



Semi-Quantitative Assessment and Quantitative AI-Driven Evaluation of CT Imaging in Chronic Thromboembolic Pulmonary Hypertension

Lojain Faisal Abdulaal

A thesis presented to the University of Sheffield in fulfilment of the thesis requirement for the degree of Doctor of Philosophy

Supervised by:

Prof AJ Swift

Prof DG Kiely

The University of Sheffield

Faculty of Medicine

Department of Clinical Medicine / Unit of Radiology

May 2025

Declaration

I, Lojain Abdulaal, confirm that the Thesis is my own work. I am aware of the University's Guidance on the Use of Unfair Means (www.sheffield.ac.uk/ssid/unfair-means). This work has not previously been presented for an award at this, or any other, university.

This is a thesis submitted in published structure. Several chapters have appeared in peer-reviewed academic journals. Additional information is presented in the 'Thesis structure' section.

Lojain Abdulaal

09 May 2025

Acknowledgments

This thesis could not have been possible without the invaluable assistance, encouragement, and support of several people who developed my academic path. I would like to acknowledge King Abdulaziz University that provided the resources and funding necessary to carry out this research.

I am deeply grateful to my exceptional supervisors and mentor, Andy Swift and David Kiely, for their help, support, insights, and encouragement throughout this process. Their dedication and expertise have been instrumental in shaping the outcomes of this work.

I would like to thank Samer Alabed, Michal Sharkey, Smitha Rajaram and Ahmed Matter, for their constructive criticism and thoughtful suggestions, which greatly strengthened the quality of this research. Their time and effort are deeply appreciated. I would also like to sincerely thank the members of the multidisciplinary team (MDT) and the pulmonary vascular disease unit (PVDU) at the Royal Hallamshire Hospital, Sheffield Teaching Hospitals NHS Foundation Trust. I am very grateful to Dr. Alex Rothman, Dr. Roger Thompson and Dr. Robin Condliffe, for their time, insightful feedback, and invaluable suggestions in reviewing my work.

I am incredibly pleased and thankful to my family and friends, who have been there for me every step of the way, offering their unwavering support, patience, and understanding during the highs and lows of my journey. To my parents, Faisal and Eman, my sisters, and my brother, thank you for always believing in me and offering the emotional support I needed to pursue my ambition. I am forever grateful for your love and support.

Finally, this thesis is a culmination of the collective efforts of many, and I am appreciative to everyone who played a part in its completion. I could not have done this without you, you have all played an integral role in my success, and I am eternally thankful for each one of you.

With all my heart, thank you

Table of Contents

Declaration	2
Acknowledgments	3
List of Tables	7
List of Figures.....	9
Abbreviations	12
Synopsis	14
Thesis structure	15
Publications and presentations	16
1 Introduction	19
1.1 Brief History	19
1.2 Pulmonary Embolism.....	20
1.3 Chronic thromboembolic pulmonary hypertension.....	21
1.4 Challenge of diagnosis of CTEPH	23
1.5 Incidence of CTEPH	23
1.6 Pathophysiology	24
1.7 Diagnostic guidance for CTEPH	25
Echocardiography.....	26
Ventilation – Perfusion Scintigraphy (V/Q)	26
Right heart catheterisation (RHC)	27
1.8 CT Imaging.....	28
CT pulmonary angiography (CTPA).....	28
CTPA features	28
CTPA Cardiac features	32
Advancement in CT imaging.....	34
1.9 Treatment	35
Anticoagulation	35
Balloon pulmonary angioplasty.....	36
Pulmonary endarterectomy	36
1.10 Semi-quantitative and quantitative CT	39
Vessel analysis.....	40
Computer-aided detection (CAD) on CT.....	40
AI approaches and QCT	41
1.11 Artificial intelligence (AI)	42
1.12 Machine learning (ML).....	43
1.13 Deep learning (DL)	43
1.14 Unsupervised vs supervised.....	47
1.15 Explainable AI (XAI)	48
1.16 Conclusion.....	49
2 Aims, Objectives, and Hypothesis	50
2.1 Hypothesis	50
2.2 Aims	50

2.3	Objectives	51
3	<i>A systematic review of artificial intelligence tools for chronic pulmonary embolism on CTPA</i>	52
3.1	Abstract.....	53
3.2	Introduction	55
3.3	Methods.....	57
	Eligibility criteria.....	58
	Search strategy.....	58
	Study selection and data extraction.....	59
3.4	Results	60
	Study 1 - Vainio et al. (2021)	63
	Study 2 - Khan et al. (2023)	64
	Study 3 - Ma et al. (2022)	65
	Study 4 - Vainio et al. (2023)	65
	Study 5 - Bird et al. (2023)	66
3.5	Discussion	68
	Models	69
	Datasets.....	71
	Performance.....	72
3.6	Conclusion.....	75
4	<i>Methodology</i>	76
4.1	Patients Database	76
4.2	CT imaging.....	77
4.3	Image analysis	78
4.4	Workflow for AI Development.....	79
4.5	Statistical analysis	82
5	<i>Lung parenchymal and cardiac appearances on CTPA impact survival in chronic thromboembolic pulmonary hypertension: results from the ASPIRE Registry</i>	83
5.1	Abstract.....	84
5.2	Introduction	86
5.3	Methods.....	88
	Study participants	88
	CTPA acquisition and evaluation	88
	Statistical analysis	91
5.4	Results	92
	Study population	92
	CTPA findings.....	95
	Distribution of CTEPH	95
	Mosaic perfusion pattern and lung infarction.....	95
	Bronchial circulation.....	95
	Parenchymal lung disease	95
	Extent of lung parenchymal abnormalities on CTPA and RHC measurements.....	96
	The extent of lung parenchymal features on CTPA, spirometry and gas transfer measurements.....	98
	Kaplan-Meier survival and Cox regression analysis for parenchymal, vascular and cardiac CT features	98

5.5	Discussion	104
6	<i>CT scoring system to Defined Thrombus Distribution in Chronic Thromboembolic Pulmonary Hypertension.....</i>	108
6.1	Abstract.....	109
6.2	Introduction	111
6.3	Methodology.....	113
	Study population	113
	CTPA protocol.....	113
	Data collection	114
	Image analysis	114
	Statistical analysis	118
6.4	Results	120
	Patient population	120
	Interobserver agreement	124
	CT, RHC and lung function measurements.....	125
	Survival of patients according to disease location	127
	Predictors of using univariate and multivariate Cox regression	127
6.5	Discussion	129
6.6	Conclusion.....	132
7	<i>Artificial Intelligence to Automate Analysis of Chronic Thromboembolic Pulmonary Disease on CTPA</i>	133
7.1	Abstract.....	134
7.2	Introduction	135
7.3	Methods.....	137
	Study cohort.....	137
	Manual segmentation	139
	Network concept and architecture	143
	Clinical evaluation	144
	Statistical analysis	145
7.4	Results	146
	Technical evaluation	149
	Segmentation analysis of testing set.....	154
	Clinical evaluation analysis with haemodynamic.....	155
	Clinical evaluation with survival analysis	157
7.5	Discussion	164
7.6	Conclusion.....	169
	Supplementary Table	170
8	<i>Discussion</i>	172
8.1	Limitations	175
9	<i>Future work.....</i>	179
10	<i>Conclusion</i>	182
	References.....	184

List of Tables

Table 1.1 Pulmonary hypertension classification adapted from ESC/ERS guidelines 2022 (Humbert et al., 2022).	22
Table 1.2 Characteristics of acute pulmonary embolism and CTEPH.....	30
Table 3.1 An overview of the literature review papers that used CTPA to identify chronic pulmonary emboli using deep learning algorithms.....	60
Table 3.2 Compliance with CLAIM checklist. Studies and the division of criteria into study description, dataset description, model description and model performance domains are shown below in (Blue/✓ =Yes) to indicate compliance, (Red/ x =No) for non-compliance and (Gray/ – =Not applicable).	61
Table 5.1 Characteristics of patients undergoing right heart catheterisation and pulmonary function tests, with a comparison between patients who underwent pulmonary endarterectomy (PEA) and those who did not (No PEA). Data are presented as mean ± standard deviation or counts (percentage). P-values (P < 0.05) indicate significant differences between the PEA and No PEA groups.....	94
Table 5.2 One-way ANOVA with post-hoc Bonferroni test to identify significant mean differences between groups. The values presented in the table are p-values, indicating the level of statistical significance for each comparison between groups.	96
Table 5.3 Findings on CTPA images in patients with CTEPH patients. (Data are mean values ± standard deviations) or counts (percentage). P-values (P < 0.05) indicate significant differences between the PEA and No PEA groups.....	99
Table 5.4 Univariate and multivariate cox-regression analysis for CT assessed vessels, cardiac changers and parenchymal change in patients undergoing and not undergoing PEA. *Multivariate including significant univariate predictors and with adjustment for age, sex, and pulmonary vascular resistance.	100
Table 6.1 Characteristics of patients who underwent right heart catheterisation and pulmonary function tests, comparing those who had pulmonary endarterectomy (PEA) versus those who did not (No PEA), as well as comparing patients with central, segmental, and distal CTEPD. Data are expressed as mean ± standard deviation or counts (percentage). P-values (P < 0.05) indicate statistically significant differences between the PEA and No PEA groups and between the three groups of CTEPD respectively. (*) indicates that a result is significantly different from the "central" reference, (#) indicates a significant difference from the "segmental" reference, and (^) indicates a significant difference from the "distal" reference.	122
Table 6.2 Interobserver reliability kappa (κ) and interclass coefficient (ICC) between observers (R1 and R2) in CT imaging to determine the number and location of CTEPH.....	124
Table 6.3 Spearman's correlations between disease locations severity and CT measurements, including RV/LV and PA/AO ratios, as well as the presence of mosaic perfusion or infarction.....	125
Table 6.4 Univariate and multivariate cox-regression analysis for CT assessed vessels, cardiac changers and parenchymal change in patients undergoing and not undergoing PEA. (P < 0.05) indicates statistically significant association with mortality. PVR group (<400=1, 400-800=2, 800-1200=3, >1200=4).....	128

Table 7.1 Characteristics of the three datasets used for developing the model (CTEPH, acute pulmonary embolism and no clot cases). Data are expressed as mean \pm standard deviation or counts (percentage).	147
Table 7.2 Patient characteristics for both model development and clinical evaluation subcohort.	148
Table 7.3 Mean \pm standard deviation of pulmonary artery (PA), pulmonary vein (PV), and thromboembolic volumes stratified by disease location, as detected using the nnU-Net-based segmentation model.	149
Table 7.4 Mean Dice Similarity Coefficient (DSC) scores for total thromboembolic volume segmentation between two independent observers.	151
Table 7.5 Interobserver agreement for chronic thromboembolic disease outputs between two observers, using intraclass correlation coefficients (ICC) with 95% confidence intervals (CI) for total, central, and non-central volumes	153
Table 7.6 Spearman correlation analysis between AI-derived volumes in millilitre (ml) of pulmonary artery (PA), pulmonary vein (PV), and thromboembolic disease with pulmonary vascular resistance (PVR), mean pulmonary arterial pressure (mPAP), and CT measurements.	156
Table 7.7 Univariate and multivariate cox-regression analysis for AI segmentation for pulmonary artery (PA), vein (PV) and thromboembolic disease (central, non-central, total clot) volumes (millilitres) in patients undergoing and not undergoing endarterectomy. (P < 0.05) indicates statistically significant association with mortality.	158
Table 7.8 Univariate cox regression analysis of central thromboembolic burden comparing AI and manual scoring across all patients (n=120), patients with endarterectomy (n=55), and those without endarterectomy (n=65). Hazard ratios (HR), 95% confidence intervals (CI), and p-values are provided for AI-derived binary classification, AI clot volume, AI binary using median>0.35, and manual binary scoring median>2.	162

List of Figures

Figure 1.1 Axial CTPA with acute PE within the lateral basal segmental artery of the left lower lobe (Red arrow), in the lateral basal segmental artery of the right lower lobe and within the superior segmental artery of the right lower lobe (Blue arrow).	31
Figure 1.2 Axial CTPA with CTEPH. (A) There is a thrombus within the left main pulmonary arteries, on the left involving the origins of the superior and inferior lingular segmental pulmonary arteries, and the left lower lobe pulmonary artery; (B) the mural thrombus involves the lobar origins of the right middle and right lower lobe pulmonary arteries.	31
Figure 1.3 Illustrates key CTPA findings associated with CTEPH. (A) demonstrates bronchial artery dilatation, a characteristic feature resulting from increased systemic collateral circulation due to chronic pulmonary artery obstruction. (B) mosaic perfusion pattern observed in both lungs, visualised through lung window reconstruction.....	32
Figure 1.4 Moderately enlarged heart with moderate to severe enlargement of the RA and RV. There is moderate RV hypertrophy. While left cardiac chambers are underfilled.	33
Figure 1.5 CTEPH therapeutic strategies reproduced with permission of the © European Society of Cardiology and European Respiratory Society 2025 (Humbert et al., 2022).	38
Figure 1.6 Illustration of the layers of CNN architectures.	45
Figure 3.1 Example of radiological features and artificial intelligence approaches in chronic thromboembolic disease detection (Images are from Sheffield institution on illustrating the diagnostic features of chronic pulmonary hypertension).	56
Figure 3.2 Process flow diagram for the inclusion and search steps.....	57
Figure 4.1 Data preparation for AI model.	80
Figure 4.2 Illustration of thromboembolic disease distribution and anatomical classification based on thrombi location within the pulmonary vasculature: central disease (main pulmonary arteries), segmental disease (segmental branches), and distal disease (subsegmental and more peripheral vessels).....	82
Figure 5.1 A) Examples of lung parenchymal features of CTEPH on CTPA. Axial CTPA images with standard lung windows from two different patients. The patient on the left showed lung infarction within the right middle lobe (yellow arrows). This typically appears as focal wedge-shaped consolidation at the lung periphery which resolves over time. Both patients exhibit mosaic perfusion. This refers to regional hyperattenuating (dashed red arrows) and hypoattenuation (solid red arrows) of the lung parenchyma, of which abnormal lung perfusion is a cause. It is important to note that neither lung infarction nor mosaic perfusion are specific to CTEPH and there is a broad differential diagnosis for both of these imaging findings. B) Examples of cardiac changes commonly seen in CTEPH on CTPA. Two axial CTPA images with standard soft tissue windows are shown. The right image shows marked dilatation of the right ventricle (RV) relative to the left ventricle (LV), with an RV/LV ratio of > 1.0, consistent with RV dysfunction. The left image shows dilatation of the pulmonary artery (PA) trunk relative to the aorta (AO), with a PA/AO ratio of > 1.0. C) Examples of CTEPH within left and right segmental disease (green circles), and emphysema lung disease in both lungs (blue arrows).....	90
Figure 5.2 Study flow diagram.....	93
Figure 5.3 Group comparison of the extent of lung mosaic perfusion (Top) and lung infarction (Bottom) with right heart catheterisation and TLCO using one-way ANOVA.	

Pulmonary vascular resistance (PVR), mean pulmonary arterial pressure (mPAP), venous oxygen saturation (SVO2), and transfer factor of the lung for carbon monoxide (TLCO). 97

Figure 5.4 Kaplan-Meier survival curve comparing survival outcomes in CTEPH patients who underwent pulmonary endarterectomy (PEA) versus those who did not, for the full cohort. 101

Figure 5.5 Kaplan-Meier survival curve comparing CTEPH patients who underwent pulmonary endarterectomy (PEA) to those who did not. along with additional curves predicting mosaic perfusion, infarction and lung disease related mortality for patients who had PEA and who did not undergo PEA after CT scan. These curves are based on CT scan findings and show numbers at risk by years..... 102

Figure 5.6 The Kaplan-Meier survival curves examining the impact of CTPA measured vessels and cardiac chambers on survival in all patients with CTEPH, those undergoing PEA and those not undergoing PEA. (pulmonary artery (PA), aorta (AO), PA/AO ratio and RV/LV ratio). 103

Figure 6.1 Axial chest CTPA slices illustrate chronic thromboembolic disease location, disease and severity classifications into central, segmental and distal subgroups (each column includes three different slices from a single patient). (A) In location classification, central included the main pulmonary artery (1) as well as the midsection of the main pulmonary artery (2 and 3) and distal aspect of the main pulmonary artery (4 and 5) of both the left and right main pulmonary arteries. (B) Segmental location, 10 segments on the right and 9 on the left (yellow arrows). (C) The presence of distal was assessed at distal segmental locations 10 segments on the right and 9 on the left (Green circle). In disease classification, (D) there is extensive central mural disease present involving both main pulmonary arteries and extending primarily into the lower lobe arteries bilaterally (red arrow). (E) In the right middle lobe, there is complex web formation at the origin of the lateral segmental branches (yellow arrow). (F) On the left side there are subsegmental attenuated vessels showing chronic thromboembolic disease (green circle). If any central disease is identified the patient is classified as having 'central' chronic thromboembolic disease. In the absence of central disease, segmental and distal are classified by the score weighting towards either category. 116

Figure 6.2 Study flow diagram..... 121

Figure 6.3 Group comparison of the right heart catheterisation with total abnormal CTEPD using one-way ANOVA. Pulmonary vascular resistance (PVR), mean pulmonary arterial pressure (mPAP), venous oxygen saturation (SVO2) and cardiac index (CI). Minor: Low clot burden. 126

Figure 6.4 Kaplan–Meier survival curves for each location (central, segmental and distal) in CTEPH patients, comparing the pulmonary endarterectomy (PEA) group with the non-surgical (no PEA) group. P-values ($P < 0.05$) indicate statistically significant differences between the subgroups of CTEPD respectively. (Red-Purple) indicates that "central" is significantly different from the "segmental", (Purple-Blue) indicates a significant difference between "segmental" and "distal" CTEPD, and (Red-Blue) indicates the difference between "central" and "distal". 127

Figure 7.1 STROBE diagram demonstrating patients with CTEPH, Acute PE and no clot selections Sheffield reference datasets. Patient subsets are also presented according to the study stage (model development and clinical evaluation). 138

Figure 7.2 AI workflow steps developed using pre trained models to create an initial mask for PA and PV segmentation..... 140

Figure 7.3 Demonstration of 3D brush tool to manually adjust and segment pulmonary vessels, and thromboembolic disease.....	140
Figure 7.4 Illustration of the manual segmentation process of pulmonary arteries (PA) and pulmonary veins (PV) from CTPA images, demonstrating the anatomical delineation required for vascular assessment.....	141
Figure 7.5 Illustration of the manual segmentation process of chronic thromboembolic disease from CTPA data, demonstrating the anatomical delineation required for CTEPH assessment.	142
Figure 7.6 Schematic representation of the nnU-Net model architecture used for automated segmentation of pulmonary arteries (PA), pulmonary veins (PV), and thromboembolic disease from CTPA images.....	144
Figure 7.7 Receiver operating characteristic (ROC) curve for the AI model in identifying thromboembolic clots on the test set. The curve demonstrates the relationship between sensitivity and specificity, and the area under the curve (AUC) represents the model's overall performance in differentiating between clot-positive and clot-negative cases.....	150
Figure 7.8 An example case that illustrates the differences in central disease segmentation between observers.	152
Figure 7.9 This case illustrates the impact of significant respiratory artefacts on segmental and distal disease, which impaired the visualisation of vascular structures and thromboembolic disease. These factors resulted in a decrease in segmentation accuracy and an increase in interobserver variability (DSC = 0.1).....	153
Figure 7.10 Examples of AI-derived pulmonary artery (PA) and pulmonary vein (PV) segmentations with corresponding clinical error scores: (A) Score 3 – no clinical error; accurate segmentation. (B) Score 2 – minor clinical error due to mild misclassification (red arrow). (C) Score 1 – significant clinical error involving major vessel segmentation inaccuracies (yellow circle).....	154
Figure 7.11 Examples of AI-derived thromboembolic disease segmentation with clinical error scoring: (A) Score 3 – no clinical error. (B) Score 2 – minor clinical error involving vessel misclassification or artefacts (red circle). (C) Score 1 – significant clinical error due to missed clot by the detection algorithm (red arrow).....	155
Figure 7.12 Kaplan–Meier survival curves for a total of 179 patients with CTEPH, compared by pulmonary endarterectomy (PEA) versus no PEA groups. The curves compare survival outcomes based on central disease detected using binary AI, and AI with median>0.4.	160
Figure 7.13 Kaplan–Meier survival curves for patients with CTEPH stratified by the presence of central thromboembolic disease, assessed using AI-derived median clot volume and manual median scoring. The cohort includes 120 patients (PEA: 55 [46%], female: 67 [56%], mean age: 57 ± 25.3 years).....	163

Abbreviations

AI	Artificial Intelligence.
AO	Ascending Aorta.
ASPIRE	Assessing The Severity of Pulmonary Hypertension in A Referral Centre.
AUC	Area Under the Curve.
BPA	Balloon Pulmonary Angioplasty.
BSA	Body Surface Area.
CAD	Computer-aided detection.
CI	Cardiac Index.
CLAIM	Checklist for Artificial Intelligence in Medical Imaging
CNN	Convolutional Neural Network.
CO	Cardiac Output.
COPD	Chronic Obstructive Pulmonary Disease.
CT	Computed Tomography.
CTEPD	Chronic Thromboembolic Pulmonary Disease
CTEPH	Chronic Thromboembolic Pulmonary Hypertension.
CTPA	Computed Tomography Pulmonary Angiography.
DECT	Dual energy CT.
DICOM	Digital Imaging and Communications in Medicine.
DL	Deep learning
ERS	European Respiratory Society.
ESC	European Society of Cardiology.
FCN	Fully Convolutional Networks
FEV1	Forced Expiratory Volume In 1 Second.
FVC	Forced Vital Capacity
HR	Hazard Ratio.
HU	Hounsfield Unit.
ICC	Interclass Correlation Coefficient.
IPAH	Idiopathic Pulmonary Arterial Hypertension.
IQR	Interquartile Range.
LV	Left Ventricle.
MDCT	Multi-Detector Computed Tomography.
MDT	Multidisciplinary Team.
MIP	Maximum Intensity Projection.
ML	Machine Learning.
MLP	Multilayer Perceptron.
mPAP	Mean Pulmonary Artery Pressure.
MRI	Magnetic Resonance Imaging.
NHS	National Health Service.
PA	Pulmonary Artery.

PAH	Pulmonary Arterial Hypertension.
PAWP	Pulmonary Artery Wedge Pressure.
PCCT	Photon-counting CT
PE	Pulmonary Embolism.
PEA	Pulmonary Endarterectomy.
PFT	Pulmonary Function Test.
PH	Pulmonary Hypertension.
PRISMA	Preferred Reporting Items for Systematic Reviews and Meta Analyses.
PVR	Pulmonary Vascular Resistance.
QCT	Qualitative CT.
RHC	Right Heart Catheterisation.
ROC	Receiver Operator Characteristics.
RV	Right Ventricle.
SD	Standard Deviation.
SVO2	Mixed Venous Oxygen Saturation.
TBV	Total Blood Volume.
TLCO	Transfer Factor of Carbon Monoxide.
VQ scan	Ventilation/Perfusion Scintigraphy.
VTE	Venous Thromboembolism.
WHO	World Health Organisation.
WU	Woods Unit.
XAI	Explainable AI.

Synopsis

Chronic thromboembolic pulmonary hypertension (CTEPH) is a severe, yet curable condition characterised by unresolved blood clots in the pulmonary arteries. Accurate diagnosis and classification of CTEPH is required for accurate treatment. The development of scar tissue from unresolved chronic thromboembolism leads to arterial narrowing, increasing pulmonary vascular resistance in the lung circulation and straining the right ventricle, which results in right heart failure if left untreated. All patients suspected of having CTEPH, without a contraindication, undergo computed tomography pulmonary angiography (CTPA) imaging to confirm diagnosis. Recent advancements in artificial intelligence (AI) using deep learning methodologies have facilitated automated quantitative analysis of medical imaging characteristics.

The primary objective was to determine the important features of CTPA for the diagnosis in the lungs and heart, and to develop a scoring system for the thromboembolic disease in the pulmonary arteries. A secondary objective was to create an automated, clinically relevant approach employing deep learning models to identify chronic pulmonary embolism and assess CTEPH severity from CTPA images, illustrating the capability of AI in detecting CTEPH occurrence and severity.

This thesis illustrates the prognostic impact of lung parenchymal abnormalities on CTPA in patients with CTEPH. The proposed scoring method for visual assessment of chronic embolic disease, which considers both disease location and extent was shown to predict survival outcomes. Furthermore, a deep learning model for chronic embolic disease segmentation and quantification was developed and clinical validated showing diagnostic value. The impact of thromboembolic disease severity on patient survival was also assessed using the AI model. The comparison of AI-derived thromboembolic disease volume with conventional manual scoring methods demonstrates improved prognostic accuracy in assessing disease severity, offering a more robust tool for clinical evaluation of CTEPH. In conclusion, our findings highlight the importance of systematically evaluating CTPA images in patients with CTEPH.

Thesis structure

This thesis is in a publication layout, as some chapters have been published as peer-reviewed journal papers. Each of these chapters consists of a comprehensive introduction, methods, results, discussion, and conclusion sections. At the start of each chapter, I have included a clear statement of my specific contributions to the relevant work. The whole work includes both these refereed research articles (Chapters 3, 5-7) and supporting chapters that provide: contextual background (Chapter 1), comprehensive methods framework (Chapter 4), an overall discussion (chapter 8), future research directions (Chapter 9), and a conclusion (Chapter 10).

Chapter 1 presented an overview of the expanding role of CT pulmonary angiography in the diagnosis and assessment of CTEPH. Chapter 2 outlined the hypothesis, aims, and objectives throughout the thesis. Chapter 3 emphasised the increasing development of studies employing AI techniques for the automated identification of chronic PE and CTEPH. Chapter 4 included a brief overview of the CTEPH imaging database building, which included clinical and radiological data obtained from the ASPIRE Registry. Chapter 5 demonstrated the prognostic impact of common CT measurements, lung parenchymal abnormalities, and cardiac changes in patients with CTEPH. Chapter 6 introduced a CTPA-based radiological scoring system for chronic thromboembolic disease, combining location and extent to predict survival outcomes. Chapter 7 developed, validated, and tested a 3D deep-learning AI model (nnU-NET) for automated chronic thromboembolic disease detection on CTPA. The study focused on pulmonary artery segmentation accuracy, clot quantification, and prognostic assessment by comparing AI-derived metrics with manual scoring to predict survival outcomes.

My future aim is to use machine learning algorithms to integrate imaging biomarkers, patient outcomes and multimodal clinical data for CTEPH assessment that may enhance diagnostic accuracy and management.

Publications and presentations

Publications and submissions directly related to this thesis

- 1- **Abdulaal, L.**, Maiter, A., Dwivedi, K., Sharkey, M.J., Alabed, S., Alkhanfar, D., Rothman, A., Rajaram, S., Condliffe, R., Kiely, D.G. and Swift, A.J., 2024. Lung parenchymal and cardiac appearances on CTPA impact survival in chronic thromboembolic pulmonary hypertension: results from the ASPIRE Registry. *ERJ Open Research*.
- 2- **Abdulaal, L.**, Maiter, A., Salehi, M., Sharkey, M., Alnasser, T., Garg, P., Rajaram, S., Hill, C., Johns, C., Rothman, A.M.K. and Dwivedi, K., 2024. A systematic review of artificial intelligence tools for chronic pulmonary embolism on CT pulmonary angiography. *Frontiers in Radiology*, 4, p.1335349.

In progress

- 3- **Abdulaal, L.**, Sharkey, M.J., Maiter, A., Alabed, S., Dwivedi, K., Rajaram, S., Condliffe, R., Kiely, D.G. and Swift, A.J., 2025. CT scoring system to Define Thrombus Distribution in Chronic Thromboembolic Pulmonary Hypertension. *Submitted to BJR*.

Publications not related to this thesis

- 4- Alnasser, T.N., **Abdulaal, L.**, Maiter, A., Sharkey, M., Dwivedi, K., Salehi, M., Garg, P., Swift, A.J. and Alabed, S., 2024. Advancements in cardiac structures segmentation: a comprehensive systematic review of deep learning in CT imaging. *Frontiers in Cardiovascular Medicine*, 11, p.1323461.

Published abstracts

- 1- **Abdulaal, L. F.**, Dwivedi, K., Sharkey, M., Alabed, S., Mamalakis, M., Alkhanfar, D. D. F., Condliffe, R., Kiely, D., & Swift, A. J. (2022). Clinical importance of CT lung parenchymal appearances in chronic thromboembolic pulmonary hypertension: a retrospective cohort study. *Insights into Imaging*, 13(Suppl 4), 205. *ECR 2022 Book of Abstracts*. <https://doi.org/10.1186/s13244-022-01337-x>
- 2- **Abdulaal, L.**, Dwivedi, K., Sharkey, M., Alabed, S., Mamalakis, M., Alkhanfar, D., Condliffe, R., Kiely, D.G., & Swift, A.J. (2022). P41 CT lung parenchymal appearances in

chronic thromboembolic pulmonary hypertension (CTEPH). *'Mission (Im)possible I' – Pulmonary vascular disease. BTS.*

- 3- **Abdulaal L**, Dwivedi K, Sharkey M, Alabed S, Alkhanfar D, Condliffe R, Rajaram S, Kiely D, Swift AJ. "Establishing and validating a scoring system for chronic thromboembolic pulmonary hypertension (CTEPH) via CT pulmonary angiography". 2023. Dec;39(12) (A-481):2301-2417. doi: 10.1007/s10554-023-02934-7. *ESCR-ESTI 2023 Berlin congress.*
- 4- Alkhanfar, D., Alabed, S., Dwivedi, K., **Abdulaal, L.**, Shahin, Y., Johns, C., Garg, P., Thompson, A.A.R., Rothman, A.M.K., Hameed, A., Charalampopoulos, A., Wild, J.M., Condliffe, R., Kiely, D.G. and Swift, A.J., 2023. CT-derived small and peel pulmonary vessel blood volume measurements as potential imaging biomarkers for the diagnosis of PAH and CTEPH. *ESCR-ESTI 2023 Berlin Congress.*
- 5- Alnasser, T.N., **Abdulaal, L.**, Maiter, A., Sharkey, M., Dwivedi, K., Salehi, M., Garg, P., Swift, A.J. and Alabed, S., 2025. 4 Advancements in cardiac structures segmentation: a comprehensive systematic review of deep learning in CT imaging. *Heart, 111*(Suppl 1), pp. A2-A2. *BSCI/BSCCT Annual Meeting 2025.*
- 6- Alnasser, T.N., Hokmabadi, A., Checkley, E.W., Sharkey, M., **Abdulaal, L.**, Alghamdi, K., Garg, P., Maiter, A., Dwivedi, K., Salehi, M. and Taylor, J., 2025. 3 A fully automated predictive model for diagnosing pulmonary hypertension and left heart disease on routine unenhanced CT. *BSCI/BSCCT Annual Meeting 2025.*

In progress

- 7- Accepted abstract to the ERS 2025 Congress in Amsterdam (27 September - 1 October 2025). Artificial intelligence in detecting and quantifying thrombotic burden compared to manual analysis using CTPA.

1 Introduction

1.1 Brief History

The term "venous thromboembolism" is credited to the pioneering work of Rudolf Virchow (McFadden and Ochsner, 2002). In 1872, surgeon Friedrich Trendelenburg, who created the German Surgery Organisation, made a sobering observation when analysing the deaths of nine patients who had pulmonary embolism (PE). Trendelenburg created a surgical technique that involved opening the pulmonary artery through a left parasternal thoracotomy to remove the embolus. However, none of those patients lived more than 37 hours. The fact that pulmonary embolism and venous thrombosis are still significant causes of morbidity and mortality today emphasises the continuing relevance of developing work in this area.

Over time, medical understanding of PE advanced, leading to the recognition of chronic thromboembolic pulmonary disease (CTEPD) and the more severe form, chronic thromboembolic pulmonary hypertension (CTEPH). In the 1950s and 1960s, autopsy findings and clinical studies revealed that unresolved thrombi could persist in the pulmonary arteries, resulting in chronic obstruction and, in some cases, pulmonary hypertension (Dunnill, 1962). The first successful pulmonary endarterectomy (PEA), a surgical procedure to remove these chronic clots, was performed in 1961 at the University of California, San Diego, which later became a leading centre for the treatment of CTEPH (Moser and Braunwald, 1973). Technological advances in imaging, particularly ventilation-perfusion (V/Q) scans and computed tomography pulmonary angiography (CTPA), significantly improved diagnostic accuracy in the following decades.

In the 1990s and early 2000s, clinical research began to differentiate CTEPD—chronic thromboembolic pulmonary obstruction without resting pulmonary hypertension—from CTEPH. In 2001, the World Health Organisation classified CTEPH as a distinct form of pulmonary hypertension (Group 4). The approval of riociguat in 2013 marked the first pharmacological treatment for inoperable CTEPH, while balloon pulmonary angioplasty (BPA) emerged as a promising alternative for non-surgical candidates. More recently, attention has

turned to patients with CTEPD who, despite normal pulmonary pressures at rest, experience significant symptoms on exertion. Ongoing scientific research continues in refining treatment strategies and enhancing patient outcomes for both CTEPD and CTEPH.

1.2 Pulmonary Embolism

PE is a condition characterised by the partial or complete blockage of one or more pulmonary arteries, typically caused by emboli formed by thrombi originating in the deep veins of the legs. The embolus can obstruct various regions of the pulmonary arterial branches, from the main pulmonary artery and its bifurcation to the right or left pulmonary arteries, as well as smaller or more distal branches, depending on its size and length (Tritschler et al., 2020). There are other causes of PE besides blood thrombi. Other potential causes include air bubbles, amniotic fluid embolism, fragments of tumours, or fat released from the marrow of a fractured long bone. Despite the fact that pulmonary embolism can affect anyone, the risk of developing this condition may be elevated by certain factors. The risk factors include older ages, obesity, cancer, varicose veins, and pre-existing medical conditions such as heart failure, high blood pressure, chronic bowel inflammation, chronic obstructive pulmonary disease (COPD), and stroke (Agusti et al., 2003).

Accurately determining the true incidence of pulmonary embolism in a population is challenging due to the wide variability in symptoms that might occur, from minor coughing or chest pain to sudden death. According to recent research in the UK, the yearly incidence of venous thromboembolism (VTE) is around 2 per 1,000 persons in the general population (Evans et al., 2020). Epidemiological research indicates that annual PE incidence rates from 39 to 115 per 100,000 people. VTE, which includes PE and deep vein thrombosis (DVT), is the third most common acute cardiovascular condition worldwide, following myocardial infarction and stroke (Righini et al., 2017, Konstantinides et al., 2020). This blockage of the pulmonary arteries can lead to an increase in right ventricle afterload, that may combine with reduced cardiac output, and cause right ventricular hypertrophy and potentially progressing to right heart failure. It also may cause CTEPH, a condition that presents with elevated arterial

pressure in the pulmonary arteries. This is a potentially fatal condition that requires instant and accurate diagnosis, followed by adequate treatment.

1.3 Chronic thromboembolic pulmonary hypertension

CTEPH is a rare disease that occurs when pulmonary emboli does not resolve despite treatment, resulting in long-term consequences and elevated pressure in the pulmonary arteries. CTEPH is a type of precapillary pulmonary hypertension (group 4). Precapillary PH also include pulmonary arterial hypertension (PAH) (group 1), pulmonary hypertension resulting from chronic lung disease and/or hypoxia (group 3), and pulmonary hypertension along with several other conditions such as blood disorders, systemic diseases, metabolic disorders, and tumours obstructing the pulmonary arteries (**Table 1.1**). The World Health Organisation created these categories to describe pulmonary hypertension based on comparable pathophysiological alterations, clinical features, and treatment approaches.

CTEPH is defined by the diagnostic threshold of mean pulmonary arterial pressure (mPAP) greater than 20 mmHg (Condon et al., 2019). The updated criteria now include pulmonary vascular resistance (PVR) to account changes in cardiac output that occur with pulmonary arterial hypertension: specifically, a PVR of 2 Wood units or greater, with a mPAP above 20 mmHg and characteristic imaging findings (ESC/ERS). Unresolved blood embolus, with thickening of the inner lining of the arteries and the creation of scar tissue, lead to higher mPAP and PVR in the blood vessels of the lungs (Klok et al., 2020). In the UK, CTEPH is life-threatening, patients with CTEPH who do not undergo surgical treatment have a 5-year survival rate of approximately 30-60% (Quadery et al., 2018). This rate may differ depending on the severity of the disease and the accessibility of alternative treatments.

Several factors related to VTE tend to risk patients to the poor resolution of thromboembolism and the development of CTEPH. The most predominant relevant risk factors for the development of CTEPH are recurrent episodes of PE and inadequate anticoagulation. This may be due to either a failure of the body to adequately activate the lytic system in dissolving large clots or to sufficiently manage the thrombus. Nevertheless,

these factors alone do not explain the majority of CTEPH cases, indicating additional underlying mechanisms (Lang et al., 2016). Patients diagnosed with CTEPH are more likely to have more comorbidities than those diagnosed with other forms of pulmonary arterial hypertension (Simonneau et al., 2017, Simonneau and Hoeper, 2019). Therefore, additional risk factors have been associated with an increased risk of CTEPH, including haematological diseases, underlying autoimmune conditions, splenectomy, thyroid replacement treatment, and a history of tumours were all identified as a factor associated with an increased risk of CTEPH (Bonderman and Lang, 2011).

Table 1.1 Pulmonary hypertension classification adapted from ESC/ERS guidelines 2022 (Humbert et al., 2022).

Group	Definition	Causes
1	Pulmonary arterial hypertension (PAH)	Idiopathic PAH Heritable PAH Drugs and toxin induced PAH Associated condition
2	Pulmonary hypertension due to left heart disease	Systolic dysfunction Diastolic dysfunction Valvular disease
3	Pulmonary Hypertension due to lung disease and /or hypoxia	Emphysema Interstitial lung disease Hypoxia without lung disease Lung disorder
4	Pulmonary Hypertension due pulmonary artery obstructions.	CTEPH Other pulmonary artery obstructions (pulmonary embolism, stenoses, in situ thrombosis, tumours)
5	Pulmonary hypertension with unclear and/or multifactorial mechanisms	Systematic and metabolic disorders Hematologic disorder

1.4 Challenge of diagnosis of CTEPH

CTEPH is difficult to diagnose since symptoms of right heart failure may not present evidence until the illness has progressed to an advanced level, and early disease phases are characterised by vague symptoms or even the lack of symptoms altogether. The fact that the signs of CTEPH are comparable to those of other kinds of pulmonary hypertension is another difficulty associated with the condition. Consequently, an accurate diagnosis may be postponed or even be missed, which affects between 2 to 4 percent of those who survive acute PE, is the most serious long-term consequence of the condition (Klok et al., 2020). Chronic PE is a challenging diagnosis and a commonly overlooked condition that's tough to spot and frequently misinterpreted. CTPA is used to diagnose CTEPH, which might be complicated to detect the radiologic features with abnormalities detected with the disease progression (Ruggiero and Screaton, 2017). Chronic PE may cause pulmonary hypertension, morbidity, and death, hence early diagnosis is critical (Doğan et al., 2015).

1.5 Incidence of CTEPH

The true prevalence of CTEPH after an acute PE remains undetermined, with studies reporting a wide range from 0.1% to 11.8% in the first two years (Delcroix et al., 2021, Konstantinides et al., 2020, Ali et al., 2012). The variability can be related to differences in study methods and patient selection criteria, and the difficulty of identifying pre-existing CTEPH from acute PE due to overlapping clinical symptoms and a frequent lack of haemodynamic data (Delcroix et al., 2021). As the ASPIRE Registry illustrates that the introduction of systematic follow-up procedures three months after acute PE enhances population-based identification of CTEPH from 5–6 cases per million to 13.2 cases per million per year in Sheffield, and increases the number of pulmonary endarterectomy procedures (Durrington et al., 2024).

Ende-Verhaar et al. (2017) conducted a systematic review and meta-analysis studying the incidence of CTEPH in patients after acute PE and according to their research, the incidence of CTEPH was between 0.56% and 3.2% (Ende-Verhaar et al., 2017). A study by Pengo et al, (2004), found that the incidence of CTEPH in patients with acute PE has grown. with 3.8% of survivors developing CTEPH within two years of their first PE incident (Pengo et al., 2004).

Similarly, (Klok et al., 2010) observed an incidence ranging from 0.57% to 1.5%, demonstrating variability in CTEPH rates across diverse patient demographics following acute PE. More recently, Valerio et al. (2022) large multicentre cohort study, which included 1,097 patients, reported that the cumulative incidence of CTEPH was approximately 2.3% (Valerio et al., 2022). According to some research, the incidence of developing CTEPH following an acute PE may reach up to 5% (Guérin et al., 2014, Mehta et al., 2010). According to studies, extensive examination of CTPA scans obtained at the time of acute PE diagnosis could result in the early detection of CTEPH in follow-up evaluations (Boon et al., 2022, Braams et al., 2021, Ende-Verhaar et al., 2019).

While PE is commonly acknowledged as a substantial risk factor for CTEPH, studies indicate that up to 25% of CTEPH patients may not have a documented history of pulmonary embolism (Pepke-Zaba et al., 2011). The study demonstrated that CTEPH is possible throughout patients who never experienced an acute pulmonary embolism.

1.6 Pathophysiology

Frequent occurrences of pulmonary embolism, along with partial resolution of emboli in the lungs, result in intimal thickening of the pulmonary arteries and fibrotic changes in the thrombi. These changes lead to arterial blockage and stenosis, which progressively increase resistance and pressure in the pulmonary vasculature, eventually causing right heart failure if not treated. The actual cause of unresolved emboli and CTEPH development remains unclear. Studies indicate that it might be influenced by a multifaceted interplay of immunologic, fibrinolytic, and hematologic dysfunction processes (Matthews and Hemnes, 2016, Lang et al., 2013, Lang et al., 2016). Studies have demonstrated that CTEPH is characterised not only by chronic thromboembolic structured in the main pulmonary arteries, but also by small and distal vessel disease, which might be a significant factor during the initiation and development of the disease (Klok et al., 2020).

Besides the mechanical blockage induced by thromboembolic, the unobstructed pulmonary vasculature experiences considerable remodelling. A study by Dorfmueller et al (2014),

performed a comparative histological examination of explanted lung tissue extracted from 17 patients with CTEPH who received lung transplants because of either an unsuccessful pulmonary endarterectomy (PEA) or inoperable distal disease. They found that patients with CTEPH exhibit altered vascular remodelling in the lungs, characterised by organised thrombosis, eccentric intimal fibrosis, and pulmonary capillary hemangiomatosis. Additionally, there was marked dilatation of the bronchial systemic vessels and vasa vasorum (Dorfmüller et al., 2014).

CTEPH is often diagnosed with significant delay because it has non-specific clinical symptoms (Delcroix et al., 2016, Ende-Verhaar et al., 2018). The patient often presents with shortness of breath, dizziness, chest pain and fatigue, which may gradually worsen over time (Kiely et al., 2013). As the disease progresses, additional symptoms may evolve, such as signs of right heart failure, peripheral oedema, abdominojugular reflux, jugular venous distention, and splenomegaly. The patient may also experience low cardiac output condition, which include tachycardia, hypotension, oliguria, and cyanosis caused by the inability of the cardiovascular system to pump blood sufficient through the lungs, resulting in poor circulation (Sabbula et al., 2024).

1.7 Diagnostic guidance for CTEPH

The 2022 European Society of Cardiology (ESC) guidelines for pulmonary hypertension state that the diagnostic method should begin with a review of the patient's medical history to identify any signs and symptoms of CTEPH. Patients with suspected CTEPH must receive anticoagulant treatment to distinguish between PE and CTEPH for a minimum of 3 months. Ventilation/perfusion (V/Q) scintigraphy should also be performed on all patients with suspected CTEPH to assess perfusion defects and confirm the diagnosis. A V/Q mismatch in a segment or a larger defect increases the chance of a CTEPH diagnosis. Additionally, the diagnosis must be corroborated with right heart catheterisation (RHC) and the identification of characteristic imaging abnormalities associated with CTEPH. Patients are often directed to specialised pulmonary hypertension centres for RHC and comprehensive imaging techniques to determine the need for surgical intervention (Humbert et al., 2022).

Additionally, the diagnosis and characterisation of CTEPH have been greatly enhanced by notable developments in CT technology. The Pulmonary Vascular Research Institute imaging task force's most recent imaging statement emphasises the significance of CTPA in the diagnostic approach. In patients with chronic PE and who are suspected of having additional emboli, it is recommended to avoid D-dimer test and rather utilise a more direct approach such as a V/Q lung scan or CTPA (Kiely et al., 2019).

Echocardiography

Echocardiography has a vital role in suspected with CTEPH, mainly for detecting evidence of pulmonary hypertension and right heart failure. It is recommended in ESC/ERS guidelines as an early, non-invasive diagnostic method by assessing tricuspid regurgitant jet velocity, if greater than 2.8m/s as it represents intermediate probability of pulmonary hypertension and if >3.4m/s infers high risk, which is a main sign of potential pulmonary hypertension (Galiè et al., 2019, Konstantinides et al., 2020). Echocardiography can also assess the cardiac chambers and atria, and secondary signs of PH can adjust a patient's risk of pulmonary hypertension as per the ESC/ERS guidelines. Additionally, echocardiography can detect leftward septal deviation during systole, which is also an indicator of elevated right-sided pressures and provides additional evidence of right ventricular strain and dysfunction (Humbert et al., 2022).

Ventilation – Perfusion Scintigraphy (V/Q)

V/Q scintigraphy is a nuclear medicine imaging technique, using radioactive isotopes to assess ventilation and perfusion of the lungs in patients suspected with CTEPH (Moradi et al., 2019). V/Q is a widely available test that is recommended in all patients with suspected CTEPH. V/Q scan can detect the typical wedge-shaped perfusion defects in the lungs, and correlation with the ventilation imaging mismatched regions can be appreciated. When CTEPH symptoms present with elevated pulmonary artery pressure, a V/Q scan becomes an effective diagnostic technique, exhibiting a sensitivity of up to 96% for CTEPH diagnosis (Tunariu et al., 2007). However, a segmental or larger perfusion defect on V/Q imaging can also occur in conditions like inflammatory responses, severe air trapping, cancers, and fibrosing mediastinitis, where pulmonary arteries are obstructed by non-thrombotic factors (Narechania et al., 2020).

The most recent developments have included single-photon emission computed tomography (SPECT) and hybrid SPECT/CT imaging, providing three-dimensional assessment and enhanced anatomical resolution. Planar V/Q is useful for screening due to its high sensitivity. SPECT or SPECT/CT improves specificity, which is important for surgical planning and reducing false positive. V/Q SPECT localises perfusion defects more accurately, and SPECT/CT provides precise anatomical correlation, helping distinguish artefacts or lung abnormalities from true thromboembolic disease (Currie and Bailey, 2023).

High sensitivity at the initial screening stage is vital to detect nearly all CTEPH cases and ensure timely referral. A V/Q scan minimises false negatives, which is important considering the progressive and curable characteristics of CTEPH disease. For surgical assessment or excluding other diagnoses, high specificity is equally important to avoid unnecessary tests or mismanagement. Consequently, V/Q SPECT or SPECT/CT enhances specificity while maintaining sensitivity, enabling more accurate and efficient treatment decisions in patients with CTEPH (Wang et al., 2020).

Right heart catheterisation (RHC)

RHC is the conclusive test for confirming PH and assessing the severity of CTEPH. The current criteria for diagnosing CTEPH with RHC include a mPAP of at least 20 mmHg, a pulmonary artery wedge pressure (PAWP) of 15 mmHg or less, and a PVR more than 3 Wood units (Humbert et al., 2022, Galiè et al., 2015). PVR also plays an important role in determining the severity of CTEPH, allowing observation of the progression of the disease and the effectiveness of treatment. While the cardiac output and cardiac index are used to determine the heart function (Galiè et al., 2015).

Exercise RHC is an additional diagnostic tool used to evaluate patients with suspected CTEPH or unexplained symptoms, even if hemodynamic measurements at rest are normal. It is particularly useful for identifying abnormal increases in mPAP during physical activity, which might indicate early pulmonary vascular disease. For instance, patients with fibrotic thrombi or chronic thromboembolic pulmonary disease, demonstrating the value of exercise RHC in unmasked hidden haemodynamic abnormalities (van Kan et al., 2016, Hoeper et al., 2013).

1.8 CT Imaging

CT pulmonary angiography (CTPA)

CTPA is a common and readily available diagnostic imaging tool to assess CTEPH. It offers fast acquisition and high-resolution imaging to assess lung parenchyma, vascular and cardiac structures (Rajaram et al., 2015, Swift et al., 2020). CTPA is the recommended option to evaluate patients with CTEPH by contrast enhanced imaging, as recommended by the European Society of Cardiology (Humbert et al., 2022).

The use of contrast media in CTPA allows a detailed assessment of the pulmonary arteries, and increases the visibility of abnormalities, including thrombi, stenoses, or lesions. Contrast media improves images substantially and separates arteries from adjacent tissue such as mediastinal tissues or lung parenchyma (McNeil and Dunning, 2007). However, may be overstated as a result of other structures of high density, including bone, calcifications, or metal. Beam-hardening artefacts by contrast media can mask pathological findings and anatomical structures (Kim et al., 2018). Post-processing algorithms and attenuation correction techniques can be used to reduce artefacts and enhance the quality of vascular imaging (Farrell et al., 2021).

CTPA features

The direct CTPA signs of the vascular abnormalities in the pulmonary arteries include complete or partial obstruction, attenuated vessels, webs, stenosis, calcified and eccentric thrombi (Gopalan et al., 2017, Delcroix et al., 2021). In CTPA, acute PE and CTEPH present distinctive radiological features that allow for differentiation. **Table 1.1** presents a comparative analysis of CTPA features observed in acute PE and CTEPH. Identifying these differences is essential for accurate diagnosis and treatment. Acute PE typically occurs near vascular bifurcations, where it can partially or completely obstruct pulmonary circulation. The presence of complete occlusion in acute PE manifests as a hypoattenuating contrast defect (dark area) that fully occupies the lumen of the involved artery in CTPA images (**Figure 1.1**) (Sin et al., 2021). Complete acute PE obstruction might lead to small lung infarctions. These infarctions may appear on CTPA images as ground-glass opacities, occasionally can be associated with reticular alterations or triangular subpleural consolidation (Kaptein et al.,

2024). On the other hand, the appearance of CTEPH differs depending on the length of time it has been present and the degree of vessel obstruction (**Figure 1.2**). Total CTEPH obstruction is characterised by an instant narrowing of the vessel width and the absence of contrast further than the obstruction. While partially obstructed vessels are presented as partially attenuated vessels, stenosis of arteries or as post-stenotic dilatation vessels distal to the obstruction. Compared to the central filling defects in acute PE, chronic thrombus is usually eccentrically adhered to the blood vessel wall (Ruggiero and Screaton, 2017, Boon et al., 2022). Within thrombi, calcification is exceedingly rare in CTEPH. Pulmonary arteries may constrict and remnant fibrotic webs or bands that form by chronic obstructions, as opposed to the dilation observed in acute PE (Nishiyama et al., 2018, Hahn et al., 2022).

In addition to vascular signs, CTEPH is characterised by common parenchymal features, such as mosaic perfusion (Grosse and Grosse, 2010). While these findings are diagnostically important, their independent association with disease severity, progression, and clinical significance requires further investigation. It is common to observe an inconsistent attenuation pattern in the lung parenchyma as a result of areas of normal blood supply and decreased blood flow (hypoperfusion). Mosaic perfusion pattern characterised by less blood flow in regions where arteries are obstructed or narrowed (Grosse et al., 2017). CTPA presents as strongly delineated low attenuation parts with tiny vascular diameters contrasted with increasing attenuation areas with greater vessels reflecting the normal/hyper pulmonary ventilation (Kligerman et al., 2015) (**Figure 1.3**). Abnormal bronchial artery dilatation is frequently present in CTPA of chronic PE and CTEPH patients that could be responsible for up to 30% of all blood flow in the body (Ruggiero and Screaton, 2017). Collaterals of systemic-to-pulmonary arteries may form; they appear on CTPA as dilated bronchial or intercostal arteries. Since lung infarction appears frequently in CTEPH cases and may be associated to left heart failure, which might decrease bronchial artery perfusion due to increased pulmonary circulation pressure (KATSUMURA and OHTSUBO, 1998). There may also be signs of prior lung infarctions, such as volume loss and subpleural scarring (Parambil et al., 2005).

Table 1.2 Characteristics of acute pulmonary embolism and CTEPH.

Feature	Acute	CTEPH
Luminal thrombus Location	Central or occlusive (main/lobar/segmental arteries)	Eccentric, wall adherent.
Thrombus Appearance	Soft, low-attenuation filling defect	Fibrotic, or organised thrombus, webs
Pulmonary Artery Changes	Dilated affected arteries	Dilated main pulmonary artery, stenosis, post-stenotic dilatation, attenuated vessels.
Collateral Formation	Absent	Often present (bronchial or intercostal arteries)
Lung Parenchyma	Normal or infarcted lung	Mosaic perfusion, infarctions, or possible volume loss
Cardiac changes	Acute RV strain	RV strain and RV hypertrophy

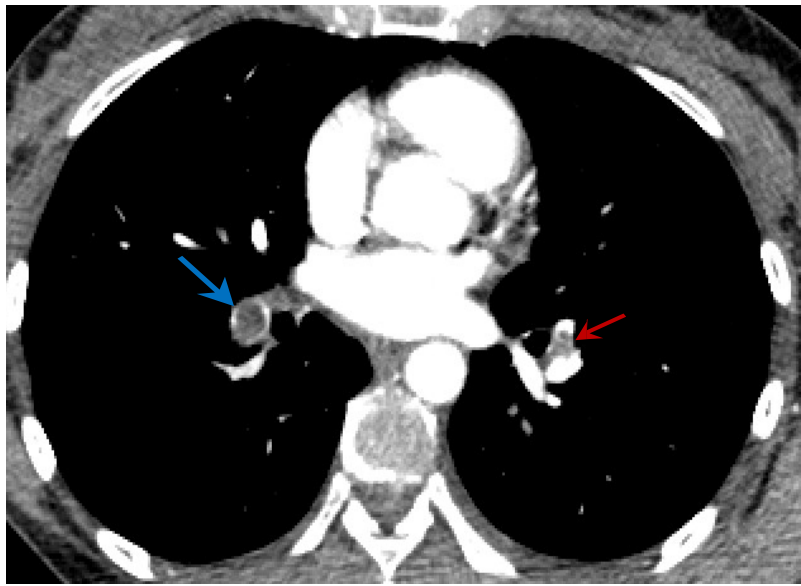


Figure 1.1 Axial CTPA with acute PE within the lateral basal segmental artery of the left lower lobe (Red arrow), in the lateral basal segmental artery of the right lower lobe and within the superior segmental artery of the right lower lobe (Blue arrow).

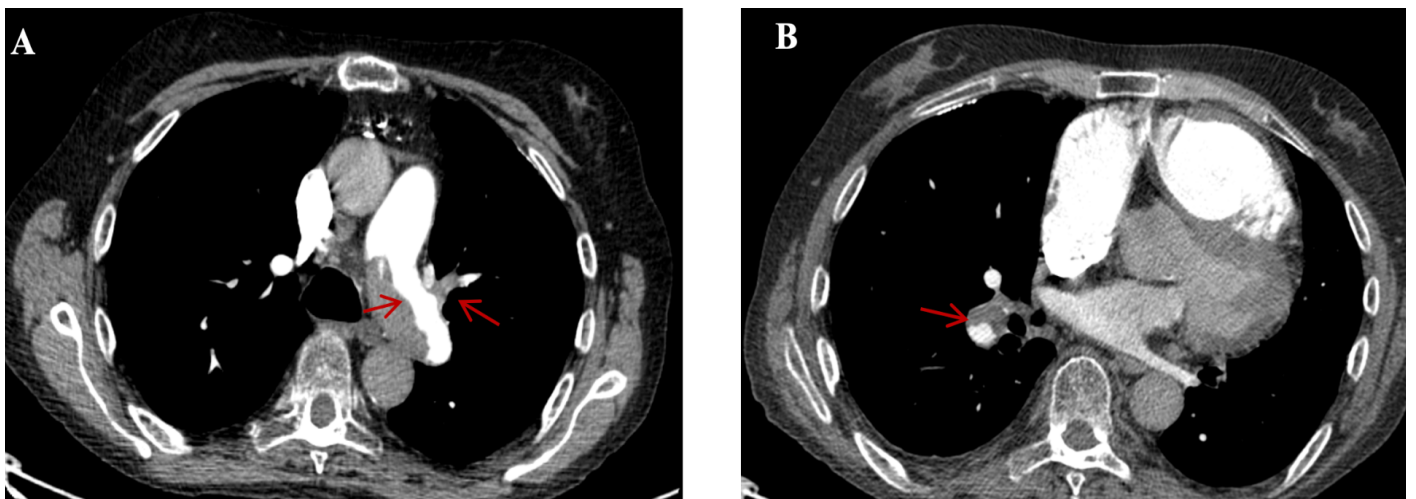


Figure 1.2 Axial CTPA with CTEPH. **(A)** There is a thrombus within the left main pulmonary arteries, on the left involving the origins of the superior and inferior lingular segmental pulmonary arteries, and the left lower lobe pulmonary artery; **(B)** the mural thrombus involves the lobar origins of the right middle and right lower lobe pulmonary arteries.

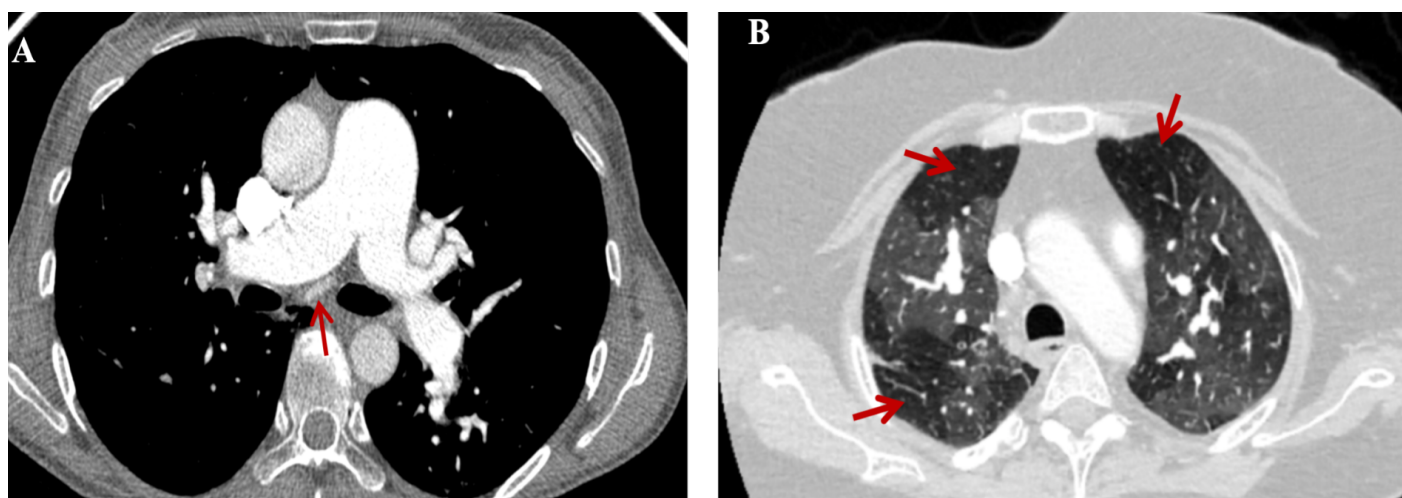


Figure 1.3 Illustrates key CTPA findings associated with CTEPH. **(A)** demonstrates bronchial artery dilatation, a characteristic feature resulting from increased systemic collateral circulation due to chronic pulmonary artery obstruction. **(B)** mosaic perfusion pattern observed in both lungs, visualised through lung window reconstruction.

CTPA Cardiac features

There are various parameters that CTPA imaging provides to evaluate CTEPH severity and stratification of risk. For instance, right cardiac strain, lung perfusion, and clot load. In addition, rising right ventricle (RV)/left ventricular (LV) ratio (greater than 1 in the axial plane, or greater than 0.90 in 4 cardiac chambers reconstruction) (**Figure 1.4**), flattening of the ventricular wall septum, and contrast material reflux into the inferior vena cava (IVC) and liver veins are all signs of right heart strain (Moore et al., 2018). The use of CT images without contrast-enhanced allows for the identification of a number of cardiac characteristics that are connected with CTEPH, such as enlargement in the size of the chambers of the heart, hypertrophy of the RV and interventricular septal deviation. The combination of pulmonary arterial diameter, RV outflow tract muscle thickness and septal deviation (or RV/LV ratio) has been shown to accurately predict the presence of pulmonary hypertension (Swift et al., 2020). Long-standing pulmonary hypertension causes compensatory thickening of the right ventricular wall (Sharifi Kia et al., 2021).

Identifying the mechanical parameters that influence right ventricular (RV) function is essential for accurately evaluating its role in disease and clinical prognosis. A study by Ruigrok et al. (2019), found that central disease in patients with CTEPH was more common with larger RV dilatation than patients with distal disease. These results demonstrate the possibility of other parameters beside standard measurements of RV afterload to significantly define RV function and flexibility in CTEPH (Ruigrok et al., 2019).

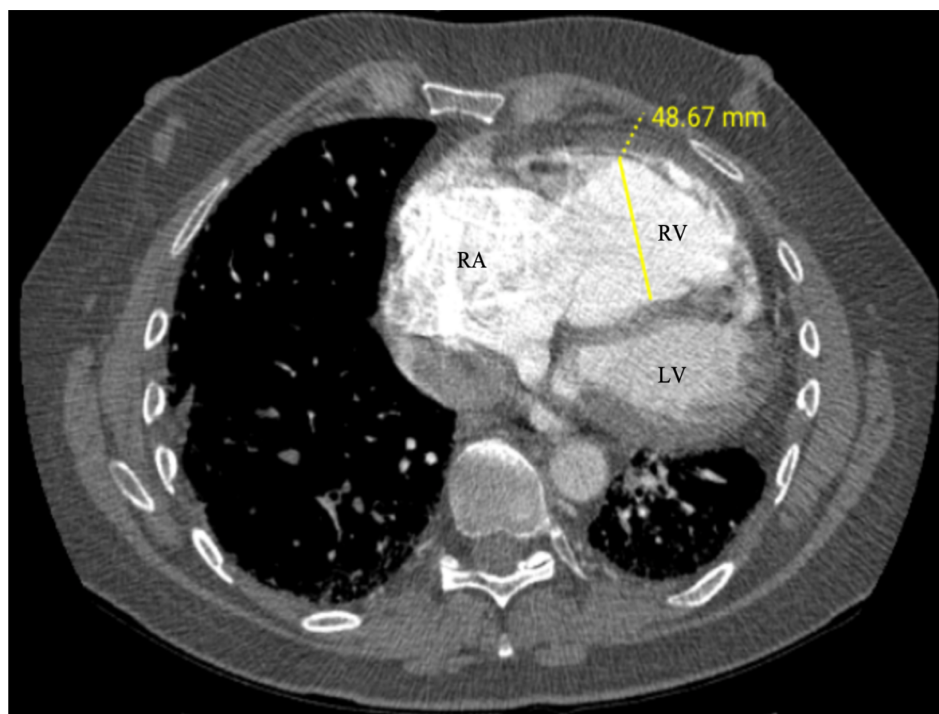


Figure 1.4 Moderately enlarged heart with moderate to severe enlargement of the RA and RV. There is moderate RV hypertrophy. While left cardiac chambers are underfilled.

Advancement in CT imaging

CT has shown substantial technical progress. by improving lung imaging and providing comprehensive anatomical and functional information. These advancements, such as the multidetector (MDCT) method, have enabled a comprehensive examination in a short amount of time and wider scan coverage, compared to the long duration of the previous system (Chaikriangkrai et al., 2014). Additionally, dual-energy CT (DECT) is capable of providing a quantitative assessment of lung perfusion simultaneously. DECT might help differentiate CTEPH from other forms of peripheral pulmonary hypertension by detecting distinct patterns of vascular irregularities and perfusion deficits. It distinguishes structures based on their X-ray absorption characteristics, using two different energies with multiple tube potentials, while reducing radiation dose (Sin et al., 2021). DECT generates color-coded perfusion maps by analysing iodine distribution within the pulmonary vasculature. This functional evaluation of blood flow enables the detection of hypoperfused regions caused by CTEPH obstructions. Lung subtraction iodine mapping (LSIM) is another novel method applied to diagnose pulmonary perfusion in patients with CTEPH. This method used a subtraction algorithm by subtracting the non-enhanced tissue from the contrast-enhanced area (pulmonary vasculature). This subtraction can produce high-resolution images of the vascular and lung parenchymal architecture as well as functional information on lung perfusion (Tamura et al., 2017).

DECT showed a sensitivity of 80-90% and a specificity of 90-95% for diagnosing CTEPH. However, its sensitivity for minor perfusion abnormalities may be lower in comparison to the VQ scan. The gold standard for identifying mismatched perfusion abnormalities predictive of CTEPH is the VQ scan, which has a sensitivity of up to 96% and a specificity of 90–95% (Kim et al., 2019). Despite its high sensitivity, the lack of the anatomical resolution requires supplemental imaging for a conclusive diagnosis. Earlier studies reported that the V/Q scan had significantly greater sensitivity compared to CTPA (97% vs. 51%) (Tunariu et al., 2007). Although this gap has decreased due to advances in CT technology, more recent studies show that both approaches have comparably high diagnostic accuracy (He et al., 2012). According to a meta-analysis by Lambert et al. (2022), CTPA has a sensitivity of 80–90% and a specificity

of above 95% for the diagnosis of CTEPH, especially when interpreted by expert radiologists (Lambert et al., 2022).

Photon-counting CT is a state-of-the-art development in imaging technology with superior spatial resolution, contrast-to-noise, and decreased exposure to ionising radiation compared to standard CT scans. PCCT has promise in improving diagnosis in CTEPH patients. It could offer high-resolution imaging of the peripheral small pulmonary arteries, which would help distinguish CTEPH from other pulmonary hypertension types and enhance clinical evaluation and disease characterisation (Kerber et al., 2023). As accessibility increases, PCCT has the potential to become the modality of first choice in the diagnosis and surgical planning of CTEPH. However, additional research is necessary to fully assess its clinical utility and to develop standardised CTEPH protocols for clinical applications (Remy-Jardin et al., 2025, Douek et al., 2023).

1.9 Treatment

According to ESC/ERS guidelines for pulmonary hypertension, the diagnostic evaluation of CTEPH should prioritise verifying the diagnosis and evaluating the patient's eligibility for surgical intervention. **Figure 1.5** shows the ESC/ERS treatment strategy for patients with CTEPH. The preferred therapy method for CTEPH is PEA, which remains the sole intervention demonstrated to improve long-term results. The treatment goal for patients who are ineligible for surgery is to eliminate symptoms, using medication or balloon pulmonary angioplasty (BPA) treatment. Moreover, constant anticoagulation is necessary for all patients diagnosed with CTEPH.

Anticoagulation

Anticoagulation therapy is the mainstay therapeutic approach prescribed in patients with CTEPH and PE. A three-month anticoagulation interval must be performed to distinguish between CTEPH and acute PE. Warfarin is considered to be the standard anticoagulant (Humbert et al., 2022). Heparin is another alternative anticoagulant that is usually administered via injection. However, direct oral anticoagulants (DOACs) have become in

preference due to their simplicity of administration and lack the need for regular monitoring. Despite their increasing usage, evidence supporting DOACs in management of CTEPH is limited. A study by Bunclark et al. 2020, reported no significant differences in functional or hemodynamic results after PEA between patients treated with warfarin and those receiving DOACs. Nevertheless, patients treated with DOACs experienced significantly higher rates of VTE (Bunclark et al., 2020).

Balloon pulmonary angioplasty

BPA was recognised as a useful alternative treatment option for inoperable CTEPH, such as high-risk surgical patients, segmental and subsegmental disease, or residual CTEPH post-PEA (Klok et al., 2018). BPA should exclusively be conducted at specialised PH centres and with extensive experience in catheter-based interventions (Kim et al., 2019). In 2018, BPA was introduced as a nationally commissioned service and became more extensively used in clinical practice across the UK. These PH centres follow a protocol of several sessions between four to six procedures for each patient to optimise results while reducing complications. Studies and clinical experiences have shown that BPA improves haemodynamic outcomes, exercise capacity, and right ventricular function for patients with inoperable and recurrent CTEPH (Fukui et al., 2014, Jaïs et al., 2022, Lang et al., 2023, Delcroix et al., 2023).

Pulmonary endarterectomy

PEA is the gold standard surgical treatment for patients with CTEPH, that involves opening the pulmonary trunk. It is performed bilaterally on the pulmonary arteries through a median sternotomy incorporated with cardiopulmonary bypass. The specific layer for incision within the arterial vessel wall is precisely identified between the lamina intima and the media (Delcroix et al., 2016). Insufficient or too deep incision into the vascular wall may result in pulmonary artery perforation, hence increasing the risk of severe haemorrhage.

Treatment options are determined by the severity and distribution of the thromboembolic disease. Severe left heart failure, distal disease and severe chronic obstructive disease are known to be limitations for PEA. However, some characteristics have been identified as potentially predicting poor postoperative outcomes. These include the lack of a history of

VTE, World Health Organisation functional class IV, right heart failure, no disease detectable in the lower lobes, and PVR more than 15 Wood units (Kim et al., 2019).

Specialised centres are currently undertaking procedures on patients with more comorbidities and distal diseases, while achieving lower mortality outcomes. PEA significantly improves symptomatic and haemodynamic outcomes for patients with CTEPH, especially when merged with medication treatments such as riociguat (Madani et al., 2012, Taniguchi et al., 2014). Cannon et al. (2016) showed excellent long-term survival and maintained functional status with marked reduction of mPAP from around 47 mmHg to 27 mmHg following endarterectomy. In research by Quadery et al. (2018) on 550 patients with CTEPH, involving 550 patients with CTEPH, those with comorbidities or who were refused surgery had much poorer survival rates at 5 years (53%) compared to patients who underwent endarterectomy (83%). Delcroix et al. (2016) analysed data from 679 patients in an international registry between 2007–2009, including 404 who underwent PEA, and found a significantly higher 3-year survival rate (89%) compared to those who did not (70%). Endarterectomy is associated with great results and much better survival rates than non-surgical therapy, regardless of patient preference or inoperable CTEPH (Delcroix et al., 2016, Quadery et al., 2018).

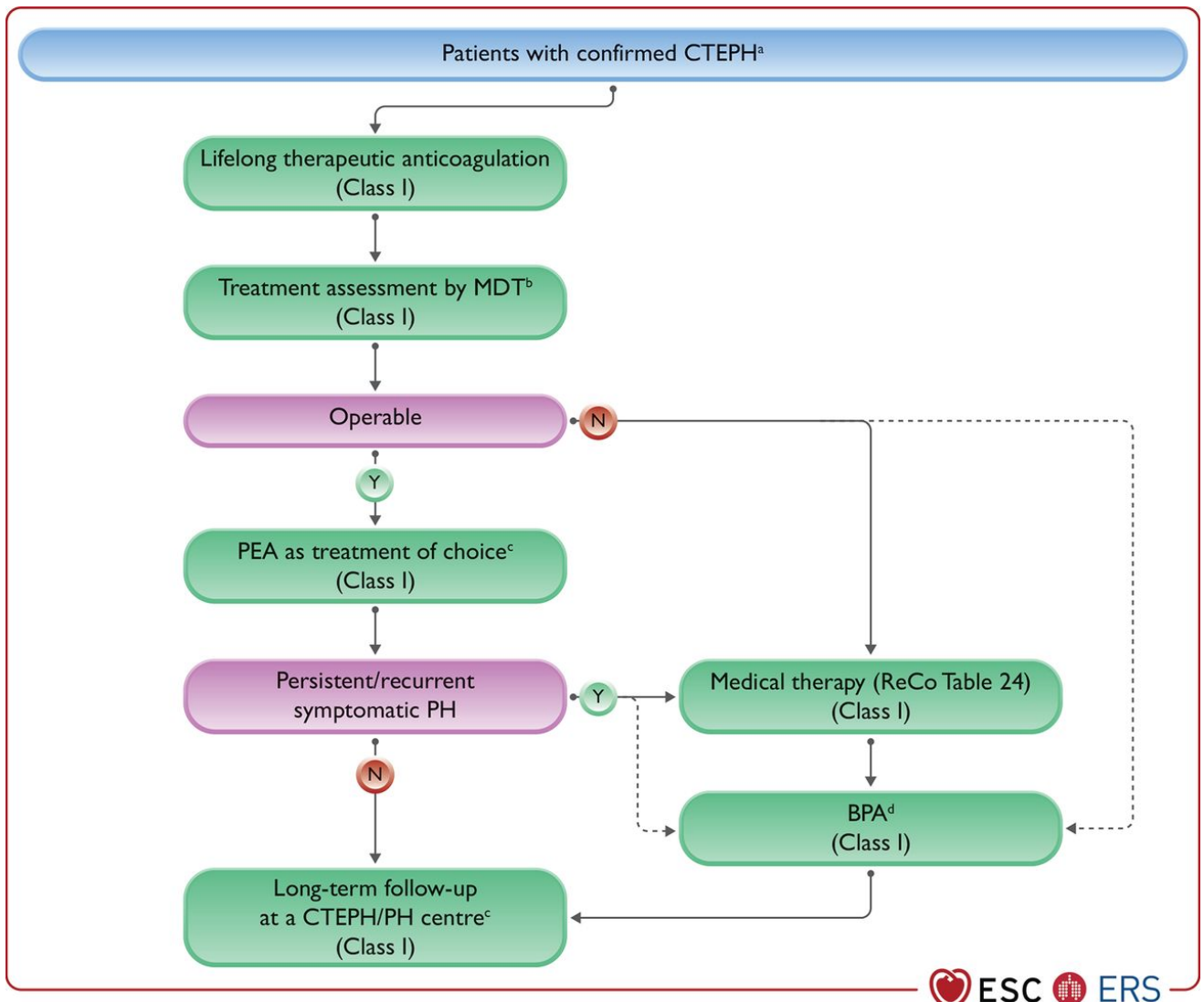


Figure 1.5 CTEPH therapeutic strategies reproduced with permission of the © European Society of Cardiology and European Respiratory Society 2025 (Humbert et al., 2022).

1.10 Semi-quantitative and quantitative CT

Semi-quantitative CT is a method for analysing CT images using qualitative visual assessment and limited numerical data to evaluate the severity or extent of a condition. Quantitative CT (QCT) is a developing research area, focusing on extracting numerical data from CT images to evaluate and quantify different pathogenic and anatomical characteristics. QCT approaches extend beyond standard visual analysis, providing quantifiable parameters to support diagnosis, disease onset, and treatment plans.

Pulmonary thrombus could be evaluated quantitatively by directly measuring the thrombus volume with advanced imaging methods, providing a better estimation of thrombus burden, or semi-quantitative assessment by numerous scores such as clot burden scores measuring the level of pulmonary arterial tree obstruction. A semi-quantitatively scoring technique is used to assess the PE severity. The existence and severity of vascular thrombosis blockage in specific branches of the pulmonary arteries were calculated to create these scores, which mostly represent the distribution of thrombus (Quadery et al., 2018). While pulmonary thrombus volume measurement relies entirely on quantitative methods using efficient image analysis techniques, a semi-automated segmentation technique may be used to measure the PE from pulmonary CTPA images with an excellent level of accuracy (Furlan et al., 2011). Accurately quantifying the size and distribution of thrombus remains challenging, thus current practice generally classifies the thrombus as central, segmental, or distal. There are radiological grading systems available, such as the QUANDILI score, which quantifies the number and severity of abnormal vascular segments on CTPA. These ratings are time-consuming and difficult to duplicate; hence they are rarely employed in clinical practice or in patients with CTEPH (Qanadli et al., 2001, Shayganfar et al., 2020). An automated technique for extracting and quantifying chronic thromboembolic disease would enable such measures to be examined in a clinical context, potentially aiding with diagnosis, risk prediction, and the tendency to develop CTEPH condition.

Vessel analysis

Enlarged proximal arteries, constricted distal vessels, and increased vascular tortuosity are some of the morphologic characteristics that are associated with CTEPH in the pulmonary arteries. As a direct result of this, research has progressed to the point where it is now possible to create a reconstruction in three-dimensional of the pulmonary vasculature in order to demonstrate these morphological alterations in pulmonary arteries. The least spanning tree model is used to begin the process of extracting this quantitative reconstruction from CTPA images. This procedure comprises the manual delineation of blood vessels to precisely label them and their branches, resulting in the creation of a comprehensive arterial-venous segmentation label map. The map considers the intricate tortuosity and complexity of the vascular network, providing an accurate representation of the vascular anatomy. In addition to perfusion scans, these 3D reconstructions may clearly illustrate the pulmonary arteries, frequently exposing a characteristic "moth-eaten" form. This characteristic feature relates to CTEPH, which might demonstrate the irregular, non-uniform arterial blockages and remodelling induced by organised thromboembolic disease. BV5 is the amount of all blood vessels in a selected area (such as a lung or lobe) that have a cross-sectional region of less than 5 mm², while (TBV) refers to the total blood vessel volume. The distal pulmonary vasculature can be quantitatively assessed by utilising the BV5/TBV ratio in combination with BV5 after normalising the anthropometric data for each patient. Both of these measures were found to be reduced—the first due to enlargement of the proximal pulmonary arteries and non-visualisation of distal vessels, and the second due to luminal narrowing in the distal vasculature (Rahaghi et al., 2016).

Computer-aided detection (CAD) on CT

Computer-Aided Detection (CAD) is a software application used in medical imaging that helps radiologists diagnose diseases. The main objective of CAD is to enhance disease identification by minimising the false negative rate resulting from observational oversights. CAD utilises algorithms to identify and highlight characteristics such as nodules, lesions, and thrombosis for additional examination (Chan et al., 2008).

Previous studies investigated automatic diagnosis of PE using CTPA have mostly focused on traditional feature-based methods. Despite demonstrating sensitivities of up to 75%, some of these approaches encounter significant limitations. These comprise the need of manual feature extraction, time-consuming and resource-intensive complicated preprocessing, and the absence of external validation to determine generalisability overfitting (Özkan et al., 2014, Tajbakhsh et al., 2015, Park et al., 2010). Nonetheless, CAD for PE has not been integrated into clinical practice, potentially due to the significant incidence of false positives generated by existing CAD algorithms (Buhmann et al., 2007, Maizlin et al., 2007). In contrast, artificial intelligence (AI) and machine learning may enhance performance measures, leading to increased interest in CAD. These developments demonstrate how important quantitative CT is for increasing the accuracy of diagnoses of patients with CTEPH.

AI approaches and QCT

This method is used for representing disease patterns and numerical information that may help the radiologist follow up the disease in a more robust and less variable fashion. This technique might provide radiologists with disease course information as well as disease diagnosis based on distinct clinical severity categories (Duzgun et al., 2021). Expert radiologists typically rely on visual evaluation to, characterise, and categorise CT imaging findings. However, CT images are interrogated with quantitative techniques to extract measurable information. There are various advantages to applying AI and QCT approaches, such as saving time, decreasing the inherent uncertainty of a visual evaluation, improving productivity, reducing errors, improving disease classification, and predicting treatment response. As a result, AI and QCT techniques can be used to enhance both radiological evaluation and clinical treatment with promising results in terms of minimising errors and enhancing sensitivity. However, it is essential to consider the limitation of AI approach in medical imaging. Breathing and motion artefacts in CT images can cause errors, and while AI can disregard data variables, it still needs human oversight (Dwivedi et al., 2021)

The incapability to see and evaluate the distal pulmonary artery vasculature, which is the site of abnormality in pulmonary hypertension and CTEPH, is a constraint shared by all currently available imaging techniques. Patients with pulmonary hypertension have large pulmonary

arteries that are dilated, thinned out, and suddenly narrow or twist (Kiely et al., 2019). The morphology of pulmonary vessels represents a method applicable for quantitative AI analysis. The vascular tree was recently segmented with 94% accuracy using a DL CNN technique (Nardelli et al., 2018). The results of clinical applications of these methods may have diagnostic and prognostic implications (Rahaghi et al., 2021).

1.11 Artificial intelligence (AI)

AI is widely used in a variety of diverse industries and healthcare services. AI uses computer system capacity to build models to accomplish tasks typically involving human intelligence. The tasks involve a wide variety of capabilities, which include problem-solving, learning, analysing, natural language understanding, pattern identification, and making decisions (Khemasuwan et al., 2020). AI systems derive the tasks through applying and merging massive data sets with sophisticated algorithms and statistical procedures. This approach facilitates ongoing improvements in patient care and diagnosis by providing assistance to radiologists in managing their increasing workloads. Research and applications on AI have developed rapidly in popularity in all aspects of healthcare, from diagnosis to therapy (Vandewinckele et al., 2020, Van Hartskamp et al., 2019).

Liu et al. 2019, compared the diagnostic accuracy of radiologist experts to that of deep-learning algorithms in a systematic review of 69 studies. The results show that deep-learning algorithms exhibited greater or equal accuracy to radiologist experts' interpretation. However, there were some limitations in this systematic review. For example, all the investigations included were retrospective and reliant on previously compiled datasets. In addition, the reporting on dealing with misplaced data in these datasets was inadequate as most studies did not specify if any data was missing and how these data were managed (Liu et al., 2019).

1.12 Machine learning (ML)

ML uses historical data (datasets, functions, and algorithms) to find a new output value. Using data analysis, expertise knowledge, training, and validation error modelling of prospective neural networks, on the other hand, are time-consuming. Consequently, it is essential to meticulously evaluate each function's capacity to align with the data and produce usable output. There are three types of machine learning including reinforcement learning, supervised learning, and unsupervised learning (Khemasuwan et al., 2020).

1.13 Deep learning (DL)

DL is a sort of ML that extracts characteristics over numerous layers that can accept input and compute an output using weights and biases. Many of these layers are included in the neural networks, giving them the capacity to learn how to generate predictions from data. DL technology improved in the 2000s and several DL algorithms became popular to demonstrate substantial ability in image processing, particularly for segmentation of medical images (Hesamian et al., 2019). DL uses deep neural network designs to analyse massive volumes of data and extract the essential features automatically in order to complete classification tasks (Du et al., 2020). One example of the most used type of DL algorithm is the convolutional neural networks (CNN), which is primarily composed of several layers, each designed to perform a particular function. Each layer uses the output of the preceding layer as its input (Yang and Yu, 2021).

The CNN algorithm is widely used for tasks such as semantic segmentation, image classification and analysis, as well as object recognition. CNNs are effective at image segmentation because they detect local patterns using shared filters. This helps them build up features from edges to shapes across multiple layers, similar to how the visual system works. CNNs are useful for recognising and analysing detailed patterns within medical images, as well as understanding the spatial relationships between these patterns and the annotated delineations provided in training data. CNNs use filters that move through the image to decompose the images down into smaller pixels, this process is identified as convolution. These filters learn to extract and recognise features automatically, for example outlines, and

object shapes. In the first layers, they begin with basic details, and in the following layers, processing more detailed features. The way the human visual system interprets images is illustrated by this hierarchical training. In image segmentation, this feature enables CNNs to accurately distinguish between various tissues or structures in an image by recognising context and spatial connections. CNNs learn directly from data, enabling more accuracy, and generalisability than traditional methods that rely on manually defined rules or features (Hesamian et al., 2019).

In contrast to the old manual learning techniques, automatic segmentation based on DL methods has been suggested, where a neural network can automatically learn image features. CNN operates according to a hierarchical data model that produces a funnel-like structure to create a completely connected layer in which all the neurons are linked, and outcome is managed. Each layer uses a differentiable function to convert one volume of activations to another (Abderrahmane et al., 2020). Convolutional, pooling, and fully connected layers are the three types of layers that make up CNN architectures (**Figure 1.6**). The most common structure of CNN comprises the first layer, which is associated with a medical image as input. The subsequent layer is the convolution layer that utilises a filter (called kernels) to combine two sets of data and generate a feature map as an output from the input images. Then, a pooling layer is used to minimise the number of parameters and computations from the convolution layer's output. As a final classification, the fully connected output layer is extracted to produce the final probabilities for each label (Khemasuwan et al., 2020).

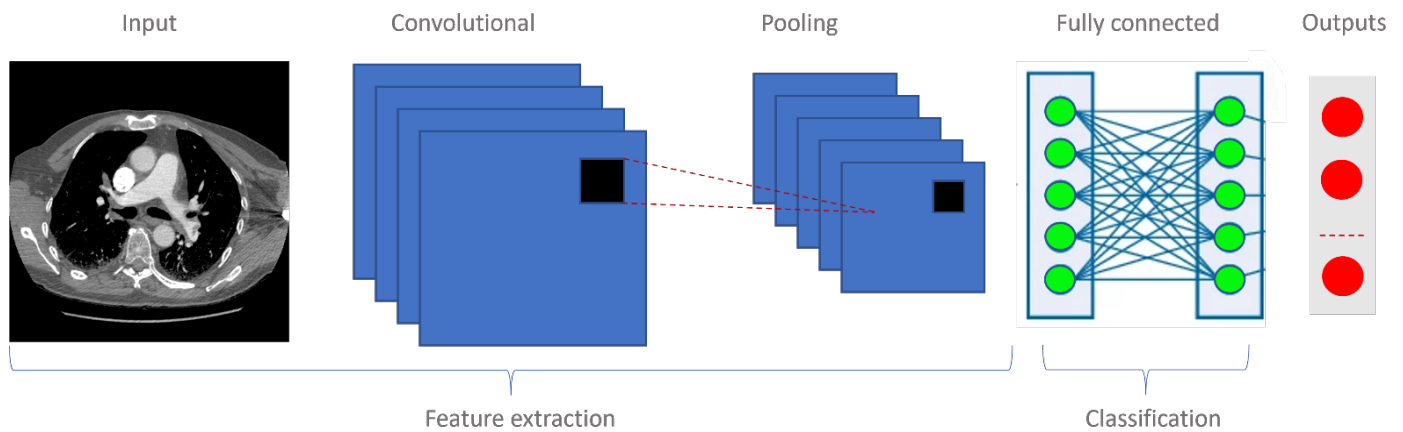


Figure 1.6 Illustration of the layers of CNN architectures.

Encoder-decoder CNNs built for image segmentation may classify each voxel in a diagnostic image as a target structure, or background tissue. This produces a segmentation mask that emphasises each area of interest at the original resolution of the input scan. These convolutional networks include two key components: an encoding path, which extracts hierarchical features like a standard CNN, and a decoding path, which replaces dense layers with transposed convolution processes. This learnt up sampling technique enables the network to restore spatial detail and provide exact segmentations that match the diagnostic image (Cardenas et al., 2019).

While previous AI approaches frequently resulted in suboptimal performance. Recent advancements in DL algorithms have demonstrated the ability to achieve performance levels comparable to human capabilities in task-specific applications. For instance, measurement of heart wall thickness in hypertrophic cardiomyopathy on magnetic resonance imaging (MRI), prediction of lung cancer risk on CT scan and diagnosis of breast cancer in mammography (Yang and Yu, 2021, Ardila et al., 2019). In addition, a recent study introduced a fully automated model for segmenting the great vessels and cardiac chambers using CTPA images, demonstrating high performance and minimal failure rates when validated on separate internal and external datasets (Sharkey et al., 2022).

In another study by Li et al. 2020, they developed a deep learning algorithm to identify coronavirus (COVID-19) using CT scan and assess the algorithm accuracy. The study included 4352 CT scans from 3322 patients at 6 different health centres. CT scans for COVID-19, community-acquired pneumonia, and other conditions not related to pneumonia, were integrated into 4352 scans of the dataset. The results showed that a deep learning algorithm could accurately identify COVID-19 and differentiate it from the many other lung disorders by the sensitivity of 90 percent and specificity of 96 percent (Li et al., 2020)

Nevertheless, Long et al. created fully convolutional networks (FCNs), which is required to address the low-resolution information caused by the final layers in CNN (fully connected layers) (Long et al., 2015). FCNs feature both encoding and decoding routes. The encoding route is similar to the standard CNNs process representing the input data by creating a high-dimensional feature. For developing accurate segmentation, the decoding process replaces the fully connected layers of CNNs with a learnt up-sampling through pixel-wise loss (Cardenas et al., 2019).

The first time a CNN method was used to identify PE was by Tajbakhsh et al. (2015); they achieved an 83 percent sensitivity for identifying individual emboli using 121 CTPA scans and 326 emboli, with two false positives results for every scan. They have demonstrated that a CNN-based approach is better than traditional ML methods (Tajbakhsh et al., 2015, Tajbakhsh et al., 2019). Another study by Liu et al. (2020) evaluated the DL algorithm to measure and identify the clot on acute PE using CTPA. This study was a retrospective study with 878 patients (232 patients without PE and 646 patients with PE). They found that the sensitivity was 94.6 percent, and specificity was 76.5 percent of the CNN algorithm to detect acute PE. They also showed that automated segmentation clot measurement was closely linked with conventional burden parameters on CTPA (Mastora and Qanadli scores) (Liu et al., 2020). On the other hand, Weikert et al. (2020) used a large training dataset of 28,000 CTPA scans to assess the functioning of the AI algorithm's ability to detect PE. The sensitivity and specificity of AI to detect PE were 92.7 percent and 95.5 percent, respectively. This study also conducted a sub-analysis of PE, which found that scans with proximal emboli had the most effective detection rates of 95.7 percent, followed by exams with segmental emboli 93.3 percent. The detection rate for subsegmental emboli was the lowest at 85.7 percent. As a consequence of

this finding, the diagnosis of PE on CTPAs, the AI algorithm was examined and had a high rate of diagnostic accuracy, which can be necessary for clinical usage. However, DL auto-segmentation has some limitations. For example, the segmentation of large structures is more accurate than segmenting small structures, such as small vessels (Weikert et al., 2020).

1.14 Unsupervised vs supervised

There are two primary kinds of machine learning methods: supervised AI and unsupervised AI. In supervised learning, the system learns from the training dataset by forecasting the data repeatedly and modifying it for the correct answer. For example, “origin PA” or “distal PA” labels for lung pulmonary artery patterns. Evaluation of the performance is based on how well these labels are predicted in a study group. Whereas supervised AI algorithms are more precise than unsupervised learning models, they require human input to recognise the information correctly. On the other hand, unsupervised learning works independently to find the structure of data that hasn't been labelled. A method that groups pixels into regions based on features, such as texture, edge information, and intensity. Common methods include clustering algorithms such as k-means and Gaussian mixture models (GMM), as well as deep learning approaches like autoencoders. These approaches attempt to divide an image into meaningful regions by learning patterns directly from the images (Liu et al., 2024). K-means and GMM cluster voxels by shared properties such as Hounsfield units, while autoencoders extract low-dimensional features for clustering in latent space, aiding anatomical structure delineation (Rajasekar et al., 2025). These methods avoid manual annotation, reducing time and subjectivity, but often require refinement to address noise or incomplete margins. In CTEPH, unsupervised methods may struggle when tissue intensities overlap. This makes it harder to group regions without some form of guidance or refinement (Ren et al., 2017, Wei, R. and Mahmood, 2020). A small quantity labelled data is merged with a larger unlabelled data to form the semi-supervised learning technique. This technique gives the advantages of both supervised and unsupervised learning while avoiding the difficulties associated with locating a large amount of labelled dataset (Barragán-Montero et al., 2021). The overwhelming majority of AI investigations in medical imaging implement supervised learning and rely on correct labelling.

1.15 Explainable AI (XAI)

The goal of the XAI system is to provide explanations to make its behaviour more understandable to humans. There are specific broad ideas that may be used to assist design AI systems that are more successful and intelligible to humans: The XAI system must be able to describe its abilities and understandings, as well as what it has performed, what it is about to accomplish, and what will occur afterwards. It should also be able to reveal the critical information on which it is functioning (Arrieta et al., 2020, Gunning et al., 2019).

There are several techniques that can be used to improve interpretation of the segmentation of the model. For example, Gradient-Weighted Class Activation Map (Grad-CAM), saliency map, and Shapley additive explanations (SHAP) ((Mundhenk et al., 2019, Bhattarai et al., 2024). The Grad-CAM approach is frequently used because of its ability to produce informative heatmaps that improve the explainability of the model (Hasannezhad and Sharifian, 2025). SHAP is a technique used to explain the model output by calculating the SHAP values and estimate the contributions of each feature to the overall prediction (Saranya and Subhashini, 2023). Although these algorithms provide valuable visual and feature-level explanations, their clinical application is limited because they lack the fine-grained, pixel-level precision that is required to identify detailed subtle abnormalities (Ennab and Mcheick, 2025b). The Pixel-Level Interpretability model, an integrated convolutional fuzzy system used to produce detailed, pixel-level visualisations, therefore improving diagnostic precision and explainability. It provides clinically significant findings and outperforms Grad-CAM in terms of interpretability, accuracy, and efficiency (Ennab and Mcheick, 2025a, Singh et al., 2025, Nasir et al., 2025).

1.16 Conclusion

This literature review described CTEPH pathophysiology, affecting factors, guidelines and classifications, imaging modality for CTEPH diagnosis and treatment techniques. Among other medical imaging techniques, the review focused on defining the CTPA scan, which is clinically acknowledged as the recommended imaging technique in CTEPH diagnosis since it is non-invasive, rapid, and has high sensitivity. CTPA technology, examination, radiographic features, CAD system and acute/chronic PE characteristics are discussed. AI is also highlighted in this review, and the impact of the AI on improving the PE diagnoses by allowing radiologists to reduce misdiagnosis. The studies suggest that DL algorithms may have greater or similar accuracy than radiologist professionals' interpretation for acute PE detection. This review highlights the lack of studies that use machine learning to detect CTEPH on CTPA, at the same time demonstrates that AI technology has great potential to predict the presence of CTEPH, assess the severity and provide an inference of the location of disease in the image.

2 Aims, Objectives, and Hypothesis

2.1 Hypothesis

The hypothesis for this thesis is that lung parenchymal and radiographic features in CTPA images are related to invasive diagnostic measurements in CTEPH. Additionally, the thesis hypothesises that automated AI tools for CTPA can enhance the detection and diagnosis of CTEPH. Most existing AI tools are developed for diagnosing acute PE, with minimal research has focused on chronic PE and CTEPH, which have significant diagnostic challenges. Additionally, AI methods developed for acute PE detection may be underutilised or inadequately modified to assess patients with CTEPH.

2.2 Aims

The first aim of this thesis is to evaluate lung parenchymal changes on CTPA and evaluate the association of mosaic perfusion and lung infarction with known prognostic indicators in patients with CTEPH. Secondly, to quantitatively analyse the extent and severity of CTEPH and assess the prognostic implications for patients undergoing PEA compared to those not undergoing PEA. The final aim of the thesis is to develop a clinically applicable method for automatically segmenting pulmonary vessels and thromboembolic disease. This approach will use deep segmentation models with CTPA images to predict patients with CTEPH, assessing both its presence and severity.

2.3 Objectives

1. Conduct a systematic review and meta-analysis on AI models to detect CTEPH and chronic PE using CT (Chapter 3).
2. Collect and establish comprehensive CTPA images diagnosed with CTEPH from the ASPIRE registry database (Chapter 4).
3. Analyse the extent and impact of cardiac and lung parenchymal abnormalities on survival outcomes in patients with CTEPH (Chapter 5).
4. Investigate a CTPA based scoring system for CTEPH, incorporating location and extent of thrombus and its relationship to radiological features and disease severity (Chapter 6).
5. Develop a fully automated deep learning model for segmentation of the pulmonary arteries (PA), pulmonary veins (PV), and thromboembolic disease on CTPA (Chapter 7).
6. Evaluate the performance of artificial intelligence in detecting and quantifying thromboembolic disease compared to manual analysis and identify its prognostic significance in patients with CTEPH (Chapter 7).

3 A systematic review of artificial intelligence tools for chronic pulmonary embolism on CTPA

***Peer-reviewed journal article published in Frontiers in Radiology (2024)**

Contribution: I led this systematic review as the primary author. My contributions included idea development, research, methodology, project management, resource communication, writing, review and editing. As part of my thesis confirmation evaluation, I completed an independent literature search, data analysis, and writing. My supervisors, DK and AS, offered invaluable help and monitoring throughout the process. The remaining authors provided modest but valued roles in the completion of this work by providing resources, project management, and assistance.

Lojain Abdulaal^{1,2*}, Ahmed Maiter^{1,3,4}, Mahan Salehi¹, Michael Sharkey¹, Turki Alnasser¹, Pankaj Garg⁵, Smitha Rajaram^{1,3,4}, Catherine Hill^{3,4}, Christopher Johns^{1,3,4}, Alex Matthew Knox Rothman¹, Krit Dwivedi^{1,3}, David G. Kiely^{1,6,7}, Samer Alabed^{1,4,6} and Andrew James Swift^{1,4,6,7}

1. Department of Infection, Immunity and Cardiovascular Disease, The University of Sheffield, UK.
2. Faculty of Applied Medical Science, King Abdulaziz University, Jeddah, Saudi Arabia.
3. Respiratory Physiology Department, Sheffield Pulmonary Vascular Disease Unit, Sheffield, UK.
4. Department of Clinical Radiology, Sheffield Teaching Hospitals NHS Foundation. Trust, Sheffield, UK.
5. Faculty of Medicine and Health Sciences, Norwich Medical School, University of East Anglia, Norwich.
6. Faculty of Engineering, INSIGNEO Institute, Institute for in Silico Medicine, The University of Sheffield, Sheffield, UK.
7. Sheffield Biomedical Research Centre, National Institute for Health Research, Sheffield, UK.

3.1 Abstract

Background: Chronic pulmonary embolism (PE) may result in pulmonary hypertension (CTEPH). Automated CT pulmonary angiography (CTPA) interpretation using artificial intelligence (AI) tools has the potential for improving diagnostic accuracy, reducing delays to diagnosis and yielding novel information of clinical value in CTEPH. This systematic review aimed to identify and appraise existing studies presenting AI tools for CTPA in the context of chronic PE and CTEPH.

Methods: MEDLINE and EMBASE databases were searched on 11 September 2023. Journal publications presenting AI tools for CTPA in patients with chronic PE or CTEPH were eligible for inclusion. Information about model design, training and testing was extracted. Study quality was assessed using compliance with the Checklist for Artificial Intelligence in Medical Imaging (CLAIM).

Results: Five studies were eligible for inclusion, all of which presented deep learning AI models to evaluate PE. First study evaluated the lung parenchymal changes in chronic PE and two studies used an AI model to classify PE, with none directly assessing the pulmonary arteries. In addition, a separate study developed a CNN tool to distinguish chronic PE using 2D maximum intensity projection reconstructions. While another study assessed a novel automated approach to quantify hypoperfusion to help in the severity assessment of CTEPH. While descriptions of model design and training were reliable, descriptions of the datasets used in training and testing were more inconsistent.

Conclusion: In contrast to AI tools for evaluation of acute PE, there has been limited investigation of AI-based approaches to characterising chronic PE and CTEPH on CTPA. Existing studies are limited by inconsistent reporting of the data used to train and test their models. This systematic review highlights an area of potential expansion for the field of AI in medical image interpretation.

There is limited knowledge of A systematic review of artificial intelligence tools for chronic pulmonary embolism in CT. This systematic review provides an assessment on research that examined deep learning algorithms in detecting CTEPH on CTPA images, the number of studies assessing the utility of deep learning on CTPA in CTEPH was unclear and should be highlighted.

3.2 Introduction

Pulmonary hypertension is defined by elevated mean pulmonary artery pressure (mPAP) and results in right ventricular failure, with significant associated morbidity and mortality. Chronic thromboembolic pulmonary hypertension (CTEPH) is a subgroup of pulmonary hypertension in which the rise in mPAP is driven by repeated and/or large volume pulmonary embolism (PE) (Simonneau and Hoeper, 2019). Surgical pulmonary endarterectomy remains the gold standard treatment for CTEPH and is potentially curative. In patients for whom endarterectomy is unsuitable, alternative treatment options include endovascular pulmonary angioplasty and medical management with anticoagulation and pulmonary vasodilators. Early initiation of treatment is important for preventing disease progression and improving patient outcomes in CTEPH, but requires prompt diagnosis (Quadery et al., 2018, Delcroix et al., 2021)

Diagnostic delays are common for CTEPH, with an average of 14 months to diagnosis from the onset of symptoms (Pepke-Zaba et al., 2011). This can be attributable to the variability of clinical presentations and overlap of symptoms such as dyspnoea with a range of other potential causes (Kim et al., 2019). Right heart catheterisation remains the gold standard for diagnosis of pulmonary hypertension and CTEPH, but is invasive and not readily accessible in most centres. CT pulmonary angiography (CTPA) is well established as a non-invasive tool for the assessment of CTEPH. The modality is widely available, frequently performed for patients with cardiorespiratory symptoms and can provide information that assists with risk stratification, treatment decisions and prognostication (Konstantinides et al., 2020). CTPA not only enables localisation and quantification of thromboembolic disease but can also yield biomarkers of disease severity (such as changes in pulmonary artery calibre and right ventricular morphology) and identify associated parenchymal lung changes (Swift et al., 2020, Kiely et al., 2019).

Automation of image identification tasks through AI offers potential improvements in diagnostic accuracy and efficiency. Various machine-learning methods have been applied to aid the detection and characterisation of acute pulmonary embolism on CTPA, with some tools licensed and in use as clinical decision aids (Long et al., 2021, Tajbakhsh et al., 2015,

Huang et al., 2020, RAPIDAI, 2022). These include deep learning (DL) algorithms utilising neural networks - these comprise layers of interconnected artificial neurons, enabling algorithms to learn patterns and relationships from data and generate models that can be used to make decisions, such as image interpretation. Convolutional neural networks (CNNs) are frequently used in DL and are capable of performing imaging classification, segmentation, and detection of objects (Yamashita et al., 2018). Existing AI-based strategies for the evaluation of PE on CTPA have included image analysis to aid classification of disease and vessel segmentation. These techniques are still being developed and their incorporation into clinical practice will need more study, refining, and validation studies to assure their efficacy and accuracy (**Figure 3.1**). While there has been considerable interest in AI for the evaluation of acute PE, it is unclear to what extent AI has been used to evaluate CTEPH on CTPA. This systematic review aimed to identify and appraise the quality of studies presenting AI tools for the evaluation of chronic PE or CTEPH on CTPA.

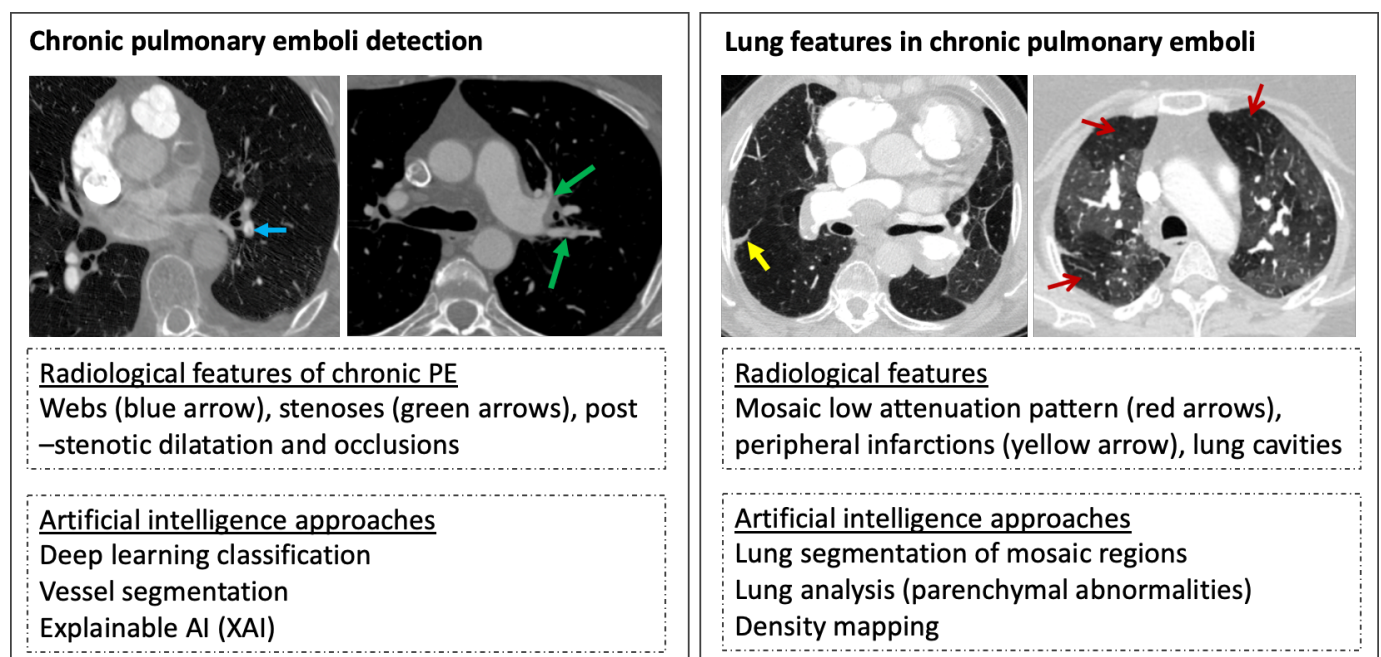


Figure 3.1 Example of radiological features and artificial intelligence approaches in chronic thromboembolic disease detection (Images are from Sheffield institution on illustrating the diagnostic features of chronic pulmonary hypertension).

3.3 Methods

The study was conducted in compliance with the Preferred Reporting Items for Systematic Reviews and Meta-Analyses (PRISMA) criteria (Page et al., 2021). The study flow is presented in **Figure 3.2**.

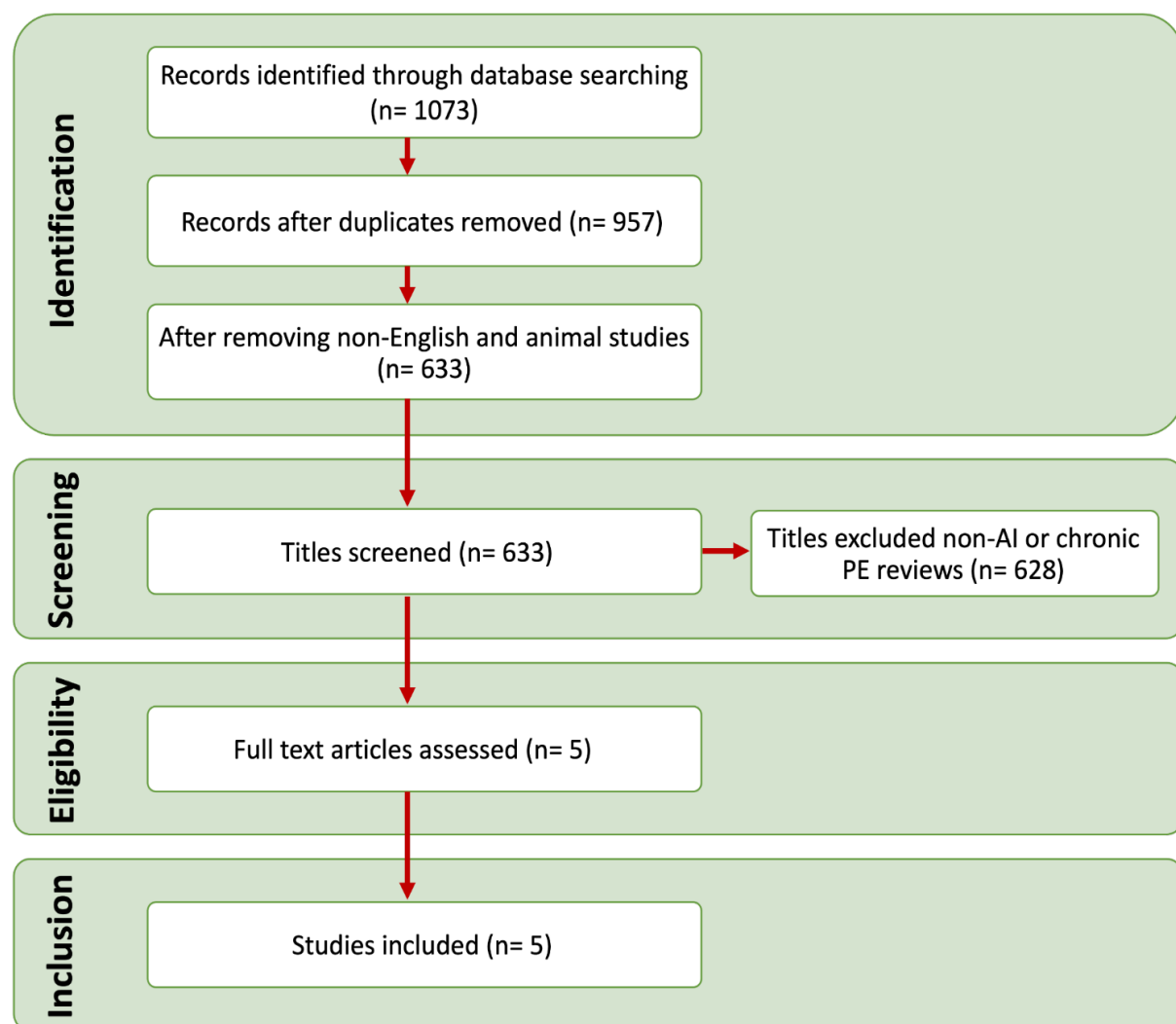


Figure 3.2 Process flow diagram for the inclusion and search steps.

Eligibility criteria

Studies published in peer-reviewed journals from 2012 onwards were eligible for inclusion if they 1) presented or assessed any type of AI tool 2) for CTPA images 3) from participants with either confirmed chronic PE or CTEPH. Exclusion criteria included non-English-language publications, non-original research (such as reviews or letters) and animal or phantom studies.

Search strategy

MEDLINE and EMBASE databases were searched on 11 September 2023.

Database search strategy

Ovid (MEDLINE and EMBASE) Search Strategy:

1. (Convolutional OR neural) ADJ1 network
2. (Deep or supervised or unsupervised or machine) AND learning
3. AI OR (Artificial ADJ1 intelligence) OR Algorithm
4. Machine Learning MESH
5. 1 OR 2 OR 3 OR 4
6. (Pulmonary emboli) OR PE OR CTEPH or CTEPD
7. Lung Embolism MESH
8. 6 OR 7
9. (CT pulmonary angiography) or CTPA
10. Computer Tomography MESH
11. 9 OR 10
12. 5 AND 8 AND 11

Study selection and data extraction

Search results were screened for eligibility by two authors (LA and AS) independently by reviewing titles and abstracts using Rayyan Systematic Review Screening Software (Ouzzani et al., 2016). Data were extracted from included studies using a standardised spreadsheet by two authors (LA and TA). Extracted data included study information (such as location, year and journal type), study design, data selection (such as number of participants, number of CTEPH cases and inclusion criteria), and the AI model being presented (such as validation and performance results). The quality of each included study was appraised by checking compliance with the individual criteria of the Checklist for Artificial Intelligence in Medical Imaging (CLAIM) (Mongan et al., 2020), which were divided into four domains (Maiter et al., 2023, Alabed et al., 2022).

3.4 Results

Five studies were eligible for inclusion (**Figure 3.2**) and are summarised in **Table 3.1** (Vainio et al., 2021, Ma et al., 2022, Khan et al., 2023, Vainio et al., 2023, Bird et al., 2023). Agreement of the studies with the criteria of CLAIM are presented in **Table 3.2**.

Table 3.1 An overview of the literature review papers that used CTPA to identify chronic pulmonary emboli using deep learning algorithms.

Study	No. Patients	Chronic PE	PE type	Setting for CTPA scan	Public (source)	AI type	Network	Outcomes
(Vainio et al., 2021)	50	25	Chronic	Multicentre	No	Segmentation	U-net-type, CNN	AUC 0.87
(Khan et al., 2023)	9446	NA	Acute and chronic	Public	RSNA (Kaggle)	Classification	DenseNet201	AUC 0.90
(Ma et al., 2022)	7279	NA	Acute and chronic	Public	RSNA (Kaggle)	Classification	3D CNN and 3D ResNet-18 model	Full cohort AUC 0.93/ Chronic PE AUC 0.68
(Vainio et al., 2023)	Public 976 Local 78	Public 244 Local 26	Chronic	Local and public	RSPECT	Classification	CNN and DenseNet201	AUC 0.94 on local
(Bird et al., 2023)	161	51	CTEPH	Local	No	Segmentation	CNN	AUC 0.84

(NA= not applicable).

Table 3.2 Compliance with CLAIM checklist. Studies and the division of criteria into study description, dataset description, model description and model performance domains are shown below in (Blue/✓ =Yes) to indicate compliance, (Red/ x =No) for non-compliance and (Gray/ – =Not applicable).

	CLAIM checklist	(Vainio et al. 2021)	(Khan et al. 2023)	(Ma et al. 2022)	(Vainio et al. 2023)	(Bird et al. 2023)
Study description	Identification as a study of AI	✓	✓	✓	✓	✓
	Structured summary of study design, methods, results, and conclusions	✓	✓	✓	✓	✓
	Scientific and clinical background	✓	✓	✓	✓	✓
	Study objectives and hypotheses	✓	✓	✓	✓	✓
	Prospective or retrospective study	✓	✓	✓	✓	✓
	Study goal	✓	✓	✓	✓	✓
	Where the full study protocol can be accessed	x	✓	✓	✓	x
Dataset description	Data sources	✓	✓	✓	✓	x
	Eligibility criteria, symptoms, results from previous tests, inclusion in registry	✓	x	x	✓	✓
	Data pre-processing steps	✓	✓	✓	✓	x
	Selection of data subsets	✓	✓	✓	✓	✓
	Definitions of data elements	✓	x	x	✓	✓
	De-identification methods	✓	✓	✓	✓	x
	How missing data were handled	x	x	x	x	x
	Flow of participants	✓	✓	✓	✓	✓
	Sample size calculation	✓	✓	x	✓	x
	How data were assigned to partitions	✓	✓	✓	✓	✓
	Level at which partitions are disjoint	✓	✓	✓	✓	✓
	Demographic and clinical characteristics	✓	x	x	✓	✓
Ground truth reference standard	Definition of ground truth reference standard	✓	x	x	x	x
	Rationale for choosing the reference standard	x	x	x	x	x
	Source of ground truth annotations	✓	x	x	✓	x
	Annotation tools	✓	✓	✓	✓	x

	inter- and intrarater variability	✓	x	x	✓	x
Model description	Detailed description of model	✓	✓	✓	✓	x
	Software libraries, frameworks, and packages	✓	✓	✓	✓	x
	Initialisation of model parameters	✓	✓	✓	✓	x
	Details of training approach	✓	✓	✓	✓	x
	Method of selecting the final model	✓	✓	✓	✓	x
	Ensembling techniques, if applicable	x	✓	✓	✓	x
Model performance	Metrics of model performance	✓	✓	✓	✓	✓
	Statistical measures of significance and uncertainty	✓	✓	✓	x	✓
	Robustness or sensitivity analysis	✓	✓	✓	✓	✓
	Methods for explainability or interpretability	x	✓	✓	✓	✓
	Validation or testing on external data	x	x	x	✓	x
	Performance metrics for optimal model on all data partitions	✓	✓	✓	✓	x
	Estimates of diagnostic accuracy	✓	✓	✓	✓	✓
	Failure analysis of incorrectly classified cases	✓	✓	✓	✓	x
Other information	Study limitations	✓	x	✓	✓	✓
	Implications for practice	✓	✓	✓	x	x
	Registration number and name of registry	—	—	—	—	—
	Sources of funding	✓	✓	✓	✓	✓
	Overall % Compliance with CLAIM	85%	76%	76%	88%	50%

Study 1 - Vainio et al. (2021)

Vainio et al. (2021) investigated the application of a 3D convolutional neural network (CNN) to identify hypoperfusion areas affected only by CTEPH from CTPA images. The overall compliance of the study with CLAIM was 85%. Compliance with the model description domain of CLAIM was 83%. The model comprised a U-net CNN (Ronneberger et al., 2015) of twelve layers and three max-pooling/upsampling phases with skip connections and one output neuron with sigmoid activation in their 3D CNN layers. The Hounsfield Unit (HU) range was linearly shifted and scaled in order to resample and normalise the CTPA volumes. The patches totally outside the lung area were eliminated after the training data were partitioned into $32 \times 32 \times 32$ voxel patches. Both learning rate adjustment and Dice loss optimisation were employed on manually labelled data to fine-tune the model and improve its accuracy during the validation process. The compliance with the dataset description criteria of CLAIM was 90%.

The study used a dataset of 50 patients of which 25 (50%) had CTEPH. A positive ventilation-perfusion (V/Q) scan for chronic PE and a CTPA with evidence of chronic PE within 3 months without signs of acute PE were the inclusion criteria for the positive patients and confirmed with a right heart catheterisation. In all cases, radiological appearances of a parenchymal disease unrelated to CTEPH that involved more than two-thirds of the lungs were eliminated. The median age of all participants was 67 years and 62% were female. These were distributed into training, validation, and testing sets containing 48%, 12% and 40% of the data respectively. The study also showed complete compliance with the ground truth description criteria of CLAIM. Manual segmentation of affected regions on CTPA by one radiologist using ventilation-perfusion scan images was used as the ground truth. The compliance with the performance description criteria of CLAIM was 62%. The 3D CNN model performed segmentation of hypoperfused lungs with a reported area under the receiver curve (AUC) of 0.87. Failure analysis identified 63 independent false positive labels frequently attributed to beam hardening artefact.

Study 2 - Khan et al. (2023)

Khan et al. (2023) presented a CNN model based on DenseNet201 (Huang et al., 2017) to classify a mixed cohort including acute and chronic PE on CTPA. The overall compliance of the study with CLAIM was 76%, including complete compliance with the model description criteria. The proposed model architecture for PE detection comprised an input module, a feature extractor module and a decision-making module. The feature extractor model, based on DenseNet201 (Huang et al., 2017), used densely connected convolutional blocks to extract rich hierarchical features from CT images, each comprising multiple convolutional layers, batch normalisation, and rectified linear activation functions (ReLU). The decision-making module took the extracted features and performed the final classification or decision-making process. This module consisted of intermediate dense and classification layers to produce the final prediction or decision regarding the presence or absence of PE. The compliance with the dataset description criteria of CLAIM was 66%. The study included 9446 CTPA scans that were gathered from the RSNA-Kaggle public database (Stein et al., 2020) (available at <https://www.kaggle.com/c/rsna-str-pulmonary-embolism-detection>). This dataset is classified into nine groups including undetermined PE, negative PE, right-side PE, Left-side PE, central PE, acute PE, chronic PE, and RV/LV ratio greater or less than 1. The dataset was annotated collaboratively by members of the RSNA and the Society of Thoracic Radiology and is a compilation of three previous datasets provided by the RSNA, with contributions from institutes in five countries (Canada, Brazil, Australia, Turkey and the USA). The 9446 exams that make up the dataset made accessible on Kaggle have been divided in this study into two sets: a training set of 7279 exams and a test set of 2167 exams. While the dataset included acute and chronic PE cases, the proportion of patients in each group was not reported and there were no confirmed CTEPH cases. Compliance with the performance description criteria of CLAIM was 87%. The model achieved an overall accuracy of 88%, sensitivity of 88%, specificity of 89%, and AUC of 0.90 for all participants in the dataset. Although chronic PE subgroup was reported to have a 95% accuracy rate, with an AUC value of 0.95. The mean ROC curve - which averages the various ROC curves for each subgroup - had an AUC of 0.90.

Study 3 - Ma et al. (2022)

Ma et al. (2022) also presented a model to identify PE on CTPA including acute and chronic PE in their dataset. The overall compliance of the study with CLAIM was 76% and the study also showed complete compliance with the model description criteria. The proposed approach entails a two-step pipeline: a 3D CNN model extracts a relevant feature sequence based on the surrounding area of slices, and a sequenced framework is used to produce study-level label predictions. The compliance with the dataset and ground truth description criteria were 58% and 20% respectively. The dataset used in this study was collected from the Kaggle competition RSNA STR Pulmonary Embolism Detection, which included 7279 studies in total (Stein et al., 2020) (available at <https://www.kaggle.com/competitions/rsna-str-pulmonary-embolism-detection/data>). The dataset includes labels at both the study and slice levels, with each slice including a label indicating if it contains any type of PE. However, the ground truth annotations used in their investigation were not defined. Compliance with the performance description criteria of CLAIM was 87%. The model performance in terms of PE identification had a reported sensitivity of 86% and specificity of 85%. For chronic PE cases, reported accuracy was 68%, sensitivity was 62% and specificity was 63%; however, the number of chronic PE cases was not reported in the paper, but it is available in the original public source.

Study 4 - Vainio et al. (2023)

Vainio et al. (2023) developed a CNN tool with the aim of identifying and differentiating chronic PE from 2D maximum intensity projection (MIP) reconstructions of CTPA. The overall compliance with CLAIM was 88%, with complete compliance with the model description criteria. Deep learning-based lung segmentation was used to prepare the CTPA images for MIP reconstructions by removing high-intensity features. A base model trained on ImageNet was used as the foundation for their architecture (Deng et al., 2009). 11 MIP images were used as input data, with each image representing a different view of the same scan. Images were processed individually before being averaged and passed through a three-layer multilayer perceptron (MLP) using ReLU activations. During training, alpha dropout and batch normalisation techniques were applied to the MLP layers. Transfer learning was also used, allowing the model to leverage pre-trained neural network architectures. Compliance for both the dataset and ground truth description domains of CLAIM was 82%. The publicly

available RSNA-STR Pulmonary Embolism CT (RSPECT) dataset was used for training. This was divided into two experiments (Colak et al., 2021). The first included 755 CTPA studies, focusing on discriminating between patients with chronic PE (RV/LV ratio ≥ 1) and a control group composed of patients with acute PE (RV/LV < 1) and those with negative PE examinations. Experiment 2 used the same groups as Experiment 1 but did not apply the RV/LV criterion, resulting in 976 CTPA scans. Additionally, a local dataset was utilised for validation and testing, consisting of 78 cases in total (26 for each of chronic PE, acute PE, and no PE).

The MIP images were modified by a radiologist manually selecting optimal colour and opacity transfer functions. Following the appearance adjustments, the researchers conducted visual inspections of the images to ensure that they accurately represented the required features and characteristics. Compliance with the performance description domain of CLAIM was 75%. In Experiment 1, DenseNet-121 with random 3-degree 2D rotations yielded the best performance, achieving an AUC of 0.70. Experiment 2, which used larger CTPA volumes for training and omitted RV/LV-based exclusion, resulted in slightly lower performance. An ensemble model was introduced, leading to a modest increase in balanced accuracy. The local dataset outperformed the public dataset significantly, with an AUC of 0.87 compared to 0.79. In the third stage, using a local dataset of 78 cases for model selection and testing led to an AUC of 0.94 and an overall accuracy of 0.89.

Study 5 - Bird et al. (2023)

This study aimed to evaluate a new automated method for quantifying hypoperfusion on dual energy CTPA to help in assessing the severity of CTEPH. An established DL CNN model for lung segmentation was utilised to automatically segment hypoperfused lung volume, effectively removing extraneous thoracic anatomy and delineating lobar boundaries. This involved processing CT images alongside iodine-water images to compute and measure the proportion of hypoperfused pixels within each lobe (Hasenstab et al., 2021). The overall compliance with CLAIM was 50%. The study referenced but did not provide any description of the CNN model (Hasenstab et al., 2021). Similarly, there was limited description of the datasets used, with 66% compliance with the dataset description criteria. The data study used a locally obtained data from, 51 CTEPH patients and 110 normal CTPA scans were retrospectively analysed. The

model automatically isolated parenchymal iodine values to delineate hypoperfusion areas and calculate hypoperfused lung volume. Compliance with the performance description criteria was 62%. The model showed that global hypoperfused lung volume distinguished CTEPH patients from controls with 0.84 AUC and 90% sensitivity cutoffs and correlated positively with hemodynamic severity and changes after surgical treatment. The study concluded that automated quantification of hypoperfused areas in CTEPH patients from dual energy CTPA may assist in clinical evaluation, especially in cases involving segmental-level disease.

3.5 Discussion

The application of AI to CTPA interpretation in the context of chronic PE and CTEPH is appealing. AI tools have the potential to aid the detection of cardiovascular and lung parenchymal changes that are important for diagnosis, risk stratification, prognostication and treatment decisions in chronic PE. Previous studies suggested that a lack of sensitivity for PE detection may affect radiologists' interpretation, which ranged from 66% to 87% (Das et al., 2008, Eng et al., 2004). AI tools for the identification of chronic PE could assist the accuracy and efficiency of CTPA interpretation by radiologists, such as by highlighting areas of potential concern for closer scrutiny. This is particularly relevant given that the changes in chronic PE may be incidental or subtle on imaging.

This systematic review aimed to identify and appraise existing studies presenting AI tools for CTPA in chronic PE patients. Five studies were eligible for inclusion, identifying a significant gap in the field. Study quality was evaluated using compliance with the criteria of CLAIM, an established structured checklist designed to aid the presentation and interpretation of studies presenting AI approaches. All five studies share a common focus on the application of deep learning techniques, particularly CNN algorithm for the detection and diagnosis of PE, using texture segmentation of the lung parenchyma without direct assessment of the pulmonary arteries. One study divided their analysis into several phases and made use of both public RSPECT and local datasets. Vainio et al. (2021) demonstrated that segmentation of the hypoperfused lungs was carried out using the CNN model resulting in an AUC of 0.87 for detecting chronic PE. Khan et al. (2023) reported that the model achieved an overall AUC of 0.90, for all participants in the dataset. Ma et al. (2022) showed promising PE detection ability whether acute or chronic, with a window-level AUC of 0.93. Vainio et al. (2023), showed that a relatively limited local dataset for model selection and testing resulted in an AUC of 0.94, indicating efficacy in diagnosing chronic PE. However, there is a potential risk of overfitting, increased variability, and uncertainty associated with using a small dataset, as it may not fully capture the variability and complexity of the underlying population.

Models

The included studies provided reliable descriptions of their respective deep learning CNN models. Khan et al. (2023) explored the use of DL CNN algorithms in computer-aided diagnosis of PE. The models were trained on a large dataset of CT scans and employed advanced techniques for feature extraction and classification to improve the accuracy of PE diagnosis. DenseNet201 is a type of neural network that employs densely connected convolutional blocks; each layer receives direct inputs from all preceding layers, resulting in enhanced feature propagation and reuse throughout the network (Huang et al., 2017). This connectivity pattern allows for better information flow and gradient propagation, potentially improving the model's ability to learn complex patterns and features relevant to PE detection. The dense connections can lead to increased memory requirements, as the outputs of all preceding layers need to be stored for gradient computation during backpropagation. DenseNet201 is a highly expressive model with a large number of parameters. In some cases, this can increase the risk of overfitting, especially if the dataset is small or not diverse enough.

In the study by Vainio et al. (2023), the model to detect chronic PE used transfer learning from a previously trained ImageNet model (Deng et al., 2009), analysed eleven MIP images, combined the image characteristics and processed them using an MLP with ReLU activations. The use of 2D MIP reconstructions for training an AI tool on CTPA images as opposed to using other approaches has benefits in terms of standardisation, computational efficiency and ease of use. However, it comes with the risk of missing essential 3D information and location-based context, which can have an influence on the tool's diagnostic accuracy. In their earlier study, Vainio et al. (2021) focused on the evaluation of a 3D CNN for the detection of hypoperfusion in patients with CTEPH. They investigated the feasibility and effectiveness of using a 3D CNN architecture to analyse CTPA images and identify regions of hypoperfusion in the lung. Ma et al. (2022) presented a multitask DL approach for the detection and identification of PE, with a CNN architecture capable of simultaneously performing multiple tasks related to PE diagnosis, such as segmenting affected lung regions, classifying the severity, and providing a score for diagnosis. The multi-task deep learning model was trained on a diverse dataset and is expected to improve the efficiency and accuracy of PE detection and identification, as the multitask learning strategy enabled the model to train and execute both PE detection and

identification tasks simultaneously. This could lead to more efficient and streamlined predictions by leveraging shared information between the tasks. The model may be able to identify frequent patterns and features for both identifying and detecting PE, improving the predictions made by the model's overall resilience and accuracy. However, multitask learning can be challenging if the tasks have conflicting or unrelated objectives. If the tasks have different characteristics or require distinct feature representations, jointly training them may hinder the performance on individual tasks. Every task needs a substantial amount of labelled data. If one task has a considerably smaller dataset or lacks labelled data, the performance of both tasks might be affected. This can result in a more complex model architecture, which may increase the risk of overfitting and require more computational resources for training and inference. While Bird et al. (2023) study focused less on developing and more on validating or assessing the algorithm. This approach can save space and reduce redundancy in the paper, authors must ensure that they follow ethical and academic standards by accurately crediting the original developers of the CNN model and providing readers with enough information to understand its implementation and performance in their study.

Overall, these papers share a common objective of leveraging DL techniques to improve the detection and diagnosis of PE from CTPA images. Some studies failed to assess the performance of their model on external datasets, potentially limiting their validity. However, only one study, conducted by Vainio et al. in 2023, addressed this limitation by testing their model on external datasets. Vainio et al. (2023) is the only study that reports a validation step during the development of their model. Assessing performance on validation data enables model fine-tuning (such as through hyperparameter optimisation) and the identification of potential issues (such as overfitting) prior to final model selection and testing. A lack of validation may limit the overall performance of these models. This raises concerns about the model's ability to function effectively and consistently in clinical practice settings. Positively, all of the research examined the causes of model underperformance and offered failure analyses of cases that were misclassified - an important step in ensuring validity.

Datasets

Descriptions of the datasets were less consistent, potentially limiting the interpretation of model performance. Each study did report their data sources, with the exception of Bird et al., 2023). Public datasets from the RSNA were used in three of the studies (Khan et al., 2023; Ma et al., 2022, Vainio et al., 2023). The use of public datasets offers ease of access to data, improves study transparency and helps comparison between models. Using diverse datasets results in a bigger annotated dataset with a broad range of samples from around the world. However, model performance may be restricted by the availability of data elements or variables in public datasets, which were not mentioned in two publications (Khan et al., 2023; Ma et al., 2022). These two studies used publicly available Kaggle datasets for the detection of acute and chronic PE. Although the proportions of acute and chronic PE cases are available from the original data source, these were not stated by the studies themselves, limiting their transparency - it is best practice for publications to provide all relevant clinical characteristics regardless of whether they can be accessed elsewhere (Maiter et al., 2023, Alabed et al., 2022). Public datasets utilised in the studies may not have had all the elements or features required for an accurate PE diagnosis, which may limit the model's ability to identify the spectrum of abnormalities related to PE. Variations in data quality may also affect model performance by affecting generalisability across datasets with distinct characteristics. While age and sex are important demographic factors, they should be complemented with additional information - such as the severity of disease or presence of comorbidities - to provide a more comprehensive understanding of generalisability in clinical populations. We observed that two out of five studies (Ma et al., 2022; Khan et al., 2023) lacked information on the demographics of these patients as well as the percentages of patients with various diseases. Studies should not assume that their audience is already acquainted with public datasets, and study methodology must be explained in sufficient detail to allow correct reproduction of the results.

Image annotations in public datasets may also be limited and restrict how the data can be used. For example, Ma et al. (2022) demonstrated that certain labels are directly taken by others and cannot be modified or changed. As a result, they do not account for the possibility of an inconsistent relationship between the labels and the predicted study-level labels in their

model. To increase the generalisability of AI models being trained, different data sets, such as retrospective and prospective data sets, might be combined. We found that one of the studies in this review was created by combining three other datasets that RSNA had previously provided with contributions from five more countries and institutions (Khan et al., 2023). The three public dataset studies did not include the description of the ground truth reference standard and the rationale for choosing the reference standard in their paper, although this information is accessible from the public source. Vainio et al. (2023) trained their model using the publicly available RSPECT dataset, but validated and tested the model using an external local dataset. Testing model performance on external data is important for ensuring generalisability and is an important consideration for clinical translation of AI tools. However, it is worth noting that only 78 cases - including only 26 cases of chronic PE - were included in this external dataset, which limits interpretation of the model's performance. It is important to carefully analyse the context and objectives of the AI model when deciding to use public data for training and local data for testing and model selection. While combining different datasets can have benefits like increased variety and generalisation, it also has drawbacks including inconsistent data, bias, and small local sample sizes. Improvements are needed in public datasets to address the lack of flexibility and adaptability in the labelling process, providing detailed information about datasets characteristics, and data augmentation applied. Some of these limitations may be addressed, and the robustness and dependability of the model can be improved, by making an effort to collect more comprehensive and diverse local data or by working with several healthcare facilities.

Performance

The Vainio et al. (2021) and Bird et al. (2023) studies were the only papers that evaluated hypoperfusion areas affected by CTEPH specifically on CTPA images using a DL model. Vainio et al. (2021) did not specifically look into the pulmonary vessels, rather evaluated the secondary effects on lung parenchyma. The AUC curve was solely used in this study to assess the model's performance. The performance of the 3D CNN model could be evaluated using various metrics such as sensitivity, specificity, accuracy, and area under the receiver operating characteristic curve (AUC-ROC). These metrics provide insights into the model's ability to correctly identify positive and negative cases of hypoperfusion. There are several metrics

available for evaluating DL models. Using merely a subset may offer a misleading overview of a model's real performance, resulting in unexpected findings when applied in a clinical setting. Therefore, it is crucial to combine several measures and analyse performance comprehensively (Hicks et al., 2022). However, the study might have compared the performance of the 3D CNN model with existing methods used for detecting hypoperfusion in CT pulmonary angiography. This could involve comparing the AUC to determine if the 3D CNN outperforms or is comparable to other approaches. The study demonstrated the feasibility of using a 3D CNN for the automated detection of hypoperfusion on CTPA images in patients with CTEPH. Furthermore, the results indicated that CNNs were able to automatically support radiologists in diagnosing and treating patients with chronic PE. Vainio et al. (2023) assessed the CNN model in several phases. The model performed inconsistently across the public and local datasets, with the local dataset producing noticeably better outcomes. The model's ability to identify chronic PE was greatly enhanced by the application of a locally optimised ensemble model, challenging model selection techniques, and the local test dataset. The model improved in cross-validation model selection, sensitivity to data augmentation, and performance on the local dataset. However, there were differences in performance, as well as the effect of different training methods. The use of a limited local dataset for early stopping presents issues regarding overfitting. However, the other two studies by Khan et al. (2023) and Ma et al. (2022) evaluated PE in general (acute and chronic) and RV/LV ratio using CNN on CTPA for classification. Nonetheless, they omitted to present the number of acute and chronic cases, which limits interpretation. Khan et al. (2023) trained an AI model without applying a validation set, which can have a number of consequences for the model's performance and reliability. Assessing performance using a validation set prior to formal testing is important for confirming that a model operates properly on unseen data and enables further refinement prior to finalisation. The lack of a validation step may limit understanding of model generalisability, increase the risk of overfitting, restrict hyperparameter optimisation and impede model selection. Finally, this study analyses the possible advantages of IoMT-enabled computer-aided diagnostics for PE classification. Gradient-weighted class activation mapping (Grad-CAM) was used by Ma et al. (2022) to improve the interpretability of the AI model, although this only applied to the first phase of training rather than going over the sequential model's parameters in the second training phase. The exclusion of Grad-CAM during the second phase of training may limit the

interpretability of the model's updated parameters. The overall results demonstrate that their model was accurate in detecting and classifying PE and has the potential to enhance acute PE diagnosis. While in chronic PE, the model does not perform effectively although they omitted to give the number of chronic PE cases.

While this review focuses on CTEPH-specific models, general-purpose tools like TotalSegmentator have shown strong performance in segmenting anatomical structures across diverse CT datasets and may aid in detecting features relevant to CTEPH (Wasserthal et al., 2023; Hinck et al., 2025). However, their effectiveness is uncertain, as CTEPH presents distinctive radiographic signs, organised thrombi and perfusion defects, which are often absent from the non-CTEPH datasets used to train such models. These models could provide a foundation, but further work is required to evaluate whether these tools can be adapted or fine-tuned for CTEPH-specific applications.

Furthermore, the usability and accessibility of the identified models remain limited. None of the five studies provided downloadable models or user-ready code for external datasets, and there is no evidence of widespread external validation or clinical use. Although some used public datasets and common DL architectures, reproducibility is restricted without open sharing of model weights and inference pipelines. Broader adoption will require open-access resources and documentation to support clinical applications.

Our systematic review has limitations. The eligibility criteria focused on chronic PE detection using AI on CTPA images; studies may have been missed if they had not clearly identified the presence of chronic PE in their datasets. Unpublished research and non-English language studies were not included. Despite the inclusion of conference abstracts within the eligibility criteria, the number of included studies was low, preventing formal meta-analysis of model performance.

3.6 Conclusion

This systematic review identified five existing studies presenting AI tools for CTPA interpretation in patients with chronic PE or CTEPH. All studies presented DL CNN approaches to the assessment of lung parenchyma, with variable performance. Assessment of studies using CLAIM identified overall reasonable reporting of AI model design and training, but inconsistent reporting of the datasets used, limiting their transparency. This study highlights an area of potential expansion for the field of AI in medical imaging.

4 Methodology

This chapter describes the steps involved in developing the radiological imaging database utilised in this thesis. Each corresponding chapter presents methods for particular analyses. It also includes introductory explanations of the AI development process.

Sheffield Teaching Hospitals NHS Foundation Trust received ethical permission, which was later authorised by the National Research Ethics Service for database study (16/YH/0352).

4.1 Patients Database

The ASPIRE (Assessing the Spectrum of Pulmonary Hypertension Identified at a Referral Centre) registry was used to identify patients with CTEPH. Patients referred for pulmonary hypertension (PH) care centre are documented in the ASPIRE registry, established by Sheffield Pulmonary Vascular Diseases Unit (SPVDU) at Sheffield Teaching Hospitals NHS Trust. Every patient transferred to the registry receives an extensive clinical and radiological examination. Along with a variety of diagnostic tests like V/Q scan, echocardiography, right heart catheterisation (RHC), pulmonary function tests (PFTs), CTPA, and MRI, this also requires a consultation with a specialist in PH. A multidisciplinary team (MDT) of specialists from radiology, cardiology, and respiratory medicine, then meets to review the condition of all patients, leading to a collaborative approach to patient management. The conclusions of the multidisciplinary team (MDT) and the outcomes of the previously described tests are systematically recorded and archived in digital forms across various databases. Additionally, the NHS Personal Demographics Service is responsible for maintaining mortality records.

The POLARIS XNAT (Pulmonary, Lung, and Respiratory Imaging Sheffield) database, which is used to identify patient data, stores medical images from the Royal Hallamshire Hospital's Academic Unit of Radiology. This includes pseudonymised CT and MRI images saved in DICOM format and only accessible with valid authentication. The DICOM CT scans from the POLARIS database were matched with clinical data from the ASPIRE registry.

Every patient at Sheffield Teaching Hospitals (STH) is assigned a one-of-a-kind identity that is connected to their individual hospital number. From the POLARIS XNAT database, the DICOM CT images of patients who were found via the ASPIRE registry were retrieved.

4.2 CT imaging

In Sheffield, CT scans are commonly performed using a GE Healthcare LightSpeed 64-slice MDCT scanner or TOSHIBA Aquilion PRIME scanner. Typical acquisition parameters are 120 kV, 0.625 mm collimation, pitch of 1, rotation duration of 0.5 seconds, and 100 mA with automatic dose reduction. These values could change based on default setups and algorithms that automatically modify settings according to characteristics such as patient body mass index. differences may also occur across various scanner types and manufacturers, since each may include distinct default settings and algorithms methods. A typical field of view of 400 mm × 400 mm with a 512 × 512 acquisition matrix is applied across all CT scans. For patients with PH in Sheffield, the standard imaging protocol involves CTPA along with HRCT reconstructions and expiratory slices acquired consecutively. During CTPA, intravenous iodinated contrast (Omnipaque 350, GE Healthcare) is given to improve opacification, which enhanced visualisation of the pulmonary vasculature.

When a CT scan is acquired, it is saved as a DICOM file in the POLARIS XNAT database and each study has its own distinct ID number. Several scans, each referred to as a "CT series," might be included in a single "study." Each CT series parameter is different that may include series with thin-slice reconstruction, lung window series, a series with mediastinal window, series with contrast or no contrast. Each DICOM file contains a list of information such as the scanner model and manufacturer, the series numbers and IDs, the reconstruction techniques that were used, slice thickness, radiation dose in Kilovoltage peak (kVp), technical parameters, scan date and number of slices. (.csv) files containing this data were created by taking the data straight out of the DICOM files. There was also a thorough validation and assessment of other factors manually, such as whether the images included IV contrast or respiratory artefacts and if the chest had been properly scanned. For each patient only CTPA series was downloaded rather than all series. In order to be eligible for AI development, the images were

viewed to confirm CTPA and manually checked for diagnostic quality and with respect to PE is it normal, acute or chronic. Included in the quality control requirements are CTPA series with slice thickness < 0.625 mm, IV contrast, no noise, more than 300 slices and a complete chest is scanned.

The inclusion criteria were all adult patients diagnosed with CTEPH at Sheffield Royal Hallamshire Hospital who had CTPA in Sheffield using the guideline criteria for CTEPH diagnosis (Humbert et al., 2022). Patients who had undergone pulmonary endarterectomy (PEA) or received medical treatment were included in the study. However, those who had balloon pulmonary angioplasty (BPA) were excluded, because BPA only became nationally commissioned in the UK starting in 2018. Furthermore, CTPA images with significant artefacts and inadequate contrast of the pulmonary arteries were excluded throughout the image processing step.

4.3 Image analysis

Radiological reports were reviewed to confirm patients with CTEPH and verify positive cases, with each positive result being evaluated radiologically. CTPA images were then analysed to identify radiological CT characteristics and lung parenchymal abnormalities, such as mosaic perfusion patterns, lung infarction, bronchial arteries, coronary calcification, and lung parenchymal disease. The purpose of the radiological assessment and data quality control was to convert raw NHS data into a format applicable for AI development. This stage critically impacts project performance, though its time-consuming and requires specialised skills. Every stage in this process was conducted by myself, a speciality trainee CT radiographer, with assistance from my supervisor, a specialist Cardiothoracic Radiologist. Data from multiple sources, including ASPIRE, POLARIS XNAT, NHS Personal Demographics Service, and DICOM files, were combined into a single database using Microsoft Excel.

Each CTPA series was manually reviewed, concentrating on the method of scan acquisition and the overall radiological quality. This comprised verifying there were no significant breathing or motion artefacts, noise interference was limited, and complete scan with full

chest coverage. In addition, I reviewed the CTPA contrast phase and confirmed the slice thickness was less than 1.25mm.

Of 1673 scans, 290 patients with CTEPH underwent thin slices, which all met the requirements for radiologically acceptable scan quality. External CTPAs and scans with significant artefacts were excluded from the analysis. Additionally, scans were excluded based on acquisition type and inconsistencies in coded DICOM information. Although several files were labelled as 'CTPA,' they did not meet the required criteria, such as correct phase timing, thin slice thickness, or presence of contrast. Despite time-consuming, the radiological evaluation and data refinement were necessary for verifying the reliability of the data before proceeding with any clinical assessment or AI model development.

4.4 Workflow for AI Development

After exporting the images from POLARIS XNAT, the DICOM files were inserted into the MIM programme (MIM Software Inc., Cleveland, Ohio, United States). We identified the pulmonary vessels, acute PE and CTEPH cases, which required the development of a process using MIM's built-in tools. This was carried out in conjunction with a clinical scientist (MS). There are two primary stages involved in the training and creation of an autonomous AI model that is capable of segmenting and identifying patients with CTEPH. First, the pulmonary arteries and veins were manually segmented using draw sphere and landmark tools in MIM software. The thromboembolic diseases were then segmented, and their anatomical locations were classified based on the definitions provided by den Exter et al. (2020): **central disease** were defined as those located in the main or lobar pulmonary arteries, while **distal disease** were defined as those in the segmental or subsegmental branches, with subsegmental arteries referring to those beyond the segmental level. An algorithm was then developed to automatically segment the pulmonary arteries and thromboembolic disease, distinguishing them from surrounding tissues, veins, and lung borders. This is done for each slice that is taken during a multi-slice CTPA.

The results of this workflow were constantly reviewed manually, with technical parameters adjusted as needed to optimise performance (**Figure 4.1**). Visual assessment was used to evaluate segmentation accuracy for the arteries, veins and thromboembolic disease.

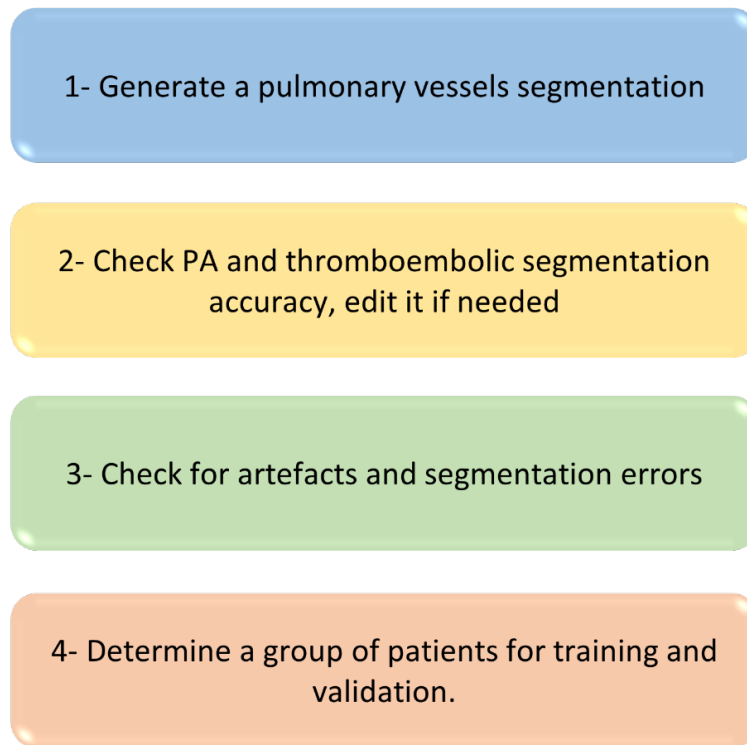


Figure 4.1 Data preparation for AI model.

Pulmonary arteries, that are included in the study and segmented for both normal and abnormal cases (Figure 4.2):

- Pulmonary artery (PA) _ Bifurcation (origin)
- Right_ PA_ (mid, distal)
- Left_ PA_ (mid, distal)
- Right_ Upper_ Anterior_ (Origin, mid, distal)
- Right_ Upper_ Apical_ (Origin, mid, distal)
- Right_ Upper_ Posterior_ (Origin, mid, distal)

- Right_Mid_Medial_ (Origin, mid, distal)
- Right_Mid_Lateral_ (Origin, mid, distal)
- Right_Lower_Anterior_ (Origin, mid, distal)
- Right_Lower_Posterior_ (Origin, mid, distal)
- Right_Lower_Medial_ (Origin, mid, distal)
- Right_Lower_Lateral_ (Origin, mid, distal)
- Right_Lower_Apical_ (Origin, mid, distal)
- Left_Upper_Anterior_ (Origin, mid, distal)
- Left_Upper_Apico Posterior_ (Origin, mid, distal)
- Left_Upper_Superior Lingula_ (Origin, mid, distal)
- Left_Upper_Inferior Lingula_ (Origin, mid, distal)
- Left_Lower_Apical_ (Origin, mid, distal)
- Left_Lower_Anterior_ (Origin, mid, distal)
- Left_Lower_Lateral_ (Origin, mid, distal)
- Left_Lower_Posterior_ (Origin, mid, distal)

In patients with CTEPH, proper segmentation of the pulmonary arteries (PA) and veins (PV) in CTPA images is important due to the diagnostic challenges associated with identifying vascular obstructions and enhances the development of AI algorithms for automated CTEPH diagnosis. In addition, CTPA scans might consist of noise or motion artefacts, which could affect accurate segmentation. noise-reduction and image enhancement methods were used to improve the accuracy of PA and PV segmentation. Considering individual variations in vascular structure and adequate contrast enhancement of CTPA is significant, which can be achieved by manual modification of segmentation parameters, hence enhancing model effectiveness to ensure consistent accuracy across different patients.

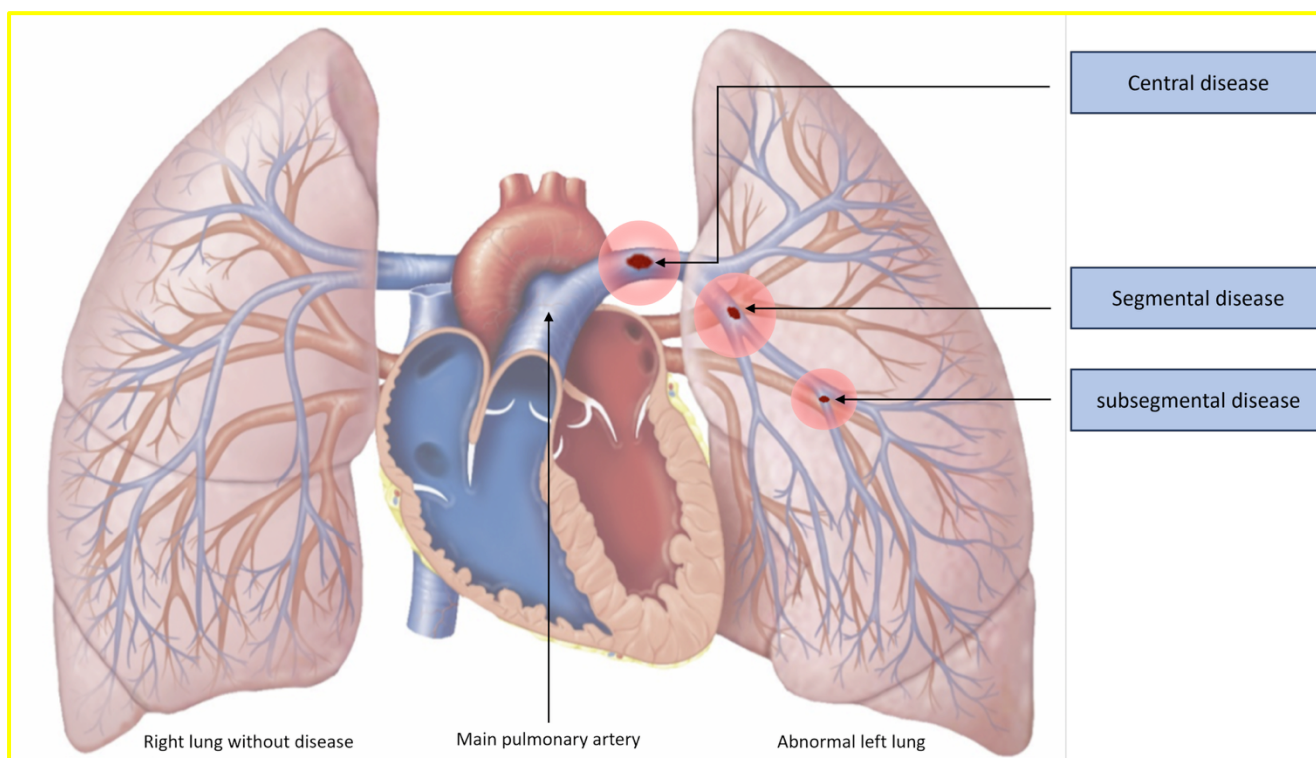


Figure 4.2 Illustration of thromboembolic disease distribution and anatomical classification based on thrombi location within the pulmonary vasculature: central disease (main pulmonary arteries), and distal disease including segmental disease (segmental branches), and (subsegmental and more peripheral vessels).

4.5 Statistical analysis

Analysis was performed using SPSS (version 27.0, IBM) and GraphPad Prism (version 9.0). Proper statistical analysis was selected based on the distribution and nature of data. For further details on the statistical methods used in each study, please see the statistical analysis sections in each chapter.

5 Lung parenchymal and cardiac appearances on CTPA impact survival in chronic thromboembolic pulmonary hypertension: results from the ASPIRE Registry

***Peer-reviewed journal article published in ERJ open (2024)**

Contribution: First author. My main contributions were completing extensive literature reviews, carrying out statistical analyses, and developing the tables and figures included in the research and integrating future amendments based on input and recommendations from my co-authors. I was also responsible for extracting and curating the dataset. This involved verifying the accuracy and completeness of clinical records and integrating these data into a cohesive and analysable format. I independently reviewed and measured all clinical cases and CTPA images used in the study.

L. Abdulaal¹, A. Maiter^{1,5}, K. Dwivedi^{1,3}, M.J. Sharkey¹, S. Alabed^{1,3,4}, D. Alkhanfar¹, A. Rothman^{1,2,3,4}, S. Rajaram⁵, R. Condliffe², D.G. Kiely^{2,3,4*} and A. J. Swift^{1,3,4*}

1. Division of Cardiovascular Medicine, University of Sheffield
2. Sheffield Pulmonary Vascular Disease Unit, Sheffield Teaching Hospitals NHS Foundation Trust
3. INSIGNEO, Institute for in silico Medicine, The University of Sheffield, Sheffield, United Kingdom.
4. National Institute for Health and Care Research, Sheffield Biomedical Research Centre, Sheffield, UK
5. Radiology Department, Sheffield Teaching Hospitals NHS Foundation Trust.

5.1 Abstract

Background: Chronic thromboembolic pulmonary hypertension (CTEPH) is commonly evaluated using CT pulmonary angiography (CTPA). We evaluated the frequency and impact of parenchymal and cardiac abnormalities on survival in CTEPH.

Methods: Patients were identified from the ASPIRE (Assessing-the-Spectrum-of-Pulmonary-Hypertension-Identified-at-a-Referral-Centre) Registry. Kaplan-Meier analysis was used to assess survival.

Results: 290 patients (55% female, mean age 65 ± 14 years) with CTEPH were included. Mosaic perfusion was noted in 83%, lung infarction in 73% and parenchymal lung disease in 28%. The severity of mosaic perfusion and lung infarction correlated with markers of disease severity ($p < 0.001$). Whereas the presence of mosaic perfusion was associated with improved survival in all patients ($p = 0.03$), it did not predict outcome in those undergoing pulmonary endarterectomy (PEA) ($p = 0.6$) and those not undergoing PEA ($p = 0.22$). The presence of lung infarction had no impact on mortality. The presence of co-existing lung disease was associated with a worse survival ($p < 0.008$), in patients not undergoing PEA. Mosaic perfusion was less common in patients with parenchymal lung disease (65%) compared to those without parenchymal lung disease (90%), $p < 0.001$. Increased right: left ventricular ratio and aortic diameter predicted worse outcome ($p < 0.002$).

Conclusion: Lung parenchymal and cardiac changes on CTPA predict outcome in CTEPH. Co-existing parenchymal lung disease is not uncommon and when present may mask the presence of mosaic perfusion. This study highlights the importance of systematically evaluating the lung parenchyma and cardiac changes in patients with CTEPH.

Advances in knowledge: Previous studies have not systematically assessed how lung parenchymal and cardiac abnormalities observed on CTPA impact survival in CTEPH. This study aims to address this gap by evaluating their frequency, correlation with disease severity, and impact on survival.

5.2 Introduction

Chronic thromboembolic pulmonary hypertension (CTEPH) is due to non-resolution of thrombus and is often accompanied by a microvasculopathy (Delcroix et al., 2021). A large prospective study and data from the ASPIRE Registry have noted a 2-year incidence of approximately 2% following an acute pulmonary embolism (Valerio et al., 2022, Durrington et al., 2024). Without treatment CTEPH is a progressive condition resulting in right heart failure and death. However, with newer approaches to treatment including pulmonary endarterectomy (PEA), balloon pulmonary angioplasty (BPA) and medical therapy outcomes are significantly improved (Delcroix et al., 2021). One of the challenges is the identification of the most appropriate therapy or therapies for treating CTEPH. Consequently, patients undergo multimodality testing, not only to characterise the extent of clot burden and estimate the severity of microvascular involvement but also assess for comorbidities which may impact significantly on decisions to proceed to PEA (Pepke-Zaba et al., 2011, Quadery et al., 2018).

Computed tomography pulmonary angiography (CTPA) plays an important role in the assessment of patients with suspected and confirmed CTEPH; it is non-invasive and is recommended in international guidelines and by expert bodies for the evaluation of patients with CTEPH (Humbert et al., 2022, Kiely et al., 2019, Remy-Jardin et al., 2021). CTPA allows for an assessment of vessels providing a roadmap of the pulmonary vasculature but in addition also allows for an assessment of cardiac chambers, lung parenchyma and mediastinal structures (Rajaram et al., 2015). Vascular abnormalities include attenuated vessels, stenosis, webs, and eccentric thrombi (Delcroix et al., 2021, Gopalan et al., 2017, Simonneau et al., 2017). Parenchymal abnormalities include mosaic perfusion and the sequelae of lung infarction. Lung infarction is more common in the setting of distal rather than central pulmonary emboli, as the lung peripheries receive less collateral supply from the bronchial arterial circulation (He et al., 2006). Although acute infarction usually appears as areas of wedge-shaped defects over time these become organised resulting in subpleural scarring and or consolidation/cavitation (Harris et al., 2008). Cardiac abnormalities reflecting the presence of pulmonary hypertension (PH) may be observed on CTPA and a combination of pulmonary

artery diameter ≥ 30 mm, right ventricular outflow tract hypertrophy ≥ 6 mm and a right ventricular: left ventricular (RV/LV) ratio of ≥ 1 is highly predictive for the presence of PH (Swift et al., 2020).

Importantly, comorbidities impact survival in patients with CTEPH (Pepke-Zaba et al., 2011, Quadery et al., 2018) and can be appreciated on imaging (Shahin et al., 2022). In patients with other forms of PH such as idiopathic pulmonary artery hypertension (IPAH) even minor parenchymal lung disease on CT predicts a higher mortality (Lewis et al., 2020, Hoeper et al., 2022), however, the impact of these changes on outcome in patients with CTEPH is not known. The aim of this study was to evaluate the frequency of mosaic perfusion, lung infarction and lung parenchymal abnormalities on CTPA in patients with CTEPH, their correlation with disease severity and impact on survival.

5.3 Methods

Study participants

Patients were identified from the ASPIRE Registry (Assessing the Spectrum of Pulmonary Hypertension Identified at a Referral Centre registry) between January 2008 and January 2018 (Hurdman et al., 2012). The ASPIRE registry includes data from patients undergoing systematic evaluation for suspected PH at the Sheffield Pulmonary Vascular Disease unit including multimodality imaging and right heart catheterisation. This is a nationally designated PH referral centre serving a population of 15-20 million and adheres to annually audited standards of care. The diagnosis of CTEPH in this study was made according to international guidelines and detailed discussion by a multidisciplinary team (MDT). Adult patients (≥ 18 years) were eligible for inclusion in the study if they underwent CTPA in Sheffield and met guideline criteria for a diagnosis of CTEPH, and patients who underwent PEA or received medical therapy. No patients who underwent BPA were included in this study; BPA was only nationally commissioned in the UK in 2018 (Humbert et al., 2022). Data on demographics, pulmonary function tests (PFT) and right heart catheterisation (RHC) were obtained from the ASPIRE Registry.

RHC was performed using a 7.5-F balloon-tipped thermodilution catheter (Becton-Dickinson, Franklin Lakes, New Jersey). Mean pulmonary artery pressure (mPAP) and pulmonary arterial wedge pressure (PAWP) were obtained using fluid-filled pressure. Cardiac output (CO) was assessed via the thermodilution method. Pulmonary vascular resistance (PVR) was calculated using the following formula: $PVR = (mPAP - PAWP)/CO$. The cardiac index (CI) was adjusted for body surface area (BSA) as: $CI = CO/BSA$.

CTPA acquisition and evaluation

CTPA studies were acquired using multidetector scanners (TOSHIBA Aquilion PRIME and GE Medical Systems) with standard acquisition parameters: tube current 80-700 mA with automatic dose reduction tube voltage 120 kV, pitch 1, slice thickness 0.5 mm x 80 mm, rotation speed 0.275. 60 mL of intravenous iodinated contrast (Omnipaque 350, GE Healthcare) was injected at a rate of 5 mL/s. Bolus tracking was performed over the

pulmonary artery using a manual fast start, with acquisition triggered over a threshold of 220 HU. Patients were excluded from the study if their CTPA images were considered to be suboptimal - for example, where contrast opacification of the pulmonary arteries was poor or there was significant movement artefact. This choice was taken during the image analysis stage, which evaluated the quality and readability of the CTPA images. Data on pulmonary endarterectomy (PEA) status was collected from patient records and surgical databases at the time of census.

A semi-quantitative approach was used to evaluate CTPA images, with visual assessment being used as a tool to identify and classify abnormalities. CTPA studies were evaluated by a single consultant cardiothoracic radiologist (AS, 13 years of experience) blinded to clinical parameters. The images were evaluated on axial slices using standard lung (level 362 HU and width 1324 HU) and soft tissue (level 40 HU and width 440 HU) windows. A standardised scoring method was used to categorise lung parenchymal disease, ensuring consistency: 0 indicating (no disease), 1 minor (1-25%), 2 mild (26–50%), and 3 moderate-to-severe (>50%). The evaluation focused on the following features, each classified as nil, minor, mild, or moderate-to-severe: 1) appearances of the lung parenchyma, including mosaic perfusion patterns, lung infarction; and any coexisting lung abnormalities (such as fibrosis, emphysema, or other lung disease); 2) vascular appearances, including the presence of CTEPH features (e.g. eccentric thrombus, strands or webs within pulmonary arteries), the distribution of thromboembolic disease (central/segmental/distal) and bronchial artery appearances (unopacified/normal/prominent/dilated); 3) technical adequacy, including the presence of artefacts. Cardiac chamber and vessel measurements were assessed by one radiographer (LA, 4 years of cardiac CT experience). All measurements were made in the axial plane following training by (AS) as previously described (Rajaram et al., 2015). The maximal diameter of the ascending aorta (AO) and pulmonary artery trunk (PA) were measured at the level of the PA bifurcation. The diameter of the right ventricle (RV) and left ventricle (LV) were measured on the slices at which they appeared maximal. The PA/AO and RV/LV ratios were subsequently calculated (**Figure 5.1**).

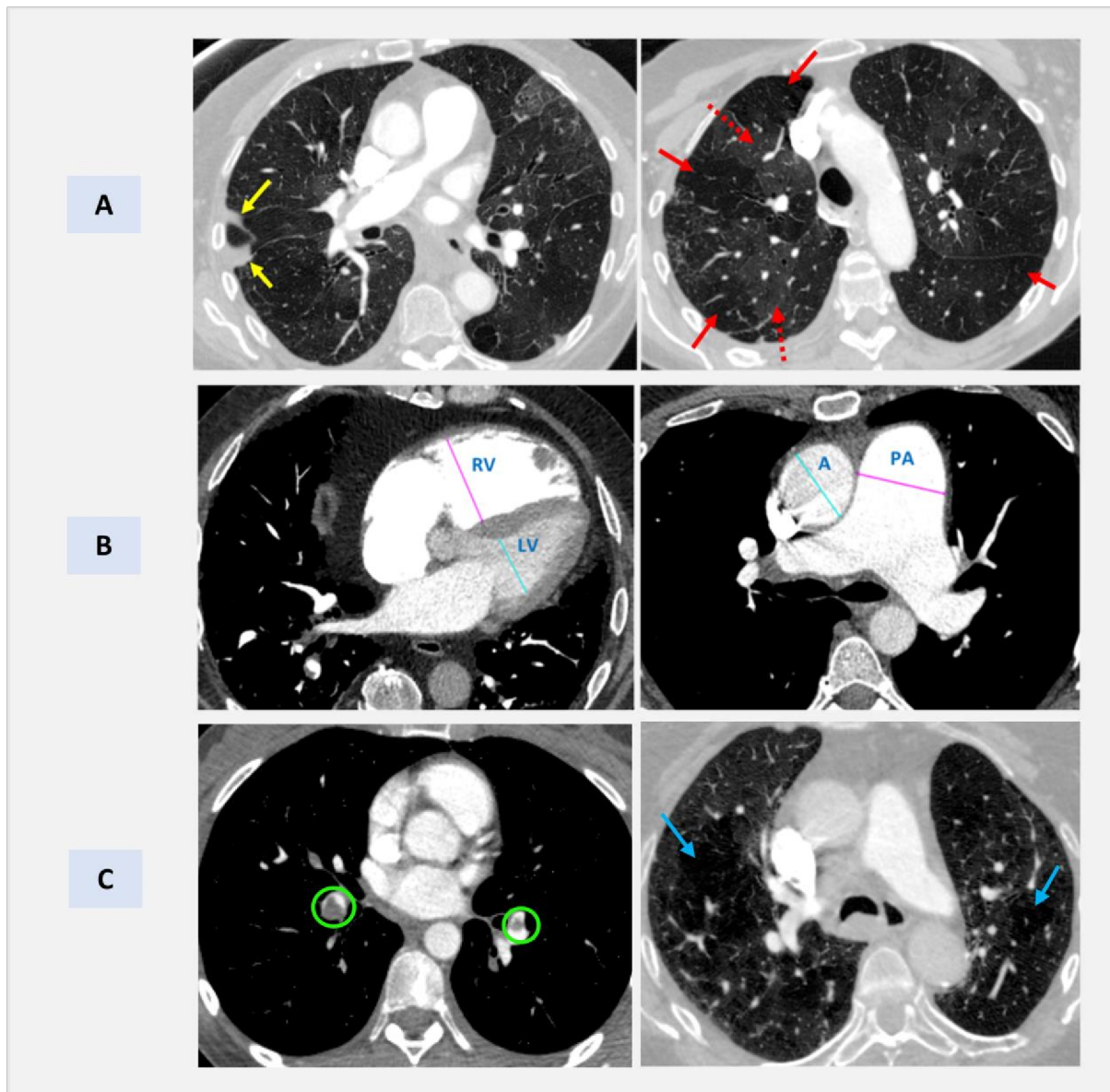


Figure 5.1 A) Examples of lung parenchymal features of CTEPH on CTPA. Axial CTPA images with standard lung windows from two different patients. The patient on the left showed lung infarction within the right middle lobe (yellow arrows). This typically appears as focal wedge-shaped consolidation at the lung periphery which resolves over time. Both patients exhibit mosaic perfusion. This refers to regional hyperattenuating (dashed red arrows) and hypoattenuation (solid red arrows) of the lung parenchyma, of which abnormal lung perfusion is a cause. It is important to note that neither lung infarction nor mosaic perfusion are specific to CTEPH and there is a broad differential diagnosis for both of these imaging findings. B) Examples of cardiac changes commonly seen in CTEPH on CTPA. Two axial CTPA images with standard soft tissue windows are shown. The right image shows marked dilatation of the right ventricle (RV) relative to the left ventricle (LV), with an RV/LV ratio of > 1.0 , consistent with RV dysfunction. The left image shows dilatation of the pulmonary artery (PA) trunk relative to the aorta (AO), with a PA/AO ratio of > 1.0 . C) Examples of CTEPH within left and right segmental disease (green circles), and emphysema lung disease in both lungs (blue arrows).

Statistical analysis

Continuous data are reported as the mean \pm standard deviation (SD) or median with interquartile range (IQR). Categorical data are reported as percentages and frequency. Pearson correlation coefficient was used to evaluate the association between two continuous variables, specifically dichotomized mosaic perfusion and infarction data (grouped as 0 and 1). Group comparisons were conducted on mosaic perfusion and infarction data compared to pulmonary hemodynamic parameters, which were categorised into four levels (nil, minor, mild, and moderate/severe), using a one-way ANOVA followed by post-hoc Bonferroni correction. Kaplan-Meier analysis was used to determine the relationship between various CT parenchyma characteristics and survival after PEA treatment, with the log-rank test used to compare survival curves. Cox proportional hazards regression was used to assess the prognostic importance of CT measurements and lung parenchymal features. SPSS Statistics (SPSS version 27, IBM) and GraphPad Prism (v10; GraphPad, La Jolla, CA, USA) were used to conduct all statistical analyses, with a significance threshold of $p < 0.05$.

As part of the national service specification for patients with pulmonary hypertension, patients receiving treatment should undergo regular assessment. There were no patients lost to follow-up during the duration of this study. Mortality data was obtained from the NHS Personal Demographics Service. The census date for the study was 10/01/2022. This study received ethical approval through the ASPIRE Registry (16/YH/0352).

5.4 Results

Study population

Between 2008 and 2018, 700 patients were diagnosed with CTEPH in Sheffield and 294 underwent CTPA in Sheffield. Four patients were excluded from the study due to poor image quality leaving 290 patients for analysis (**Figure 5.2**). Of these 272 patients (93.7%) had available RHC data and 260 patients (89.6%) had available PFT data.

The mean age was 65 ± 14 years and 55% were female (**Table 5.1**). mPAP was 45 ± 12 mmHg and PVR 645 ± 414 dyne.s.cm⁻⁵. Twenty-five patients (9%) were in WHO Function Class II, 231 (79%) WHO FC III and 30 (10%) WHO FC IV.

Pulmonary endarterectomy was performed in 119 patients (41%) with a median duration of 7 months (IQR 0 to 11) to surgery.

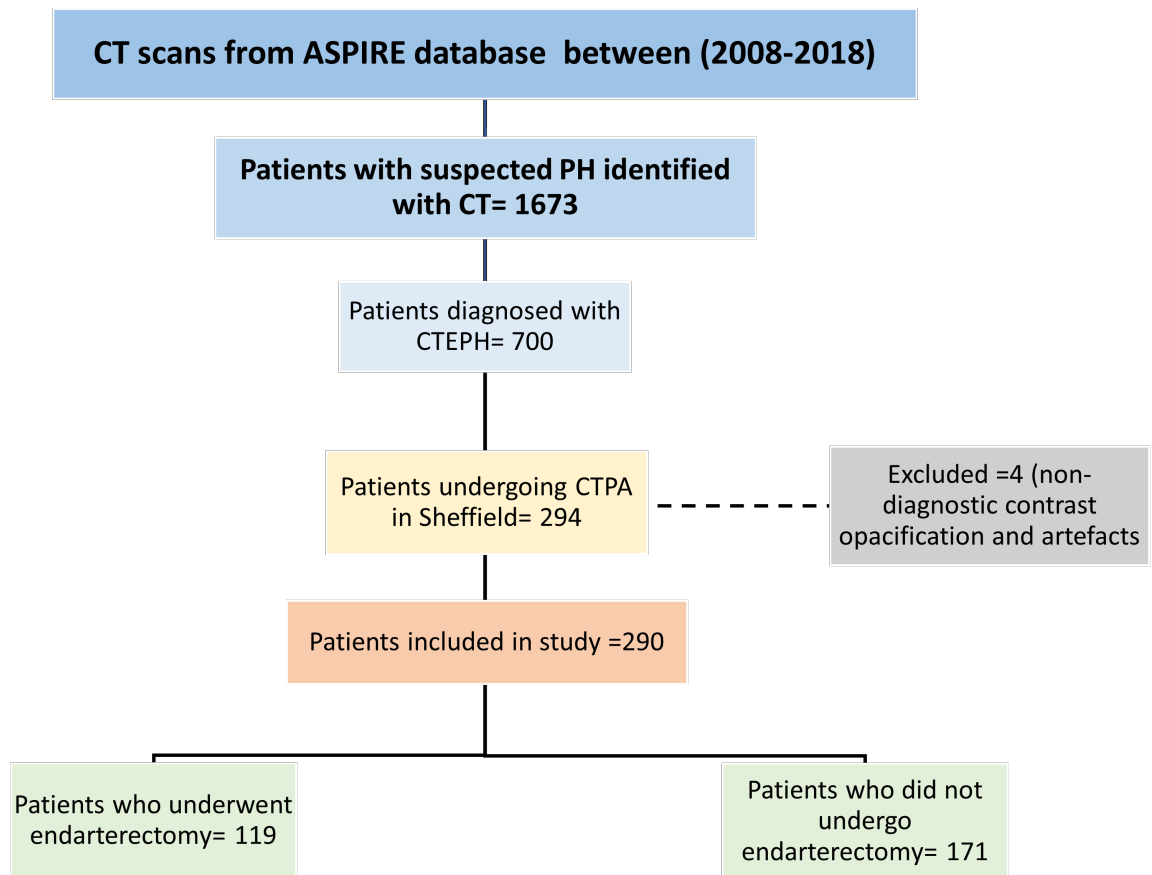


Figure 5.2 Study flow diagram.

Table 5.1 Characteristics of patients undergoing right heart catheterisation and pulmonary function tests, with a comparison between patients who underwent pulmonary endarterectomy (PEA) and those who did not (No PEA). Data are presented as mean \pm standard deviation or counts (percentage). P-values ($P < 0.05$) indicate significant differences between the PEA and No PEA groups.

Patient characteristics	Full cohort 290	Endarterectomy 119 (41%)	No Endarterectomy 171 (59%)	P value
Age (years)	65 \pm 14	60 \pm 14	67 \pm 14	<0.001
Sex (Female)	158 (54.5%)	68 (57%)	90 (53%)	0.44
WHO FC	II (25), III (231), IV (30)	II (6), III (101), IV (10)	II (19), III (130), IV (20)	0.47
Right heart catheterisation	n=272 (94%)	n=112 (94%)	n=160 (94%)	P value
PVR (dyne·s·cm ⁻⁵)	646 \pm 414	666 \pm 424	631 \pm 409	0.5
mPAP (mmHg)	45 \pm 12	45 \pm 12	45 \pm 12	0.99
PAWP (mmHg)	12.6 \pm 5.1	12.6 \pm 4.7	12.7 \pm 5.4	0.72
SVO ₂ (%)	62 \pm 9	63 \pm 8	61 \pm 9.1	0.16
SaO ₂ (%)	94 \pm 3.8	93 \pm 4.1	94 \pm 3.4	0.3
CI (L/min/m ²)	2.6 \pm 0.8	2.5 \pm 0.8	2.6 \pm 0.9	0.22
CO (L/min)	4.7 \pm 1.6	4.6 \pm 1.5	4.9 \pm 1.8	0.12
Pulmonary function test	n=260 (90%)	n=114 (96%)	n=146 (85%)	P value
Predicted FEV ₁ (%)	76.3 \pm 20.3	80.1 \pm 19.06	73.3 \pm 20.8	0.008
Predicted FVC (%)	88.4 \pm 21.5	91.8 \pm 20.07	85.8 \pm 22.2	0.02
Predicted TLCO (%)	60.2 \pm 18.3	62 \pm 15.8	59 \pm 20	0.17

Abbreviations: World health organisation (WHO), pulmonary vascular resistance (PVR), mean pulmonary arterial pressure (mPAP), pulmonary artery wedge pressure (PAWP), venous oxygen saturation (SVO₂), oxygen saturation (SaO₂), cardiac index (CI), and cardiac output (CO). Pulmonary function, include forced expiratory volume (FEV₁), forced vital capacity (FVC), and transfer factor of the lung for carbon monoxide (TLCO).

CTPA findings

Distribution of CTEPH

Of patients with CTEPH, 25% had central or lobar disease, 61% segmental disease and 14% subsegmental disease. The distribution of CTEPH did not correlate with either extent of lung infarction ($r=-0.07$, $p=0.18$) or mosaic perfusion ($r=-0.03$, $p=0.61$).

Mosaic perfusion pattern and lung infarction

Mosaic perfusion and lung infarction were present in 83% and 73% of patients respectively, with both present in 69% (**Table 5.3**). The severity of mosaic perfusion showed a significant correlation with RV/LV ratio ($r= 0.22$, $p <0.001$). There was no significant correlation found between lung infarction and RV/LV ratio ($r= 0.06$, $p=0.29$). No correlation was found between mosaic perfusion or lung infarction with PA/AO ratio ($r= 0.01$, $p=0.73$ and $r= -0.02$, $p=0.79$ respectively).

Bronchial circulation

Dilated bronchial arteries were found in 78% of patients. Bronchial artery dilatation showed a weak statistical association with mosaic perfusion ($r= 0.12$, $p=0.035$). Bronchial artery dilatation showed no statistical association with infarction ($r= 0.02$, $p=0.72$).

No statistically significant correlation was identified for either age or sex with different chronic PE distributions, mosaic perfusion, bronchial artery dilatation or PA diameter.

Parenchymal lung disease

81 of 290 patients (28%) had coexisting parenchymal lung disease. Of the total cohort of CTEPH, emphysema was present in 45 (15.5%), interstitial lung disease 11 (3.8%) and other parenchymal abnormalities in 25 (9%) including air trapping 7 (2.4%), consolidation 4 (1.4%), ground glass 2 (0.7%), bronchiectasis 6 (2.1%), lung cyst 2 (0.7%) and pleural involvement (pleural plaques/effusion) 4 (1.4%).

Mosaic perfusion was present in 53 out of 81 (65%) of patients with parenchymal lung disease compared to 188 out of 209 (90%) of patients without parenchymal lung disease, $p<0.001$. Lung infarction was also less common in patients with parenchymal lung disease and was present in 45 out of 81 patients (56%) compared to 166 out of 209, (79%) of patients without parenchymal lung disease, $p<0.001$.

Extent of lung parenchymal abnormalities on CTPA and RHC measurements

RHC was performed at a median of 0 days (IQR 0 to 1 days) around CTPA. The extent of mosaic perfusion and lung infarction correlated positively with PVR ($r=0.32$, $p<0.001$ and $r=0.24$, $p<0.001$), and negatively with SVO2 ($r=-0.31$, $p<0.001$ and $r=-0.24$, $p<0.001$). Whilst the extent of mosaic perfusion ($r=0.20$, $p<0.001$) correlated with mPAP there was no correlation between infarction severity ($r=0.07$, $p=0.20$) and mPAP. **Table 5.2** and **Figure 5.3** present the one-way ANOVA analysis of the severity levels of mosaic perfusion and lung infarction.

Table 5.2 One-way ANOVA with post-hoc Bonferroni test to identify significant mean differences between groups. The values presented in the table are p-values, indicating the level of statistical significance for each comparison between groups.

CT feature	mPAP	PVR	SVO2	TLCO	RV/LV ratio
Mosaic perfusion	0.002	<0.001	<0.001	NS	<0.001
Infarction	NS	<0.001	<0.001	0.03	NS
Lung disease	NS	NS	NS	0.002	NS
Clot location	0.041	0.034	<0.001	NS	NS
Bronchial arteries	0.03	0.004	<0.001	NS	<0.001

Abbreviations: include pulmonary vascular resistance (PVR), mean pulmonary arterial pressure (mPAP), venous oxygen saturation (SVO2) and predicted transfer factor of the lung for carbon monoxide (TLCO).

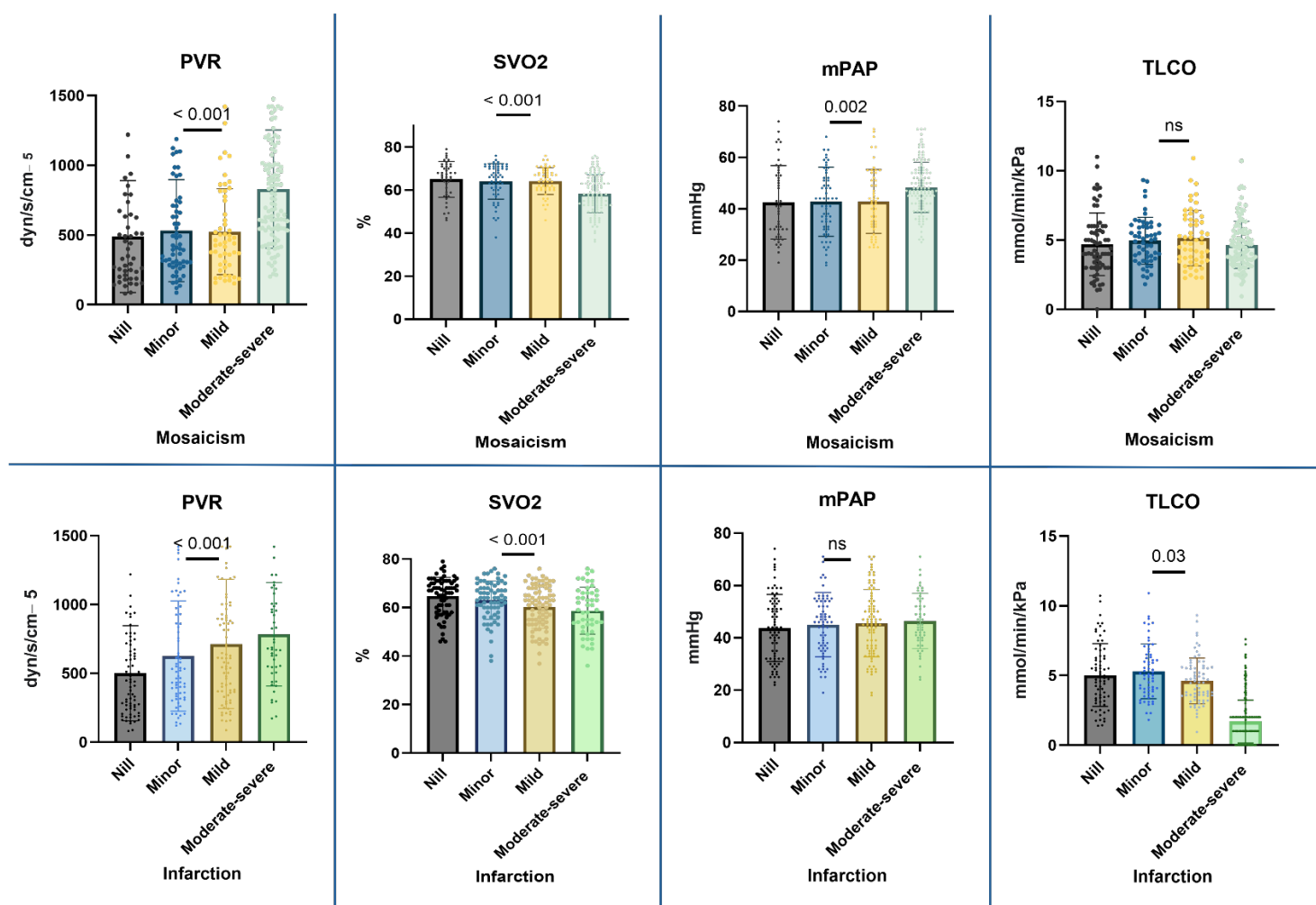


Figure 5.3 Group comparison of the extent of mosaic perfusion (Top) and lung infarction (Bottom) with right heart catheterisation and TLCO using one-way ANOVA. Pulmonary vascular resistance (PVR), mean pulmonary arterial pressure (mPAP), venous oxygen saturation (SVO2), and transfer factor of the lung for carbon monoxide (TLCO).

The extent of lung parenchymal features on CTPA, spirometry and gas transfer measurements

There was no correlation between the extent of mosaic perfusion with FEV1 or FVC ($r = -0.1$, $p = 0.1$ and $r = -0.05$, $p = 0.4$). The extent of infarction showed a weak negative correlation with FEV1 ($r = -0.13$, $p = 0.02$) but not with FVC ($r = -0.07$, $p = 0.25$).

There was no correlation between the extent of mosaic perfusion and TLCO whereas the extent of infarction correlated negatively ($r = -0.15$, $p = 0.015$) with TLCO.

Kaplan-Meier survival and Cox regression analysis for parenchymal, vascular and cardiac CT features

For all patients, the presence of mosaic perfusion was associated with improved survival with 1- and 3-year survival of 90 and 77% compared to 91 and 65%, in patients without mosaic perfusion, respectively, $p = 0.03$. In contrast, the presence of lung infarction had no impact on mortality. For all patients, the presence of parenchymal lung disease was associated with a worse outcome with 1- and 3-year survival of 81 and 61% compared to 93 and 79% in patients without parenchymal disease, respectively, $p = 0.004$. For patients undergoing PEA, there was no significant difference in survival rates at 1 year (97 vs. 96%), 3 years (96 vs. 88%) and 5 years (89 vs. 82%) between those with and without parenchymal lung disease, respectively ($p = 0.98$). For patients not undergoing PEA, the presence of parenchymal lung disease had lower survival rates at 1 year (73 vs. 91%), 3 years (48 vs. 72%), and 5 years (41 vs. 57%) compared to patients without parenchymal lung disease, respectively ($p = 0.008$).

Patients with CTEPH who had pulmonary endarterectomy (PEA) had significantly better survival outcomes than those who did not (log rank = 31.8, $p < 0.001$) (**Figure 5.4**). Kaplan-Meier curves examining the impact of mosaic perfusion, lung infarction, co-existing lung disease and CT measurements on survival in all patients, those undergoing PEA and those not undergoing PEA are presented in **Figure 5.5 and 5.6**. Characteristics of patients and Cox regression analysis of major vessels, and cardiac chambers for patients undergoing and not undergoing PEA are shown in **Tables 5.3 and 5.4**.

Table 5.3 Findings on CTPA images in patients with CTEPH patients. (Data are mean values \pm standard deviations) or counts (percentage). P-values ($P < 0.05$) indicate significant differences between the PEA and No PEA groups.

Variables	Full cohort 290	Endarterectomy 119 (41%)	No Endarterectomy 171 (59%)	P value
Central CTEPH	73 (25%)	26 (22%)	46 (27%)	0.4
Segmental CTEPH	177 (61%)	75 (63%)	102 (60%)	0.64
Subsegmental CTEPH	40 (14%)	18 (15%)	22 (13%)	0.7
Mosaic perfusion	241 (83%)	105 (88%)	136 (80%)	0.07
Lung infarction	211 (73%)	90 (76%)	121 (71%)	0.43
Abnormal Bronchial artery	228 (78%)	90 (76%)	138 (81%)	0.37
Lung disease (Emphysema/Fibrosis/other)	81 (28%) (45/11/25) (16%,4%,9%)	25 (21%) (17/3/5) (14%,3%,4%)	56 (33%) (27/7/22) (16%,4%,13%)	0.03
Lung cavity	11 (3.8%)	6 (5%)	5 (3%)	0.36
Coronary artery disease	189 (65%)	69 (58%)	120 (70%)	0.03
Kidney Disease	21 (7%)	5 (4%)	16 (9%)	0.1
Calcific aortic valve	24 (8%)	7 (6%)	17 (10%)	0.28
Pulmonary artery diameter (centimetre)	3.4 \pm 0.49	3.4 \pm 0.55	3.4 \pm 0.44	0.85
Aorta (centimetre)	3.26 \pm 0.44	3.17 \pm 0.44	3.3 \pm 0.43	0.007
Right ventricle (centimetre)	4.46 \pm 0.68	4.32 \pm 0.7	4.57 \pm 0.67	0.003
Left ventricle (centimetre)	3.52 \pm 0.68	3.6 \pm 0.68	3.48 \pm 0.69	0.16
PA/AO ratio	1.05 \pm 0.17	1.08 \pm 0.17	1.03 \pm 0.17	0.03
RV/LV ratio	1.31 \pm 0.34	1.25 \pm 0.33	1.36 \pm 0.34	0.005

Table 5.4 Univariate and multivariate cox-regression analysis for CT assessed vessels, cardiac changers and parenchymal change in patients undergoing and not undergoing PEA. *Multivariate including significant univariate predictors and with adjustment for age, sex, and pulmonary vascular resistance.

Variables	Univariate analysis			Multivariate analysis*		
Endarterectomy (119)	HR	95% CI	P value	HR	95% CI	P value
Pulmonary artery diameter (centimetre)	1.48	0.79 to 2.79	0.22	NA		
Aorta (centimetre)	8.33	3.38 to 20.5	<0.001	6.93	2.5 to 18.6	<0.001
PA/AO ratio	0.07	0.006 to 0.9	0.04	NA		
Right ventricle (centimetre)	1.53	0.92 to 2.5	0.09	NA		
Left ventricle (centimetre)	0.93	0.56 to 1.5	0.7	NA		
RV/LV ratio	1.7	0.64 to 4.9	0.26	NA		
mosaic perfusion	0.76	0.26 to 2.18	0.6	NA		
Infarction	2.02	0.7 to 5.8	0.19	NA		
Lung disease	1	0.43 to 2.3	0.9	NA		
No endarterectomy (171)	HR	95% CI	P value	HR	95% CI	P value
Pulmonary artery diameter (centimetre)	0.76	0.4 to 1.19	0.24	NA		
Aorta (centimetre)	1.29	0.85 to 1.96	0.22	NA		
PA/AO ratio	0.29	0.09 to 0.93	0.03	NA		
Right ventricle(centimetre)	1.51	1.14 to 2.02	0.004	NA		
Left ventricle(centimetre)	0.6	0.45 to 0.85	0.003	NA		
RV/LV ratio	3.59	2.08 to 6.2	<0.001	3.9	2.2 to 6.9	<0.001
mosaic perfusion	0.75	0.48 to 1.18	0.22	NA		
Infarction	1.09	0.71 to 1.68	0.67	NA		
Lung disease	1.68	1.13 to 2.4	0.009	1.79	1.1 to 2.7	0.005

Abbreviations: Hazard ratio (HR). Confidence intervals (95%CI).

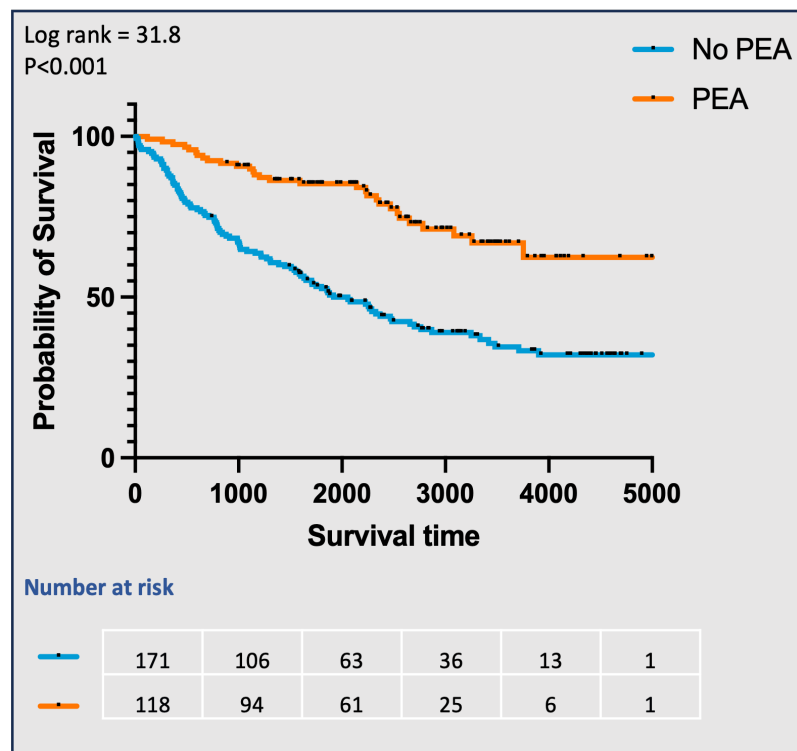


Figure 5.4 Kaplan-Meier survival curve comparing survival outcomes in CTEPH patients who underwent pulmonary endarterectomy (PEA) versus those who did not, for the full cohort.

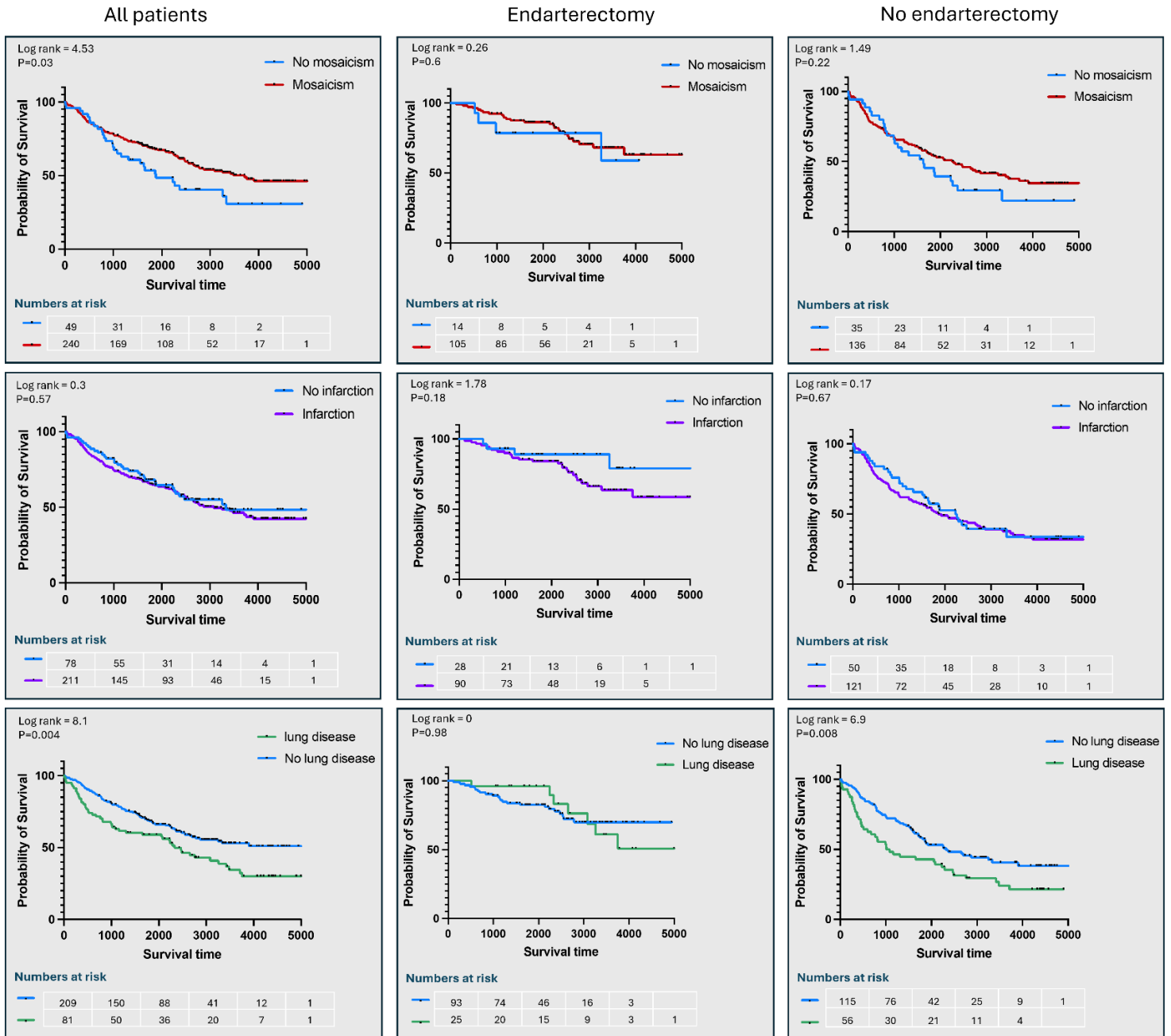


Figure 5.5 Kaplan-Meier survival curve comparing CTEPH patients who underwent pulmonary endarterectomy (PEA) to those who did not. along with additional curves predicting mosaic perfusion, infarction and lung disease related mortality for patients who had PEA and who did not undergo PEA after CT scan. These curves are based on CT scan findings and show numbers at risk by years.

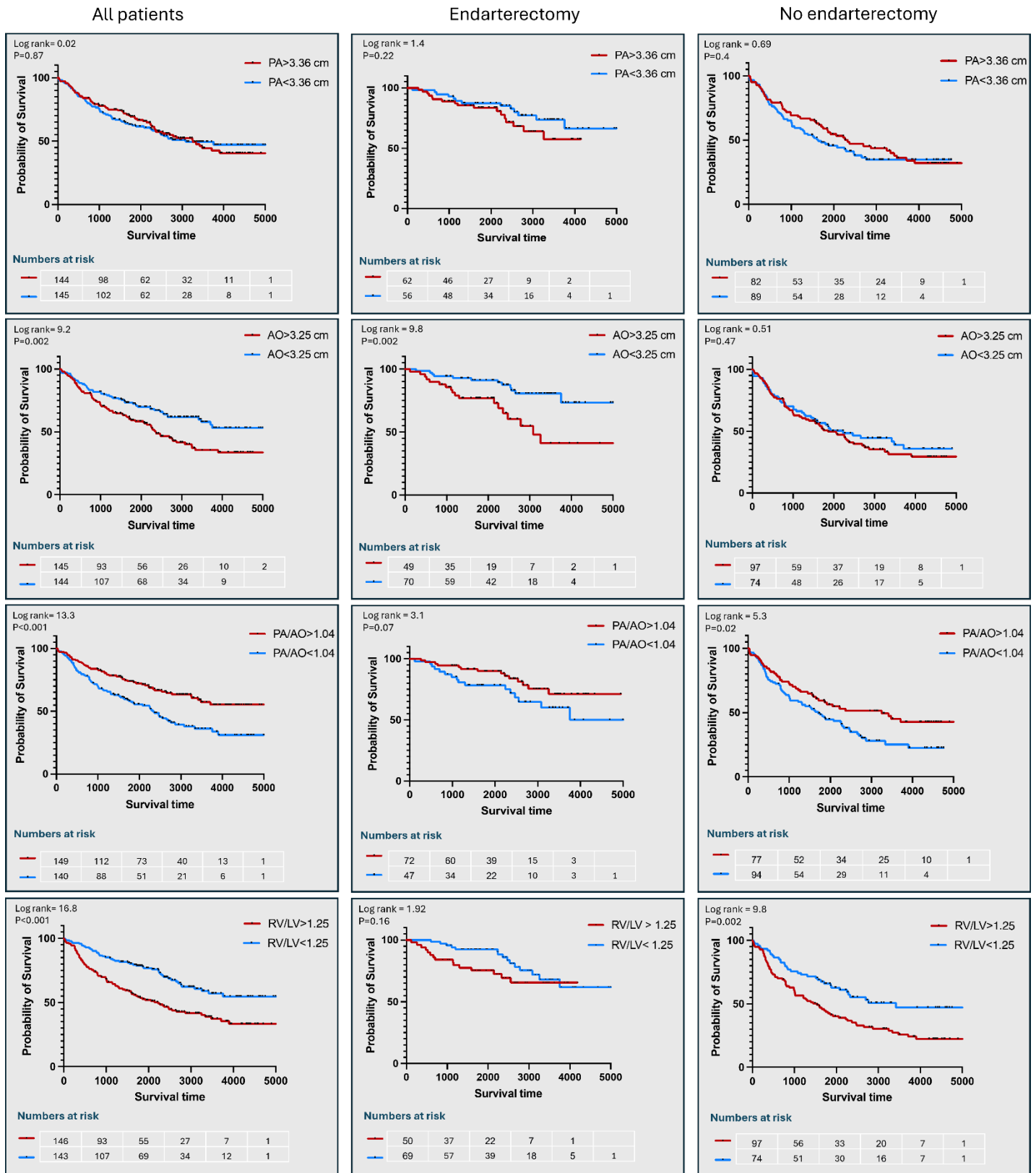


Figure 5.6 The Kaplan-Meier survival curves examining the impact of CTPA measured vessels and cardiac chambers on survival in all patients with CTEPH, those undergoing PEA and those not undergoing PEA. (pulmonary artery (PA), aorta (AO), PA/AO ratio and RV/LV ratio).

5.5 Discussion

In this study we have shown that the presence of parenchymal lung changes on CTPA is common in CTEPH, and we have demonstrated for the first time that it impacts negatively on survival. In addition, to our knowledge we have shown for the first time that an increase in aortic diameter predicts worse outcomes, likely due to the impact of underlying comorbidities. In addition, measurements of vessels and cardiac chambers have prognostic value in CTEPH. We have also confirmed that mosaic perfusion and lung infarction are common features of CTEPH and correlate albeit weakly with indicators of disease severity. This study highlights the value of systematically evaluating vessels, cardiac chambers and the lung parenchyma in patients with CTEPH and the adverse impact of parenchymal lung disease on survival.

Despite a number of registries reporting on the frequency of comorbidities in patients with CTEPH (Pepke-Zaba et al., 2011, Quadery et al., 2018) there is relatively limited published data on CT parenchymal lung disease in patients with CTEPH and their correlation with outcome. A key finding from this study is the high prevalence of co-existing lung disease (28%) noted on imaging in patients with CTEPH including the presence of emphysema in 15.5% and interstitial lung disease in 3.8%. This is higher than the prevalence of chronic obstructive pulmonary disease (COPD) (9.5%) and interstitial lung disease (1.3%) noted in the first International CTEPH Registry (Pepke-Zaba et al., 2011). In patients who meet guideline criteria for IPAH the presence of even minor degrees of lung disease impact negatively on survival (Lewis et al., 2020). In our study, moderate to severe lung disease was associated with the poorest mortality outcomes in both the PEA and non-PEA patients. The absence of patients with severe lung diseases from PEA eligibility is possibly the reason for the increased incidence and severity of parenchymal abnormalities seen in the non-PEA group. As a result, PEA patients with parenchymal abnormalities commonly present with less severe lung disease. However, regardless of PEA intervention, the extent and severity of parenchymal abnormalities remain critical in determining the prognosis of the patient. This is thought to reflect environmental factors, such as smoking, and their impact on the pattern of pulmonary vascular involvement (Olsson et al., 2023). In our study, the presence of lung disease was associated with a worse outcome in patients with CTEPH with the exception of patients

undergoing surgery. However, in the surgical population those with more significant lung disease were excluded due to concerns of increased risk of peri-operative mortality and this is reflected in significantly higher FEV1 and FVC in those undergoing surgery compared to those who did not. Previous studies in patients with CTEPH have identified a number of other comorbidities such as malignancy and chronic kidney disease that were independent predictors of a worse outcome in patients with CTEPH (Quadery et al., 2018), however, the adverse impact of parenchymal lung disease on outcome in CTEPH, has not to our knowledge, been previously reported. For patients with CTEPH, associated CT findings of parenchymal lung disease may reflect additional deleterious pulmonary vascular involvement and loss of the capillary vascular bed. This form of pulmonary vascular involvement may explain why such patients have a worse prognosis. This study highlights the importance of identifying parenchymal lung disease given the negative impact it has on survival.

Our study confirms the finding of previous studies that features such as mosaic perfusion and lung infarction are common in patients with CTEPH. Previous studies have shown significant correlations between the presence of mosaic perfusion and key indicators of disease severity in pulmonary hypertension. Haemodynamic markers such as PVR and TLCO have prognostic value in various forms of pulmonary hypertension, including CTEPH (Quadery et al., 2018, Saouti et al., 2009, Delcroix et al., 2016). In this study, the extent of mosaic perfusion and lung infarction correlated positively with PVR and negatively with SvO₂ consistent with the observation that these imaging characteristics reflect more severe pulmonary vascular disease. Patients with lung infarction compared to those without infarction also had a significantly lower TLCO whereas the presence or absence of mosaic perfusion did not impact on TLCO. In the present study lower TLCO was also associated with the presence of co-existing lung disease. We identified 11 patients with lung cavity (3.8%), the presence of lung cavity was not associated with mortality.

Several studies have explored the correlation between mosaic perfusion and hemodynamic parameters in CTEPH. A study found that in 145 patients with CTEPH, both mPAP and PVR demonstrated a significant correlation with the degree of mosaic perfusion (Leone et al., 2017). Another study showed that in 27 patients with CTEPH, 25 of whom had RHC data, mosaic perfusion had a significant positive correlation with PVR but no correlation with mPAP

(Kasai et al., 2017). Our study showed a significant though modest correlation between mosaic perfusion with mPAP, PVR and SVO₂. In addition to confirming the association of mosaic perfusion with disease severity, we have also shown that lung infarction is associated with more severe haemodynamic disease but also abnormalities of gas exchange, reflected in a lower TLCO.

It has been noted that patients with CTEPH without mosaic perfusion exhibit a higher mortality than patients with mosaic perfusion, although the rationale for this is not clear. We postulate this may in part be due to the higher incidence of co-existing parenchymal lung disease in patients without mosaic perfusion. In addition to the association of lung disease with more widespread vascular damage, parenchymal lung disease by impacting on lung attenuation may mask the detection of mosaic perfusion. Our findings suggest that for patients undergoing PEA, the presence of mosaic perfusion or infarction does not significantly impact all-cause mortality. While in patients not undergoing PEA, the absence of mosaic perfusion is associated with increased mortality, likely relating to the higher proportion of patients with parenchymal lung disease in this group. However, in patients without lung disease, the extent of mosaic perfusion did not predict mortality. These findings highlight the importance of comprehensively assessing both vascular and parenchymal abnormalities in patients with CTEPH.

Finally, we have shown that CTPA features of vessels and cardiac chambers have prognostic value in patients with CTEPH. In particular, we have shown that an increase in RV diameter and an increase in RV/LV ratio predict a worse outcome in patients with CTEPH regardless of whether patients undergo or do not undergo PEA. The adverse prognostic impact of an increased RV:LV ratio has been demonstrated in other forms of PH, but to our knowledge it is the first time it has been observed in a large cohort of patients with CTEPH (Doğan et al., 2015, Forfia et al., 2006). It is known that more severe haemodynamic disease, characterised by severe increases in PVR identify patients with CTEPH at high risk of surgical intervention (Mayer et al., 2011), whether an elevation for RV:LV ratio over a particular threshold could also be used to identify a high-risk group requires further exploration. We have also shown that an increased aortic diameter predicts a worse outcome in CTEPH regardless of whether patients underwent PEA. An increase in aortic diameter occurs with increasing age but is also

a marker of other comorbidities such as hypertension. In CTEPH a large left atrium (frequently the sequelae of systemic hypertension) is a risk factor for a worse outcome following PEA (Shahin et al., 2022). Lower PA/Ao ratio was found to be a risk factor for worse outcome in those not undergoing endarterectomy, we suspect this may again be driven by the relative increase in aortic diameter, though further studies are required to confirm. Given that left heart disease may be unmasked following PEA, and the left atrial size and pulmonary arterial wedge pressure measurement may be less reliable markers of left heart disease in the presence of high right sided pressures, further exploration of the aortic diameter as a risk factor in patients with CTEPH requires further study.

There are a number of limitations in this study. Patients were retrospectively identified from a single centre and a number of the CT assessments are qualitative and were read by a single experienced Radiologist. Further work to evaluate the utility of imaging derived lung patterns for prediction of outcomes following BPA is required. Surgical resection rates were 41% for this population similar to the 43% in the UK as reported in the 14th UK National Audit of pulmonary hypertension of 4103 patients with CTEPH undergoing evaluation; suggesting that this population is representative of the UK CTEPH population.

In conclusion, systematic assessment of patients with CTEPH undergoing CTPA highlights that mosaic perfusion, lung infarction and parenchymal lung disease are commonly observed. Parenchymal lung disease and CT features of more severe pulmonary hypertension impact negatively on survival regardless of whether patients undergo pulmonary endarterectomy and should be considered when counselling patients.

6 CT scoring system to Defined Thrombus Distribution in Chronic Thromboembolic Pulmonary Hypertension

***Peer-reviewed journal article submitted in BJR (2025)**

Contribution: First author. My main contributions were completing extensive literature reviews, carrying out statistical analyses, and developing the tables and figures included in the research and integrating future amendments based on input and recommendations from my co-authors. In addition, I was responsible for the systematic labelling of thromboembolic disease across all CTPA cases and performed detailed image reviews to ensure the consistency and accuracy. I also designed and implemented a structured scoring system to standardise disease assessment, which was applied across the dataset to support robust and reproducible analysis.

Authors

L. Abdulaal^{1,6}, M.J. Sharkey¹, A. Maiter^{4,5}, S. Alabed^{1,3,4}, K. Dwivedi^{1,3}, S. Rajaram⁵, R. Condliffe², D.G. Kiely^{2,3,4}, and A. J. Swift^{1,3,4}*

1. Division of Cardiovascular Medicine, University of Sheffield
2. Sheffield Pulmonary Vascular Disease Unit, Sheffield Teaching Hospitals NHS Foundation Trust
3. INSIGNEO, Institute for in silico Medicine, The University of Sheffield, Sheffield, United Kingdom.
4. National Institute for Health and Care Research, Sheffield Biomedical Research Centre, Sheffield, UK
5. Radiology Department, Sheffield Teaching Hospitals NHS Foundation Trust.
6. Faculty of Applied Medical Science, King Abdulaziz University, Jeddah, Saudi Arabia.

6.1 Abstract

Objective: Characterisation of thrombus is important for guiding treatment in chronic thromboembolic pulmonary hypertension (CTEPH). This study presents a novel scoring system for visual assessment of CTEPH on CT pulmonary angiography (CTPA), incorporating both disease location and extent to determine the impact on survival outcomes.

Methods: Patients with CTEPH were identified retrospectively from the ASPIRE registry. The scoring system emphasises disease based on their predominant location as central, segmental and distal disease. Survival analysis was conducted using Cox-regression and Kaplan–Meier survival curves.

Results: 208 patients with CTEPH were included (mean age 66 ± 13.6 years, 52.4% female). Mosaic perfusion and infarction were commonly seen in patients with distal disease (92% and 88%). The severity score demonstrated a statistically significant correlation with haemodynamics ($p < 0.001$), higher severity scores were associated with elevated pulmonary vascular resistance, reduced mixed venous oxygen saturation and cardiac index. Central and distal disease showed similar survival, whereas survival was worse in central compared to segmental disease for all patients ($p < 0.001$), including those undergoing ($p < 0.04$) and not undergoing endarterectomy ($p < 0.001$). Central disease was an independent predictor of mortality in those not undergoing endarterectomy (hazard ratio 1.9, $p < 0.01$).

Conclusion: Our scoring system showed excellent interobserver agreement. Thromboembolic disease location was shown to be a predictor of mortality, with central disease independently associated with shorter survival in patients not undergoing pulmonary endarterectomy.

Advances in knowledge: This is a novel scoring system for characterising CTEPH on CTPA, considering disease location and extent. It provides disease location as a predictor of survival, introducing a new framework for patient stratification and clinical decision-making.

6.2 Introduction

Chronic thromboembolic pulmonary hypertension (CTEPH) occurs in approximately 2% of patients following acute pulmonary embolism (PE) due to incomplete resolution of thrombus within the pulmonary arteries (Klok et al., 2020). Accurate and early diagnosis of CTEPH is increasingly important given the growing number of therapeutic options available (Konstantinides et al., 2020). Identifying the optimal therapeutic strategy for managing CTEPH poses a significant challenge, and patients often undergo a number of investigations to assess their thrombus burden, severity of pulmonary hypertension and comorbidities (Pepke-Zaba et al., 2011, Quadery et al., 2018). In particular, characterisation of thromboembolic disease, including location and extent is important for determining suitability for and predicting the success of pulmonary endarterectomy and balloon angioplasty (He et al., 2012). Addressing the precise localisation of thromboembolic and the relationship with disease severity may provide essential insights into the pathogenesis of CTEPH, facilitating risk stratification and treatment management.

The current preferred method for confirming suspected CTEPH is CT pulmonary angiography (CTPA), which allows not only for assessment of specific abnormalities in CTEPH – such as intraluminal stenosis, webs and eccentric thrombus within the pulmonary arteries – but also for evaluation of lung parenchymal and cardiac changes (Gopalan et al., 2017, Simonneau et al., 2017, Delcroix et al., 2021). However, assessing chronic thromboembolic disease on CTPA can present significant challenges. CTPA interpretation requires extensive experience due to the potential for misinterpretation of subtle abnormalities, which can result in diagnostic delays or inappropriate management (Lambert et al., 2022).

The scoring system refers to a standardised tool to quantitatively assess specific findings on imaging evaluations, with the potential to enhance interobserver agreement and ensure consistent assessment of CTEPH for accurate clinical decisions. Several widely used scoring systems have previously been developed to characterise thromboembolism on CTPA in acute PE. These have incorporated the number and size of emboli, their location within the pulmonary vasculature, and their influence on haemodynamics (Qanadli et al., 2001, Mastora

et al., 2003). Scoring systems for evaluating CTEPH are infrequently used in routine clinical practice due to their complexity and dependence on modern imaging technology. Dual-Energy CT (DECT) scans, for example, are designed to detect and quantify perfusion abnormalities in the lungs, which are frequently associated with haemodynamic parameters to determine disease severity and operability (Takagi et al., 2016, Renapurkar et al., 2024). However, to our knowledge, no scoring system has been developed for the characterisation of chronic thromboembolic disease on CTPA in CTEPH.

This study aimed to characterise chronic thromboembolic disease features on CTPA in patients with CTEPH and assess their relationship with disease severity and survival outcomes.

6.3 Methodology

This retrospective study received ethical approval from our institution with consent waived and the National Research Ethics Service (16/YH/0352).

Study population

Patients were identified through the ASPIRE (Assessing the Spectrum of Pulmonary Hypertension Identified at a Referral Centre registry) database from January 2008 to January 2018 (Hurdman et al., 2012). ASPIRE comprises de-identified data obtained during routine clinical care from patients who have undergone evaluation for suspected pulmonary hypertension at the Pulmonary Vascular Disease unit. The research included adult patients aged ≥ 18 years who underwent CTPA and met guideline criteria for a diagnosis of CTEPH (Humbert et al., 2022). Patients who underwent pulmonary endarterectomy or received medical therapy were included. Balloon pulmonary angioplasty (BPA) was not nationally commissioned in the UK until 2018 and therefore no patients underwent this intervention during the conduct of the study. Patients who had external CTPA performed in other institutions and those who had severe artefacts were excluded.

CTPA protocol

CTPA scans were conducted utilising multidetector scanners (TOSHIBA Aquilion PRIME and GE Medical Systems) with the following standard acquisition parameters: a tube current ranging from 80 to 700 mA with automatic dose reduction, tube voltage of 120 kV, pitch of 1, slice thickness of 0.5 mm, and a rotation speed of 0.275. Intravenous contrast media (Omnipaque 350, GE Healthcare) was administered at a rate of 5 ml/s with a total volume of 60 ml. Bolus tracking was performed in the pulmonary artery utilising a manual fast start, initiating image acquisition when contrast reached the predefined threshold of 220 Hounsfield units (HU).

Data collection

The demographics, clinical, and laboratory information of the patients were collected from an electronic medical database and document reviews. In addition to the CTPA studies, the following data were also retrieved for each included patient where available.

1. Pulmonary function tests (PFTs). Baseline forced vital capacity (FVC), Forced expiratory volume (FEV) and transfer factor of the lung for carbon monoxide (TLCO) closest to the date of RHC.
2. Right heart catheterisation (RHC) data. RHC was undertaken using a balloon tipped 7.5-F thermodilution catheter (Becton-Dickinson, Franklin Lakes, New Jersey). Mean pulmonary artery pressure (mPAP) and pulmonary arterial wedge pressure (PAWP) were measured by fluid filled pressure. Cardiac output (CO) was measured using the thermodilution technique. PVR was determined as follows: $PVR = (mPAP - PAWP)/CO$. Cardiac index (CI) was corrected for the patient's body surface area (BSA): $CI = CO/BSA$. Right heart catheterisation was obtained from the ASPIRE registry.
3. Mortality data obtained from the NHS Personal Demographics Service at the time of census. All pulmonary hypertension patients getting treatment are subjected to routine follow-up in accordance with the national service guidance.

Image analysis

Two observers independently evaluated the CTPA images, blinded to clinical information and patient demographic to minimise the risk of interpretation bias. The evaluations were conducted using MIM software, which was employed for clot segmentation and analysis. In addition to disease location, the observers recorded other relevant CTEPH-related features, such as lung parenchymal abnormalities, including mosaic attenuation, bronchial artery changes, and infarction. CT axial plane was used for all CT cardiac measurements including the maximum diameters of the ascending aorta (AO), pulmonary artery (PA), the right and left ventricles (RV and LV). Then, the RV/LV and PA/AO ratios were calculated for each patient as part of the analysis.

The scoring system is designed to classify chronic thromboembolic disease based on their predominant location in the pulmonary arterial tree, providing uniformity and clarity in determining the severity and anatomical extent of CTEPH. The score mainly represents a simplified method for visual assessment of disease distribution and highlights the predominant location of CTEPH involvement. Each location is associated with a score that reflects the number of diseases present within a specific range.

Chronic thromboembolic disease location within the pulmonary vasculature was classified as follows according to conventional anatomical descriptions (**Figure 6.1**). "**Central**" disease was defined as a thromboembolic involvement in the main pulmonary artery, in addition to the proximal segments of the left and right pulmonary arteries (including mid and distal in the main branches). Patients identified as having central disease may also have had disease in segmental and distal arteries, but when central involvement was present, patients were defined as having central disease regardless of extent of clot burden elsewhere. "**Segmental**" was defined as disease in the branches distal to the central arteries, beginning at the lobar arteries. Patients with segmental disease may also have had distal involvement, but the dominant feature was segmental (higher score than distal). "**Distal**" involves the smaller, more peripheral subsegmental arteries. Patients with distal disease may also have segmental involvement, but the dominant characteristic is distal.

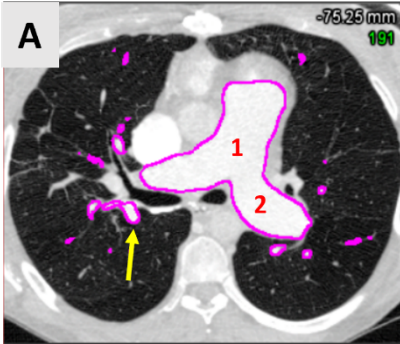
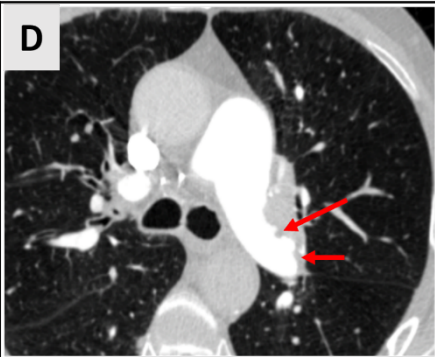
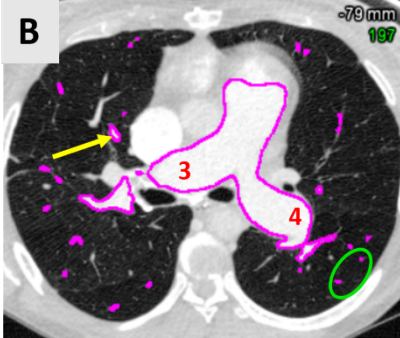
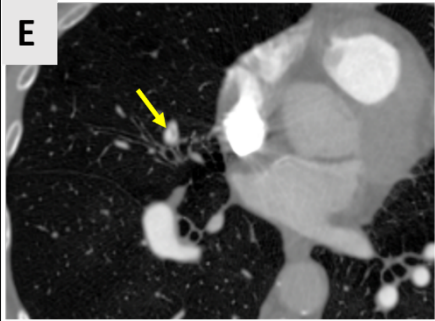
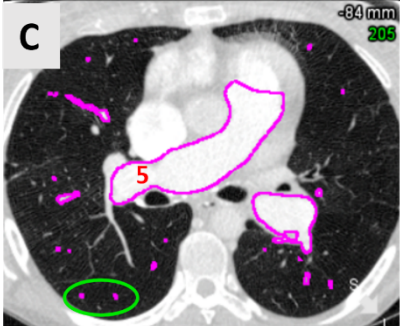
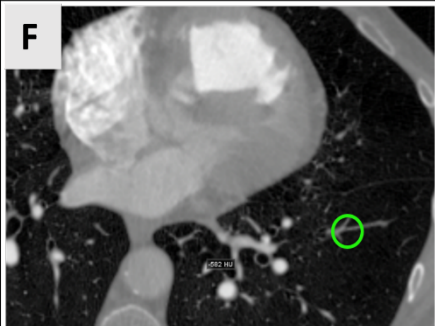
1 Location classification	2 Disease classification	3 Severity classification	
<div>A</div> 	<div>D</div> 	<div>“Central CTEPD”</div> <div>Any central disease</div>	<div>Minor</div> <div>(Total Score: 1–3)</div> <div>or</div>
<div>B</div> 	<div>E</div> 	<div>“Segmental CTEPD”</div> <div>No central disease</div> <div>Segmental CTEPD ≥ Distal CTEPD</div>	<div>Mild</div> <div>(Total Score: 4–6)</div> <div>or</div>
<div>C</div> 	<div>F</div> 	<div>“Distal CTEPD”</div> <div>No central disease</div> <div>Segmental CTEPD < Distal CTEPD</div>	<div>Moderate</div> <div>(Total Score: 7–9)</div> <div>or</div> <div>Severe</div> <div>(Total Score: 10–13)</div> <div>Combined for analysis.</div>

Figure 6.1 Axial chest CTPA slices illustrate chronic thromboembolic disease location, disease and severity classifications into central, segmental and distal subgroups (each column includes three different slices from a single patient). (A) In location classification, central included the main pulmonary artery (1) as well as the midsection of the main pulmonary artery (2 and 3) and distal aspect of the main pulmonary artery (4 and 5) of both the left and right main pulmonary arteries. (B) Segmental location, 10 segments on the right and 9 on the left (yellow arrows). (C) The presence of distal was assessed at distal segmental locations 10 segments on the right and 9 on the left (Green circle). In disease classification, (D) there is extensive central mural disease present involving both main pulmonary arteries and extending primarily into the lower lobe arteries bilaterally (red arrow). (E) In the right middle lobe, there is complex web formation at the origin of the lateral segmental branches (yellow arrow). (F) On the left side there are subsegmental attenuated vessels showing chronic thromboembolic disease (green circle). If any central disease is identified the patient is classified as having ‘central’ chronic thromboembolic disease. In the absence of central disease, segmental and distal are classified by the score weighting towards either category.

Step 1 (central arteries): evaluate central based on disease involvement in the five main central pulmonary artery locations. Assign one point for each thrombus in central, Calculate the score as the sum of all involved locations, with a maximum score of 5.

Step 2 Determine the predominant non-central classification: evaluate the segmental and distal scores if there is no central disease involvement (Central Score = 0). Segmental and distal classifications were simplified using 19 pulmonary arteries for each location. This approach simplifies the original scheme (19 segmental and 19 distal branches) into a more standardised framework. The scoring system for chronic thrombi operates on a simple quantitative categorisation, by assessing the number of thrombi within a specific range and assigning a corresponding score based on predefined intervals:

1. **Score of 1:** Assigned when the thrombi count is between 1 and 5.
2. **Score of 2:** Assigned when the thrombi count is between 6 and 10.
3. **Score of 3:** Assigned when the thrombi count is between 11 and 14.
4. **Score of 4:** Assigned when the thrombi count is between 15 and 19.

Then, assess the differences between the segmental and distal scores, using the higher score as the predominant score.

Step 3 Calculate the Total Score: Combine all three locations to calculate the total score:

Total Score = Central Score+ Segmental Score+ Distal Score.

Maximum Total Score: 5 (Central)+4 (Segmental)+4 (Distal)=13 (predominant location).

Clinical example:

- Central disease in 0 locations → **Central Score = 0.**
- Segmental disease in 15 arteries → **Segmental Score = 4.**
- Distal disease in 5 arteries → **Distal Score = 1.**
- **Total Score = 0 (Central) + 4 (Segmental) + 1 (Distal) = 5 (segmental).**
- The classification as segmental overall based on segmental disease having the higher score (4) than distal disease (1), which prioritises the location with the higher score if no central disease.

The total score can be grouped into four categories based on severity and extent of the chronic thromboembolic disease: **Minor (Total Score: 1–3)** reflects minimal disease involvement. **Mild (Total Score: 4–6)** represents a moderate disease distribution. **Moderate (Total Score: 7–9)** indicates significant disease involvement affecting multiple regions. Finally, **Severe (Total Score: 10–13)** highlights extensive disease widespread distribution. All patients within the severe group by definition have central disease in addition to segmental and distal disease in order for their total score to be 10 or more. This is due to the fact that segmental and distal disease is unable to achieve the threshold score of 10 under the scoring methodology employed in this study. If central involvement is absent (Central Score = 0), classification is based on the higher score between segmental and distal disease. When both are present, their combined score (e.g., 4 + 4 = 8) places the patient in the severe category (Total Score: 10–13) if central disease is present; otherwise, a total score of 8 categorised into moderate (Total Score: 7–9). This system provides a structured way to evaluate and grade disease presence and severity, offering a standardised method for categorisation in clinical research settings.

In a blinded sub-study, the CTPA of 20 patients with CTEPH was assessed by two observers with different levels of CT imaging experience (AS, 13 years as a cardiothoracic radiologist and LA, a radiographer with 8 years of experience). This sub-study, as part of the overall research, aimed to evaluate interobserver agreement and validate the robustness and consistency of the scoring system across different levels of imaging expertise.

Statistical analysis

Statistical analyses were conducted using SPSS Statistics (version 27, IBM) and GraphPad Prism (v10; GraphPad, La Jolla, CA, USA), with a significance threshold of $p < 0.05$. The main goal of the study was to examine a disease location for CTEPH assessment. To achieve this, we examined the correlations between chronic thromboembolic disease location and several clinical and hemodynamic metrics using Spearman's correlation coefficient with 95% confidence intervals. Descriptive statistics are presented as the mean \pm standard deviation (SD) or median and interquartile range (IQR) for continuous variables, and as percentages and frequencies for categorical data. Comparison of total scoring disease severity groups (i.e.,

minor, mild, and moderate-severe) were performed using a one-way ANOVA with post-hoc Bonferroni correction. Due to the small number of patients in the severe group ($n = 7$), they were merged with the moderate group for analysis, forming a combined "moderate-severe" category. Interobserver agreement was measured using Cohen's weighted κ (linear weights) for categorical variables, in addition to intraclass correlation coefficient (ICC) for continuous variables. Kappa value was interpreted using the thresholds defined by McHugh(2012): as 0.01–0.20 indicates slight agreement, (0.21–0.40) fair agreement, (0.41–0.60) moderate agreement, (0.61–0.80) substantial agreement, and (0.81–0.99) for excellent agreement (McHugh, 2012). The ICC values were interpreted as follows according to established thresholds: (< 0.50) indicated poor agreement, (0.50 - 0.75) fair or moderate agreement, (0.75 - 0.90) moderate to good agreement, (> 0.90) indicated excellent agreement (Koo and Li, 2016). Correlations between disease location and severity were evaluated by Cox regression and Kaplan-Meier analysis.

6.4 Results

Patient population

A total of 208 patients with CTEPH were included in the study (mean age 66 ± 13.6 , 52.4% female) (**Figure 6.2**). Of these 195 patients (94%) had available RHC data and 185 patients (89%) had available PFT data. Their clinical characteristics are summarised in full in **Table 6.1**. 37% (77/208) had central chronic thromboembolic disease, 38% (80/208) had segmental disease, and 25% (51/208) had distal disease. Of the patients, 18 (9%) were categorised as WHO Functional Class (FC) II, 165 (79%) as WHO FC III, and 21 (10%) as WHO FC IV.

The chronic thromboembolic disease scores were categorised into four groups based on the severity of the disease. The distribution of patients across these groups was as follows: 64 (31%) patients were classified as minor, 92 (44%) as mild, 45 (22%) as moderate, and 7 (3%) as severe. By combining the moderate and severe groups, a total of 52 (25%) patients were classified as moderate-severe disease ($45 + 7 = 52$). When grouped by severity score, patients with moderate-severe disease demonstrated significantly higher PVR ($p < 0.001$) and lower cardiac index ($p < 0.001$).

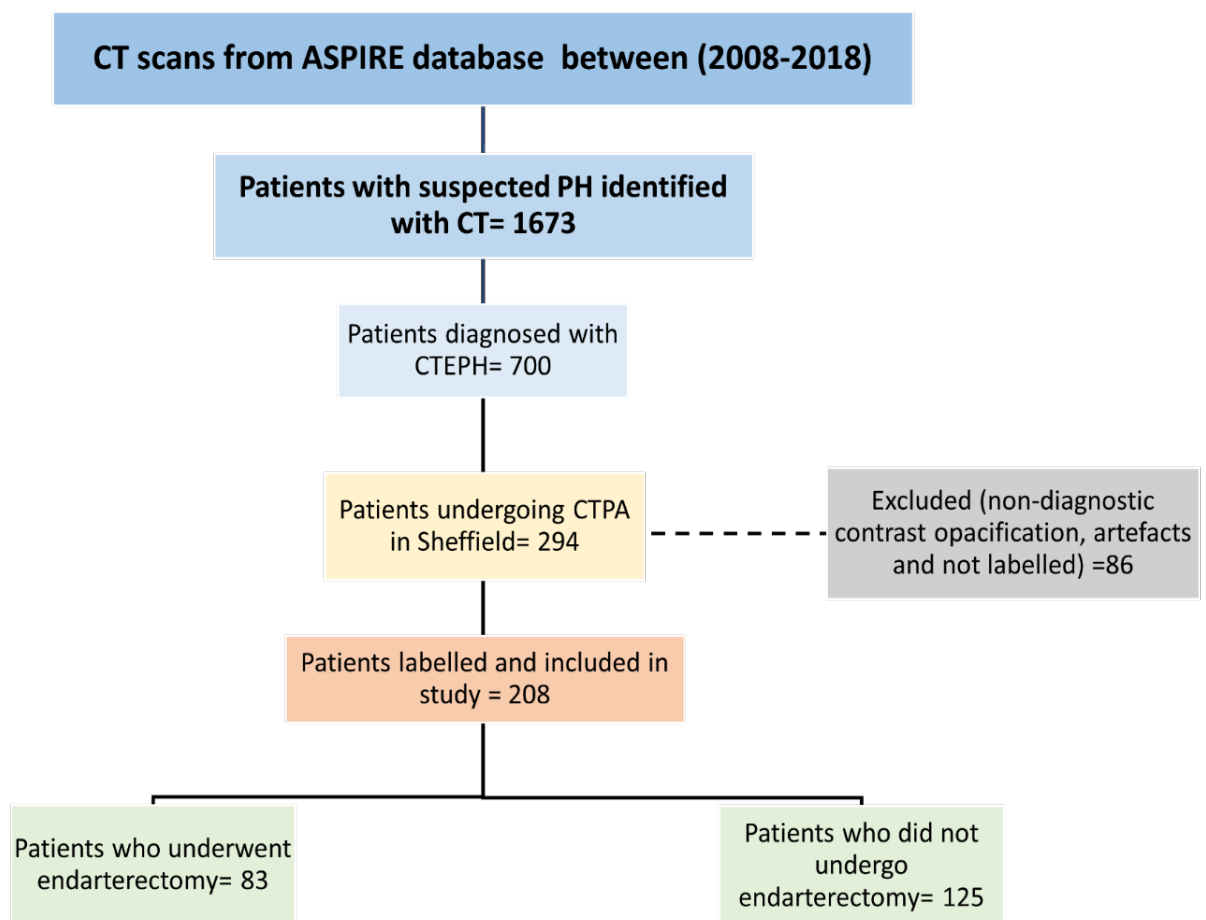


Figure 6.2 Study flow diagram.

Table 6.1 Characteristics of patients who underwent right heart catheterisation and pulmonary function tests, comparing those who had pulmonary endarterectomy (PEA) versus those who did not (No PEA), as well as comparing patients with central, segmental, and distal CTEPD. Data are expressed as mean \pm standard deviation or counts (percentage). P-values ($P < 0.05$) indicate statistically significant differences between the PEA and No PEA groups and between the three groups of CTEPD respectively. (*) indicates that a result is significantly different from the "central" reference, (#) indicates a significant difference from the "segmental" reference, and (^) indicates a significant difference from the "distal" reference.

Patient characteristics	Full cohort 208	PEA 83(40%)	No PEA 125(60%)	P value	Central 77(37%)	Segmental 80(38%)	Distal 51(25%)	P value
Age (years)	66 \pm 13.6	62 \pm 13.01	68 \pm 13.6	0.002	67.2 \pm 12.8	64.7 \pm 13.2	65.5 \pm 15.5	0.51
Sex (Female)	109(52%)	46(55%)	63(50%)	0.48	36(47%)	42(53%)	31(61%)	0.3
WHO FC	II (18), III (165), IV (21)	II (3), III (70), IV (8)	II (15), III (95), IV (13)	0.16	II (3), III (62), IV (11) #	II (12), III (67), IV (1)*^	II (3), III (36), IV (9) #	<0.001
Mosaic perfusion	177(85%)	77(93%)	100(80%)	0.01	66 (86%)	64 (80%)	47(92%)	0.16
Infarction	159(76%)	67(81%)	92(74%)	0.23	63(82%) #	51(64%)*^	45(88%) #	0.002
Lung disease	57(27%)	16(19%)	41(33%)	0.03	24(31%)	25(31%)	8(16%)	0.09
Coronary artery disease	140(67%)	51(61%)	89(71%)	0.14	56(73%)	51(64%)	33(65%)	0.44
RHC	195(94%)	78(94%)	117(94%)	P value	69(90%)	77(96%)	49(96%)	P value
PVR (wood unit)	8.5 \pm 5.4	9.07 \pm 5.4	8.1 \pm 5.4	0.22	9.9 \pm 5.9#	6.3 \pm 3.7*^	10 \pm 6.06#	<0.001
mPAP (mmHg)	46 \pm 12.01	47.4 \pm 11.2	45 \pm 12.4	0.15	47.4 \pm 12.6	44.6 \pm 12.7	45.8 \pm 9.5	0.34
PAWP (mmHg)	12.1 \pm 4.6	12.2 \pm 4.4	12.1 \pm 4.8	0.89	12.5 \pm 4.5	12.5 \pm 5	11.09 \pm 4	0.29
SVO2 (%)	61.5 \pm 8.7	62 \pm 8.3	61.3 \pm 9	0.62	58.5 \pm 9.3#	65 \pm 6.4*^	60.3 \pm 9.4 #	<0.001

SaO2 (%)	93.2±3.8	92.7±4.1	93.5±3.5	0.2	93±4	93.4±3.6	92.9±3.8	0.73
CI (L/min/m2)	2.5±0.87	2.5±0.85	2.6±0.89	0.3	2.4±0.95#	2.9±0.83* ^	2.3±0.66 #	<0.001
PFT	185 (89%)	77 (93%)	108 (86%)	P value	70 (91%)	69 (86%)	46(90%)	P value
Predicted FEV1 (%)	76.8±20.2	80.5±18.7	74.1±20.8	0.03	75.8±21.5	76.5±18.8	78.7±20.5	0.73
Predicted FVC (%)	90.2±22.5	93.5±21.3	87.9±23.1	0.09	89.5±23.3	89.4±22.2	92.3±22	0.75
Predicted TLCO (%)	61±18.5	61.3±15.9	60.2±20.3	0.69	56.5±21#	65.9±15.4 *	59±17.2	0.009

Abbreviations: right heart catheterisation (RHC): pulmonary vascular resistance (PVR), mean pulmonary arterial pressure (mPAP), pulmonary artery wedge pressure (PAWP), venous oxygen saturation (SvO2), arterial oxygen saturation (SaO2), cardiac index (CI), and cardiac output (CO). Pulmonary function tests (PFT): predicted forced expiratory volume in one second (FEV1), predicted forced vital capacity (FVC), and predicted transfer factor of the lung for carbon monoxide (TLCO).

Interobserver agreement

The agreement among observers for the detection of 20 patients with CTEPH was 89% for central location, 80% for segmental, and 66% distal. Kappa values and intraclass correlation coefficients were utilised to evaluate interobserver agreement for disease location and extent assessment, as presented in **Table 6.2**.

Table 6.2 Interobserver reliability kappa (κ) and interclass coefficient (ICC) between observers (R1 and R2) in CT imaging to determine the number and location of CTEPH.

Disease location	R1-R2 _ K(95%CI)
Central clot ICC	0.97 (0.92-0.98)
weighted kappa	0.89 (0.74-1)
Segmental ICC	0.93 (0.83-0.97)
weighted kappa	0.8 (0.62-0.99)
Distal ICC	0.88 (0.63-0.96)
weighted kappa	0.66 (0.46-0.86)
Total abnormal ICC	0.92 (0.82-0.97)
weighted kappa	0.78 (0.58-0.98)

CT, RHC and lung function measurements

Table 6.3 presents the correlations found between chronic thromboembolic location with CT measurements (RV/LV and PA/AO ratios), mosaic perfusion and infarction.

Patients with central and distal disease had more severe pulmonary haemodynamics and lower TLCO but similar spirometry to those with segmental disease ($p<0.001$), **Table 6.1**.

In all 208 patients, highly significant statistical differences were demonstrated between the score system (disease severity) and the hemodynamic parameters (PVR, Svo₂ and cardiac index), with ($p<0.001$). Patients with moderate-severe disease demonstrated significantly higher PVR and lower cardiac index (**Figure 6.3**).

Table 6.3 Spearman's correlations between disease locations severity and CT measurements, including RV/LV and PA/AO ratios, as well as the presence of mosaic perfusion or infarction.

Disease location	RV/LV ratio	PA/AO ratio	Mosaic perfusion	Infarction
Central	$r=-0.07, p=0.27$	$r=0.19, p=0.009^*$	$r=0.85, p=0.08$	$r=0.09, p=0.21$
Segmental	$r=-0.1, p=0.01^*$	$r=0.05, p=0.43$	$r=-0.1, p=0.09$	$r=-0.2, p<0.001$
Distal	$r=0.1, p=0.12$	$r=-0.07, p=0.28$	$r=0.27, p<0.001$	$r=0.17, p=0.01$
Total	$r=0.14, p=0.04$	$r=0.06, p=0.36$	$r=0.19, p=0.009^*$	$r=0.22, p=0.003$

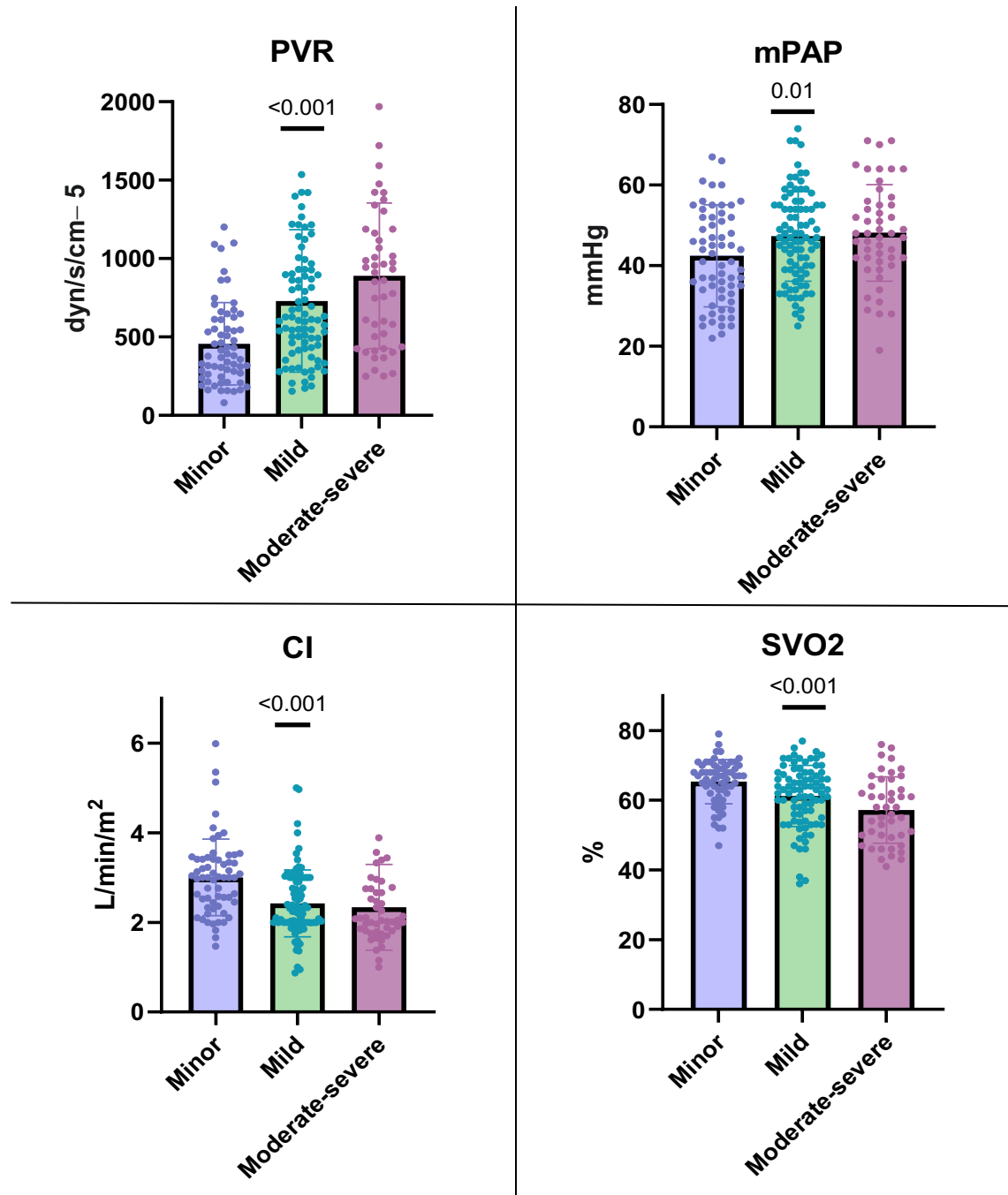


Figure 6.3 Group comparison of the right heart catheterisation with total abnormal CTEPD using one-way ANOVA. Pulmonary vascular resistance (PVR), mean pulmonary arterial pressure (mPAP), venous oxygen saturation (SVO2) and cardiac index (CI). Minor: Low clot burden.

Survival of patients according to disease location

Endarterectomy was performed in 40% (83/208) patients, at a median time of 7 months (IQR 0 to 11) from CTPA. Notably, there were no instances of patients being lost to follow-up during the study period.

The results of the Kaplan-Meier survival analyses are shown in **Figure 6.4**. Patients with central and distal disease demonstrated similar survival rates. Survival rates were worse for patients with central disease compared to segmental disease for all patients ($p < 0.001$), those undergoing endarterectomy ($p < 0.04$) and those not undergoing endarterectomy ($p < 0.001$).

Predictors of using univariate and multivariate Cox regression

Multivariate Cox-regression adjusting for age, sex and haemodynamics parameters (mPAP, PVR) is shown in **Table 6.4**. Whereas central disease remained an independent predictor of a worse outcome in those not undergoing endarterectomy (hazard ratio (HR) 1.9, $p < 0.01$), its presence did not impact on survival in those having endarterectomy.

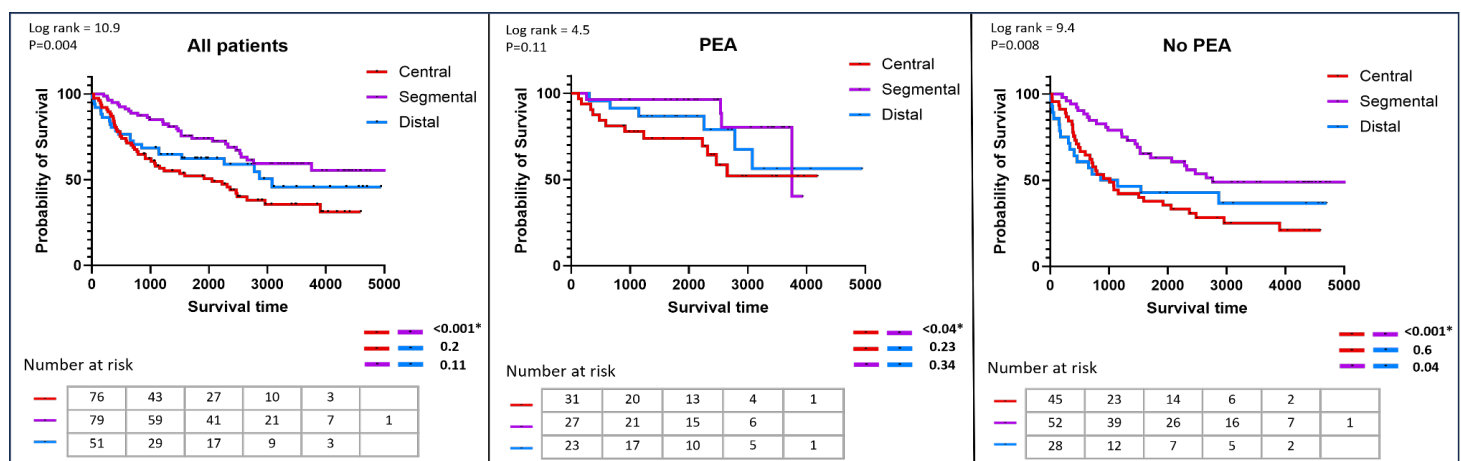


Figure 6.4 Kaplan–Meier survival curves for each location (central, segmental and distal) in CTEPH patients, comparing the pulmonary endarterectomy (PEA) group with the non-surgical (no PEA) group. P-values ($P < 0.05$) indicate statistically significant differences between the subgroups of CTEPD respectively. (Red-Purple) indicates that "central" is significantly different from the "segmental", (Purple-Blue) indicates a significant difference between "segmental" and "distal" CTEPD, and (Red-Blue) indicates the difference between "central" and "distal".

Table 6.4 Univariate and multivariate cox-regression analysis for CT assessed vessels, cardiac changers and parenchymal change in patients undergoing and not undergoing PEA. (P < 0.05) indicates statistically significant association with mortality. PVR group (<400=1, 400-800=2, 800-1200=3, >1200=4).

Variables	Univariate analysis			Multivariate adjusting for age, sex, mPAP and PVR		
Endarterectomy	HR	95% CI	P value	HR	95% CI	P value
Central disease	2.64	0.9 to 7.08	0.05	NA		
Segmental disease	0.37	0.12 to 1.12	0.08	NA		
Distal disease	0.8	0.18 to 3.5	0.77	NA		
No endarterectomy	HR	95% CI	P value	HR	95% CI	P value
Central disease	1.91	1.19 to 3.05	0.007	1.9	1.1 to 3.1	0.01
Segmental disease	0.47	0.29 to 0.77	0.003	NA		
Distal disease	1.2	0.65 to 2.3	0.49	NA		

Abbreviations: mean pulmonary artery pressure (mPAP), pulmonary vascular resistance (PVR). Hazard ratio (HR). Confidence intervals (95%CI).

6.5 Discussion

This study aimed to address how chronic thromboembolic disease location in CTEPH is assessed on CTPA and relates to key clinical outcomes. We developed a scoring system for the categorisation of chronic thromboembolic disease location on visual assessment of CTPA studies. The scores showed high kappa and ICC values, indicating excellent interobserver agreement between two observers. Central disease was an independent predictor of outcome in patients not undergoing pulmonary endarterectomy. While in patients who underwent endarterectomy the pattern was less clear with no independent predictive value identified.

Prior studies have assessed the severity of CTEPH including clinical, hemodynamic, and imaging investigations (Meinel et al., 2014, Abozeed et al., 2022, Gharepapagh et al., 2023). A prior study used DECT to assess changes in lung perfused blood volume based on the extent of pulmonary hypoperfusion, highlighting the value of assessing lung parenchymal tissue and perfusion in the setting of suspected chronic thromboembolic (Takagi et al., 2016). Another study proposed a CT scoring system in 145 patients with CTEPH, based on CTEPH radiological signs and haemodynamic changes, which includes mosaic perfusion, tricuspid regurgitation, pulmonary artery diameter, and Unilateral/Bilateral thrombus (Leone et al., 2017). However, we are unaware of prior studies that have assessed disease location in the pulmonary artery tree compared with haemodynamics, surgical intervention and mortality in CTEPH.

Grafham et al. (2023) established a proximity-based CT pulmonary angiography scoring system, exhibiting moderate interobserver agreement among 40 patients with CTEPH and demonstrating the value of extensive pulmonary artery location evaluation. The highest degree of agreement was found at the main and lobar levels, but as expected decreased agreement was found distally. Interestingly the authors evaluated different vessel appearances such as webs, eccentric thickening and occlusions and showed variable agreement demonstrating the challenge of accurate evaluation in chronic thromboembolic disease (Grafham et al., 2023). In contrast, Hrdlicka et al. (2024) found that radiologists, even non-experts, had good sensitivity and interreader agreement when diagnosing CTEPH on

CTPA, however in our experience of clinical practice, such high agreement may not be achieved (Hrdlicka et al., 2024). These findings emphasise the importance of comprehensive scoring systems and the need for standardised methods to assess disease impact and distribution. In the present study, the interobserver agreement demonstrated good consistency between the two observers in determining the extent of disease. However, inaccurate results may arise due to subtle or small thrombi, vessel wall thickening or luminal irregularity, alterations in the surrounding lung tissue, or artefacts (Delcroix et al., 2021). The lowest level of agreement was found in patients with distal disease, likely due to the fact that distal arteries are smaller, and the disease is more challenging to interpret in the distal regions.

The results indicate that broad classes of disease location showed clear clinical value, central location is independently associated with mortality and distal location with PVR. The more detailed scoring system provided may be useful for therapeutic intervention planning, but further work is needed to determine if there is incremental clinical value in the haemodynamic assessment or mortality prediction.

Distal disease presents a significant challenge in the management of CTEPH due to a lower accessibility of endarterectomy and is associated with worse outcomes (Suntharalingam et al., 2007). In our study, distal disease was associated with mortality rates comparable to central disease. A study by Gan et al. (2010) found that distal disease was a significant predictor of mortality compared to proximal CTEPH in both endarterectomy and non-endarterectomy groups. Several factors could indicate the reason why distal disease outcomes are similar to central disease. Distal disease, albeit affecting smaller arteries, can cause severe pulmonary hypertension due to the cumulative impact of many blockages, leading to a haemodynamic impact comparable to that of central disease. In the present study, PVR was similarly high in distal and central disease, for both of these chronic embolic disease locations PVR was higher than that found in segmental disease, suggesting similarly severe vascular obstruction in distal and central disease. This is consistent with previous study, demonstrating the significance of identifying distal disease as a high-risk characteristic in chronic thromboembolic disease, which has been associated with high PVR and severe pulmonary hypertension (Gan et al., 2010).

The lack of effectiveness of existing scoring systems to precisely evaluate distal disease demonstrates the importance of accurately characterising the haemodynamics and parenchymal alterations associated with distal disease in patients with CTEPH. Additionally, our study also highlights the important relationship between distal disease with lung parenchymal abnormalities such as mosaic attenuation (indicating abnormal perfusion) and infarction. Distal disease may indirectly affect lung parenchyma through alterations in regional blood flow dynamics and subsequent tissue ischemia (Suki et al., 2011, McCabe et al., 2020). The presence of mosaic pattern attenuation and infarction may indeed aid the diagnosis of CTEPH when distal diseases are not clearly identified (Gopalan et al., 2017).

This study demonstrated that higher chronic thromboembolic disease scores are associated with higher PVR and mPAP, indicating a relationship between greater thrombus burden and more severe haemodynamic abnormalities in CTEPH. Previous studies have shown that CTEPH scoring systems significantly correlate with PVR and mPAP, this associations are either determined by visually assessing haemodynamic changes in CT imaging (Leone et al., 2017), or by quantifying pulmonary blood volume using DECT (Abozeed et al., 2022). Thrombus impedes flow, and it is unsurprising that a greater burden is associated with larger alterations in the haemodynamics of the pulmonary circulation.

We acknowledge the limitations of our research. Eligible patients were identified from a single-centre registry and only two observers assessed scans. This could affect the generalisability of our findings. Additionally, intra-observer variability when using the scoring system was not assessed. Patients were identified retrospectively, which limited the ability to control for potential confounders. While CTPA was performed on all patients, contemporaneous PFT and RHC data were not fully complete. Results can be impacted by a variety of factors, including treatment efficacy, comorbidities, and the overall condition of the patient. Future research could focus on using AI to better characterise the location and burden of chronic thromboembolic disease, potentially improving diagnosis accuracy in patients with CTEPH (Abdulaal et al., 2024). AI algorithms, utilising deep learning models, may analyse CTPA images with more accuracy, detecting subtle patterns and estimating disease burden more reliably than conventional approaches.

6.6 Conclusion

This study presents a scoring system for chronic thromboembolic disease location and extent in CTEPH on CTPA. Distal disease was associated with elevated PVR and lung parenchymal abnormalities. Our results confirm the effectiveness of determining the chronic thromboembolic disease location and extent in the assessment of CTEPH severity and risk prediction. The scoring system may still help with planning and reporting, even if it does not add clear prognostic value. Further research is needed to determine its additional benefits in haemodynamic assessment and mortality prediction.

7 Artificial Intelligence to Automate Analysis of Chronic Thromboembolic Pulmonary Disease on CTPA

Research article (Ready for submission)

Contribution: First author. My main contributions were completing extensive literature reviews, carrying out statistical analyses, and developing the tables and figures included in the research. I was primarily responsible for the manual segmentation and detailed correction of pulmonary arteries, pulmonary veins, and thromboembolic disease on CTPA scans, creating a ground truth dataset for training and validating the AI model. I thoroughly reviewed all patient cases and imaging datasets used in this chapter and contributed to the radiological assessment and interpretation of imaging findings. This included reviewing all imaging data integrating future amendments based on input and recommendations from my co-authors.

Authors

L. Abdulaal¹, M.J. Sharkey¹, K. Dwivedi^{1,3}, S. Rajaram⁵, S. Alabed^{1,3,4}, M. Saleh¹, A. Rothman^{1,2,3,4}, R. Condliffe², D.G. Kiely^{2,3,4} and A. J. Swift^{1,3,4}

1. Division of Cardiovascular Medicine, University of Sheffield
2. Sheffield Pulmonary Vascular Disease Unit, Sheffield Teaching Hospitals NHS Foundation Trust
3. INSIGNEO, Institute for in silico Medicine, The University of Sheffield, Sheffield, United Kingdom.
4. National Institute for Health and Care Research, Sheffield Biomedical Research Centre, Sheffield, UK
5. Radiology Department, Sheffield Teaching Hospitals NHS Foundation Trust.

7.1 Abstract

Aim: Develop a clinically applicable artificial intelligence (AI) model to quantify the severity of chronic thromboembolic pulmonary disease (CTEPD) on computed tomography pulmonary angiography (CTPA). Evaluate the performance of the AI model in quantifying CTEPD compared to manual clot scoring and determine the prognostic value in patients with CTEPH.

Methods: An nnU-Net-based segmentation model was developed using 256 patients (161 training / 41 validation / 54 testing) from the Sheffield centre, including cases of CTEPH, acute pulmonary embolism (PE), and no clot. A separate clinical evaluation of 179 patients with CTEPH was used to assess the clinical utility of the segmentation model and its association with survival. A subcohort of 120 patients with CTEPH was selected to match cases with available manual scoring (as developed on Chapter 6), assessing both accuracy and reliability.

Results: The model achieved a Dice Similarity Coefficient (DSC) of 0.95 for pulmonary vessels segmentations and of 0.58 for thromboembolic disease segmentation. Interobserver agreement for thromboembolic disease was 0.69. Internal testing on cases including acute PE, CTEPH, and no clot achieved an AUC of 0.92. There were no segmentation failures in the test set. The mean DSC between two observer accuracy for thromboembolic segmentation was 0.59 ± 0.21 . Survival analysis demonstrated that AI-derived thromboembolic disease volume was associated with mortality (central: (HR=1.14, $p=0.01$); total: (HR=1.04, $p=0.03$), and in those who did not undergo endarterectomy (central: (HR=1.32, $p<0.001$); total: (HR=1.05, $p=0.01$). In contrast, patients who underwent endarterectomy thromboembolic disease volume was not associated with mortality. In the subcohort of 120 patients, AI-derived thromboembolic disease volume demonstrated a significant correlation with manual scoring ($r=0.72$, $p<0.001$).

Conclusion: This model enables accurate segmentation of PA and PV. Lower performance in thromboembolic disease may reflect variation in manual labels used to train the model. An AI approach to segment chronic thromboembolic pulmonary disease may have high diagnostic accuracy for detection, and also prognostication.

7.2 Introduction

Chronic thromboembolic pulmonary hypertension (CTEPH) is a rare but severe condition that may lead to a high mortality rate if not treated (Pepke-Zaba et al., 2013). Patients suspected of having CTEPH are routinely referred for computed tomography pulmonary angiography (CTPA), which has become the preferred imaging modality for visualising pulmonary vasculature, cardiac structures, and parenchymal abnormalities. However, accurate diagnosis of CTEPH remains challenging, as it relies on expert qualitative interpretation. This approach introduces subjectivity, interobserver variability, accurate assessments can be time-consuming, and where disease is missed may cause diagnostic delays (Delcroix et al., 2020; Pepke-Zaba et al., 2011; Klok et al., 2022). The lack of standardised quantitative frameworks constrains the reproducibility of diagnostic outcomes, highlighting the clinical need for automated tools to support accurate diagnosis. Prior research has evaluated the performance of deep learning algorithms in identifying pulmonary embolism (PE) in CTPA, demonstrating promising performance with reported sensitivities ranging from 73% to 96% and specificities between 77% and 96% (Weikert et al., 2020, Soffer et al., 2021, Cheikh et al., 2022, Buls et al., 2021). In contrast, as shown in Chapter 3, research on automated CTPA analysis for diagnosing CTEPH remains limited (Abdulaal et al., 2024). Developing a universal model for automatic evaluation of CTEPH is challenging due to the complexity of the disease.

Recent breakthroughs in artificial intelligence (AI) have transformed medical imaging, facilitating detailed assessment of complicated vascular structures. Integrating AI with pulmonary vessel segmentation has shown potential in reducing diagnostic delays and improving the accuracy of thromboembolic disease detection (Yuan et al., 2021, Chan et al., 2008). CTEPH occurs in the pulmonary artery (PA), hence improving the accuracy of segmenting the arteries is critical for detecting thromboembolic disease characteristics. AI-based pulmonary vascular segmentation enhances diagnostic methods by automating abnormality detection, lowering interobserver variability, and providing quantitative values for thromboembolism disease categorisation (Chu et al., 2025, Ming et al., 2025, Pu et al., 2022, Zhai et al., 2023). Furthermore, these methodologies allow for the creation of advanced biomarkers, such as clot load indices, which can increase diagnostic accuracy. As AI continues to advance, challenges remain in accurately segmenting the thin and intricately branching

distal pulmonary arteries, where segmentation errors can contribute to false negatives (Zhou et al., 2023). Therefore, accurate pulmonary vessel segmentation is essential for correctly identifying the region of interest, as segmentation errors can negatively affect the entire data analysis workflow.

This work develops of a nnU-Net-based framework for the automated segmentation of PA, pulmonary vein (PV), and thromboembolic disease using CTPA imaging.

This study aims to:

- Develop a clinically applicable AI model for patients with CTEPH.
- Evaluate the performance of PA, PV, and thromboembolic disease segmentation outputs generated by the proposed algorithm.
- Conduct a clinical evaluation of the segmentation results, including scoring and validation of the outcomes.
- Analyse disease location and distribution, quantify clot volume, and compare AI-generated results with manual clot scoring (Chapter 6) to assess prognostic significance and its potential for predicting survival outcomes in patients with CTEPH.

7.3 Methods

A retrospective CTPA dataset from the ASPIRE (Assessing the Spectrum of Pulmonary Hypertension Identified at a Referral Centre registry) at Sheffield, UK. All analyses were conducted at the patient level, with one CT scan corresponding to each patient. The North Sheffield Ethics Committee and review board granted ethical approval for this study. The National Research Ethics Service also approved the retrospective analysis with a waiver of informed consent, (16/YH/0352).

Study cohort

Datasets were obtained from the ASPIRE registry, with its details previously reported (Hurdman et al., 2012). The registry systematically collects extensive clinical and radiological information about patients sent to a specialised medical centre for assessment of suspected pulmonary hypertension. The confirmed diagnosis of CTEPH, acute PE, and no clot in this study were established in accordance with international guidelines and through detailed discussions by the multidisciplinary team (MDT). Cases with no clot were identified based on the selection of patients without a primary or secondary diagnosis of CTEPH. All scans were conducted using two scanners (General Healthcare Lightspeed and TOSHIBA Aquilion PRIME). Scanning parameters comprised thin-slice volumetric contrast-enhanced scans as part of the CTPA protocol. The study included adult patients aged ≥ 18 years old who underwent CTPA in Sheffield and met the diagnostic criteria for either acute PE or CTEPH. This included patients who received medical management or underwent pulmonary endarterectomy (PEA) as part of their treatment for CTEPH.

The dataset was divided at the patient level, with each patient corresponding to a distinct CTPA scan. The reference dataset included a varied cohort of 275 patients with CTEPH, 209 patients with acute PE, and 120 patients without thromboembolic disease as determined using chest CTPA findings. The cohort used for model development is further separated into three groups: training, validation, and testing (**Figure 7.1**). The model was not tested on an external dataset.

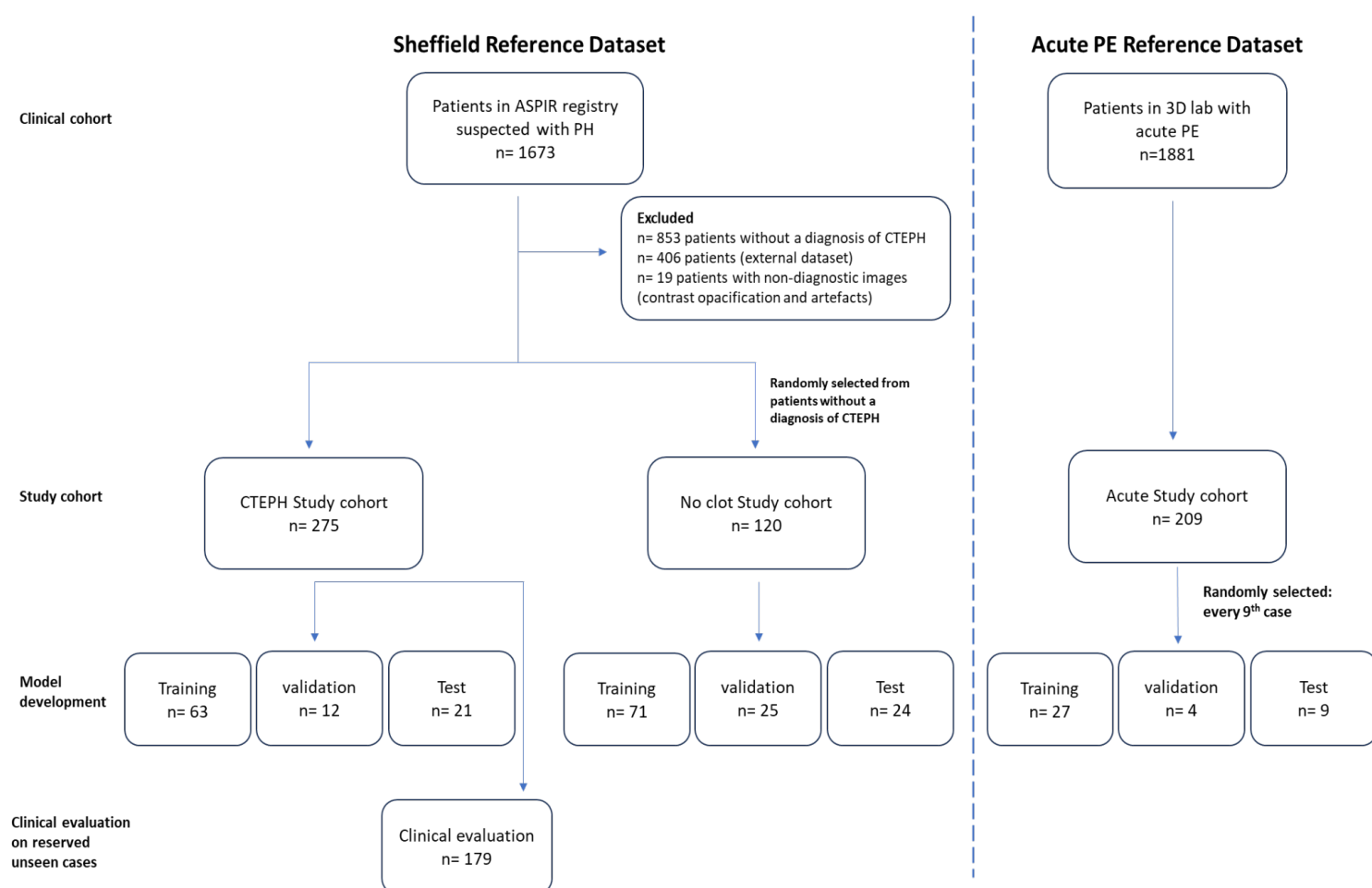


Figure 7.1 STROBE diagram demonstrating patients with CTEPH, Acute PE and no clot selections Sheffield reference datasets. Patient subsets are also presented according to the study stage (model development and clinical evaluation).

Manual segmentation

Manual ground truth segmentation masks for PA, PV, and thromboembolic diseases were created using MIM (Software, Cleveland, USA). A structured workflow was established with built-in operators for pre-trained models, to generate an initial segmentation mask. Each stage of this workflow was systematically reviewed by an expert radiologist (AS) and a trained radiographer (LA). The process was executed in a series of defined phases (**Figure 7.2**).

Axial slice-based segmentation was first employed to create a 2D whole-body mask, followed by 3D lung segmentation and cropping (Sharkey et al., 2023). Subsequently, segmentations of eight cardiac structures and the main pulmonary artery (MPA) were performed using a pre-trained nnU-Net model (Sharkey et al., 2022). The MPA structure was extracted as a 3D volumetric mask. The region grow tool was then used to segment the MPA and PV from the lung structures, with manual error correction applied. Threshold values were set at 228 to 713 Hounsfield Units (HU) for the PA and 117 to 407 HU for the PV. The workflow underwent a continuous manual assessment, with window width and level adjusted as appropriate to allow accurate delineation of the chronic thromboembolic disease and pulmonary vessels in general. We manually refined and segmented vessels and thromboembolic disease on a slice-by-slice basis using a 3D brush tool (**Figure 7.3**). This final annotated image and segmentation served as the ground truth for model development and training.

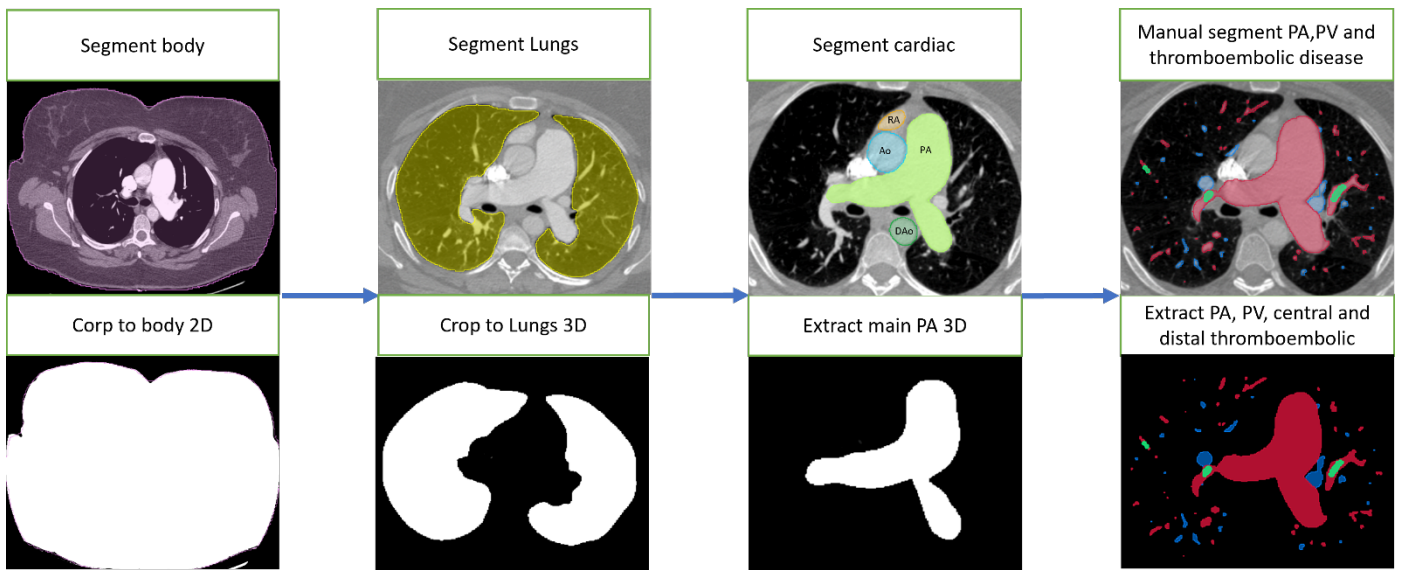


Figure 7.2 AI workflow steps developed using pre trained models to create an initial mask for PA and PV segmentation.

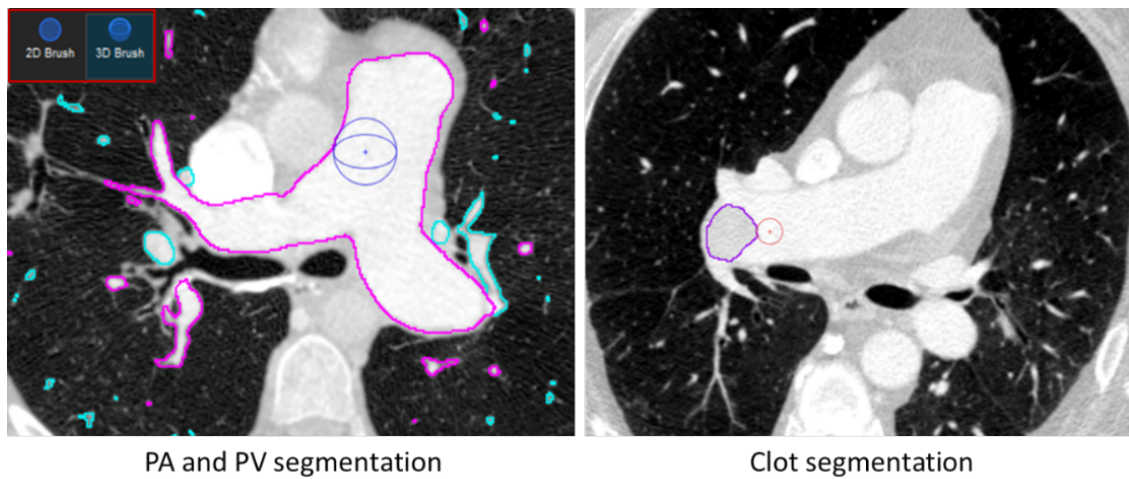


Figure 7.3 Demonstration of 3D brush tool to manually adjust and segment pulmonary vessels, and thromboembolic disease.

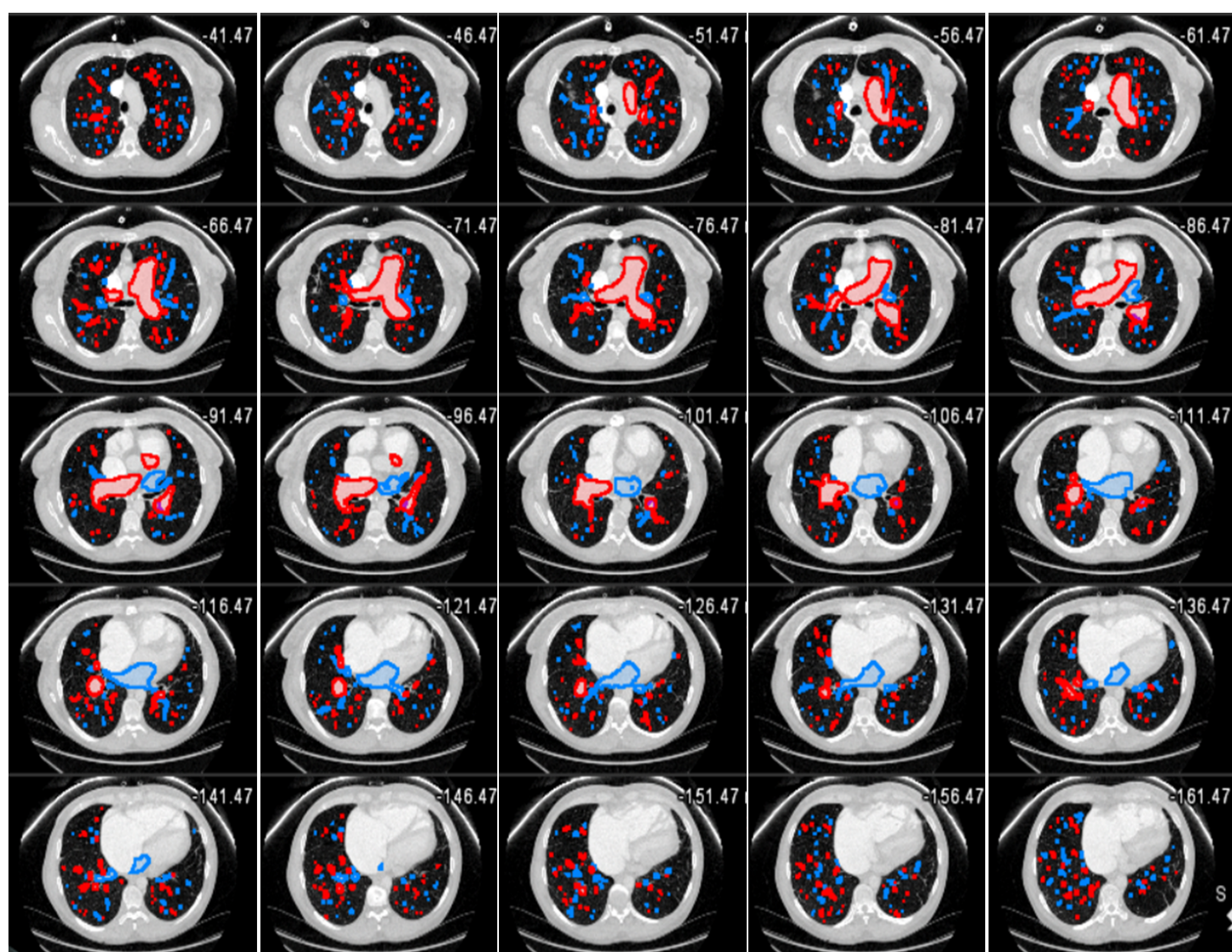


Figure 7.4 Illustration of the manual segmentation process of pulmonary arteries (PA) and pulmonary veins (PV) from CTPA images, demonstrating the anatomical delineation required for vascular assessment.

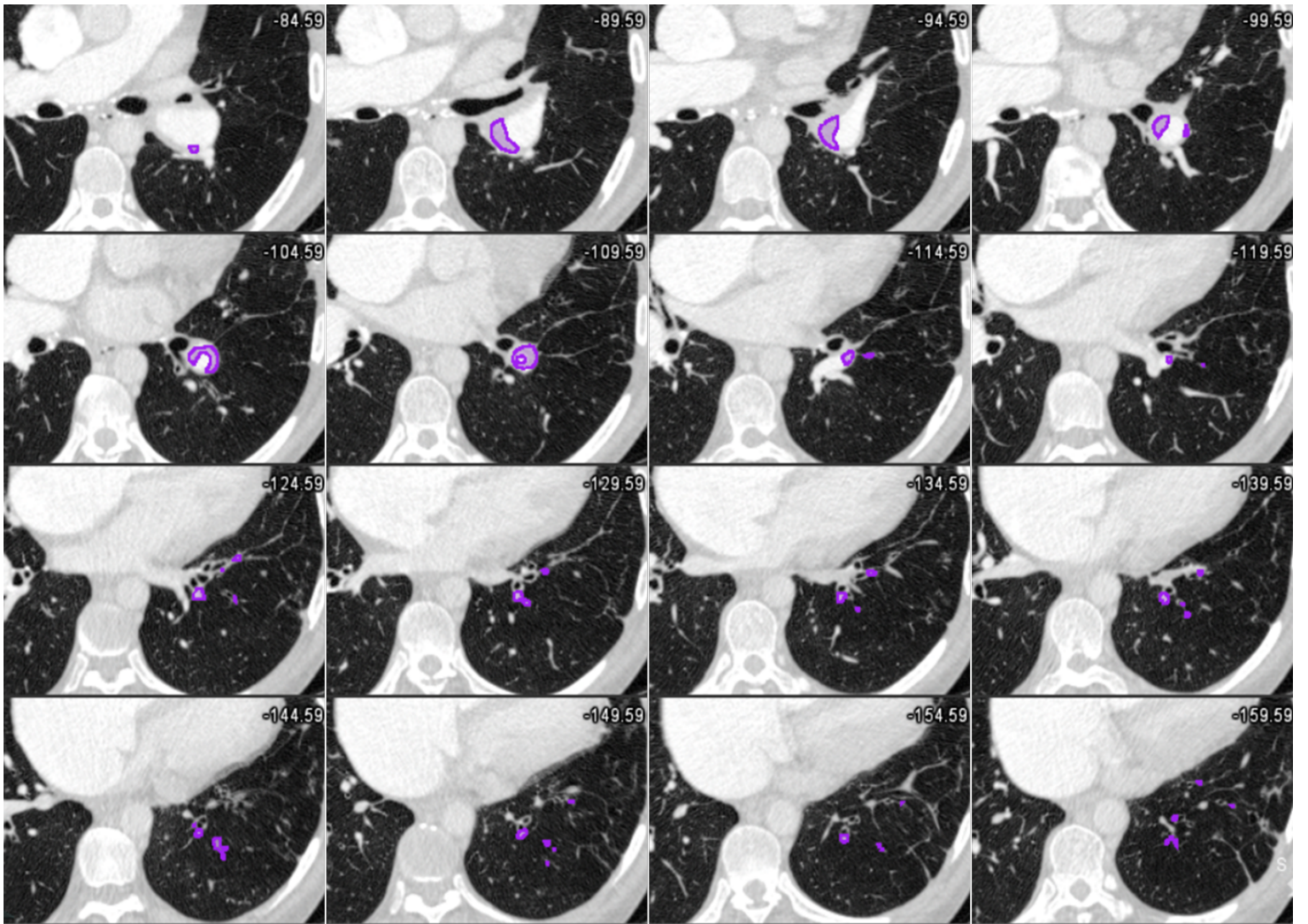


Figure 7.5 Illustration of the manual segmentation process of chronic thromboembolic disease from CTPA data, demonstrating the anatomical delineation required for CTEPH assessment.

Network concept and architecture

The nnU-Net model was utilised for the segmentation of PA, PV, and thromboembolic disease in CTPA images. nnU-Net is a pioneering publicly accessible deep learning segmentation model that automatically adapts image preprocessing, network design, data training, and post-processing for new imaging task (Isensee et al., 2021). A schematic representation of the nnU-Net architecture is presented in **Figure 7.6**.

CTPA Images and masks underwent pre-processing with resampling all volumetric CTPA data to a median pixel spacing of $0.738 \times 0.738 \times 0.625$ mm (x,y,z). Images were obtained using a 512×512 matrix, with median number of slices per volume 358 slices. CTPA intensity values were normalised and clipped to the [0.5th, 99.5th] percentile range to exclude outliers using foreground classes. The data was clipped to the range of -608 to 753 HU, then normalised by subtracting the mean (140.85) and dividing by the standard deviation (291.91). A patch sizes of $192 \times 350 \times 256$ was used. A two-stage cascade 3D nnU-Net architecture with seven convolutional stages was trained on the dataset using a batch size of 2. Each convolutional stage employed a kernel size $3 \times 3 \times 3$, feature maps per stage (23, 64, 128, 256, 320, 320, 320), and Leaky ReLU activation function without dropout layer. A single-fold training method was utilised, with a total of 1000 epochs and early stopping at 212 epochs.

Additionally, we applied data augmentation tools to enhance generalisability of the segmentation model. Spatial transformation, Gaussian noise, Gaussian smoothing, intensity scaling, and random axis flipping, all applied to increase diversity of the training dataset. Dice Similarity Coefficient (DSC) metrics were calculated for the test cohort (n=54). DSC score was applied as a metric to assess the overlap between the predicted segmentation and the ground truth annotations.

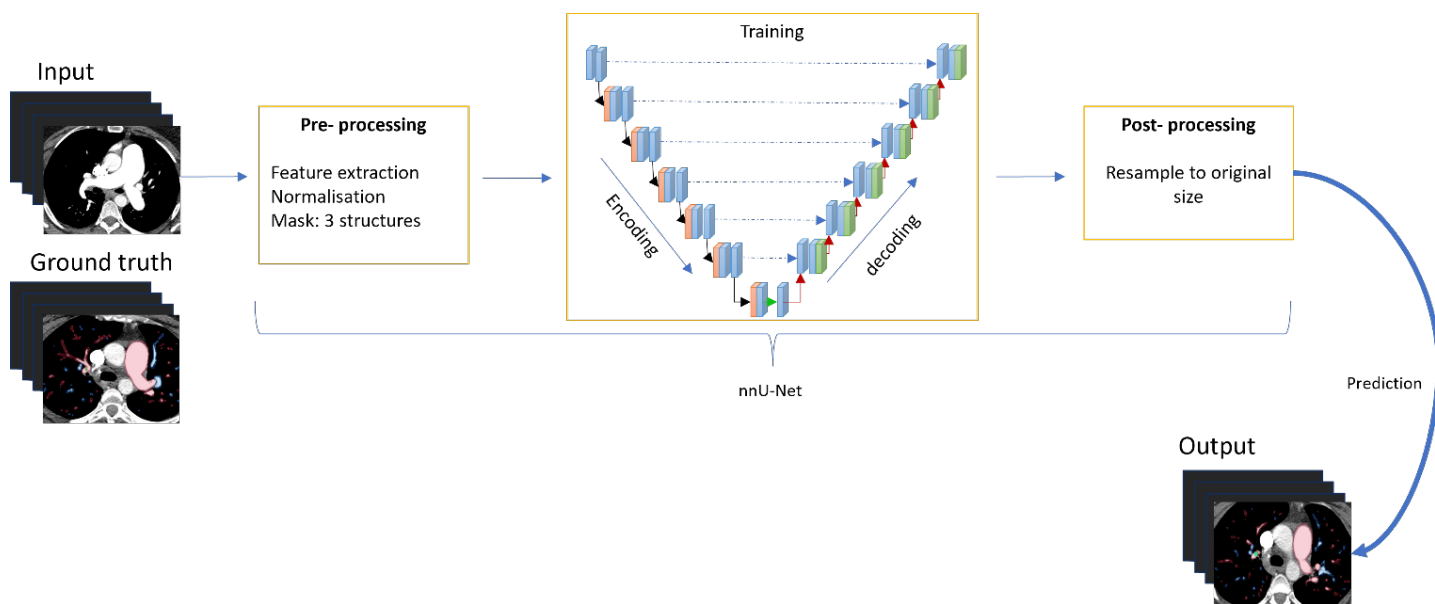


Figure 7.6 Schematic representation of the nnU-Net model architecture used for automated segmentation of pulmonary arteries (PA), pulmonary veins (PV), and thromboembolic disease from CTPA images.

Clinical evaluation

The segmentation outputs were reviewed through a clinical evaluation by a radiologist (AS) with 13 years of experience and a radiographer (LA) with 4 years of experience in interpreting thoracic CT images. Test set segmentations of the PA, PV, and thromboembolic disease were independently reviewed. The following criteria were used to designate an ordinal segmentation score to each segmentation output:

- 0:** Segmentation failed entirely.
- 1:** Segmentation was generated but contains major clinically significant errors.
- 2:** Segmentation includes minor errors that are clinically insignificant.
- 3:** Segmentation is accurate, with no clinically significant errors identified.

Thromboembolic disease volume segmentations were extracted from each CT scan using an automated AI segmentation model. Moreover, to assess the accuracy and reproducibility of chronic thromboembolic segmentation, an interobserver comparison was conducted on a subset of test patients ($n = 10$), involving the two reviewers independently.

Statistical analysis

All statistical analyses were performed using SPSS software (version 29.0, IBM), Excel (Microsoft Corporation, Redmond, USA), and GraphPad Prism (version 10). Continuous variables were summarised as means with standard deviations (SD), while categorical variables were reported as counts and percentages. Area Under the Curve (AUC) values were produced to assess model performance and minimise variability between ground truth segmentation and automated AI outcomes in the test dataset.

Spearman correlation coefficients were calculated to evaluate associations between AI-driven segmentation and both CT-based measurements and haemodynamic parameters. Cox regression was employed to examine the association between PA, PV and thromboembolic volume and patient survival in the clinical evaluation cohort. Hazard ratios (HRs) were reported with 95% confidence intervals (CIs), and p -values < 0.05 were considered statistically significant. AI-derived data were analysed using both univariate and multivariate models, adjusted for known prognostic variables including age, sex, mean pulmonary arterial pressure (mPAP), and pulmonary vascular resistance (PVR). Kaplan–Meier survival curves were used to compare survival outcomes from the time of diagnostic assessment, using the log-rank test. Interobserver comparison was conducted using DSC for thromboembolic disease segmentations, and Intraclass correlation coefficients (ICC) for volumetric measurements (Maier-Hein et al., 2024). ICC values were interpreted as follows, values < 0.5 indicate poor agreement, 0.5–0.75 moderate, 0.75–0.90 good, and > 0.90 excellent agreement. (Koo and Li, 2016).

7.4 Results

Patient clinical characteristics with CTEPH, acute PE and no clot cohorts are summarised in **Table 7.1**. The CTEPH cohort (n=275) was subdivided into two datasets: a model development (n=96) and clinical evaluation (n=179) (**Figure 7.1**). This was established to differentiate between cases utilised for the model or technical development from the clinical evaluation cases. The patients showed a wide range of haemodynamic, spirometry, and demographic features.

Baseline clinical characteristics of technical development are presented in **Table 7.2**. A total of 161 patients were randomly assigned to different groups: 63 CTEPH, 27 acute PE, and 71 no clots for training; 41 patients (12 CTEPH, 4 acute PE, 25 no clots) for validation; and 54 patients (21 CTEPH, 9 acute PE, 24 no clots) for technical performance testing.

Table 7.1 Characteristics of the three datasets used for developing the model (CTEPH, acute pulmonary embolism and no clot cases). Data are expressed as mean \pm standard deviation or counts (percentage).

Characteristics	CTEPH full cohort n= 275	Acute PE n= 40	ASPIRE no clot n=120
Age (years)	65 \pm 14	78 \pm 18	63 \pm 13
Sex (Female)	158 (54.5%)	27 (67.5%)	80 (66.6%)
WHO FC	II (25), III (225), IV (25)	NA	II (19), III (86), IV (11)
Right heart catheterisation	n=272 (94%)	NA	n=82 (68%)
PVR (dyne·s·cm ⁻⁵)	646 \pm 414	NA	393 \pm 275.4
mPAP (mmHg)	45 \pm 12	NA	35 \pm 12.2
SVO2 (%)	62.1 \pm 9	NA	65.6 \pm 13.5
CI (L/min/m2)	2.6 \pm 0.8	NA	2.8 \pm 0.83
Pulmonary function tests	n=260(90%)	NA	n=71 (59%)
Predicted FEV1 (%)	76.3 \pm 20.3	NA	67.6 \pm 23.8
Predicted FVC (%)	88.4 \pm 21.5	NA	76.3 \pm 23.6
Predicted TLCO (%)	60.2 \pm 18.3	NA	47.4 \pm 21.3

Abbreviations: World Health Organisation (WHO), pulmonary vascular resistance (PVR), mean pulmonary arterial pressure (mPAP), pulmonary artery wedge pressure (PAWP), venous oxygen saturation (SvO2), and cardiac index (CI). Forced expiratory volume in one second (FEV1), forced vital capacity (FVC), and transfer factor of the lung for carbon monoxide (TLCO).

Table 7.2 Patient characteristics for both model development and clinical evaluation subcohort.

Characteristics	Model development			Clinical evaluation
	Training n=161	Validation n= 41	Testing n=54	CTEPH =179
Age (years)	67 ± 15.2	65 ± 16.2	65 ±15.7	64 ± 14
Sex (Female)	95 (59%)	26 (63%)	37 (69%)	99 (55%)
WHO FC	II (19), III (95), IV (15)	II (5), III (27), IV (4)	II (6), III (35), IV (4)	II (17), III (144), IV (18)
Right heart catheterisation	n=113	n=27	n=35	n=165
PVR (dyne·s·cm ⁻⁵)	583 ± 397.6	449 ± 287.7	582.4 ±373	611.6 ±424.5
mPAP (mmHg)	41 ± 14.3	41 ± 11	41 ±14	44.2 ±12.6
SVO2 (%)	63 ± 9.6	66.3 ± 9.2	59 ±17.5	62.6 ±8.4
CI (L/min/m2)	2.66 ± 0.9	2.9 ±0.93	2.44 ±0.64	2.6 ±0.86
Pulmonary function tests	n=99	n=14	n=26	n=159
Predicted FEV1 (%)	70.6 ± 23.3	73 ± 19.2	67.7 ±17.4	76.8 ± 20.3
Predicted FVC (%)	81.3 ± 22.7	83 ± 18.9	82.7 ±19.6	88.8 ±21.6
Predicted TLCO (%)	54.5 ±22.3	61.5 ± 25.5	54.6 ±19.4	60.2 ±16.5

Abbreviations: World Health Organisation (WHO), pulmonary vascular resistance (PVR), mean pulmonary arterial pressure (mPAP), pulmonary artery wedge pressure (PAWP), venous oxygen saturation (SvO2), and cardiac index (CI). Forced expiratory volume in one second (FEV1), forced vital capacity (FVC), and transfer factor of the lung for carbon monoxide (TLCO).

Technical evaluation

The model achieved a mean DSC of 0.95 for PA and PV segmentations in the test set. In contrast, thromboembolic disease segmentation showed a significantly lower mean DSC of 0.58. Sensitivity across the whole test dataset was 80% overall, 93% for PA and PV, and 54% for thromboembolic disease. DSC and sensitivity scores for PA, PV, and thromboembolic disease segmentations are provided for each patient in (**Supplementary table S1**).

Mean volumetric measurements of the PA, PV, and thromboembolic disease across different patient groups, and clinical evaluation CTEPH cohort are summarised in **Table 7.3**.

Table 7.3 Mean \pm standard deviation of pulmonary artery (PA), pulmonary vein (PV), and thromboembolic volumes stratified by disease location, as detected using the nnU-Net-based segmentation model.

Structure Millilitres (ml)	Testing set 54			Clinical evaluation
	CTEPH (n=21)	Acute PE (n=9)	No clot (n=24)	CTEPH (n=179)
Main PA	120.55 \pm 48.5	87.42 \pm 35.4	119.32 \pm 65.7	126.02 \pm 40.3
PA	232.42 \pm 89.1	172.6 \pm 47.3	234.6 \pm 90.2	243.83 \pm 68.1
PV	145.28 \pm 42.1	156.36 \pm 31.7	180.75 \pm 60.2	174.32 \pm 46.1
Central disease	1.18 \pm 2.1	0.09 \pm 0.18	0	0.49 \pm 1.77
Non-central disease*	4.62 \pm 4.6	1.54 \pm 2.7	0.04 \pm 0.06	3.12 \pm 4.15
Total clot volume	5.8 \pm 5.5	1.63 \pm 2.9	0.04 \pm 0.06	3.61 \pm 5.22

*Non-central disease includes segmental and distal.

The test results including cases of (acute PE, CTEPH, no clot) achieved an AUC of 0.92, indicating excellent classification performance. When specifically distinguishing CTEPH from no clot cases, the model demonstrated even higher accuracy with an AUC of 0.97. However, predictive performance was lower for differentiating acute PE from no clot cases, with an AUC of 0.78 (**Figure 7.7**).

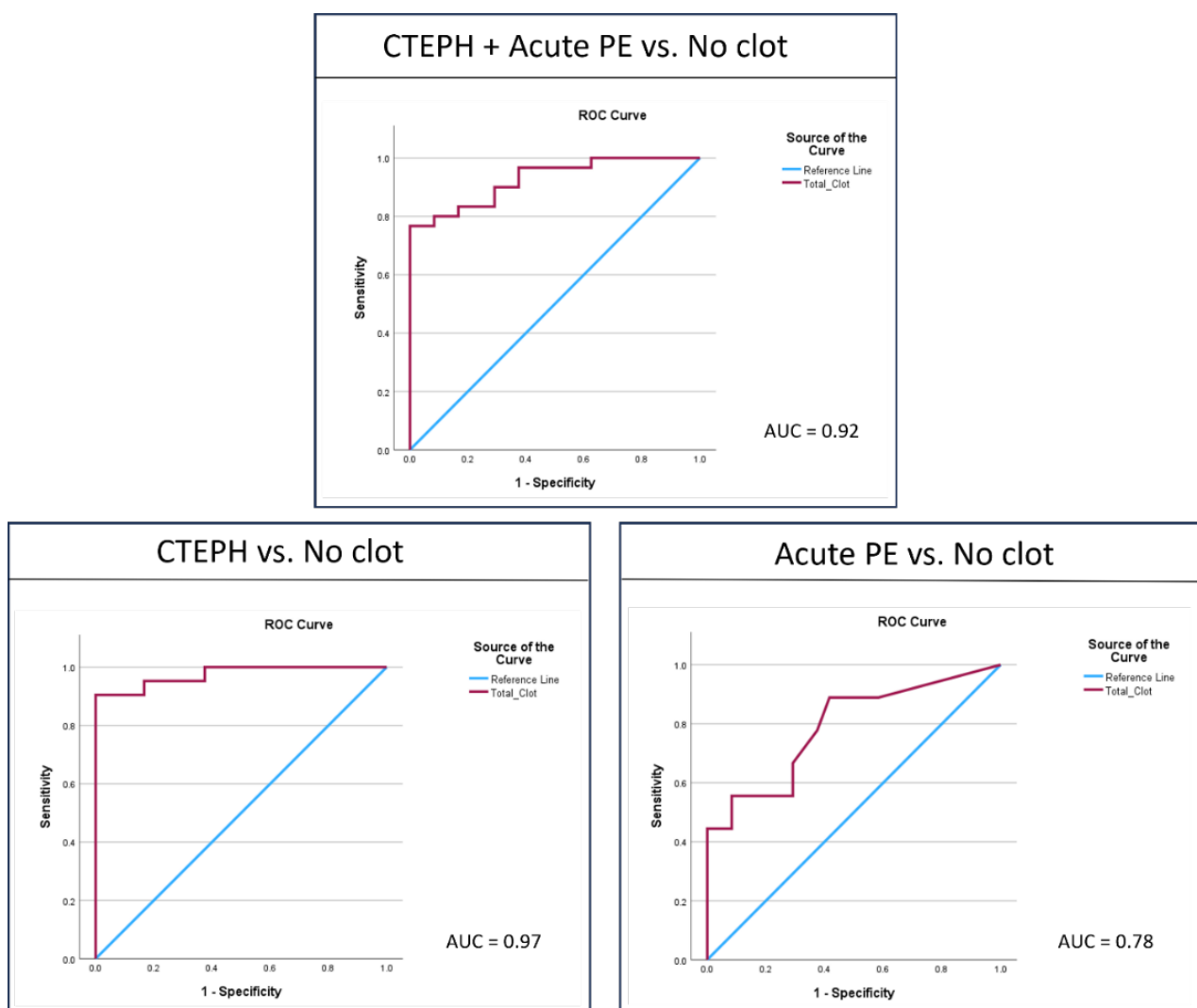


Figure 7.7 Receiver operating characteristic (ROC) curve for the AI model in identifying thromboembolic clots on the test set. The curve demonstrates the relationship between sensitivity and specificity, and the area under the curve (AUC) represents the model's overall performance in differentiating between clot-positive and clot-negative cases.

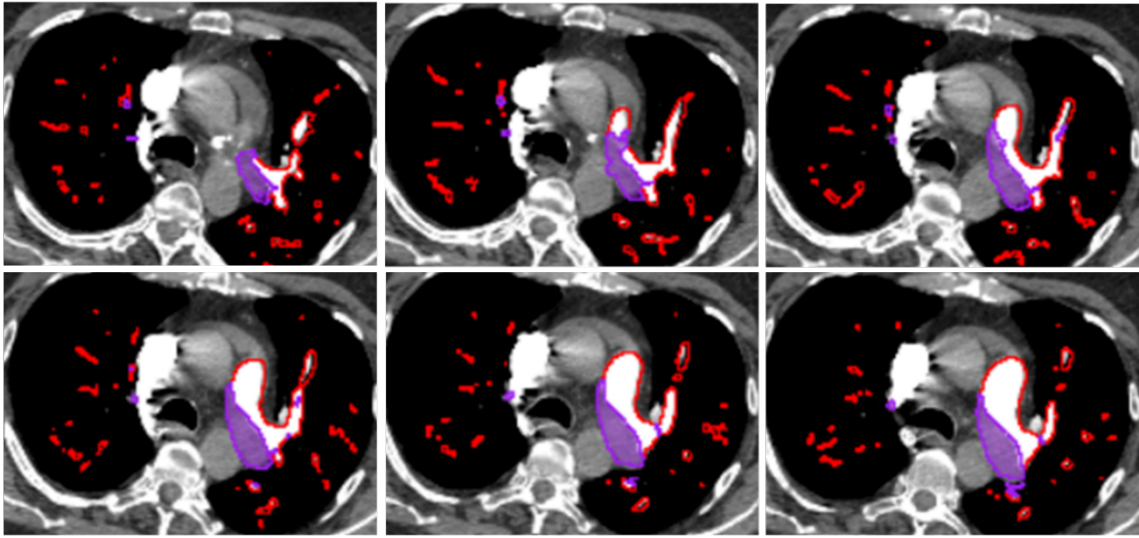
The DSC between observers for thromboembolic disease segmentation on CTPA images (n = 10) was 0.59 ± 0.21 , indicating moderate agreement. Mean DSC scores for total thromboembolic volume segmentation between the two independent observers were calculated for each case and presented in **Table 7.4**.

In terms of the clot volume results, interobserver agreement was highest for central disease segmentation, with an ICC of 0.89 (**Figure 7.8**). In comparison, total clot volume showed moderate agreement (ICC = 0.69), while non central disease segmentation demonstrated the lowest agreement with ICC of 0.57, reflecting greater variability in the segmentation of peripheral thromboembolic disease (**Table 7.5**). The subtle and varied appearance of chronic thrombotic disease and the existence of imaging artefacts that may mask thrombus are possible causes of this performance reduction (**Figure 7.9**).

Table 7.4 Mean Dice Similarity Coefficient (DSC) scores for total thromboembolic volume segmentation between two independent observers.

Cases	Observer1	Observer 2	DSC
	Total clot volume (ml)	Total clot volume (ml)	
1	4.93	4.81	0.97
2	7.17	5.41	0.64
3	4.21	2.77	0.69
4	1.67	0.54	0.1
5	1.39	0.85	0.5
6	12.55	11.49	0.77
7	3.87	3.13	0.53
8	4.44	3.49	0.74
9	28.86	8.97	0.41
10	1.98	1.26	0.48

Observer 1



Observer 2

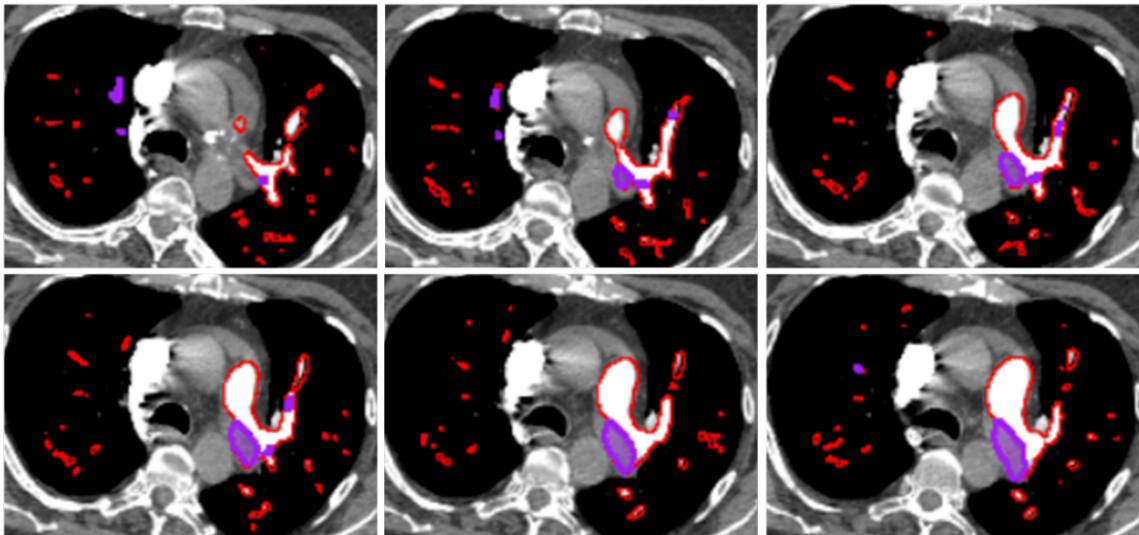
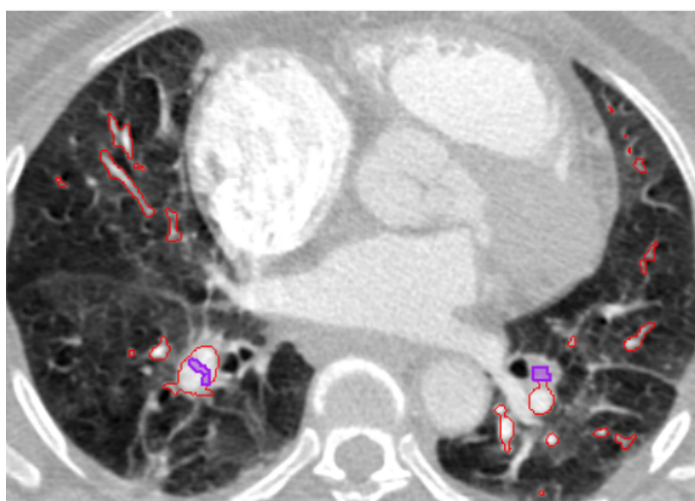


Figure 7.8 An example case that illustrates the differences in central disease segmentation between observers.

Table 7.5 Interobserver agreement for chronic thromboembolic disease outputs between two observers, using intraclass correlation coefficients (ICC) with 95% confidence intervals (CI) for total, central, and non-central volumes

Segmentation Region	ICC	95% CI	P value	Interpretation
Central disease	0.89	0.61 to 0.97	0.001	Good agreement
Non-central disease	0.57	-0.39 to 0.88	0.09	Moderate agreement
Total clot volume	0.69	-0.07 to 0.92	0.03	Moderate agreement

Observer 1



Observer 2

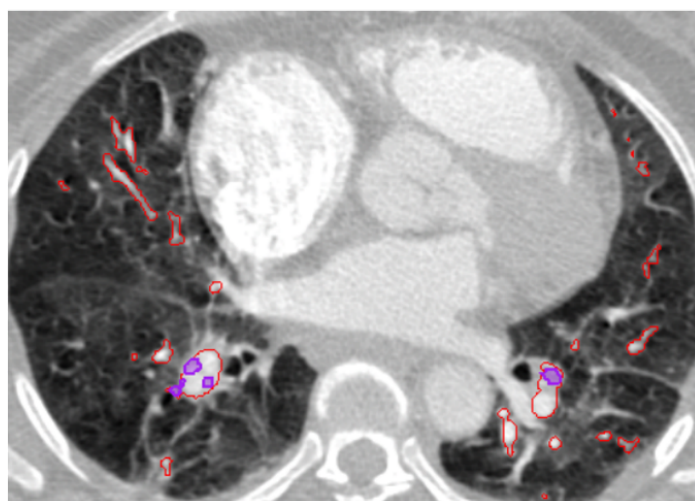


Figure 7.9 This case illustrates the impact of significant respiratory artefacts on segmental and distal disease, which impaired the visualisation of vascular structures and thromboembolic disease. These factors resulted in a decrease in segmentation accuracy and an increase in interobserver variability (DSC = 0.1).

Segmentation analysis of testing set

The algorithm successfully segmented all cases (n=54), and there were no failures in PA or PV segmentation (**Figure 7.10**). Out of these cases, 30 (56%) achieved PA/PV segmentation with no clinically relevant errors (score 3), 19 (35%) exhibited minor clinically insignificant errors (score 2), and 5 (9%) showed major clinically significant errors (score 1). Segmentation errors were primarily attributed to imaging artefacts (71%), suboptimal contrast opacification (46%), and lung parenchymal abnormalities (42%), with some cases exhibiting more than one contributing factor.

In the test set of 30 cases, 21 (70%) had excellent clot segmentation without any clinically significant error (score 3). Minor clinical errors (score 2) were observed in 6 cases (20%), while 3 cases (10%) exhibited major clinically significant errors (score 1), as shown in **Figure 7.11**. The most common reasons for segmentation errors were PA and PV segmentations errors (27%), poor opacification (17%), artefacts (23%) and distal disease (20%).

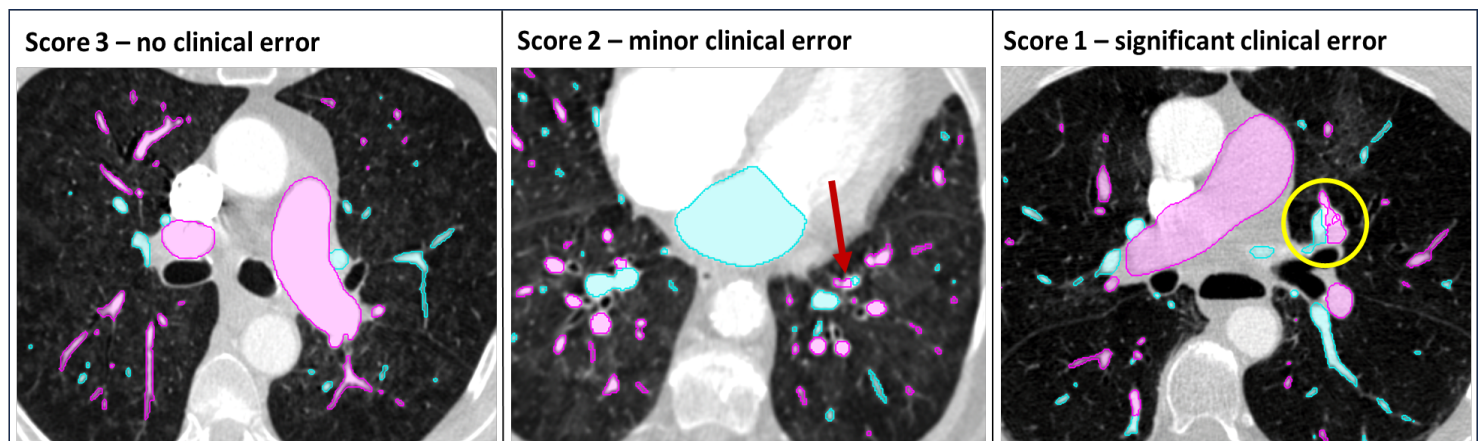


Figure 7.10 Examples of AI-derived pulmonary artery (PA) and pulmonary vein (PV) segmentations with corresponding clinical error scores: (A) Score 3 – no clinical error; accurate segmentation. (B) Score 2 – minor clinical error due to mild misclassification (red arrow). (C) Score 1 – significant clinical error involving major vessel segmentation inaccuracies

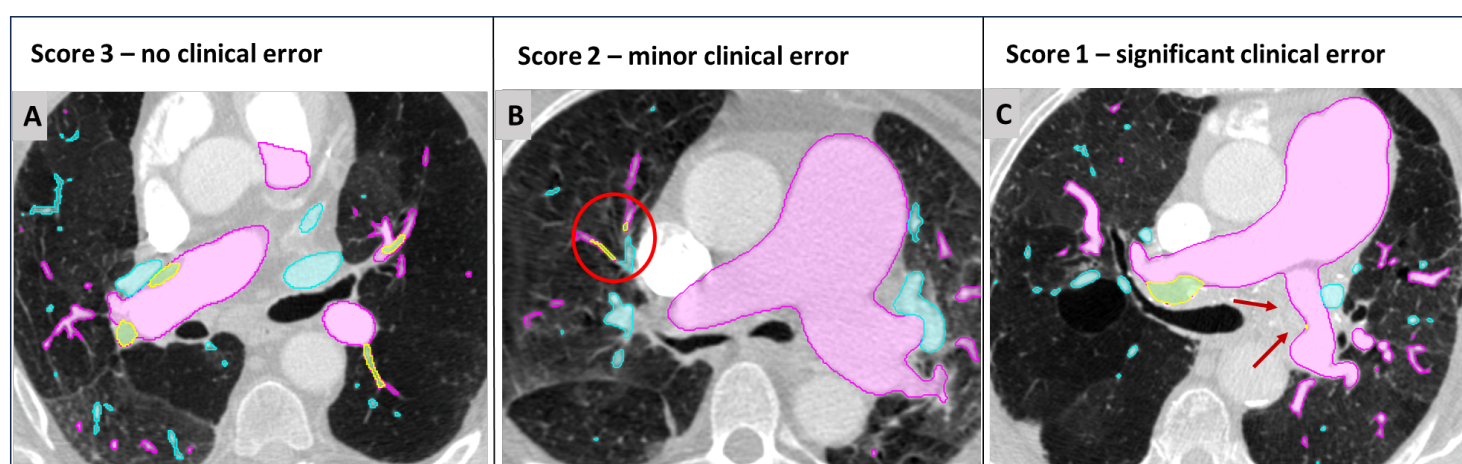


Figure 7.11 Examples of AI-derived thromboembolic disease segmentation with clinical error scoring: (A) Score 3 – no clinical error. (B) Score 2 – minor clinical error involving vessel misclassification or artefacts (red circle). (C) Score 1 – significant clinical error due to missed clot by the detection algorithm (red arrow).

Clinical evaluation analysis with haemodynamic

Clinical evaluation was conducted on a cohort of 179 patients with CTEPH. A modest significant correlation was observed between AI-derived central and non-central (segmental and distal) thromboembolic segmentations and pulmonary vascular resistance (PVR) ($r=0.21$, $p=0.005$). Notably, non-central disease volume demonstrated a marginally stronger significant correlation with PVR ($r=0.26$, $p<0.001$).

Modest significant correlations were found between non central clot volume and key imaging markers of the lung parenchyma. Specifically, associations were observed with mosaic perfusion ($r=0.21$, $p=0.005$) and lung infarction ($r=0.21$, $p=0.004$). In contrast, central clot volume showed no significant association with either mosaic perfusion ($r=0.09$, $p=0.23$) or infarction ($r=0.05$, $p=0.43$).

Additionally, the PA to aorta (PA/AO) ratio was modestly associated with central clot volume ($r=0.17$, $p=0.024$), while the right ventricle to left ventricle (RV/LV) ratio showed a significant correlation with non-central clot volume ($r=0.25$, $p<0.001$), as presented in **Table 7.6**.

No significant correlation was observed between transfer factor of the lung for carbon monoxide (TLCO) and central disease ($r=0.04$, $p=0.5$), non-central disease ($r=0.08$, $p=0.29$), or total clot volume ($r=0.07$, $p=0.38$). Similarly, no significant associations were identified between clot burden and any other PFT parameters.

Table 7.6 Spearman correlation analysis between AI-derived volumes in millilitre (ml) of pulmonary artery (PA), pulmonary vein (PV), and thromboembolic disease with pulmonary vascular resistance (PVR), mean pulmonary arterial pressure (mPAP), and CT measurements.

AI Variables (179)	PVR (dyne.s.cm ⁻⁵)	mPAP (mmHg)	SVO2 (%)	PA/AO ratio	RV/LV ratio
Central volume (ml)	0.14, $p=0.06$	0.06, $p=0.38$	-0.05, $p=0.5$	0.15, $p=0.03$	0.09, $p=0.2$
Non central volume (ml)	0.26, <0.001	0.18, $p=0.01$	-0.19, $p=0.01$	0.08, $p=0.27$	0.26, <0.001
Total clot volume(ml)	0.26, <0.001	0.17, $p=0.02$	-0.18, $p=0.01$	0.07, $p=0.29$	0.25, <0.001
Main PA volume(ml)	0.12, $p=0.11$	0.24, <0.001	-0.12, $p=0.12$	0.34, <0.001	0.02, $p=0.71$
PA volume (ml)	0.08, $p=0.29$	0.26, <0.001	-0.06, $p=0.4$	0.29, <0.001	0.04, $p=0.53$
PV volume(ml)	-0.37, <0.001	-0.2, $p=0.008$	0.23, $p=0.003$	-0.01, $p=0.85$	-0.27, <0.001
PA/PV ratio	0.43, <0.001	0.47, <0.001	-0.29, $p<0.001$	0.28, <0.001	0.26, <0.001

Clinical evaluation with survival analysis

Of 179 CTEPH patients, 77 (43%) had endarterectomy, and 102 (57%) did not undergo endarterectomy. The median time to pulmonary endarterectomy was 7 months (IQR: 0 to 11). The outcome of mortality was observed in 81 (45%) patients. Notably, no patients in this cohort underwent balloon pulmonary angioplasty or lung transplantation.

The presence of AI-derived central thromboembolic disease volume was analysed in two ways: first, as a binary variable (1 = presence of any central volume, 0 = absence); and second, using a median-based severity threshold, where central volume > 0.4 millilitre (mL) were assigned a value of 1. The rationale for including the median-based method was to explore whether a higher burden of central volume provided additional prognostic value.

Univariate and multivariate analyses examining the association between AI-derived clot volume location and mortality are summarised in **Table 7.7**. In univariate analysis, both central clot volume and total clot volume were significantly associated with mortality, both in the entire cohort and specifically among patients who did not undergo endarterectomy. After adjusting for demographic and clinical variables, including age, sex, mPAP, and PVR, the presence of central clot volume remained a significant predictor of mortality ($p < 0.001$) in the subgroup of patients who did not undergo endarterectomy.

According to Kaplan-Meier survival analysis, patients with higher thromboembolic burden demonstrated poorer survival outcomes (**Figure 7.12**). The presence of AI central disease showed no significant difference in survival (log=1.4, $p=0.22$). While AI central median>0.4 ml was significantly associated with worse survival in the overall cohort (log=4.3, $p=0.03$) and in patients who did not undergo pulmonary endarterectomy (log=6.7, $p=0.009$). However, patients who underwent endarterectomy were associated with improved survival outcomes (log=0.06, $p=0.79$).

Table 7.7 Univariate and multivariate cox-regression analysis for AI segmentation for pulmonary artery (PA), vein (PV) and thromboembolic disease (central, non-central, total clot) volumes (millilitres) in patients undergoing and not undergoing endarterectomy. (P < 0.05) indicates statistically significant association with mortality.

Variables	Univariate analysis			Multivariate analysis		
All patients 179	HR	95% CI	P value	HR	95% CI	P value
Central clot volume	1.14	1.02 to 1.3	0.01	NA		
Central (median >0.4)	1.7	0.9 to 3.4	0.1	NA		
Non-central clot volume	1.04	0.9 to 1.1	0.09	NA		
Total clot volume	1.04	1 to 1.1	0.03	NA		
Main PA volume	1	0.99 to 1	0.15	NA		
PA volume	1	0.99 to 1	0.62	NA		
PV volume	1	0.99 to 1	0.62	NA		
PA/PV ratio	1.1	0.69 to 1.1	0.61	NA		
Endarterectomy 77	HR	95% CI	P value	HR	95% CI	P value
Central clot volume	1.17	0.98 to 1.4	0.07	NA		
Central (median >0.4)	1.2	0.27 to 5.3	0.79	NA		
Non-central clot volume	1	0.87 to 1.14	0.9	NA		
Total clot volume	1.03	0.94 to 1.12	0.49	NA		
Main PA volume	1	0.99 to 1.02	0.1	NA		
PA volume	1	0.99 to 1	0.92	NA		
PV volume	1	0.99 to 1.02	0.11	NA		
PA/PV ratio	0.45	0.1 to 1.9	0.29	NA		

No endarterectomy 102	HR	95% CI	P value	HR	95% CI	P value
Central	1.32	1.1 to 1.55	<0.001	1.42	1.1 to 1.73	<0.001
Central (median >0.4)	2.2	1 to 4.6	0.03	NA		
Non-central	1.05	0.99 to 1.1	0.059	NA		
Total clot volume	1.05	1 to 1.1	0.01	NA		
Main PA volume	1	0.99 to 1	0.65	NA		
PA volume	1	0.99 to 1	0.55	NA		
PV volume	0.99	0.99 to 1	0.5	NA		
PA/PV ratio	1.3	0.83 to 2.2	0.21	NA		

Not applicable (NA). Volumes in millilitres (ml).

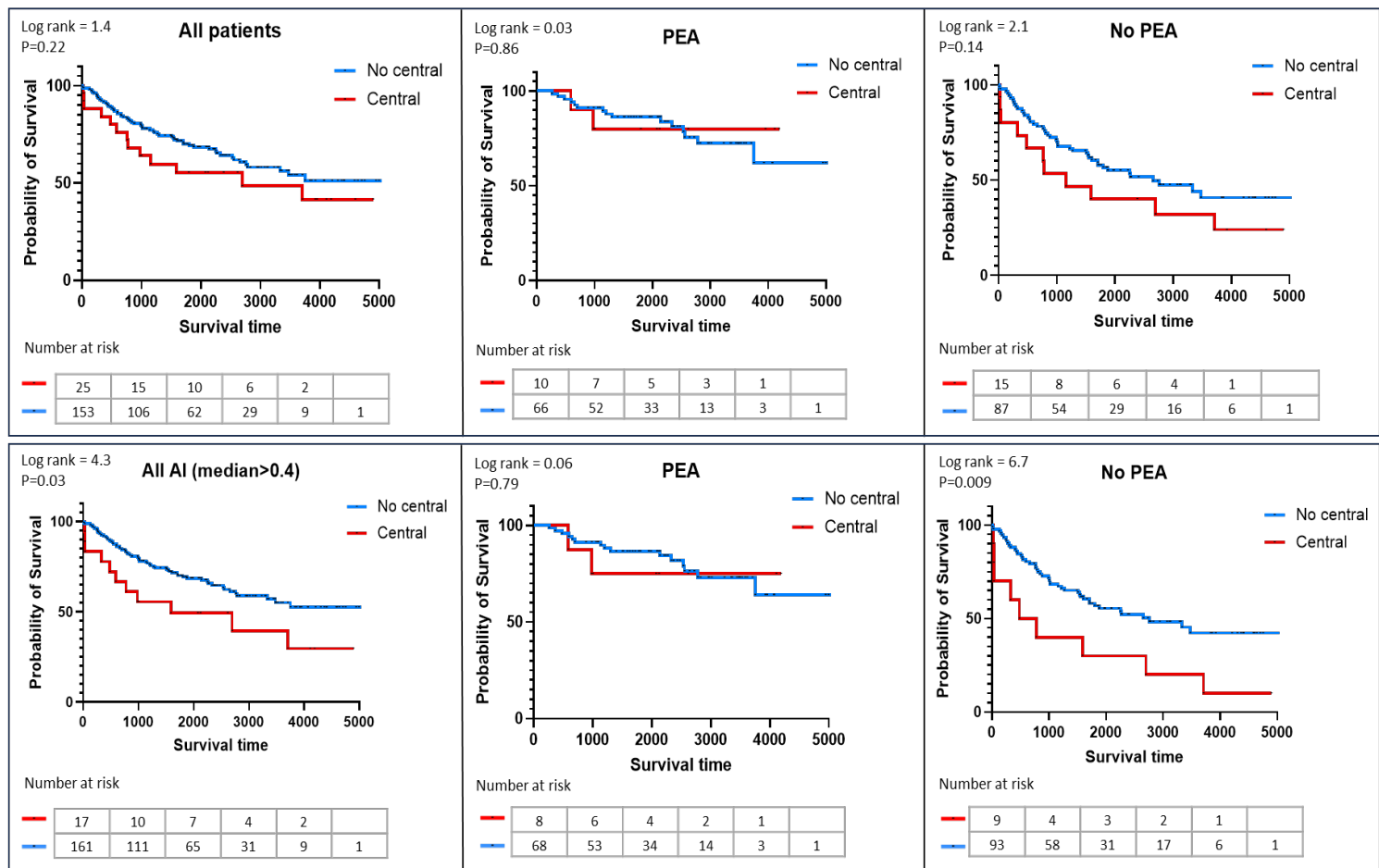


Figure 7.12 Kaplan–Meier survival curves for a total of 179 patients with CTEPH, compared by pulmonary endarterectomy (PEA) versus no PEA groups. The curves compare survival outcomes based on central disease detected using binary AI, and AI with median>0.4.

AI-derived clot volume vs. manual scoring system (As described in Chapter 6)

A strong positive correlation was observed between the manual total scoring (scored out of 13) and the AI-derived total clot volume, as measured by Spearman's correlation (0.72, 95% CI: 0.61 to 0.80, $p < 0.001$).

A subset of 120 patients with CTEPH was used to compare central disease severity between AI-derived clot volume and manual scoring outcomes. Including patients who underwent endarterectomy ($n=55$) and those not undergoing endarterectomy ($n=65$). Binary labels were generated by thresholding the median value, with an AI-derived median > 0.35 ml and a manual median score > 2 were assigned a value of 1; all others were labelled as 0 (1 = central, 0 = no central).

Univariate Cox regression analysis identified several significant predictors of mortality in central disease based on both AI-derived and manual scoring (**Table 7.8**). In the full cohort, both AI-derived central volume ($HR=1.2$, $p=0.001$) and AI-derived median central ($HR=2.6$, $p=0.008$) were significantly associated with worse outcomes. While manual median scoring showed a weaker association with outcomes ($HR=1.89$, $p=0.03$), the central manual score was ($HR=1.7$, $p=0.05$).

Kaplan–Meier survival analysis on AI-derived median > 0.35 ml and manual scoring median > 2 , are demonstrated in **Figure 7.13**. AI-derived median was significantly associated with worse survival in the overall cohort ($p=0.006$) and in patients who did not undergo endarterectomy ($p=0.01$). No significant difference in survival was observed in the endarterectomy subgroup. Likewise, in the manual scoring median-based, there was a significant difference between patients with central and no central disease ($p=0.03$). However, in patients who did not undergo endarterectomy, there was no significant difference in survival between central and no central disease ($p=0.22$).

Table 7.8 Univariate cox regression analysis of central thromboembolic burden comparing AI and manual scoring across all patients (n=120), patients with endarterectomy (n=55), and those without endarterectomy (n=65). Hazard ratios (HR), 95% confidence intervals (CI), and p-values are provided for AI-derived binary classification, AI clot volume, AI binary using median>0.35, and manual binary scoring median>2.

Variables	Univariate analysis		
All patients (120)	HR	95% CI	P value
Central (AI clot volume) (ml)	1.2	1.07 to 1.34	0.001
Central (AI median>0.35)	2.6	1.2 to 5.51	0.008
Central (manual scoring)	1.7	0.99 to 3.1	0.05
Central (manual median>2)	1.89	1.03 to 3.4	0.03
Endarterectomy (55)	HR	95% CI	P value
Central (AI clot volume) (ml)	1.2	1 to 1.42	0.03
Central (AI median>0.35)	1.88	0.41 to 8.4	0.41
Central (manual scoring)	2.1	0.75 to 5.8	0.15
Central (manual median>2)	2.8	1.04 to 8.01	0.04
No endarterectomy (65)	HR	95% CI	P value
Central (AI clot volume) (ml)	1.2	1.07 to 1.52	0.005
Central (AI median)	2.7	1.18 to 6.3	0.01
Central (manual scoring)	1.58	0.78 to 3.1	0.2
Central (manual median>2)	1.6	0.74 to 3.4	0.22

Volumes in millilitres (ml).

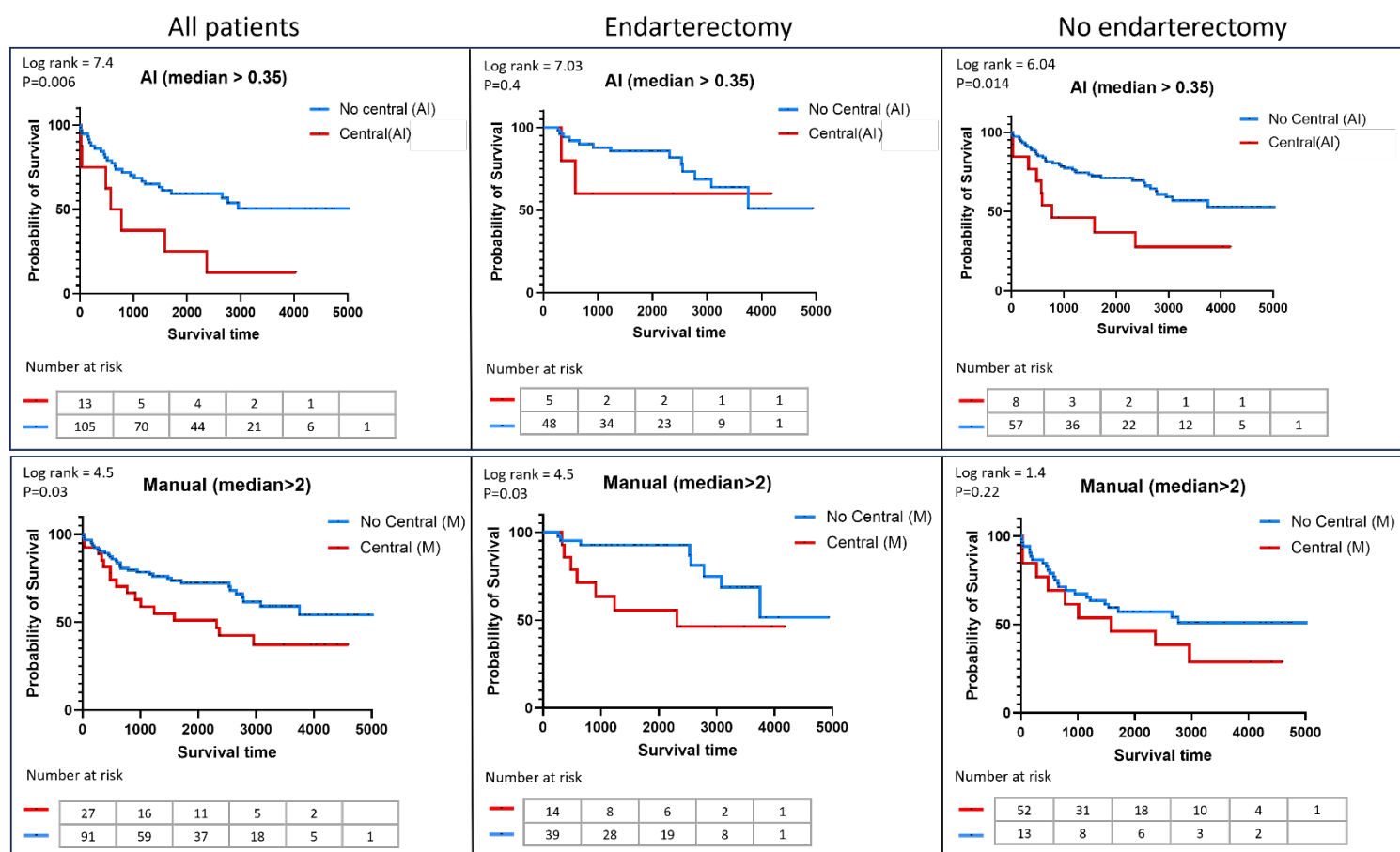


Figure 7.13 Kaplan–Meier survival curves for patients with CTEPH stratified by the presence of central thromboembolic disease, assessed using AI-derived median clot volume and manual median scoring. The cohort includes 120 patients (PEA: 55 [46%], female: 67 [56%], mean age: 57 ± 25.3 years).

7.5 Discussion

This study presents an automated 3D segmentation for PA, PV and thromboembolic disease with clinical validation using clinical CTPA cohorts. The model achieved high accuracy for PA and PV segmentation but demonstrated lower accuracy for prediction of the manual thromboembolic disease segmentations. To the best of our knowledge, this study is the first to apply a volumetric segmentation framework using nnU-Net to automate the segmentation of chronic thromboembolic disease, highlighting both the potential and limitations of this method. The primary finding of this study is that an AI-driven clot segmentation model applied to CT imaging may predict both the presence of CTEPH and patient survival. This work has shown that central disease detected by AI may serve as a prognostic indicator for patients with CTEPH. AI-driven quantification may reduce interobserver variability, providing a more objective and reliable method for detecting high-risk patients (Shin et al., 2025). The strong positive correlation between our manual scores and AI-derived clot volumes further supports the clinical validity of these automated tools. These results show the possibilities of AI-based measurements to improve manual assessment, resulting in enhancing prognosis and along with clinical decision-making.

The high Dice score for PA and PV are indicative of a high degree of agreement between the model predictions and the ground truth annotations. Our performance metrics are comparable to those previously reported in vascular segmentation deep learning methods. Prior studies have achieved DSC of 0.94 (Nardelli et al., 2018), 0.92 (Zhang et al., 2019), 0.84 (Wu et al., 2023), 0.89 (Chu et al., 2025), 0.87 (Zhou et al., 2023), 0.86 (Ming et al., 2025), and 0.82 (Qin et al., 2021) for segmentation of the PA and PV compared with a DSC of 0.95 in this study. The structure of pulmonary vasculature differs across patients, including variations in pulmonary vessels diameter, angulation and presence of disease. Accurate differentiation between the PA and PV is essential for identifying and treating pulmonary diseases. Clinical diagnosis, thrombus localisation, and treatment planning can all depend on the automated segmentation of PA and PV in CTPA images.

In contrast, segmentation of thromboembolic disease achieved a lower agreement with DSC of 0.58. PE segmentation has demonstrated good accuracy, with reported DSC of 0.64 (Pu et al., 2023), and 0.74 (Ajmera et al., 2022). Interobserver variability in segmenting chronic thromboembolic disease remains a challenge, as demonstrated by the variation in DSC scores between the two observers. This variability results from the complex vascular remodelling caused by the presence of organised thromboembolic material, leading to intimal abnormalities, stenoses, and webs, which further increase the difficulty of the segmentation task (Cui et al., 2019, Gopalan et al., 2017). Furthermore, pulmonary arteries and veins show in similar grayscale on CT images, especially in smaller distal vessels, challenging both manual and AI-based segmentation. Despite these challenges, our study demonstrated moderate interobserver agreement for total clot volume quantification (ICC = 0.69). Previous studies using CT-based classification have reported comparable findings, with reported kappa values of 0.51 (Grafham et al., 2023), 0.55 (Eberhard et al., 2022), and 0.64 (McInnis et al., 2020), highlighting the reproducibility radiological assessment of disease extent in patients with CTEPH. In addition, our study observed an excellent agreement for central disease, reflecting the relative ease of identifying larger, more proximal thromboembolic disease. In contrast, agreement for non-central (segmental and subsegmental) disease was lower with ICC = 0.57, in line with the low agreement for distal thromboembolic disease reported by Grafham et al. (2023), with kappa values of 0.31. This highlights the challenge of reliably assessing distal thromboembolic disease. Advanced imaging techniques combined with AI models may help address the underdiagnosis of distal disease, often caused by the limited visualisation of conventional CTPA (Gotta et al., 2024).

In our test set, the proposed model achieved an overall AUC of 0.92 for thromboembolic disease prediction, with a specifically higher AUC of 0.97 for patients with CTEPH. Our model performed better at distinguishing chronic thromboembolic disease from no clot cases compared to acute PE, which may be attributed to datasets imbalance, artefacts and the increased anatomical variability. The lower number of acute PE cases compared to CTEPH cases may lead to biased performance estimation towards the most frequent cases (Lobo et al., 2008), in addition there was a lower volume of clot in the PE cases as compared to clot volume in CTEPH. In contrast, Ma et al. (2022) observed lower detection performance for chronic PE with AUC of 0.69, compared to acute PE with AUC of 0.93, thus highlighting the

diagnostic difficulties related with chronic PE and the possibility of our approach in addressing this gap. While Vainio et al. (2023) achieved an AUC of 0.94 using a multi-network ensemble model, their use of maximum intensity projection-derived images resulted in the loss of critical spatial detail, limiting the model's ability to detect important features for the diagnosis of CTEPH. Our volumetric approach used important spatial features, which may help explain the improved performance of our model in patients with CTEPH. In a recent abstract, Nardelli et al. (2023) developed an AI-based method for the detection and quantification of pulmonary micro thrombi in patients with CTEPH using CTPA images. The model achieved excellent diagnostic performance, with an AUC of 0.89, but more validation is required to ensure its robustness and reliability.

We established a standardised radiological grading system to assess the accuracy of segmentation in the test set based on the diagnostic impact. Our study demonstrates that AI-driven segmentation of PA, PV and thromboembolic disease achieve good clinical performance, with no segmentation failure. However, even minor errors, such as incorrectly classifying arteries or failing to fully segment distal arteries, might have a significant clinical impact on the evaluation of thromboembolic disease. Previous research has shown a lower sensitivity in detecting thrombi in distal arteries compared to central disease, highlighting the challenge of identifying less prominent abnormalities in these peripheral areas (Sugiura et al., 2013, Rogberg et al., 2019). Additionally, misclassification of thrombus, for example false negatives in distal arteries, may have clinical impact in patients with CTEPH (Delcroix et al., 2016, Wittram et al., 2004). Expert radiological evaluation is still required, for small, distal, or low-attenuation thromboembolism disease.

The strong correlation between AI-derived clot volumes and manual scoring demonstrates the clinical validity of automated quantification for patients with CTEPH. Recent studies have evaluated AI-based PE detection, highlighting the need for better methods to support CTEPH diagnosis (Ayobi et al., 2024, Cheikh et al., 2022). Our results show evidence for the clinical relevance of AI-based clot volume quantification in patients with CTEPH. The study showed that segmental and distal disease burden demonstrated a stronger correlation with PVR compared to central disease, although the overall strength of the correlation was modest. This result is corroborated by previous studies demonstrating that distal pulmonary

vasculopathy might elevates PVR in patients with CTEPH (Delcroix et al., 2021, Dorfmueller et al., 2014). Furthermore, studies have shown that the performance of pulmonary endarterectomy in patients with distal CTEPH, which includes segmental and subsegmental disease, is both can be feasible and effective (Yang et al., 2023, Fernandes et al., 2023).

On univariate survival analysis both central and total clot volume exhibited substantial relationships with mortality throughout the whole population, with notably strong correlations in patients who did not undergo pulmonary endarterectomy. In patients not having endarterectomy, central clot volume continued to be a significant predictor of mortality, after adjusting for demographic and clinical factors. This demonstrates that central clot volume independently correlates to worse survival outcomes and may serve as a key prognostic marker in patients who did not undergo endarterectomy.

This study also demonstrated that central thromboembolic burden, quantified using both AI-derived and manual scoring defined by median-based, is significantly associated with survival in patients with CTEPH. Notably, AI-derived central median was associated with worse outcomes compared to manual scoring median. Although AI might provide consistency and scalability, it may over or underestimate disease severity in certain cases due to limitations in training data and an inability to fully account for clinical details that experienced clinicians consider during manual assessments (Norori et al., 2021). Additionally, our manual scoring identified a significant survival difference between patients with central disease severity, supporting the clinical importance of visually assessed thromboembolic distribution. These findings may support the integration of AI-derived clot burden as a prognostic tool, particularly for identifying high-risk patients who may not be surgical candidates.

Manual segmentation was a time-consuming task, often requiring up to an hour per case based on the anatomical variability and CT image quality. On the other hand, the AI-based model performed segmentation in approximately 2-3 minutes, indicating a potential enhancement in workflow efficiency.

However, our study is subject to several limitations. The model was trained using data gathered from a single institution, although it was generated using scanners from multiple

manufacturers. The proposed model was not tested on an external cohort, which is required to assess its generalisability and performance. The test set included only a limited number of patients with suspected CTEPH, which may restrict the generalisability of our findings. The evaluation of scans was performed by only two observers. Patients were identified retrospectively, limiting our capacity to account for possible confounders. AI performance may be limited by imaging artefacts, poor vascular opacification, and segmentation errors in the pulmonary arteries. Severe artefacts impede typical visual evaluation for radiologists and can lead to misinterpretations. Furthermore, there is a significant methodological difference between AI-based and manual scoring: in AI segmentation, central disease includes involvement of the lobar arteries, whereas in manual scoring, central disease is defined as affecting only the main pulmonary arteries (left and right). This inconsistency may have an influence on direct comparisons between AI and manual evaluations, thereby impacting model performance interpretation. In addition, this study did not compare AI-derived volumes and manual volumes directly for survival prediction. Future work is required to explicitly analyse the clinical impact of AI-based evaluations compared to manual to determine if AI gives similar or better results in clinical assessment.

7.6 Conclusion

A PA, PV, and thromboembolic diseases nnU-Net segmentation model was developed with high accuracy for vascular segmentation and moderate for thromboembolic disease segmentation. The AI-driven analysis highlights the potential in quantifying the volumetric measurements of the chronic thromboembolic disease, predicting CTEPH presence, and providing prognostic insight into patient survival. Interobserver comparison in segmenting CTEPH demonstrated moderate agreement overall, with the highest consistency achieved in the segmentation of central thromboembolic disease. AI-derived volumetric measures correlated strongly with haemodynamic parameters and demonstrated performance comparable to manual assessments in patients with CTEPH. Future work should focus on enhancing model accuracy for non-central disease, expanding annotated datasets, and improving the reliability of AI-based assessments across diverse clinical settings.

Supplementary Table

Table S1. DSC and Sensitivity scores for each patient in performance testing including (CTEPH, Acute PE, and no clot) cases.

Case	Dice Similarity Coefficient (DSC)			Sensitivity		
	PA	PV	Clots	PA	PV	Clots
1	0.90	0.91	0.27	0.92	0.89	0.19
2	0.93	0.94	0.63	0.91	0.93	0.59
3	0.95	0.94	0.71	0.93	0.92	0.68
4	0.92	0.93	NA	0.88	0.88	NA
5	0.93	0.95	0.40	0.89	0.92	0.48
6	0.93	0.94	0.79	0.88	0.91	0.87
7	0.96	0.97	0.22	0.94	0.95	0.16
8	0.95	0.96	0.40	0.92	0.94	0.37
9	0.96	0.97	0.21	0.94	0.96	0.12
10	0.96	0.95	0.34	0.94	0.93	0.21
11	0.96	0.94	0.86	0.95	0.92	0.92
12	0.97	0.96	NA	0.95	0.95	NA
13	0.97	0.96	NA	0.96	0.96	NA
14	0.96	0.97	0.77	0.95	0.95	0.65
15	0.94	0.94	0.72	0.90	0.90	0.78
16	0.94	0.96	0.65	0.92	0.94	0.50
17	0.94	0.91	NA	0.95	0.94	NA
18	0.97	0.95	0.74	0.95	0.93	0.78
19	0.96	0.96	0.45	0.95	0.94	0.35
20	0.95	0.93	0.59	0.92	0.90	0.64
21	0.95	0.95	NA	0.94	0.93	NA
22	0.96	0.96	0.71	0.94	0.94	0.83
23	0.96	0.95	0.74	0.94	0.94	0.73
24	0.96	0.96	NA	0.93	0.94	NA
25	0.95	0.95	0.49	0.94	0.93	0.45
26	0.98	0.97	NA	0.97	0.96	NA
27	0.98	0.97	0.55	0.96	0.96	0.90
28	0.95	0.95	NA	0.92	0.91	NA
29	0.95	0.95	0.63	0.94	0.94	0.48

30	0.95	0.95	0.72	0.94	0.92	0.63
31	0.96	0.96	NA	0.96	0.96	NA
32	0.96	0.97	0.79	0.96	0.96	0.72
33	0.96	0.95	0.58	0.95	0.94	0.62
34	0.93	0.93	NA	0.90	0.90	NA
35	0.95	0.96	NA	0.93	0.94	NA
36	0.94	0.95	0.45	0.93	0.93	0.31
37	0.94	0.96	0.57	0.94	0.95	0.44
38	0.95	0.96	0.00	0.92	0.94	NA
39	0.97	0.96	NA	0.96	0.95	NA
40	0.95	0.94	0.58	0.93	0.91	0.53
41	0.94	0.97	NA	0.90	0.94	NA
42	0.95	0.96	NA	0.90	0	NA
43	0.94	0.95	0.23	0.92	0.89	0.74
44	0.96	0.97	NA	0.91	0.93	NA
45	0.97	0.96	NA	0.93	0.92	NA
46	0.97	0.96	NA	0.88	0.88	NA
47	0.95	0.95	NA	0.89	0.92	NA
48	0.98	0.97	NA	0.88	0.91	NA
49	0.97	0.95	NA	0.94	0.95	NA
50	0.97	0.97	NA	0.92	0.94	NA
51	0.96	0.97	NA	0.94	0.96	NA
52	0.96	0.96	NA	0.94	0.93	NA
53	0.97	0.96	NA	0.95	0.92	NA
54	0.96	0.95	0.07	0.95	0.95	0.04
Mean ± SD (95% Confidence Interval)	0.95 ± 0.01 (0.95 to 0.95)	0.95 ± 0.01 (0.95 to 0.95)	0.58 ± 0.19 (0.49 to 0.67)	0.93 ± 0.02 (0.92 to 0.94)	0.93 ± 0.01 (0.93 to 0.94)	0.54 ± 0.24 (0.45 to 0.64)

8 Discussion

This is a chapter overview discussion of the work. For a full discussion of each chapter of the thesis, kindly review each of the associated chapters.

This thesis evaluated CT lung parenchymal characteristics as predictive indicators in CTEPH patients. It also presented a scoring system for visual assessment of chronic thromboembolic on CTPA, which incorporates both location and extent to determine the impact of disease location on survival outcomes. In addition, we conducted a systematic review of deep learning applications in chronic thromboembolic disease and developed a novel AI-based segmentation model. This model was clinically validated for automated quantification of thromboembolic burden and evaluation of its prognostic significance.

The Methods chapter outlines two key contributions of this thesis in addition to the scientific findings and published manuscripts. These contributions described the creation of a clinical radiological database and the establishment of a procedure for AI application in patients with CTEPH using CTPA. A combination of NHS imaging datasets presented some challenges, specifically variations in image quality and acquisition settings. The segmentation of vascular and thromboembolic disease requires not only technical expertise but also a thorough understanding of the clinical relevance of imaging findings. Additionally, my involvement in CT image assessment helped me better understand imaging artefacts, anatomical variances, parenchymal features, and disease appearances as a clinical academic radiographer.

Chapter three presented the systematic review (published in *Frontiers in Radiology*) that forms fundamental research into the potential function of artificial intelligence in diagnosing and detecting CTEPH using CTPA. This review highlighted both the potential advantages and the challenges inherent in this approach, presenting a critical assessment of existing studies and identifying gaps in current research, to indicate areas for future study. The results showed that, despite the massive research on acute PE, there are limited studies investigating AI

applications for chronic PE and CTEPH. However, the study highlighted the potential of AI in interpreting CTPA for patients with CTEPH, improving diagnostic accuracy.

In chapter five (published in European Respiratory Journal Open Access), the study demonstrated the significance of CT systematic evaluation of parenchymal and cardiac chambers abnormalities in patients with CTEPH. A semi-quantitative methodology was employed, incorporating CT reports and subjective visual assessments to evaluate the scans within the database. This study is the first to report that increased aortic diameter is associated with adverse outcomes, potentially reflecting the burden of underlying comorbidities. Mosaic perfusion and lung infarction demonstrated as common radiographic findings of CTEPH, which correlate with signs of disease severity. In patients who underwent PEA, the presence of mosaic perfusion or infarction had no significant influence on mortality. However, in patients who did not undergo PEA, the absence of mosaic perfusion was associated with increased mortality, potentially due to a higher prevalence of underlying parenchymal lung disease. In addition, the study found a significant frequency of co-existing lung diseases in patients with CTEPH, indicating their importance in determining clinical outcomes. These findings offer valuable insight into the relationship between vascular involvement, parenchymal lung abnormalities, and disease severity indicators, providing crucial information for the risk assessment and management of patients with CTEPH.

Chapter six (submitted to BJR) described the development and clinical assessment of a novel clot scoring system in patients with CTEPH using CTPA. The scoring system was created to account for both disease location and extent, resulting in a formal framework for assessing disease burden and its effect on survival outcomes. Quantitative CT evaluation of clot burden, anatomical distribution, and severity in CTEPH might provide useful diagnostic assistance for radiologists. We found that central disease presence is a predictor of mortality in patients who do not undergo PEA. The scoring method demonstrated significant interobserver agreement, proving its reliability and repeatability in analysing CTEPH distribution. However, interobserver agreement was lower in distal disease cases, most likely due to the difficulty in evaluating smaller, more peripheral arteries. This highlights the need of utilising clinically appropriate AI model resolutions or advanced imaging methods to help improve distal disease detection. Additionally, significant correlations were found between distal disease with PVR

and lung parenchymal abnormalities such mosaic perfusion and lung infarction, which may contribute to disease development through changes in pulmonary blood flow and pulmonary tissue ischaemia. A significant correlation was observed between disease burden and haemodynamic abnormalities. A greater chronic thromboembolic disease scores were associated with higher PVR and mPAP, reflecting the expectation that greater thrombus load leads to increased right ventricular afterload.

In chapter seven, we developed AI segmentation models for PA, PV and thromboembolic disease using CTPA imaging. The model achieved high accuracy of (0.95) for PA and PV, but performed moderately for thromboembolic disease (0.58), with no failures in segmentation of the three structures. Interobserver comparison demonstrated that the distal disease segmentation showed the most variation between observers. the difficulties of segmenting CTEPH resulting from anatomical diversity, organised thrombus, imaging artefacts, and a lack of annotated images. We also conducted a clinical evaluation of the AI-driven thromboembolic segmentation to assess the prognostic value of volume-based disease location in patients with CTEPH. This study found that central disease was a significant predictor of mortality in those who did not undergo endarterectomy. The accuracy of AI-driven thromboembolic segmentation was supported by the high correlation between automated thromboembolic disease volume and manual scoring analysis (as previously described in chapter 6). The integration of radiological assessment with AI-driven thromboembolic segmentation enhances the prognostic prediction capability of CTPA imaging as a robust imaging biomarker for CTEPH.

8.1 Limitations

The purpose of the thesis was to address critical gaps in CTEPH imaging studies by: (1) conducting a systematic evaluation of parenchymal and cardiac CT abnormalities and their prognostic significance, (2) establishing a standardised thromboembolic burden quantification method, and (3) developing an AI algorithm to perform a comprehensive clinical evaluation of the segmentation results.

One overarching limitation is that all analyses were conducted on retrospective data. Retrospective studies use previously acquired data rather than designing and conducting new research to address certain questions. Bias and other restrictions may result from this, which might compromise the reliability and applicability of the results. While all patients underwent CTPA, varying numbers underwent right heart catheterisation (RHC), pulmonary function test (PFT) and pulmonary endarterectomy. None of the patients included in this thesis underwent balloon pulmonary angioplasty (BPA), as this treatment option was not available during the study period (2008–2018). In the UK, they are currently accepted plan of treatment for patients with inoperable CTEPH. We did not have any information on anticoagulant strategies and postoperative targeted medications.

We created a CTEPH clinical radiology database from the ASPIRE registry. The results of this thesis were verified in a realistic clinical cohort utilising two CT scanners. Although the ASPIRE registry has data from many centres, both the semi-qualitative CT assessments and the application of the AI model in this work were carried out using data from a single site (Sheffield). Consequently, the generalisability of the findings could be limited. In Addition, this thesis did not use any advanced CT technologies, such as dual-energy CT or photon-counting CT, which might restrict the visualisation and the detection of small distal disease and minor vascular changes in patients with CTEPH. Advanced CT scanners help to improve the image quality and diagnostic accuracy of CTEPH.

A radiologist and a radiographer (both experienced in cardiothoracic imaging) conducted all labelling, segmentation, CT measurements, and evaluations of CTPA images. However, the

degree of the interobserver variability could limit the generalisability of the study findings, specifically in distal disease. For example, RV/LV measurements on CTPA have been shown to be poorly reproducible even among experienced radiologists (Lanham et al., 2022). While interobserver agreement was assessed through this thesis, variability in interpreting distal disease may still influence the consistency and applicability of certain results.

In the systematic review (chapter 3), despite including conference abstracts in the eligibility criteria, only five studies met the inclusion requirements, limiting the ability to perform a formal meta-analysis of model performance. The review was limited to studies that specifically investigated the application of AI for diagnosing chronic pulmonary embolism (PE) or CTEPH on CTPA imaging. Methodological techniques and the reporting of dataset characteristics, including demographics, disease severity, and the number of chronic PE patients, vary between the included studies. This inconsistency affects the ability to accurately assess the generalisability and clinical applicability of the AI algorithms.

In chapter 5, The study classified lung parenchymal anomalies (such as mosaic perfusion and lung infarction, using a semi-quantitative scoring method. However, the definitions and thresholds for these classifications were not standardised, which may limit the comparability of the findings with other studies. The study did not evaluate the impact of treatments (such as, medical therapy or PEA), which limits the correlation between CT features and outcomes. Understanding treatment impact on quality of life offers valuable insight for patient management.

The findings from chapter 6 may not fully apply to broader populations with different clinical characteristics or treatment approaches. Another limitation is that intra-observer variability was not assessed. Although interobserver agreement was high, the consistency of individual observers over time remains unknown. Furthermore, the scoring system is still a semi-quantitative approach that depends on visual assessment; however, it successfully classifies the distribution of diseases.

In chapter 7, the primary limitations of AI research in medical imaging for CTEPH are the inadequate number of expert annotated training datasets, the lack of extensive clinical

datasets, and a limited diversity of patient demographics for model validation. Following prospective validation and, if feasible, randomised controlled studies for PA and PV segmentation, the next step towards routine clinical application was the initiation of clinical trials. While the lower performance in thromboembolic segmentation, emphasises the requirement of additional methods for model and data refining. The test set contained only a limited number of patients with CTEPH and acute PE, which may limit the reliability of performance in general clinical practice. The absence of external validation is a key gap, as the model's performance has yet to be evaluated across multiple institutions, scanner types, and patient groups. Without multicentre validation, we cannot analyse possible biases in our single-centre dataset, such as institutional imaging techniques and patient selection criteria. Artefacts, suboptimal contrast opacification, and pulmonary artery segmentation errors can degrade AI performance to identify thromboembolic disease. Severe artefacts, which also challenge radiologists, may lead to misclassification in both AI predictions and manual radiological assessments.

It is crucial to acknowledge the inherent challenges in achieving a universally accepted, ground-truth segmentation of thromboembolic pulmonary disease, as inter-reader variability remains a well-documented limitation across medical imaging disciplines (Webb et al., 2021, Wilson et al., 2021). AI diagnosis models inherently possess biases that are challenging to quantify, shaped by the characteristics of their training datasets. Specifically, the model's learning process is influenced by the subjective interpretations, preferences, and biases of the two observers responsible for labelling and segmenting the training data. For instance, differences in radiologists' capacity to identify small-vessel thrombosis or distinguish between organised thrombi and vascular remodelling may introduce bias into the model. Distal disease poses a significant diagnostic challenge to identify due to their small size, peripheral location, and often subtle imaging appearance, which can contribute to interobserver variability. To enhance the robustness and generalisability of the model, incorporating a more diverse group of radiologists with varying levels of expertise could improve its applicability across a wider range of clinical settings.

Every AI model is specifically trained to address a particular clinical question, with the main objective of this thesis is to assess the prognostic impact of diagnosing thromboembolic

disease. Therefore, the AI algorithm was trained on a biased dataset consisting of patients with preassigned diagnoses of acute PE and CTEPH. Although the algorithm shows promising results in segmenting and predicting thromboembolic pulmonary disease, it is therefore limited to this particular group of patients and cannot be generalised to other diseases or conditions. Additionally, The AI model also lacks the ability to distinguish patients with CTEPH and acute PE, therefore suggesting a diagnostic disadvantage of the model. As a result, without additional training, transfer learning, or adaptive techniques the algorithm is ineffective as a diagnostic tool in larger clinical applications. AI algorithms are constrained and biased by the demographics, disease subgroups, and data quality of the training dataset. These limitations reflect the difficulties encountered even by expert radiologists in identifying organised thromboembolic disease in patients with CTEPH. This highlights the importance of continuously refining and validating AI models in order to improve diagnosis accuracy and clinical applicability.

An important methodological distinction exists between the AI and manual scoring approaches regarding disease localisation. The AI system adopts a more inclusive definition of central disease, incorporating both main pulmonary arteries (left and right) and lobar arteries in its assessment. In contrast, the manual analysis considers only main pulmonary artery, left and right involvement as central disease, classifying lobar artery involvement as segmental disease. This difference in classification criteria introduces potential challenges when comparing AI and manual performance metrics, as cases with isolated lobar involvement would be categorised differently by each method. Such inconsistencies may have an impact on the apparent agreement between automated and manual assessments and should be carefully evaluated when analysing comparative performance outcomes.

Despite these limitations, our study shows both the promise and opportunity for further development in AI-derived thromboembolism disease segmentation.

9 Future work

Building on the results given in this thesis, there are a number of potential opportunities for future study that might increase our understanding of the diagnosis and treatment of patients with CTEPH.

This thesis presents research based on retrospective analysis. Further research to establish a prospective cohort to assess the diagnostic value of chronic thromboembolic disease, as well as pulmonary vascular and cardiac measurements, could be helpful. The validity and valuable relevance of these results would be further improved by carrying out larger, multi-centre investigations and prospective experiments.

The study offers a solid basis for identifying the method by which CTEPH is associated with CTPA characteristics, including parenchymal lung disease, mosaic perfusion, and lung infarction. However, several directions for additional research might be developed based on these outcomes to further progress the field of study. One area for further research is to evaluate the effect of CTPA features on outcomes in patients undergoing balloon pulmonary angioplasty (BPA). Incorporating patients who have undergone BPA, which is recently utilised as a treatment method for CTEPH, may provide a more comprehensive understanding of how imaging characteristics affect results across various treatment modalities. Additionally, assessing changes in CT features after treatments such as pulmonary endarterectomy (PEA) or BPA, may be helpful in determining treatment effectiveness. In order to find more prognostic indicators and enhance risk stratification, future research should also investigate the function of new biomarkers, such as genetic and inflammatory markers, along with radiomics. Longitudinal studies with extensive follow-up periods can be used to estimate the long-term effects of CT characteristics on mortality, functional outcomes, and progression of CTEPH disease.

While this work had complete CTPA data for all patients, the diversity in the number of patients who received right heart catheterisation (RHC) and pulmonary function testing (PFT), may restrict comparison analysis. To overcome this, future prospective research should

prioritise standardised data collection of multiple tests that ensure diagnostic techniques are applied consistently across all study participants. This would provide more comprehensive comparisons and correlations between imaging results and haemodynamic or functional outcomes. This possible investigation utilising standardised diagnostic approaches might confirm and enhance our findings, hence improving patient decision-making.

Further segmentation of chronic thromboembolic disease in patients with CTEPH could be considered to improve the performance of the model. However, to enhance our AI model, future work should first focus on enhancing the diversity of training data by incorporating larger and multi-institutional datasets that include a wider range of CTEPH cases. Second, the model architecture should be optimized to reduce overfitting and improve performance across diverse patient populations, imaging protocols, and techniques. Several strategies might be considered in the future to improve segmentation of chronic thromboembolic disease, including patch-based image analysis methods to enhance detection and the use of generative techniques to reduce image artefacts. While these generative methods show promise for improving segmentation accuracy and model reliability, the risk of image hallucination remains a critical concern, as it could introduce false features that may mislead clinical interpretation. We are also exploring semi-supervised learning techniques, including black-box models capable of utilising both labelled and unlabelled datasets. Tools such as Grad-CAM or occlusion sensitivity maps can be used for understanding decisions in image classification and highlight the most significant regions of the image. Third, integrating CTPA findings with haemodynamic parameters may provide valuable background data to improve the diagnostic accuracy of the model. Finally, the pretrained models will be further analysed by performing additional fine-tuning and comparing them to the standard pretrained models. Further model refinement, training with more diverse and annotated datasets, and external validation are essential before clinical application.

The AI methodology and processes applied in this thesis to quantify acute PE and CTEPH can be developed to automatically quantify additional imaging characteristics. Possible requirements in a chest CTPA scan include quantification of mosaic perfusion, lung infarction, air trapping and consolidation. At the same time, some initial development work has been done on these approaches. Segmentation of imaging features, including mosaic perfusion,

lung infarction, air trapping, and consolidation is initially started using MIM software in patients with CTEPH. The aim is to develop an integrated and comprehensive CTPA model that combines multiple AI systems to automatically analyse and quantify a variety of imaging characteristics in patients with CTEPH. CTPA might then measure the abnormalities in the lung parenchyma associated with CTEPH, analyse the pulmonary arteries, and determine the severity of CTEPH. This would considerably improve radiological reporting and give quantifiable outcomes for measuring prognostic effects.

Advanced imaging techniques, such as dual-energy computed tomography (DECT), lung subtraction iodine mapping (CT LSIM), and high-resolution imaging with photon-counting CT, have not yet been fully utilised by AI tools. Future research could build on this thesis by exploring the integration of AI with these modalities, which hold the potential to enhance diagnostic workflows and help in earlier detection of CTEPH.

Another interesting area for future work is to comprehensively examine the correlation between haemodynamic flow patterns in the main pulmonary arteries and AI-derived central clot volume. Such a study could offer deeper insight into the mechanisms underlying chronic thromboembolic disease formation in the main pulmonary arteries. Central chronic thromboembolic disease, presumably located in the main pulmonary arteries, may reflect slow or turbulent flow in the proximal pulmonary arteries as a consequence of severe pulmonary hypertension and reduced cardiac output. Advanced imaging techniques, such as computational fluid dynamics (CFD) or 4D flow magnetic resonance imaging (MRI), can be utilised to assess flow patterns, including turbulence, shear stress, and velocity characteristics, in patients with severe pulmonary hypertension. Using advanced imaging techniques to assess patients with severe pulmonary hypertension could help evaluate whether a higher thrombus burden is associated with more severe turbulent flow.

10 Conclusion

This thesis proposes semi-quantitative assessments and AI-driven quantitative analyses to evaluate the role of CTPA in patients with CTEPH. The results demonstrated that parenchymal lung changes on CTPA are common in CTEPH and have an adverse impact on survival. An increase in aortic diameter predicts poorer outcomes, likely attributable to the influence of underlying comorbidities. Patients with CTEPH should undergo a systematic evaluation of the lung parenchyma, cardiac chambers and pulmonary vessels, to emphasise its prognostic importance. It further presented a novel scoring system to assess the location and severity of chronic thromboembolic disease. The presence of central disease was found to be an independent risk factor for worse outcome in patients not undergoing endarterectomy. Distal thromboembolic disease demonstrated the lowest interobserver agreement compared to central and segmental disease. The thesis also developed an automated AI model for quantifying PA, PV and thromboembolic disease. Although the segmentation accuracy for thromboembolic disease was suboptimal relating to the challenging human task of thromboembolic segmentation, the model demonstrated high classification performance and robust correlations with haemodynamic parameters. This demonstrates the potential to assist in the diagnosis, prognosis, and quantification of the chronic thromboembolic disease burden. This work has enhanced understanding of thromboembolic burden in CTEPH and demonstrates its potential to help in refining diagnosis, risk stratification, and patient management.

This work also acknowledged several limitations and outlined potential future developments, including the enhancement of distal disease detection, dataset diversity, and the requirement for external validation. An AI model that can both automatically analyse and provide a prediction about the outcome of CTEPH would be a ground-breaking in the field of pulmonary embolism disease.

References

- ABDERRAHMANE, N., LEMAIRE, E. & MIRAMOND, B. 2020. Design space exploration of hardware spiking neurons for embedded artificial intelligence. *Neural Networks*, 121, 366-386.
- ABDULAAL, L., MAITER, A., SALEHI, M., SHARKEY, M., ALNASSER, T., GARG, P., RAJARAM, S., HILL, C., JOHNS, C. & ROTHMAN, A. M. K. 2024. A systematic review of artificial intelligence tools for chronic pulmonary embolism on CT pulmonary angiography. *Frontiers in Radiology*, 4, 1335349.
- ABOZEED, M., CONIC, S., BULLEN, J., RIZK, A., SAEEDAN, M. B., KARIM, W., HERESI, G. A. & RENAPURKAR, R. D. 2022. Dual energy CT based scoring in chronic thromboembolic pulmonary hypertension and correlation with clinical and hemodynamic parameters: a retrospective cross-sectional study. *Cardiovascular Diagnosis and Therapy*, 12, 305.
- AGUSTI, A., NOGUERA, A., SAULEDA, J., SALA, E., PONS, J. & BUSQUETS, X. 2003. Systemic effects of chronic obstructive pulmonary disease. *European Respiratory Journal*, 21, 347-360.
- AJMERA, P., KHARAT, A., SETH, J., RATHI, S., PANT, R., GAWALI, M., KULKARNI, V., MARAMRAJU, R., KEDIA, I. & BOTCHU, R. 2022. A deep learning approach for automated diagnosis of pulmonary embolism on computed tomographic pulmonary angiography. *BMC Medical Imaging*, 22, 195.
- ALABED, S., MAITER, A., SALEHI, M., MAHMOOD, A., DANIEL, S., JENKINS, S., GOODLAD, M., SHARKEY, M., MAMALAKIS, M. & RAKOCEVIC, V. 2022. Quality of reporting in AI cardiac MRI segmentation studies—A systematic review and recommendations for future studies. *Frontiers in Cardiovascular Medicine*, 9, 956811.
- ALI, J. M., HARDMAN, G., PAGE, A. & JENKINS, D. P. 2012. Chronic thromboembolic pulmonary hypertension: an underdiagnosed entity? *Hospital Practice*, 40, 71-79.
- ARDILA, D., KIRALY, A. P., BHARADWAJ, S., CHOI, B., REICHER, J. J., PENG, L., TSE, D., ETEMADI, M., YE, W. & CORRADO, G. 2019. End-to-end lung cancer screening with three-dimensional deep learning on low-dose chest computed tomography. *Nature medicine*, 25, 954-961.
- ARRIETA, A. B., DÍAZ-RODRÍGUEZ, N., DEL SER, J., BENNETOT, A., TABIK, S., BARBADO, A., GARCÍA, S., GIL-LÓPEZ, S., MOLINA, D. & BENJAMINS, R. 2020. Explainable Artificial Intelligence (XAI): Concepts, taxonomies, opportunities and challenges toward responsible AI. *Information fusion*, 58, 82-115.
- AYOBI, A., CHANG, P. D., CHOW, D. S., WEINBERG, B. D., TASSY, M., FRANCIOSINI, A., SCUDELER, M., QUENET, S., AVARE, C. & CHAIBI, Y. 2024. Performance and clinical utility of an artificial intelligence-enabled tool for pulmonary embolism detection. *Clinical Imaging*, 113, 110245.
- BARRAGÁN-MONTERO, A., JAVAID, U., VALDÉS, G., NGUYEN, D., DESBORDES, P., MACQ, B., WILLEMS, S., VANDEWINCKELE, L., HOLMSTRÖM, M. & LÖFMAN, F. 2021. Artificial intelligence and machine learning for medical imaging: A technology review. *Physica Medica*, 83, 242-256.
- BHATTARAI, P., THAKURI, D. S., NIE, Y. & CHAND, G. B. 2024. Explainable AI-based DeepSHAP for mapping the multivariate relationships between regional neuroimaging biomarkers and cognition. *European Journal of Radiology*, 174, 111403.

- BIRD, E., HASENSTAB, K., KIM, N., MADANI, M., MALHOTRA, A., HAHN, L., KLIGERMAN, S., HSIAO, A. & CONTIJOCH, F. 2023. Mapping the spatial extent of hypoperfusion in chronic thromboembolic pulmonary hypertension using multienergy CT. *Radiology: Cardiothoracic Imaging*, 5, e220221.
- BONDERMAN, D. & LANG, I. M. 2011. Risk factors for chronic thromboembolic pulmonary hypertension. *Textbook of Pulmonary Vascular Disease*, 1253-1259.
- BOON, G. J., ENDE-VERHAAR, Y. M., BEENEN, L. F., COOLEN, J., DELCROIX, M., GOLEBIEWSKI, M., HUISMAN, M. V., MAIRUHU, A. T., MEIJBOOM, L. J. & MIDDELDORP, S. 2022. Prediction of chronic thromboembolic pulmonary hypertension with standardised evaluation of initial computed tomography pulmonary angiography performed for suspected acute pulmonary embolism. *European Radiology*, 1-10.
- BRAAMS, N. J., BOON, G. J., DE MAN, F. S., VAN ES, J., DEN EXTER, P. L., KROFT, L. J., BEENEN, L. F., HUISMAN, M. V., NOSSENT, E. J. & BOONSTRA, A. 2021. Evolution of CT findings after anticoagulant treatment for acute pulmonary embolism in patients with and without an ultimate diagnosis of chronic thromboembolic pulmonary hypertension. *European Respiratory Journal*, 58.
- BUHMANN, S., HERZOG, P., LIANG, J., WOLF, M., SALGANICOFF, M., KIRCHHOFF, C., REISER, M. & BECKER, C. H. 2007. Clinical evaluation of a computer-aided diagnosis (CAD) prototype for the detection of pulmonary embolism. *Academic radiology*, 14, 651-658.
- BULS, N., WATTÉ, N., NIEBOER, K., ILSSEN, B. & DE MEY, J. 2021. Performance of an artificial intelligence tool with real-time clinical workflow integration—detection of intracranial hemorrhage and pulmonary embolism. *Physica Medica*, 83, 154-160.
- BUNCLARK, K., NEWNHAM, M., CHIU, Y. D., RUGGIERO, A., VILLAR, S. S., CANNON, J. E., COGHLAN, G., CORRIS, P. A., HOWARD, L. & JENKINS, D. 2020. A multicenter study of anticoagulation in operable chronic thromboembolic pulmonary hypertension. *Journal of Thrombosis and Haemostasis*, 18, 114-122.
- CARDENAS, C. E., YANG, J., ANDERSON, B. M., COURT, L. E. & BROCK, K. B. Advances in auto-segmentation. *Seminars in radiation oncology*, 2019. Elsevier, 185-197.
- CHAIKRIANGKRAI, K., CHOI, S. Y., NABI, F. & CHANG, S. M. 2014. Important advances in technology and unique applications to cardiovascular computed tomography. *Methodist DeBakey cardiovascular journal*, 10, 152.
- CHAN, H.-P., HADJIISKI, L., ZHOU, C. & SAHINER, B. 2008. Computer-aided diagnosis of lung cancer and pulmonary embolism in computed tomography—a review. *Academic radiology*, 15, 535-555.
- CHEIKH, A. B., GORINCOUR, G., NIVET, H., MAY, J., SEUX, M., CALAME, P., THOMSON, V., DELABROUSSE, E. & CROMBÉ, A. 2022. How artificial intelligence improves radiological interpretation in suspected pulmonary embolism. *European Radiology*, 32, 5831-5842.
- CHU, Y., LUO, G., ZHOU, L., CAO, S., MA, G., MENG, X., ZHOU, J., YANG, C., XIE, D. & MU, D. 2025. Deep learning-driven pulmonary artery and vein segmentation reveals demography-associated vasculature anatomical differences. *Nature Communications*, 16, 2262.
- COLAK, E., KITAMURA, F. C., HOBBS, S. B., WU, C. C., LUNGREN, M. P., PREVEDELLO, L. M., KALPATHY-CRAMER, J., BALL, R. L., SHIH, G. & STEIN, A. 2021. The RSNA pulmonary embolism CT dataset. *Radiology: Artificial Intelligence*, 3, e200254.

- CONDON, D. F., NICKEL, N. P., ANDERSON, R., MIRZA, S. & DE JESUS PEREZ, V. A. 2019. The 6th World Symposium on Pulmonary Hypertension: what's old is new. *F1000Research*, 8.
- CUI, H., LIU, X. & HUANG, N. Pulmonary vessel segmentation based on orthogonal fused U-Net++ of chest CT images. Medical Image Computing and Computer Assisted Intervention–MICCAI 2019: 22nd International Conference, Shenzhen, China, October 13–17, 2019, Proceedings, Part VI 22, 2019. Springer, 293-300.
- CURRIE, G.M. & BAILEY, D.L., 2023. V/Q SPECT and SPECT/CT in Pulmonary Embolism. *Journal of nuclear medicine technology*, 51(1), pp.9-15.
- DAS, M., MÜHLENBRUCH, G., HELM, A., BAKAI, A., SALGANICOFF, M., STANZEL, S., LIANG, J., WOLF, M., GÜNTHER, R. W. & WILDBERGER, J. E. 2008. Computer-aided detection of pulmonary embolism: influence on radiologists' detection performance with respect to vessel segments. *European radiology*, 18, 1350-1355.
- DELCROIX, M., DE PERROT, M., JAÏS, X., JENKINS, D. P., LANG, I. M., MATSUBARA, H., MEIJBOOM, L. J., QUARCK, R., SIMONNEAU, G. & WIEDENROTH, C. B. 2023. Chronic thromboembolic pulmonary hypertension: realising the potential of multimodal management. *The Lancet Respiratory Medicine*, 11, 836-850.
- DELCROIX, M., LANG, I., PEPKE-ZABA, J., JANSÁ, P., D'ARMINI, A. M., SNIJDER, R., BRESSER, P., TORBICKI, A., MELLEMKJÆR, S. & LEWCZUK, J. 2016. Long-term outcome of patients with chronic thromboembolic pulmonary hypertension: results from an international prospective registry. *Circulation*, 133, 859-871.
- DELCROIX, M., TORBICKI, A., GOPALAN, D., SITBON, O., KLOK, F. A., LANG, I., JENKINS, D., KIM, N. H., HUMBERT, M. & JAIS, X. 2021. ERS statement on chronic thromboembolic pulmonary hypertension. *European Respiratory Journal*, 57.
- DENG, J., DONG, W., SOCHER, R., LI, L.-J., LI, K. & FEI-FEI, L. Imagenet: A large-scale hierarchical image database. 2009 IEEE conference on computer vision and pattern recognition, 2009. Ieee, 248-255.
- DOĞAN, H., DE ROOS, A., GELEIJNS, J., HUISMAN, M. V. & KROFT, L. J. 2015. The role of computed tomography in the diagnosis of acute and chronic pulmonary embolism. *Diagnostic and Interventional Radiology*, 21, 307.
- DORFMÜLLER, P., GÜNTHER, S., GHIGNA, M.-R., DE MONTPRÉVILLE, V. T., BOULATE, D., PAUL, J.-F., JAÏS, X., DECANTE, B., SIMONNEAU, G. & DARTEVELLE, P. 2014. Microvascular disease in chronic thromboembolic pulmonary hypertension: a role for pulmonary veins and systemic vasculature. *European Respiratory Journal*, 44, 1275-1288.
- DOUEK, P. C., BOCCALINI, S., OEI, E. H., CORMODE, D. P., POURMORTEZA, A., BOUSSEL, L., SI-MOHAMED, S. A. & BUDDE, R. P. 2023. Clinical applications of photon-counting CT: a review of pioneer studies and a glimpse into the future. *Radiology*, 309, e222432.
- DU, G., CAO, X., LIANG, J., CHEN, X. & ZHAN, Y. 2020. Medical Image Segmentation based on U-Net: A Review. *Journal of Imaging Science & Technology*, 64.
- DUNNILL, M. 1962. Quantitative methods in the study of pulmonary pathology. *Thorax*, 17, 320.
- DURRINGTON, C., HURDMAN, J. A., ELLIOT, C. A., MACLEAN, R., VAN VEEN, J., SACCULLO, G., DE-FONESKA, D., SWIFT, A. J., SMITHA, R. & HILL, C. 2024. Systematic pulmonary embolism follow-up increases diagnostic rates of chronic thromboembolic

- pulmonary hypertension and identifies less severe disease: results from the ASPIRE Registry. *European Respiratory Journal*, 63.
- DUZGUN, S. A., DURHAN, G., DEMIRKAZIK, F. B., IRMAK, I., KARAKAYA, J., AKPINAR, E., AKPINAR, M. G., INKAYA, A. C., OCAL, S. & TOPELI, A. 2021. AI-based quantitative CT analysis of temporal changes according to disease severity in COVID-19 pneumonia. *Journal of Computer Assisted Tomography*, 45, 970-978.
- DWIVEDI, K., SHARKEY, M., CONDLIFFE, R., UTHOFF, J. M., ALABED, S., METHERALL, P., LU, H., WILD, J. M., HOFFMAN, E. A. & SWIFT, A. J. 2021. Pulmonary hypertension in association with lung disease: quantitative CT and artificial intelligence to the rescue? State-of-the-art review. *Diagnostics*, 11, 679.
- EBERHARD, M., MCINNIS, M., DE PERROT, M., LICHTBLAU, M., ULRICH, S., INCI, I., OPITZ, I. & FRAUENFELDER, T. 2022. Dual-energy CT pulmonary angiography for the assessment of surgical accessibility in patients with chronic thromboembolic pulmonary hypertension. *Diagnostics*, 12, 228.
- ENDE-VERHAAR, Y. M., HUISMAN, M. V. & KLOK, F. A. 2017. To screen or not to screen for chronic thromboembolic pulmonary hypertension after acute pulmonary embolism. *Thrombosis Research*, 151, 1-7.
- ENDE-VERHAAR, Y. M., MEIJBOOM, L. J., KROFT, L. J., BEENEN, L. F., BOON, G. J., MIDDELDORP, S., NOSSENT, E. J., SYMERKY, P., HUISMAN, M. V. & BOGAARD, H. J. 2019. Usefulness of standard computed tomography pulmonary angiography performed for acute pulmonary embolism for identification of chronic thromboembolic pulmonary hypertension: results of the InShape III study. *The Journal of Heart and Lung Transplantation*, 38, 731-738.
- ENDE-VERHAAR, Y. M., VAN DEN HOUT, W. B., BOGAARD, H. J., MEIJBOOM, L. J., HUISMAN, M. V., SYMERKY, P., VONK-NOORDEGRAAF, A. & KLOK, F. A. 2018. Healthcare utilization in chronic thromboembolic pulmonary hypertension after acute pulmonary embolism. *Journal of Thrombosis and Haemostasis*, 16, 2168-2174.
- ENG, J., KRISHNAN, J. A., SEGAL, J. B., BOLGER, D. T., TAMARIZ, L. J., STREIFF, M. B., JENCKES, M. W. & BASS, E. B. 2004. Accuracy of CT in the diagnosis of pulmonary embolism: a systematic literature review. *American Journal of Roentgenology*, 183, 1819-1827.
- ENNAB, M. & MCHEICK, H. 2025a. Advancing AI Interpretability in Medical Imaging: A Comparative Analysis of Pixel-Level Interpretability and Grad-CAM Models. *Machine Learning and Knowledge Extraction*, 7, 12.
- ENNAB, M. & MCHEICK, H. 2025b. A novel convolutional interpretability model for pixel-level interpretation of medical image classification through fusion of machine learning and fuzzy logic. *Smart Health*, 35, 100535.
- EVANS, C. R., HONG, C.-P., FOLSOM, A. R., HECKBERT, S. R., SMITH, N. L., WIGGINS, K., LUTSEY, P. L. & CUSHMAN, M. 2020. Lifestyle moderates genetic risk of venous thromboembolism: the ARIC study. *Arteriosclerosis, thrombosis, and vascular biology*, 40, 2756-2763.
- FARRELL, C. M., PINSON, J.-A. & DENNETT, A. M. 2021. CT Attenuation correction and its impact on image quality of myocardial perfusion imaging in coronary artery disease: A systematic review. *Asia Oceania Journal of Nuclear Medicine and Biology*, 9, 31.
- FERNANDES, T. M., KIM, N. H., KERR, K. M., AUGER, W. R., FEDULLO, P. F., POCH, D. S., YANG, J., PAPAMATHEAKIS, D. G., ALOTAIBI, M. & BAUTISTA, M. A. 2023. Distal vessel pulmonary thromboendarterectomy: results from a single institution. *The Journal of Heart and Lung Transplantation*, 42, 1112-1119.

- FORFIA, P. R., FISHER, M. R., MATHAI, S. C., HOUSTEN-HARRIS, T., HEMNES, A. R., BORLAUG, B. A., CHAMERA, E., CORRETTI, M. C., CHAMPION, H. C. & ABRAHAM, T. P. 2006. Tricuspid annular displacement predicts survival in pulmonary hypertension. *American journal of respiratory and critical care medicine*, 174, 1034-1041.
- FUKUI, S., OGO, T., MORITA, Y., TSUJI, A., TATEISHI, E., OZAKI, K., SANDA, Y., FUKUDA, T., YASUDA, S. & OGAWA, H. 2014. Right ventricular reverse remodelling after balloon pulmonary angioplasty. *European Respiratory Journal*, 43, 1394-1402.
- FURLAN, A., PATIL, A., PARK, B., CHANG, C.-C. H., ROBERTS, M. S. & BAE, K. T. 2011. Accuracy and reproducibility of blood clot burden quantification with pulmonary CT angiography. *American Journal of Roentgenology*, 196, 516-523.
- GALIÈ, N., CHANNICK, R. N., FRANTZ, R. P., GRÜNIG, E., JING, Z. C., MOISEEVA, O., PRESTON, I. R., PULIDO, T., SAFDAR, Z. & TAMURA, Y. 2019. Risk stratification and medical therapy of pulmonary arterial hypertension. *European Respiratory Journal*, 53.
- GALIÈ, N., HUMBERT, M., VACHIER, J.-L., GIBBS, S., LANG, I., TORBICKI, A., SIMONNEAU, G., PEACOCK, A., NOORDEGRAAF, A. V. & BEGHETTI, M. 2015. 2015 ESC/ERS Guidelines for the diagnosis and treatment of pulmonary hypertension. *Polish Heart Journal (Kardiologia Polska)*, 73, 1127-1206.
- GAN, H.-L., ZHANG, J.-Q., BO, P., ZHOU, Q.-W. & WANG, S.-X. 2010. The actuarial survival analysis of the surgical and non-surgical therapy regimen for chronic thromboembolic pulmonary hypertension. *Journal of thrombosis and thrombolysis*, 29, 25-31.
- GHAREPAPAGH, E., RAHIMI, F., KOOHI, A., BAKHSHANDEH, H., MOUSAVI-AGHDAS, S. A., SADEGHIPOOR, P., FAKHARI, A., AMIRNIA, M., JAVADRASHID, R. & RASHIDI, F. 2023. Clot Burden As a Predictor of Chronic Thromboembolic Pulmonary Hypertension After Acute Pulmonary Embolism: A Cohort Study. *Thoracic Research and Practice*, 24, 276.
- GOPALAN, D., DELCROIX, M. & HELD, M. 2017. Diagnosis of chronic thromboembolic pulmonary hypertension. *European Respiratory Review*, 26.
- GOTTA, J., KOCH, V., GEYER, T., MARTIN, S. S., BOOZ, C., MAHMOUDI, S., EICHLER, K., RESCHKE, P., D'ANGELO, T. & KLIMEK, K. 2024. Imaging-based risk stratification of patients with pulmonary embolism based on dual-energy CT-derived radiomics. *European Journal of Clinical Investigation*, 54, e14139.
- GRAFHAM, G. K., BAMBRICK, M., HOUBOIS, C., MAFELD, S., DONAHOE, L., DE PERROT, M. & MCINNIS, M. C. 2023. Enhancing preoperative assessment in chronic thromboembolic pulmonary hypertension: A comprehensive analysis of interobserver agreement and proximity-based CT pulmonary angiography scoring. *Heliyon*, 9.
- GROSSE, A., GROSSE, C. & LANG, I. M. 2017. Distinguishing chronic thromboembolic pulmonary hypertension from other causes of pulmonary hypertension using CT. *American Journal of Roentgenology*, 209, 1228-1238.
- GROSSE, C. & GROSSE, A. 2010. CT findings in diseases associated with pulmonary hypertension: a current review. *Radiographics*, 30, 1753-1777.
- GUÉRIN, L., COUTURAUD, F., PARENT, F., REVEL, M.-P., GILLIAZEAU, F., PLANQUETTE, B., PONTAL, D., GUÉGAN, M., SIMONNEAU, G. & MEYER, G. 2014. Prevalence of chronic thromboembolic pulmonary hypertension after acute pulmonary embolism. *Thrombosis and haemostasis*, 112, 598-605.

- GUNNING, D., STEFIK, M., CHOI, J., MILLER, T., STUMPF, S. & YANG, G.-Z. 2019. XAI—Explainable artificial intelligence. *Science robotics*, 4, eaay7120.
- HAHN, L. D., PAPAMATHEAKIS, D. G., FERNANDES, T. M., POCH, D. S., YANG, J., SHEN, J., HOH, C. K., HSIAO, A., KERR, K. M. & PRETORIUS, V. 2022. Multidisciplinary approach to chronic thromboembolic pulmonary hypertension: role of radiologists. *Radiographics*, 43, e220078.
- HARRIS, H., BARRACLOUGH, R., DAVIES, C., ARMSTRONG, I., KIELY, D. G. & VAN BEEK, E. J. 2008. Cavitating lung lesions in chronic thromboembolic pulmonary hypertension. *Journal of radiology case reports*, 2, 11.
- HASANNEZHAD, A. & SHARIFIAN, S. 2025. Explainable AI enhanced transformer based UNet for medical images segmentation using gradient weighted class activation map. *Signal, Image and Video Processing*, 19, 321.
- HASENSTAB, K. A., YUAN, N., RETSON, T., CONRAD, D. J., KLIGERMAN, S., LYNCH, D. A., HSIAO, A. & INVESTIGATORS, C. 2021. Automated CT staging of chronic obstructive pulmonary disease severity for predicting disease progression and mortality with a deep learning convolutional neural network. *Radiology: Cardiothoracic Imaging*, 3, e200477.
- HE, H., STEIN, M. W., ZALTA, B. & HARAMATI, L. B. 2006. Pulmonary infarction: spectrum of findings on multidetector helical CT. *Journal of thoracic imaging*, 21, 1-7.
- HE, J., FANG, W., LV, B., HE, J.-G., XIONG, C.-M., LIU, Z.-H. & HE, Z.-X. 2012. Diagnosis of chronic thromboembolic pulmonary hypertension: comparison of ventilation/perfusion scanning and multidetector computed tomography pulmonary angiography with pulmonary angiography. *Nuclear medicine communications*, 33, 459-463.
- HESAMIAN, M. H., JIA, W., HE, X. & KENNEDY, P. 2019. Deep learning techniques for medical image segmentation: achievements and challenges. *Journal of digital imaging*, 32, 582-596.
- HICKS, S. A., STRÜMKE, I., THAMBAWITA, V., HAMMOU, M., RIEGLER, M. A., HALVORSEN, P. & PARASA, S. 2022. On evaluation metrics for medical applications of artificial intelligence. *Scientific reports*, 12, 5979.
- HINCK, D., SEGEROTH, M., MIAZZA, J., BERDAJS, D., BREMERICH, J., WASSERTHAL, J. & PRADELLA, M., 2025. Automatic segmentations of cardiovascular structures on chest CT data Sets: An Update of the TotalSegmentator. *European Journal of Radiology*, p.112006.
- HOEPER, M. M., BOGAARD, H. J., CONDLIFFE, R., FRANTZ, R., KHANNA, D., KURZYNA, M., LANGLEBEN, D., MANES, A., SATOH, T. & TORRES, F. 2013. Definitions and diagnosis of pulmonary hypertension. *Journal of the American College of Cardiology*, 62, D42-D50.
- HOEPER, M. M., DWIVEDI, K., PAUSCH, C., LEWIS, R. A., OLSSON, K. M., HUSCHER, D., PITTROW, D., GRÜNIG, E., STAEHLER, G. & VIZZA, C. D. 2022. Phenotyping of idiopathic pulmonary arterial hypertension: a registry analysis. *The Lancet Respiratory Medicine*, 10, 937-948.
- HRDLICKA, J., JURKA, M., BIRCAKOVA, B., AMBROZ, D., JANSÁ, P., BURGETOVA, A. & LAMBERT, L. 2024. Even non-expert radiologists report chronic thromboembolic pulmonary hypertension (CTEPH) on CT pulmonary angiography with high sensitivity and almost perfect agreement. *European Radiology*, 34, 1086-1093.

- HUANG, G., LIU, Z., VAN DER MAATEN, L. & WEINBERGER, K. Q. Densely connected convolutional networks. *Proceedings of the IEEE conference on computer vision and pattern recognition*, 2017. 4700-4708.
- HUANG, S.-C., PAREEK, A., ZAMANIAN, R., BANERJEE, I. & LUNGREN, M. P. 2020. Multimodal fusion with deep neural networks for leveraging CT imaging and electronic health record: a case-study in pulmonary embolism detection. *Scientific reports*, 10, 22147.
- HUMBERT, M., KOVACS, G., HOEPER, M. M., BADAGLIACCA, R., BERGER, R. M., BRIDA, M., CARLSEN, J., COATS, A. J., ESCRIBANO-SUBIAS, P. & FERRARI, P. 2022. 2022 ESC/ERS Guidelines for the diagnosis and treatment of pulmonary hypertension: Developed by the task force for the diagnosis and treatment of pulmonary hypertension of the European Society of Cardiology (ESC) and the European Respiratory Society (ERS). Endorsed by the International Society for Heart and Lung Transplantation (ISHLT) and the European Reference Network on rare respiratory diseases (ERN-LUNG). *European heart journal*, 43, 3618-3731.
- HURDMAN, J., CONDLIFFE, R., ELLIOT, C. A., DAVIES, C., HILL, C., WILD, J. M., CAPENER, D., SEPHTON, P., HAMILTON, N. & ARMSTRONG, I. 2012. ASPIRE registry: assessing the Spectrum of Pulmonary hypertension Identified at a REferral centre. *European Respiratory Journal*, 39, 945-955.
- ISENSE, F., JAEGER, P. F., KOHL, S. A., PETERSEN, J. & MAIER-HEIN, K. H. 2021. nnU-Net: a self-configuring method for deep learning-based biomedical image segmentation. *Nature methods*, 18, 203-211.
- JÄS, X., BRENOT, P., BOUVAIST, H., JEVIKAR, M., CANUET, M., CHABANNE, C., CHAOUAT, A., COTTIN, V., DE GROOTE, P. & FAVROLT, N. 2022. Balloon pulmonary angioplasty versus riociguat for the treatment of inoperable chronic thromboembolic pulmonary hypertension (RACE): a multicentre, phase 3, open-label, randomised controlled trial and ancillary follow-up study. *The Lancet Respiratory Medicine*, 10, 961-971.
- KAPTEIN, F. H., STÖGER, J. L., VAN DAM, L. F., NINABER, M. K., MERTENS, B. J., HUISMAN, M. V., KLOK, F. A. & KROFT, L. J. 2024. Computed tomography diagnosis of pulmonary infarction in acute pulmonary embolism. *Thrombosis Research*, 241, 109071.
- KASAI, H., TANABE, N., FUJIMOTO, K., HOSHI, H., NAITO, J., SUZUKI, R., MATSUMURA, A., SUGIURA, T., SAKAO, S. & TATSUMI, K. 2017. Mosaic attenuation pattern in non-contrast computed tomography for the assessment of pulmonary perfusion in chronic thromboembolic pulmonary hypertension. *Respiratory investigation*, 55, 300-307.
- KATSUMURA, Y. & OHTSUBO, K. I. 1998. Correlation between clinical and pathological features of pulmonary thromboemboli and the development of infarcts. *Respirology*, 3, 203-206.
- KHAN, M., SHAH, P. M., KHAN, I. A., ISLAM, S. U., AHMAD, Z., KHAN, F. & LEE, Y. 2023. IoMT-Enabled Computer-Aided Diagnosis of Pulmonary Embolism from Computed Tomography Scans Using Deep Learning. *Sensors*, 23, 28.
- KHEMASUWAN, D., SORESENSEN, J. S. & COLT, H. G. 2020. Artificial intelligence in pulmonary medicine: computer vision, predictive model and COVID-19. *European respiratory review*, 29.
- KIELY, D. G., ELLIOT, C. A., SABROE, I. & CONDLIFFE, R. 2013. Pulmonary hypertension: diagnosis and management. *Bmj*, 346.
- KIELY, D. G., LEVIN, D. L., HASSOUN, P. M., IVY, D., JONE, P.-N., BWIKA, J., KAWUT, S. M., LORDAN, J., LUNGU, A. & MAZUREK, J. A. 2019. Statement on imaging and

- pulmonary hypertension from the Pulmonary Vascular Research Institute (PVRI). *Pulmonary circulation*, 9, 2045894019841990.
- KIM, C., KIM, D., LEE, K. Y., KIM, H., CHA, J., CHOO, J. Y. & CHO, P.-K. 2018. The optimal energy level of virtual monochromatic images from spectral CT for reducing beam-hardening artifacts due to contrast media in the thorax. *American Journal of Roentgenology*, 211, 557-563.
- KIM, N. H., DELCROIX, M., JAIS, X., MADANI, M. M., MATSUBARA, H., MAYER, E., OGO, T., TAPSON, V. F., GHOFrani, H.-A. & JENKINS, D. P. 2019. Chronic thromboembolic pulmonary hypertension. *European Respiratory Journal*, 53.
- KLIGERMAN, S. J., HENRY, T., LIN, C. T., FRANKS, T. J. & GALVIN, J. R. 2015. Mosaic attenuation: etiology, methods of differentiation, and pitfalls. *Radiographics*, 35, 1360-1380.
- KLOK, F., DELCROIX, M. & BOGAARD, H. 2018. Chronic thromboembolic pulmonary hypertension from the perspective of patients with pulmonary embolism. *Journal of Thrombosis and Haemostasis*, 16, 1040-1051.
- KLOK, F. A., COUTURAUD, F., DELCROIX, M. & HUMBERT, M. 2020. Diagnosis of chronic thromboembolic pulmonary hypertension after acute pulmonary embolism. *European Respiratory Journal*, 55.
- KLOK, F. A., VAN KRALINGEN, K. W., VAN DIJK, A. P., HEYNING, F. H., VLIEGEN, H. W. & HUISMAN, M. V. 2010. Prospective cardiopulmonary screening program to detect chronic thromboembolic pulmonary hypertension in patients after acute pulmonary embolism. *haematologica*, 95, 970.
- KONSTANTINIDES, S. V., MEYER, G., BECATTINI, C., BUENO, H., GEERSING, G.-J., HARJOLA, V.-P., HUISMAN, M. V., HUMBERT, M., JENNINGS, C. S. & JIMÉNEZ, D. 2020. 2019 ESC Guidelines for the diagnosis and management of acute pulmonary embolism developed in collaboration with the European Respiratory Society (ERS) The Task Force for the diagnosis and management of acute pulmonary embolism of the European Society of Cardiology (ESC). *European heart journal*, 41, 543-603.
- KOO, T. K. & LI, M. Y. 2016. A guideline of selecting and reporting intraclass correlation coefficients for reliability research. *Journal of chiropractic medicine*, 15, 155-163.
- LAMBERT, L., MICHALEK, P. & BURGETOVA, A. 2022. The diagnostic performance of CT pulmonary angiography in the detection of chronic thromboembolic pulmonary hypertension—systematic review and meta-analysis. *European Radiology*, 32, 7927-7935.
- LANG, I. M., ANDREASSEN, A. K., ANDERSEN, A., BOUVAIST, H., COGHLAN, G., ESCRIBANO-SUBIAS, P., JANSÁ, P., KOPEC, G., KURZYNA, M. & MATSUBARA, H. 2023. Balloon pulmonary angioplasty for chronic thromboembolic pulmonary hypertension: a clinical consensus statement of the ESC working group on pulmonary circulation and right ventricular function. *European heart journal*, 44, 2659-2671.
- LANG, I. M., DORFMÜLLER, P. & NOORDEGRAAF, A. V. 2016. The pathobiology of chronic thromboembolic pulmonary hypertension. *Annals of the American Thoracic Society*, 13, S215-S221.
- LANG, I. M., PESAVENTO, R., BONDERMAN, D. & YUAN, J. X. 2013. Risk factors and basic mechanisms of chronic thromboembolic pulmonary hypertension: a current understanding. *European Respiratory Journal*, 41, 462-468.
- LEONE, M. B., GIANNOTTA, M., PALAZZINI, M., CEFARELLI, M., MARTÌN SUÀREZ, S., GOTTI, E., BACCHI REGGIANI, M. L., ZOMPATORI, M. & GALIÈ, N. 2017. A new CT-score as index

- of hemodynamic changes in patients with chronic thromboembolic pulmonary hypertension. *La radiologia medica*, 122, 495-504.
- LEWIS, R. A., THOMPSON, A. R., BILLINGS, C. G., CHARALAMPOPOULOS, A., ELLIOT, C. A., HAMILTON, N., HILL, C., HURDMAN, J., RAJARAM, S. & SABROE, I. 2020. Mild parenchymal lung disease and/or low diffusion capacity impacts survival and treatment response in patients diagnosed with idiopathic pulmonary arterial hypertension. *European Respiratory Journal*, 55.
- LI, L., QIN, L., XU, Z., YIN, Y., WANG, X., KONG, B., BAI, J., LU, Y., FANG, Z. & SONG, Q. 2020. Using artificial intelligence to detect COVID-19 and community-acquired pneumonia based on pulmonary CT: evaluation of the diagnostic accuracy. *Radiology*, 296, E65-E71.
- LIU, W., LIU, M., GUO, X., ZHANG, P., ZHANG, L., ZHANG, R., KANG, H., ZHAI, Z., TAO, X. & WAN, J. 2020. Evaluation of acute pulmonary embolism and clot burden on CTPA with deep learning. *European radiology*, 30, 3567-3575.
- LIU, X., FAES, L., KALE, A. U., WAGNER, S. K., FU, D. J., BRUYNSEELS, A., MAHENDIRAN, T., MORAES, G., SHAMDAS, M. & KERN, C. 2019. A comparison of deep learning performance against health-care professionals in detecting diseases from medical imaging: a systematic review and meta-analysis. *The lancet digital health*, 1, e271-e297.
- LOBO, J. M., JIMÉNEZ-VALVERDE, A. & REAL, R. 2008. AUC: a misleading measure of the performance of predictive distribution models. *Global ecology and Biogeography*, 17, 145-151.
- LONG, J., SHELHAMER, E. & DARRELL, T. Fully convolutional networks for semantic segmentation. Proceedings of the IEEE conference on computer vision and pattern recognition, 2015. 3431-3440.
- LONG, K., TANG, L., PU, X., REN, Y., ZHENG, M., GAO, L., SONG, C., HAN, S., ZHOU, M. & DENG, F. 2021. Probability-based Mask R-CNN for pulmonary embolism detection. *Neurocomputing*, 422, 345-353.
- MA, X., FERGUSON, E. C., JIANG, X., SAVITZ, S. I. & SHAMS, S. 2022. A multitask deep learning approach for pulmonary embolism detection and identification. *Scientific reports*, 12, 13087.
- MADANI, M. M., AUGER, W. R., PRETORIUS, V., SAKAKIBARA, N., KERR, K. M., KIM, N. H., FEDULLO, P. F. & JAMIESON, S. W. 2012. Pulmonary endarterectomy: recent changes in a single institution's experience of more than 2,700 patients. *The Annals of thoracic surgery*, 94, 97-103.
- MAIER-HEIN, L., REINKE, A., GODAU, P., TIZABI, M. D., BUETTNER, F., CHRISTODOULOU, E., GLOCKER, B., ISENSEE, F., KLEESIEK, J. & KOZUBEK, M. 2024. Metrics reloaded: recommendations for image analysis validation. *Nature methods*, 21, 195-212.
- MAITER, A., SALEHI, M., SWIFT, A. J. & ALABED, S. 2023. How should studies using AI be reported? Lessons from a systematic review in cardiac MRI. *Frontiers in radiology*, 3, 1112841.
- MAIZLIN, Z. V., VOS, P. M., GODOY, M. B. & COOPERBERG, P. L. 2007. Computer-aided detection of pulmonary embolism on CT angiography: initial experience. *Journal of thoracic imaging*, 22, 324-329.
- MASTORA, I., REMY-JARDIN, M., MASSON, P., GALLAND, E., DELANNOY, V., BAUCHART, J.-J. & REMY, J. 2003. Severity of acute pulmonary embolism: evaluation of a new spiral

- CT angiographic score in correlation with echocardiographic data. *European radiology*, 13, 29-35.
- MATTHEWS, D. T. & HEMNES, A. R. 2016. Current concepts in the pathogenesis of chronic thromboembolic pulmonary hypertension. *Pulmonary circulation*, 6, 145-154.
- MAYER, E., JENKINS, D., LINDNER, J., D'ARMINI, A., KLOEK, J., MEYNS, B., ILKJAER, L. B., KLEPETKO, W., DELCROIX, M. & LANG, I. 2011. Surgical management and outcome of patients with chronic thromboembolic pulmonary hypertension: results from an international prospective registry. *The Journal of thoracic and cardiovascular surgery*, 141, 702-710.
- MCCABE, C., DIMOPOULOS, K., PITCHER, A., ORCHARD, E., PRICE, L. C., KEMPNEY, A. & WORT, S. J. 2020. Chronic thromboembolic disease following pulmonary embolism: time for a fresh look at old clot. *European Respiratory Journal*, 55.
- MCFADDEN, P. M. & OCHSNER, J. L. 2002. A history of the diagnosis and treatment of venous thrombosis and pulmonary embolism. *Ochsner Journal*, 4, 9-13.
- MCHUGH, M. L. 2012. Interrater reliability: the kappa statistic. *Biochemia medica*, 22, 276-282.
- MCINNIS, M. C., WANG, D., DONAHOE, L., GRANTON, J., THENGANATT, J., TAN, K., KAVANAGH, J. & DE PERROT, M. 2020. Importance of computed tomography in defining segmental disease in chronic thromboembolic pulmonary hypertension. *ERJ Open Research*, 6.
- MCNEIL, K. & DUNNING, J. 2007. Chronic thromboembolic pulmonary hypertension (CTEPH). *Heart*, 93, 1152-1158.
- MEHTA, S., HELMERSEN, D., PROVENCHER, S., HIRANI, N., RUBENS, F. D., DE PERROT, M., BLOSTEIN, M., BOUTET, K., CHANDY, G. & DENNIE, C. 2010. Diagnostic evaluation and management of chronic thromboembolic pulmonary hypertension: a clinical practice guideline. *Canadian respiratory journal*, 17, 301-334.
- MEINEL, F., GRAEF, A., THIERFELDER, K., ARMBRUSTER, M., SCHILD, C., NEUROHR, C., REISER, M. & JOHNSON, T. Automated quantification of pulmonary perfused blood volume by dual-energy CTPA in chronic thromboembolic pulmonary hypertension. *RöFo-Fortschritte auf dem Gebiet der Röntgenstrahlen und der bildgebenden Verfahren*, 2014. © Georg Thieme Verlag KG, 151-156.
- MING, Y., LUO, S., ZHAO, L., XU, Q. & SONG, W. 2025. High Accuracy Pulmonary Vessel Segmentation for Contrast and Non-contrast CT Images and Its Clinical Evaluation. *arXiv preprint arXiv:2503.16988*.
- MONGAN, J., MOY, L. & KAHN JR, C. E. 2020. Checklist for artificial intelligence in medical imaging (CLAIM): a guide for authors and reviewers. Radiological Society of North America.
- MORADI, F., MORRIS, T. A. & HOH, C. K. 2019. Perfusion scintigraphy in diagnosis and management of thromboembolic pulmonary hypertension. *Radiographics*, 39, 169-185.
- MOSER, K. M. & BRAUNWALD, N. S. 1973. Successful surgical intervention in severe chronic thromboembolic pulmonary hypertension. *Chest*, 64, 29-35.
- MUNDHENK, T. N., CHEN, B. Y. & FRIEDLAND, G. 2019. Efficient saliency maps for explainable AI. *arXiv preprint arXiv:1911.11293*.
- NARDELLI, P., JIMENEZ-CARRETERO, D., BERMEJO-PELAEZ, D., WASHKO, G. R., RAHAGHI, F. N., LEDESMA-CARBAYO, M. J. & ESTÉPAR, R. S. J. 2018. Pulmonary artery-vein

- classification in CT images using deep learning. *IEEE transactions on medical imaging*, 37, 2428-2440.
- NARECHANIA, S., RENAPURKAR, R. & HERESI, G. A. 2020. Mimickers of chronic thromboembolic pulmonary hypertension on imaging tests: a review. *Pulmonary Circulation*, 10, 2045894019882620.
- NASIR, B., ZIA, T., NAWAZ, M. & MOREIRA, C. 2025. Weakly Supervised Pixel-Level Annotation with Visual Interpretability. *arXiv preprint arXiv:2502.17824*.
- NISHIYAMA, K. H., SABOO, S. S., TANABE, Y., JASINOWODOLINSKI, D., LANDAY, M. J. & KAY, F. U. 2018. Chronic pulmonary embolism: diagnosis. *Cardiovascular diagnosis and therapy*, 8, 253.
- NORORI, N., HU, Q., AELLEN, F. M., FARACI, F. D. & TZOVARA, A. 2021. Addressing bias in big data and AI for health care: A call for open science. *Patterns*, 2.
- OLSSON, K. M., CORTE, T. J., KAMP, J. C., MONTANI, D., NATHAN, S. D., NEUBERT, L., PRICE, L. C. & KIELY, D. G. 2023. Pulmonary hypertension associated with lung disease: new insights into pathomechanisms, diagnosis, and management. *The Lancet Respiratory Medicine*, 11, 820-835.
- OUZZANI, M., HAMMADY, H., FEDOROWICZ, Z. & ELMAGARMID, A. 2016. Rayyan—a web and mobile app for systematic reviews. *Systematic reviews*, 5, 1-10.
- ÖZKAN, H., OSMAN, O., ŞAHİN, S. & BOZ, A. F. 2014. A novel method for pulmonary embolism detection in CTA images. *Computer methods and programs in biomedicine*, 113, 757-766.
- PAGE, M. J., MCKENZIE, J. E., BOSSUYT, P. M., BOUTRON, I., HOFFMANN, T. C., MULROW, C. D., SHAMSEER, L., TETZLAFF, J. M., AKL, E. A. & BRENNAN, S. E. 2021. The PRISMA 2020 statement: an updated guideline for reporting systematic reviews. *bmj*, 372.
- PARAMBIL, J. G., SAVCI, C. D., TAZELAAR, H. D. & RYU, J. H. 2005. Causes and presenting features of pulmonary infarctions in 43 cases identified by surgical lung biopsy. *Chest*, 127, 1178-1183.
- PARK, S. C., CHAPMAN, B. E. & ZHENG, B. 2010. A multistage approach to improve performance of computer-aided detection of pulmonary embolisms depicted on CT images: Preliminary investigation. *IEEE transactions on biomedical engineering*, 58, 1519-1527.
- PENGO, V., LENSING, A. W., PRINS, M. H., MARCHIORI, A., DAVIDSON, B. L., TIOZZO, F., ALBANESE, P., BIASIOLO, A., PEGORARO, C. & ILICETO, S. 2004. Incidence of chronic thromboembolic pulmonary hypertension after pulmonary embolism. *New England Journal of Medicine*, 350, 2257-2264.
- PEPKE-ZABA, J., DELCROIX, M., LANG, I., MAYER, E., JANSÁ, P., AMBROZ, D., TREACY, C., D'ARMINI, A. M., MORSOLINI, M. & SNIJDER, R. 2011. Chronic thromboembolic pulmonary hypertension (CTEPH) results from an international prospective registry. *Circulation*, 124, 1973-1981.
- PEPKE-ZABA, J., JANSÁ, P., KIM, N. H., NAEIJE, R. & SIMONNEAU, G. 2013. Chronic thromboembolic pulmonary hypertension: role of medical therapy. *European Respiratory Journal*, 41, 985-990.
- PU, J., GEZER, N. S., REN, S., ALPAYDIN, A. O., AVCI, E. R., RISBANO, M. G., RIVERA-LEBRON, B., CHAN, S. Y.-W. & LEADER, J. K. 2023. Automated detection and segmentation of pulmonary embolisms on computed tomography pulmonary angiography (CTPA) using deep learning but without manual outlining. *Medical image analysis*, 89, 102882.

- PU, J., LEADER, J. K., SECHRIST, J., BEECHE, C. A., SINGH, J. P., OCAK, I. K. & RISBANO, M. G. 2022. Automated identification of pulmonary arteries and veins depicted in non-contrast chest CT scans. *Medical image analysis*, 77, 102367.
- QANADLI, S. D., EL HAJJAM, M., VIEILLARD-BARON, A., JOSEPH, T., MESUROLLE, B., OLIVA, V. L., BARRÉ, O., BRUCKERT, F., DUBOURG, O. & LACOMBE, P. 2001. New CT index to quantify arterial obstruction in pulmonary embolism: comparison with angiographic index and echocardiography. *American journal of roentgenology*, 176, 1415-1420.
- QIN, Y., ZHENG, H., GU, Y., HUANG, X., YANG, J., WANG, L., YAO, F., ZHU, Y.-M. & YANG, G.-Z. 2021. Learning tubule-sensitive CNNs for pulmonary airway and artery-vein segmentation in CT. *IEEE transactions on medical imaging*, 40, 1603-1617.
- QUADERY, S. R., SWIFT, A. J., BILLINGS, C. G., THOMPSON, A. A., ELLIOT, C. A., HURDMAN, J., CHARALAMPOPOULOS, A., SABROE, I., ARMSTRONG, I. J. & HAMILTON, N. 2018. The impact of patient choice on survival in chronic thromboembolic pulmonary hypertension. *European Respiratory Journal*, 52.
- RAHAGHI, F. N., NARDELLI, P., HARDER, E., SINGH, I., SÁNCHEZ-FERRERO, G. V., ROSS, J. C., ESTÉPAR, R. S. J., ASH, S. Y., HUNSAKER, A. R. & MARON, B. A. 2021. Quantification of arterial and venous morphologic markers in pulmonary arterial hypertension using CT imaging. *Chest*, 160, 2220-2231.
- RAHAGHI, F. N., ROSS, J. C., AGARWAL, M., GONZÁLEZ, G., COME, C., DIAZ, A., VEGAS-SÁNCHEZ-FERRERO, G., HUNSAKER, A., ESTÉPAR, R. S. J. & WAXMAN, A. 2016. Pulmonary vascular morphology as an imaging biomarker in chronic thromboembolic pulmonary hypertension. *Pulmonary circulation*, 6, 70-81.
- RAJARAM, S., SWIFT, A., CONDLIFFE, R., JOHNS, C., ELLIOT, C., HILL, C., DAVIES, C., HURDMAN, J., SABROE, I. & WILD, J. 2015. CT features of pulmonary arterial hypertension and its major subtypes: a systematic CT evaluation of 292 patients from the ASPIRE Registry. *Thorax*, 70, 382-387.
- RAJASEKAR, E., CHANDRA, H., PEARS, N., VAIRAVASUNDARAM, S. & KOTTECHA, K., 2025. Lung image quality assessment and diagnosis using generative autoencoders in unsupervised ensemble learning. *Biomedical signal processing and control*, 102, p.107268.
- RAPIDAI. 2022. *Why RapidAI for PE* [Online]. <https://www.rapidai.com/rapid-pe> RAPIDAI. [Accessed 31 May 2023].
- REMY-JARDIN, M., FLOHR, T. & REMY, J. 2025. Thoracic applications of photon-counting CT: where are WE after three years of clinical implementation? *British Journal of Radiology*, tqaf026.
- REMY-JARDIN, M., RYERSON, C. J., SCHIEBLER, M. L., LEUNG, A. N., WILD, J. M., HOEPER, M. M., ALDERSON, P. O., GOODMAN, L. R., MAYO, J. & HARAMATI, L. B. 2021. Imaging of pulmonary hypertension in adults: a position paper from the Fleischner Society. *Radiology*, 298, 531-549.
- RENAPURKAR, R. D., BULLEN, J., RIZK, A., ABOZEED, M., KARIM, W., SAEEDAN, M. B., TONG, M. Z. & HERESI, G. A. 2024. A Novel Dual Energy Computed Tomography Score Correlates With Postoperative Outcomes in Chronic Thromboembolic Pulmonary Hypertension. *Journal of Thoracic Imaging*, 39, 178-184.
- RIGHINI, M., ROBERT-EBADI, H. & LE GAL, G. 2017. Diagnosis of acute pulmonary embolism. *Journal of Thrombosis and Haemostasis*, 15, 1251-1261.

- ROGBERG, A. N., GOPALAN, D., WESTERLUND, E. & LINDHOLM, P. 2019. Do radiologists detect chronic thromboembolic disease on computed tomography? *Acta Radiologica*, 60, 1576-1583.
- RONNEBERGER, O., FISCHER, P. & BROX, T. U-net: Convolutional networks for biomedical image segmentation. Medical image computing and computer-assisted intervention–MICCAI 2015: 18th international conference, Munich, Germany, October 5-9, 2015, proceedings, part III 18, 2015. Springer, 234-241.
- RUGGIERO, A. & SCREATON, N. 2017. Imaging of acute and chronic thromboembolic disease: state of the art. *Clinical radiology*, 72, 375-388.
- RUIGROK, D., MEIJBOOM, L. J., WESTERHOF, B. E., IN'T VELD, A. H., VAN DER BRUGGEN, C. E., MARCUS, J. T., NOSSENT, E. J., VONK NOORDEGRAAF, A., SYMERSKY, P. & BOGAARD, H.-J. 2019. Right ventricular load and function in chronic thromboembolic pulmonary hypertension: differences between proximal and distal chronic thromboembolic pulmonary hypertension. *American Journal of Respiratory and Critical Care Medicine*, 199, 1163-1166.
- SABBULA, B. R., SANKARI, A. & AKELLA, J. 2024. Chronic Thromboembolic Pulmonary Hypertension. *StatPearls [Internet]*. StatPearls Publishing.
- SAOUTI, N., DE MAN, F., WESTERHOF, N., BOONSTRA, A., TWISK, J., POSTMUS, P. E. & NOORDEGRAAF, A. V. 2009. Predictors of mortality in inoperable chronic thromboembolic pulmonary hypertension. *Respiratory medicine*, 103, 1013-1019.
- SARANYA, A. & SUBHASHINI, R. 2023. A systematic review of Explainable Artificial Intelligence models and applications: Recent developments and future trends. *Decision analytics journal*, 7, 100230.
- SHAHIN, Y., ALABED, S., REHAN QUADERY, S., LEWIS, R. A., JOHNS, C., ALKHANFAR, D., SUKHANENKO, M., ALANDEJANI, F., GARG, P. & ELLIOT, C. A. 2022. CMR measures of left atrial volume index and right ventricular function have Prognostic Value in Chronic Thromboembolic Pulmonary Hypertension. *Frontiers in Medicine*, 9, 840196.
- SHARIFI KIA, D., KIM, K. & SIMON, M. A. 2021. Current understanding of the right ventricle structure and function in pulmonary arterial hypertension. *Frontiers in physiology*, 12, 641310.
- SHARKEY, M. J., DWIVEDI, K., ALABED, S. & SWIFT, A. J. 2023. Deep learning automated quantification of lung disease in pulmonary hypertension on CT pulmonary angiography: A preliminary clinical study with external validation. *arXiv preprint arXiv:2303.11130*.
- SHARKEY, M. J., TAYLOR, J. C., ALABED, S., DWIVEDI, K., KARUNASAAGARAR, K., JOHNS, C. S., RAJARAM, S., GARG, P., ALKHANFAR, D. & METHERRALL, P. 2022. Fully automatic cardiac four chamber and great vessel segmentation on CT pulmonary angiography using deep learning. *Frontiers in Cardiovascular Medicine*, 9, 983859.
- SHAYGANFAR, A., HAJIAHMADI, S., ASTARAKI, M. & EBRAHIMIAN, S. 2020. The assessment of acute pulmonary embolism severity using CT angiography features. *International Journal of Emergency Medicine*, 13, 1-5.
- SHIN, Y., LEE, M., LEE, Y., KIM, K. & KIM, T. 2025. Artificial Intelligence-Powered Quality Assurance: Transforming Diagnostics, Surgery, and Patient Care—Innovations, Limitations, and Future Directions. *Life*, 15, 654.
- SIMONNEAU, G. & HOEPER, M. M. 2019. The revised definition of pulmonary hypertension: exploring the impact on patient management. *European Heart Journal Supplements*, 21, K4-K8.

- SIMONNEAU, G., TORBICKI, A., DORFMÜLLER, P. & KIM, N. 2017. The pathophysiology of chronic thromboembolic pulmonary hypertension. *European Respiratory Review*, 26.
- SIN, D., MCLENNAN, G., RENGIER, F., HADDADIN, I., HERESI, G. A., BARTHOLOMEW, J. R., FINK, M. A., THOMPSON, D. & PARTOVI, S. 2021. Acute pulmonary embolism multimodality imaging prior to endovascular therapy. *The international journal of cardiovascular imaging*, 37, 343-358.
- SINGH, R., CHAUDHARY, A. & RAY, S. 2025. Decoding Challenges using Mathematics of Fuzzy Theory in Interpretability, Shifts, Adaptation and Trust. *Biomedical and Pharmacology Journal*, 18, 179-190.
- SOFFER, S., KLANG, E., SHIMON, O., BARASH, Y., CAHAN, N., GREENSPAN, H. & KONEN, E. 2021. Deep learning for pulmonary embolism detection on computed tomography pulmonary angiogram: a systematic review and meta-analysis. *Scientific reports*, 11, 15814.
- STEIN, A., WU, C., CARR, C., SHIH, G., RUDIE, J. & MONGAN, J. 2020. RSNA STR Pulmonary Embolism Detection. *United States: Radiological Society of North America*.
- SUGIURA, T., TANABE, N., MATSUURA, Y., SHIGETA, A., KAWATA, N., JUJO, T., YANAGAWA, N., SAKAO, S., KASAHARA, Y. & TATSUMI, K. 2013. Role of 320-slice CT imaging in the diagnostic workup of patients with chronic thromboembolic pulmonary hypertension. *Chest*, 143, 1070-1077.
- SUKI, B., STAMENOVIC, D. & HUBMAYR, R. 2011. Lung parenchymal mechanics. *Comprehensive Physiology*, 1, 1317.
- SUNTHARALINGAM, J., HUGHES, R., GOLDSMITH, K., DOUGHTY, N., GEORGE, P., TOSHNER, M., SHEARES, K. & PEPKE-ZABA, J. 2007. Acute haemodynamic responses to inhaled nitric oxide and intravenous sildenafil in distal chronic thromboembolic pulmonary hypertension (CTEPH). *Vascular pharmacology*, 46, 449-455.
- SWIFT, A. J., DWIVEDI, K., JOHNS, C., GARG, P., CHIN, M., CURRIE, B. J., ROTHMAN, A. M., CAPENER, D., SHAHIN, Y. & ELLIOT, C. A. 2020. Diagnostic accuracy of CT pulmonary angiography in suspected pulmonary hypertension. *European Radiology*, 30, 4918-4929.
- TAJBAKHS, N., GOTWAY, M. B. & LIANG, J. Computer-aided pulmonary embolism detection using a novel vessel-aligned multi-planar image representation and convolutional neural networks. Medical Image Computing and Computer-Assisted Intervention--MICCAI 2015: 18th International Conference, Munich, Germany, October 5-9, 2015, Proceedings, Part II 18, 2015. Springer, 62-69.
- TAJBAKHS, N., SHIN, J. Y., GOTWAY, M. B. & LIANG, J. 2019. Computer-aided detection and visualization of pulmonary embolism using a novel, compact, and discriminative image representation. *Medical image analysis*, 58, 101541.
- TAKAGI, H., OTA, H., SUGIMURA, K., OTANI, K., TOMINAGA, J., AOKI, T., TATEBE, S., MIURA, M., YAMAMOTO, S. & SATO, H. 2016. Dual-energy CT to estimate clinical severity of chronic thromboembolic pulmonary hypertension: Comparison with invasive right heart catheterization. *European journal of radiology*, 85, 1574-1580.
- TAMURA, M., YAMADA, Y., KAWAKAMI, T., KATAOKA, M., IWABUCHI, Y., SUGIURA, H., HASHIMOTO, M., NAKAHARA, T., OKUDA, S. & NAKATSUKA, S. 2017. Diagnostic accuracy of lung subtraction iodine mapping CT for the evaluation of pulmonary perfusion in patients with chronic thromboembolic pulmonary hypertension: correlation with perfusion SPECT/CT. *International journal of cardiology*, 243, 538-543.

- TANIGUCHI, Y., MIYAGAWA, K., NAKAYAMA, K., KINUTANI, H., SHINKE, T., OKADA, K., OKITA, Y., HIRATA, K.-I. & EMOTO, N. 2014. Balloon pulmonary angioplasty: an additional treatment option to improve the prognosis of patients with chronic thromboembolic pulmonary hypertension. *EuroIntervention*, 10, 518-25.
- TRITSCHLER, T., KRAAIJPOEL, N., GIRARD, P., BÜLLER, H. R., LANGLOIS, N., RIGHINI, M., SCHULMAN, S., SEGERS, A. & LE GAL, G. 2020. Definition of pulmonary embolism-related death and classification of the cause of death in venous thromboembolism studies: communication from the SSC of the ISTH. *Journal of thrombosis and haemostasis*, 18, 1495-1500.
- TUNARIU, N., GIBBS, S. J., WIN, Z., GIN-SING, W., GRAHAM, A., GISHEN, P. & ADIL, A.-N. 2007. Ventilation-perfusion scintigraphy is more sensitive than multidetector CTPA in detecting chronic thromboembolic pulmonary disease as a treatable cause of pulmonary hypertension. *Journal of nuclear medicine*, 48, 680-684.
- VAINIO, T., MÄKELÄ, T., ARKKO, A., SAVOLAINEN, S. & KANGASNIEMI, M. 2023. Leveraging open dataset and transfer learning for accurate recognition of chronic pulmonary embolism from CT angiogram maximum intensity projection images. *European radiology experimental*, 7, 33.
- VAINIO, T., MÄKELÄ, T., SAVOLAINEN, S. & KANGASNIEMI, M. 2021. Performance of a 3D convolutional neural network in the detection of hypoperfusion at CT pulmonary angiography in patients with chronic pulmonary embolism: a feasibility study. *European radiology experimental*, 5, 1-12.
- VALERIO, L., MAVROMANOLI, A. C., BARCO, S., ABELE, C., BECKER, D., BRUCH, L., EWERT, R., FAEHLING, M., FISTERA, D. & GERHARDT, F. 2022. Chronic thromboembolic pulmonary hypertension and impairment after pulmonary embolism: the FOCUS study. *European heart journal*, 43, 3387-3398.
- VAN HARTSKAMP, M., CONSOLI, S., VERHAEGH, W., PETKOVIC, M. & VAN DE STOLPE, A. 2019. Artificial intelligence in clinical health care applications. *Interactive journal of medical research*, 8, e12100.
- VAN KAN, C., VAN DER PLAS, M. N., REESINK, H. J., VAN STEENWIJK, R. P., KLOEK, J. J., TEPASKE, R., BONTA, P. I. & BRESSER, P. 2016. Hemodynamic and ventilatory responses during exercise in chronic thromboembolic disease. *The Journal of thoracic and cardiovascular surgery*, 152, 763-771.
- VANDEWINCKELE, L., CLAESSENS, M., DINKLA, A., BROUWER, C., CRIJNS, W., VERELLEN, D. & VAN ELMPT, W. 2020. Overview of artificial intelligence-based applications in radiotherapy: Recommendations for implementation and quality assurance. *Radiotherapy and Oncology*, 153, 55-66.
- WANG, M., WU, D., MA, R., ZHANG, Z., ZHANG, H., HAN, K., XIONG, C., WANG, L. & FANG, W., 2020. Comparison of V/Q SPECT and CT angiography for the diagnosis of chronic thromboembolic pulmonary hypertension. *Radiology*, 296(2), pp.420-429.
- WASSERTHAL, J., BREIT, H.C., MEYER, M.T., PRADELLA, M., HINCK, D., SAUTER, A.W., HEYE, T., BOLL, D.T., CYRIAC, J., YANG, S. & BACH, M., 2023. TotalSegmentator: robust segmentation of 104 anatomic structures in CT images. *Radiology: Artificial Intelligence*, 5(5), p.e230024.
- WEBB, J. M., ADUSEI, S. A., WANG, Y., SAMREEN, N., ADLER, K., MEIXNER, D. D., FAZZIO, R. T., FATEMI, M. & ALIZAD, A. 2021. Comparing deep learning-based automatic segmentation of breast masses to expert interobserver variability in ultrasound imaging. *Computers in biology and medicine*, 139, 104966.

- WEI, R. & MAHMOOD, A., 2020. Recent advances in variational autoencoders with representation learning for biomedical informatics: A survey. *Ieee Access*, 9, pp.4939-4956.
- WEIKERT, T., WINKEL, D. J., BREMERICH, J., STIELTJES, B., PARMAR, V., SAUTER, A. W. & SOMMER, G. 2020. Automated detection of pulmonary embolism in CT pulmonary angiograms using an AI-powered algorithm. *European radiology*, 30, 6545-6553.
- WILSON, M., CHOPRA, R., WILSON, M. Z., COOPER, C., MACWILLIAMS, P., LIU, Y., WULCZYN, E., FLOREA, D., HUGHES, C. O. & KARTHIKESALINGAM, A. 2021. Validation and clinical applicability of whole-volume automated segmentation of optical coherence tomography in retinal disease using deep learning. *JAMA ophthalmology*, 139, 964-973.
- WITTRAM, C., MAHER, M. M., YOO, A. J., KALRA, M. K., SHEPARD, J.-A. O. & MCLOUD, T. C. 2004. CT angiography of pulmonary embolism: diagnostic criteria and causes of misdiagnosis. *Radiographics*, 24, 1219-1238.
- WU, Y., QI, S., WANG, M., ZHAO, S., PANG, H., XU, J., BAI, L. & REN, H. 2023. Transformer-based 3D U-Net for pulmonary vessel segmentation and artery-vein separation from CT images. *Medical & Biological Engineering & Computing*, 61, 2649-2663.
- YAMASHITA, R., NISHIO, M., DO, R. K. G. & TOGASHI, K. 2018. Convolutional neural networks: an overview and application in radiology. *Insights into imaging*, 9, 611-629.
- YANG, J., MADANI, M. M., MAHMUD, E. & KIM, N. H. 2023. Evaluation and Management of Chronic Thromboembolic Pulmonary Hypertension. *CHEST*, 164, 490-502.
- YANG, R. & YU, Y. 2021. Artificial convolutional neural network in object detection and semantic segmentation for medical imaging analysis. *Frontiers in oncology*, 11, 638182.
- YUAN, H., SHAO, Y., LIU, Z. & WANG, H. 2021. An improved faster R-CNN for pulmonary embolism detection from CTPA images. *IEEE Access*, 9, 105382-105392.
- ZHAI, Z., BOON, G. J., STARING, M., VAN DAM, L. F., KROFT, L. J., HERNÁNDEZ GIRÓN, I., NINABER, M. K., BOGAARD, H. J., MEIJBOOM, L. J. & VONK NOORDEGRAAF, A. 2023. Automated quantification of the pulmonary vasculature in pulmonary embolism and chronic thromboembolic pulmonary hypertension. *Pulmonary Circulation*, 13, e12223.
- ZHANG, C., SUN, M., WEI, Y., ZHANG, H., XIE, S. & LIU, T. 2019. Automatic segmentation of arterial tree from 3D computed tomographic pulmonary angiography (CTPA) scans. *Computer Assisted Surgery*, 24, 79-86.
- ZHOU, Q., TAN, W., LI, Q., LI, B., ZHOU, L., LIU, X., YANG, J. & ZHAO, D. 2023. A new segment method for pulmonary artery and vein. *Health Information Science and Systems*, 11, 47.